PL-TR--
94-1056

INFLATABLE TORUS SOLAR ARRAY TECHNOLOGY PROGRAM PHASE II

Kevin Davey
Koorosh Guidanean
Pat Malone
Geoff Williams

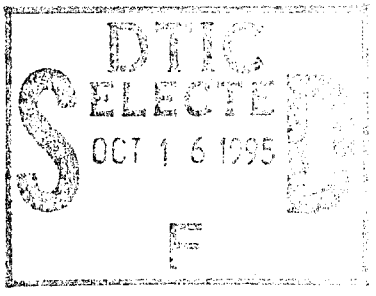

L'Garde, Inc.
15181 Woodlawn Avenue
Tustin, CA 92680

January 1994

Final Report

PHILLIPS LABORATORY
Space and Missiles Technology Directorate
AIR FORCE MATERIEL COMMAND
KIRTLAND AIR FORCE BASE, NM 87117-5776

AD NUMBER

AD- B204 206

NEW LIMITATION CHANGE

TO

DISTRIBUTION STATEMENT A -
Approved for public release; Distribution unlimited.

Limitation Code: 1

FROM

DISTRIBUTION STATEMENT -

Limitation Code:

AUTHORITY

Janet E. Mosher, Phillips Lab., Kirtland AFB, N.M.

PL-TR--94-1056

This final report was prepared by L'Garde, Inc., Tustin, CA, under Contract F29601-90-C-0006, with Phillips Laboratory, Kirtland Air Force Base, New Mexico. The Laboratory Project Officer-in-Charge was Lt. Randy Boswell (VTPC).

If your address has changed, if you wish to be removed from the mailing list, or if your organization no longer employs the addressee, please notify PL/VTRP, 3550 Aberdeen Ave SE, Kirtland AFB, NM 87117-5776 to help maintain a current mailing list.

This report has been reviewed and is approved for publication.

Randy L Boswell

RANDY L. BOSWELL, 1 Lt, USAF
Project Officer

FOR THE COMMANDER

David H Kristensen

DAVID H. KRISTENSEN, Lt Col, USAF
Chief, Power & Thermal Management Div

Henry L Pugh Jr

HENRY L. PUGH, JR., Col, USAF
Director of Space and Missiles Technology

DO NOT RETURN COPIES OF THIS REPORT UNLESS CONTRACTUAL OBLIGATIONS OR NOTICE ON A SPECIFIC DOCUMENT REQUIRES THAT IT BE RETURNED.

The following notice applies to any unclassified (including originally classified and now declassified) technical reports released to "qualified U.S. contractors" under the provisions of DoD Directive 5230.25, Withholding of Unclassified Technical Data From Public Disclosure.

NOTICE TO ACCOMPANY THE DISSEMINATION OF EXPORT-CONTROLLED TECHNICAL DATA

1. Export of information contained herein, which includes, in some circumstances, release to foreign nationals within the United States, without first obtaining approval or license from the Department of State for items controlled by the International Traffic in Arms Regulations (ITAR), or the Department of Commerce for items controlled by the Export Administration Regulations (EAR), may constitute a violation of law.

2. Under 22 U.S.C. 2778 the penalty for unlawful export of items or information controlled under the ITAR is up to two years imprisonment, or a fine of $100,000, or both. Under 50 U.S.C., Appendix 2410, the penalty for unlawful export of items or information controlled under the EAR is a fine of up to $1,000,000, or five times the value of the exports, whichever is greater; or for an individual, imprisonment of up to 10 years, or a fine of up to $250,000, or both.

3. In accordance with your certification that establishes you as a "qualified U.S. Contractor", unauthorized dissemination of this information is prohibited and may result in disqualification as a qualified U.S. contractor, and may be considered in determining your eligibility for future contracts with the Department of Defense.

4. The U.S. Government assumes no liability for direct patent infringement, or contributory patent infringement or misuse of technical data.

5. The U.S. Government does not warrant the adequacy, accuracy, currency, or completeness of the technical data.

6. The U.S. Government assumes no liability for loss, damage, or injury resulting from manufacture or use for any purpose of any product, article, system, or material involving reliance upon any or all technical data furnished in response to the request for technical data.

7. If the technical data furnished by the Government will be used for commercial manufacturing or other profit potential, a license for such use may be necessary. Any payments made in support of the request for data do not include or involve any license rights.

8. A copy of this notice shall be provided with any partial or complete reproduction of these data that are provided to qualified U.S. contractors.

D E S T R U C T I O N N O T I C E

For classified documents, follow the procedures in DoD 5200.22-M, Industrial Security Manual, Section II-19 or DoD 5200.1-R, Information Security Program Regulation, Chapter IX. For unclassified, limited documents, destroy by any method that will prevent disclosure of contents or reconstruction of the document.

DRAFT SF 298

1. Report Date (dd-mm-yy) January 1994	2. Report Type Final	3. Dates covered (from... to) Mar 92 - Dec 93
4. Title & subtitle INFLATABLE TORUS SOLAR ARRAY TECHNOLOGY PROGRAM PHASE II		5a. Contract or Grant # F29601-90-C-0006
		5b. Program Element # 62601F
6. Author(s) Kevin Davey Koorosh Guidanean Pat Malone Geoff Williams		5c. Project # DRPB 5d. Task # AA 5e. Work Unit # 04
7. Performing Organization Name & Address L'Garde, Inc. 15181 Woodlawn Avenue Tustin, CA 92680		8. Performing Organization Report # LTR-93-GW-072B
9. Sponsoring/Monitoring Agency Name & Address Phillips Laboratory 3550 Aberdeen Avenue, SE Kirtland AFB, NM 87117-5776		10. Monitor Acronym 11. Monitor Report # PL-TR--94-1056

12. Distribution/Availability Statement
Distribution authorized to DoD components only, PROPRIETARY INFORMATION; January 1994. Other requests shall be referred to AFMC/STI.

13. Supplementary Notes

14. Abstract This Phase II of the Inflatable Torus Solar Array Technology (ITSAT) Program took the Inflatable Solar Array all the way from prototype development through thermal vacuum testing. The design consists of two inflatable/rigidizable tubes on either side of a flexible solar array. The tubes are mounted to an enclosure which attaches to the host spacecraft, while the lid to the enclosure completes the rectangular structure for the array.

During the program, a flexible solar array was developed for the application and was used for all testing. The program ended with deployment, natural frequency measurement, and thermal cycling in the thermal vacuum chamber at the Naval Research Laboratory.

15. Subject Terms
Inflatable Solar Array Rigidized Structures
Inflatable Structures Flexible Solar Arrays

Security Classification of			19. Limitation of Abstract	20. # of Pages	21. Responsible Person (Name and Telephone #)
16. Report Unclassified	17. Abstract Unclassified	18. This Page Unclassified	Limited	228	Randy L. Boswell (505) 846-9632

ACKNOWLEDGEMENTS

The authors would like to express their deep appreciation to the following individuals:

Colonel Lee Demitry at the Advanced Research Projects Agency (ARPA) for his support throughout the program; Lt Randy Boswell and Dorothy Sandoval at Phillips Laboratory, and Tricia Tiernan at Space Applications Corporation for their thorough review of this report; Rod Dobson at Applied Solar Energy Corporation for delivering the solar cells on time and within budget; Joe Hauser and the staff at the Naval Research Laboratory for their long hours of support during thermal vacuum testing; Alec Garcia at Aerospace Corporation, and David Brinker and Dr Dennis Flood at the NASA Lewis Research Center for sharing their expertise in photovoltaics; and for preparing and making the numerous revisions required for this report Judy Flickinger and Bonnie Lowe, respectively, at L'Garde.

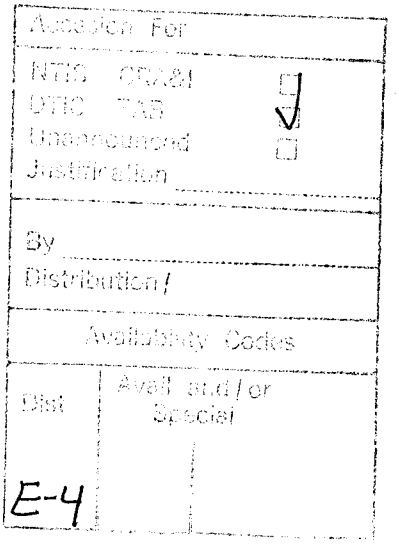

CONTENTS

CONTENTS (Continued)

CONTENTS (Concluded)

FIGURES

FIGURES (Continued)

FIGURES (Continued)

FIGURES (Continued)

FIGURES (Continued)

FIGURES (Continued)

FIGURES (Concluded)

TABLES

TABLES (Continued)

TABLES (Concluded)

CONVERSION FACTORS TO SI UNITS

Item	Units	Multiply by	To Convert to SI Units
acceleration	g	9.81	m/s^2
angular momentum	lb in^2/sec	2.926×10^{-4}	kg m^2/sec
angular velocity	rps	6.283	rad/s
energy	erg	1×10^{-7}	J
force	lbs	4.448	N
impulse	taps $\left(\frac{g}{cm\ sec}\right)$	0.1	$\frac{kg}{m\ sec}$
length	ft	.3048	m
length	kft	304.8	m
length	inch	.0254	m
length	mil	2.54×10^{-5}	m
moment of inertia	lb in^2	2.926×10^{-4}	kg m^2
pressure	atm	1.013×10^5	Pa or N/m^2
pressure	kilobar	1×10^8	Pa or N/m^2
pressure	Mbar	1×10^{11}	Pa or N/m^2
pressure	psi	6.895×10^3	Pa or N/m^2
temperature	^oC	add 273.16	K
velocity	kfps	304.8	m/sec
volume	in^3	1.639×10^{-5}	m^3
weight	lbs	.4536	kg

1.0 EXECUTIVE SUMMARY

1.1 INTRODUCTION

The Inflatable Torus Solar Array Technology (ITSAT) Phase II protoflight development and demonstration program has been successfully completed. Over 6 years ago, the Inflatable Solar Array was conceptualized as a means to meet anticipated future requirements of advanced microsatellites. The dominant requirements for solar power were high power densities, flexible packaging envelope, short fabrication and delivery schedules, and low cost. Using L'Garde's state-of-the-art technology, several approaches to developing an inflatably-deployed-then-rigidized structure were proposed in response to an Advanced Research Projects Agency (ARPA) Broad Area Announcement (BAA). Subsequently a program was awarded to L'Garde to further define and develop prototype and protoflight solar array systems.

1.2 HISTORY

During Phase I of the program 15 point designs were studied. The parameters for these studies included: orbit altitude, inclination, performance life, deployed configuration, cell types, cost, and overall performance. The studies concluded that an inflatably-deployed-then-rigidized structural support system using thin film solar cell substrate technology would provide power densities that were more than double the state-of-the-art flexible panel technology. The key was the inflatable-then-rigidized structural members. Figure 1 presents the typical performance of various solar array systems.

1.3 PHASE II

Phase II of ITSAT studied array sizes of 200 to 1000 W per wing, End-of-Life (EOL) in a 3-year Low-Earth-Orbit (LEO) at any inclination (0-90 deg). This phase ended with a successful thermal vacuum deployment test of a 200-W-EOL thin-film substrate prototype unit at the Naval Research Laboratory (NRL) test chamber. The program was completed in approximately 22 months from contract award. The effort included system design, space-qualified material research, testing and selection, development testing of various

subsystems, fabrication of the structure, deployment system and solar array blanket, and partial qualification testing and deployment in a space-like environment. The resulting protoflight unit has a specific power of 59.1 W/kg and an areal power density of 113 W/m^2. A production array will have a specific power of 93.0 W/kg and an areal power density of 113 W/m^2. A comprehensive list of performance specifications for the protoflight and the production unit is shown in Table 1, ITSAT Performance Specifications. Larger sizes shown in Figure 1 are scaled from the protoflight unit.

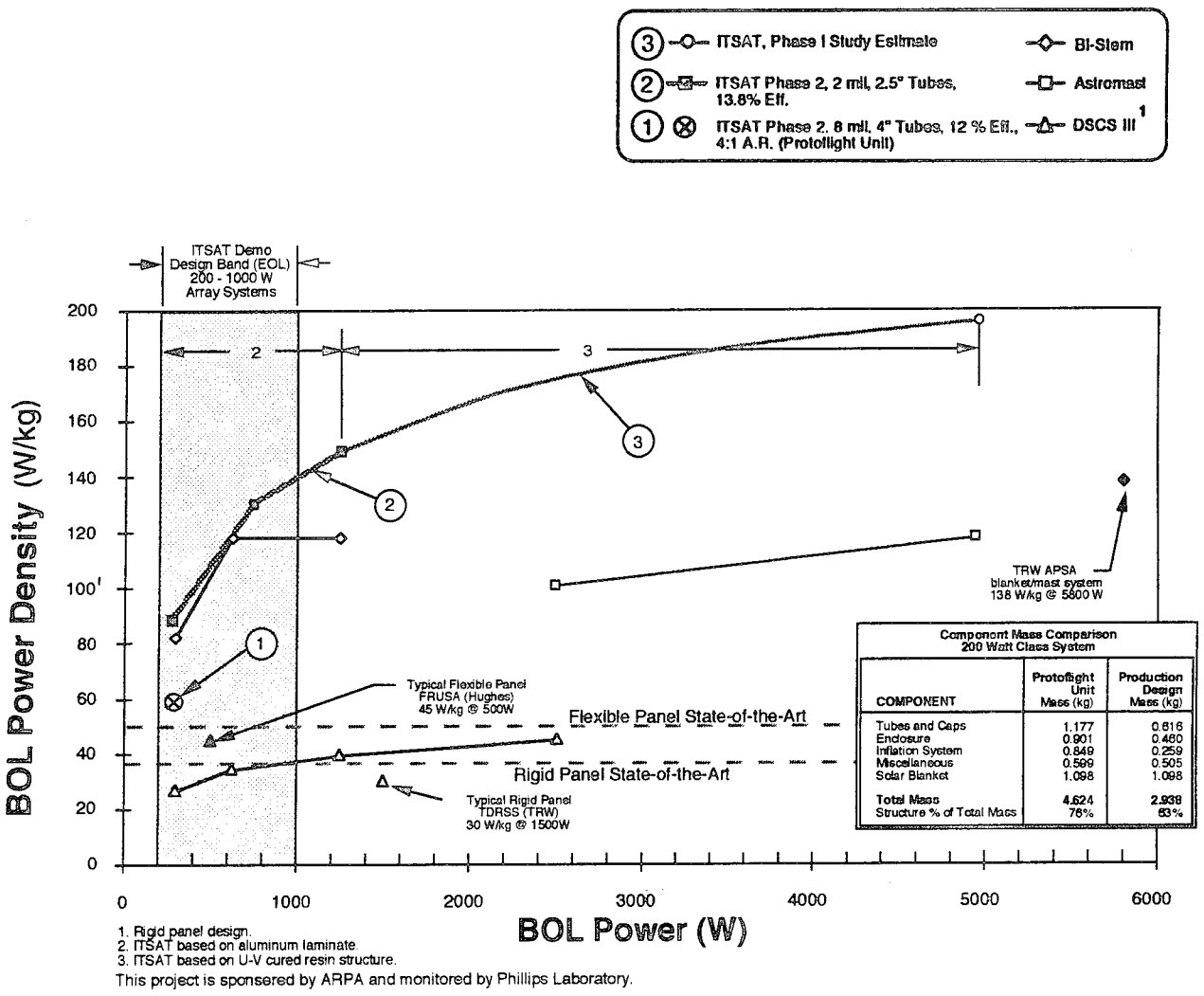

Figure 1. Typical performance of various solar array systems.

Table 1. The ITSAT performance specifications.

SPECIFICATION	REQUIREMENTS/ GOALS	PROTOFLIGHT ACTUALS	PRODUCTION GOALS
OVERALL SYSTEM			
FULLY POPULATED (HYPOTHETICAL)			
BOL Power	---	274.9 W	274.9 W
EOL Power	200 W [R]	221.4 W	221.4 W
Weight	---	9.65 lb (4.38 kg)	7.14 lb (3.24 kg)
Structure (% of weight)	---	75%	66%
BOL Power/Weight	90 W/kg [G]	28.5 W/lb (59.1 W/kg)	38.5 W/lb (93.0 W/kg)
EOL Power/Weight	---	22.9 W/lb (47.6 W/kg)	31.0 W/lb (74.9 W/kg)
Packaged Volume	---	2360 in^3	1850 in^3
Dimensions (Packaged)	---	44.6 x 8.4 x 6.4 in	44.6 x 8.4 x 5.1 in
Overall Dimensions (deployed)	---	142.5 x 44.6 x 8.4 in	142.5 x 44.6 x 8.4 in
Moment of Inertia (deployed)	---		
I_{xx}	---	TBD	TBD
I_{yy}	---	TBD	TBD
I_{zz}	---	TBD	TBD
Natural Frequency (packaged)	> 20 Hz [G]	105 Hz[a]	TBD
Natural Frequency (deployed)			
X-axis	> 1Hz [R]	> 1 Hz	> 1 Hz
Y-axis	> 1Hz [R]	> 1 Hz	> 1 Hz
Z-axis	> 1Hz [R]	1.04 Hz	> 1 Hz
Mounting Type	---	4 bolt pattern	4 bolt pattern
Thread Size	---	1/4-20 UNC-2B	1/4-20 UNC-2B
Dimensions	---	3.500 in bolt circle	3.500 in bolt circle
ARRAY			
Type	---	Rigid Cells on Flexible Blanket	Rigid Cells on Flexible Blanket
Cell Thickness	---	2.2 mil (baseline)	2.2 mil
Coverglass Thickness	---	2.9 mil	2.9 mil
Cell Efficiency	---	13.8%	13.8%

Table 1. The ITSAT performance specifications (continued).

SPECIFICATION	REQUIREMENTS/ GOALS	PROTOFLIGHT ACTUALS	PRODUCTION GOALS
Substrate Thickness	---	2 mil	2 mil
Blanket Dimensions	---	29.2 x 128.2 in	29.2 x 128.2 in
Distance Between Blanket Foldlines	---	7.1 in	7.1 in
Aspect Ratio (Blanket Only)	> 4:1 [G]	4.38 : 1	4.38 : 1
Population Density (Test Article)	~ 10% [G]	9.7%	9.7%
BOL Power/Blanket Area	---	10.5 W/ft^2 (113 W/m^2)	10.5 W/ft^2 (113 W/m^2)
EOL Power/Blanket Area	---	8.5 W/ft^2 (91 W/m^2)	8.5 W/ft^2 (91 W/m^2)
Blanket Area	> 21.5 ft^2 (2m^2) [G]	26.0 W/ft^2 (2.42 m^2)	26.0 W/ft^2 (2.42 m^2)
STRUCTURE			
Type	---	Twin Boom, Inflated/Rigidized	Twin Boom, Inflated/Rigidized
Tube Diameter	---	4 in	2.5 in
Tube Length	---	140 in	140 in
Tube Rigidization Pressure:	---		
In Eclipse	---	17.5 psi	28.0 psi
In Sunlight	---	19.7 psi	31.5 psi
Tube Burst Pressure	---	43.0 psi (test data)	69 psi
INFLATION SYSTEM			
Inflatant	---	Nitrogen	Nitrogen
Valve Type	---	Pyrotechnic	Pyrotechnic
Tank Pressure	---	2870 psi	TBD
Inflatant Mass	---	0.221 lb	TBD
Flow Regulation	---	Flow Restrictors	Flow Restrictors
Fill Valve	---	Flare-Type	Flare-Type
Tank Fill Port Specification	---	MS33656-2	MS33656-2
DEPLOYMENT CHARACTERISTICS			
Deployment Time	---	30 s	30 s
Additional Time Required for Rigidization	---	70 s	70 s
ORBITAL PARAMETERS			
Lifetime	3 yr [R]	≥ 3 yr	---

Table 1. The ITSAT performance specifications (concluded).

SPECIFICATION	REQUIREMENTS/ GOALS	PROTOFLIGHT ACTUALS	PRODUCTION GOALS
Altitude	600-800 km (750 km nominal) [R]	[b]	---
Apogee	(Circular)	[b]	---
Perigee	(Circular)	[b]	---
Inclination	Design for eclipse every orbit [R]	---	---
Pointing Requirements	TBD	---	---
Acceleration when Deployed	0.03 g [R]	---	---
Tube Temperature when deployed		-172 to 540 R (160 to 300 k)	---
LAUNCH ENVIRONMENTS			
Temperature in Storage	-40 to 150°F	Tested to -40 to 150°F	(-40 to 150°F)
Temperature During Launch	(0 to 135°F)	---	---
Steady State Acceleration	10 g nominal (see Fig. 6)		---
Vibration	Figure 7	Tested to Figure 7	---
Shock	Figure 8	Tested w/Actual Pyros	---

[a] Estimated
[b] Meets or exceeds all orbit parameters within the altitude requirement (600 - 800 km).

Figure 2 shows the 200-W-EOL-class protoflight unit that was fabricated, demonstrated, and tested under flight-like conditions during Phase II.

This protoflight unit utilizes thin crystalline silicon solar cells. The structure is designed such that almost any type of solar cell mosaic can be used. Cell sizes used on the protoflight unit were 2 x 4 cm in surface area and 2.2 mils thick. Other cell types and sizes can be used to increase the system power density.

The ITSAT represents a major step in the evolution of highly efficient solar array technology in the few hundred to the few thousand Watt power output ranges. Space-qualified inflatable-rigidizable structural components were developed, fabricated, tested and demonstrated.

The flexible solar array blanket consists of thin crystalline silicon solar cells, a foldable Kapton® substrate, associated wiring and assembly fittings. This blanket approach yields a two to three-fold improvement in power density over systems that are currently available.

- Successful deployment at about -95° C, after pyroshock* and launch vibration environments

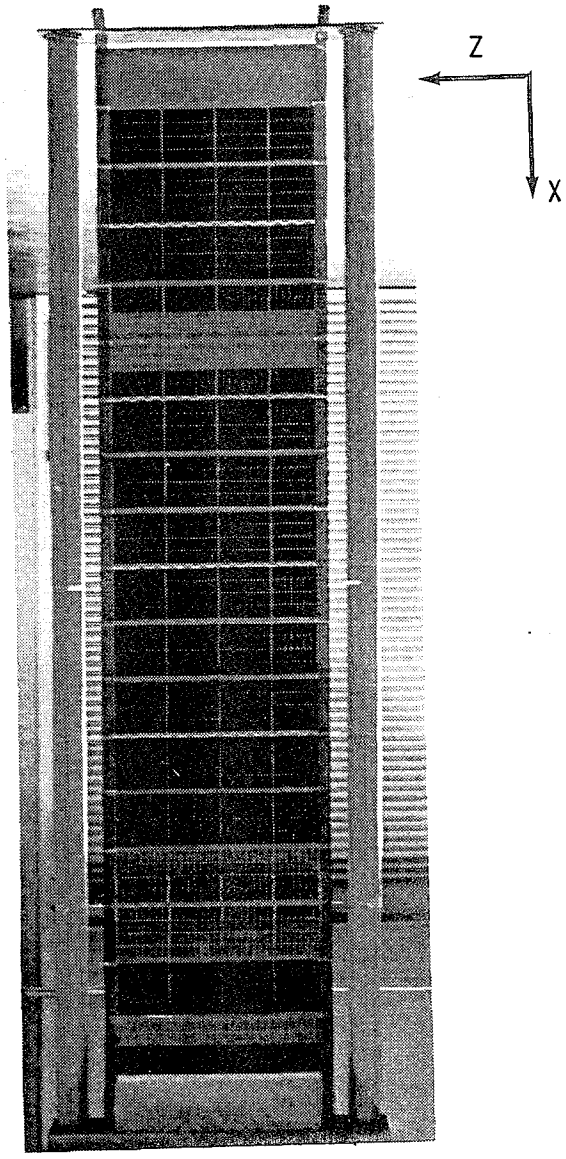

Figure 2. The ITSAT qualification array - deployed.

*Pyroshock was applied to the development unit by the cable cutters which were installed on the housing. These self-induced pyroshock environments were also applied to the qualification unit by the cable cutters and the inflation system puncture cutters during deployment at NRL.

- Successful inflation and rigidization of the tubular structural members
- Demonstration of excellent rigidity, yielding a natural frequency of 1.04 Hz
- No adverse effects due to thermal cycling
- Solar cell string resistances and output voltages unaffected by all events

1.4 FUTURE

The next step must be to refurbish the ITSAT protoflight unit for an actual space flight test and evaluation. The flight experiment will measure the ITSAT performance during deployment and on orbit. Typical measurements include deployment dynamics, output power, temperature of the structure and solar array, and natural frequency. Additional parameters during a 1-year monitoring effort can include cell degradation, atomic oxygen (AO) survivability of the structure and array substrate, and other age-sensitive factors.

The effort needed to prepare the ITSAT hardware for flight includes replacement of the tube struts, refurbishment and cleaning of the inflation system, checkout of the array blanket, packaging, acceptance testing, and integration with the spacecraft. To support the overall experiment, the programmatic tasks include, but are not limited to, the experiment plan, safety reports, integration plan, and other mission-specific efforts.

1.5 ESTIMATED PRODUCTION PRICES

The price estimates for ITSAT systems in the power range of 200 to 1000 W are given in Table 2. The prices are based on the specifications of Table 1 (scaled for larger systems). The price estimates presented are for fabrication of hardware and acceptance testing, per unit. The solar cells consume the largest fraction of the price.

Table 2. Summary table.

ARRAY SYSTEM POWER (EOL W)	DELIVERY TIME FOLLOWING FAB & ACCEPTANCE TESTING	ROM PRICE $ (Millions)	ROM PRICE PER WATT ($)
200	14 Months ARO	$0.61	$3,000
600	16 Months ARO	$1.41	$2,350
1200	18 Months ARO	$2.33	$2,330

Typical prices for other state-of-the-art systems with power ranges greater than 1000 W average $5000/W*. Thus the advanced ITSAT provides much better performance in weight, volume, packaging, and reliability for a significantly lower cost than current systems.

* Data from teleconferences with NASA, Aerospace Corporation and TRW.

2.0 ITSAT PHASE II INTRODUCTION

The purpose of the ITSAT Demonstration Program was to

- Develop the technology required to fly a working experimental prototype of an inflatably deployed and rigidized solar array

- Further advance the required materials, experiment and prototype design through the requisite development test program culminating at the prototype qualification test including thermal vacuum chamber tests at the end of Phase II

- Demonstrate this technology by flying this prototype at the end of the optional Phase III of this program.

This report covers the design, fabrication, and testing performed during Phase II.

2.1 DESIGN

The Phase I design consisted of a four sided torus which surrounded the array. The side elements were joined together at their corners, which presented a fabrication problem.

The Phase II ITSAT array and structure is shown in Figure 3. It is packaged into a lightweight rectangular graphite composite enclosure. The enclosure remains stationary (i.e., attached to the satellite drive assembly) while the lid is attached to the outboard end of two inflated/rigidized tubes. The array is stretched in between the four sides of the structure (the two booms, the lid, and the enclosure). This design eliminates the need for corner elements on the torus. The packaged array is shown in Figure 4, and the deployed array is shown in Figure 2.

The solar array is a thin-film Kapton® substrate utilizing thin crystalline silicon cells. The array is only partially populated with actual cells (about 10%) to reduce cost while the rest of the blanket is covered by mass simulators. The actual breakdown of cell/simulators is given in Table 3.

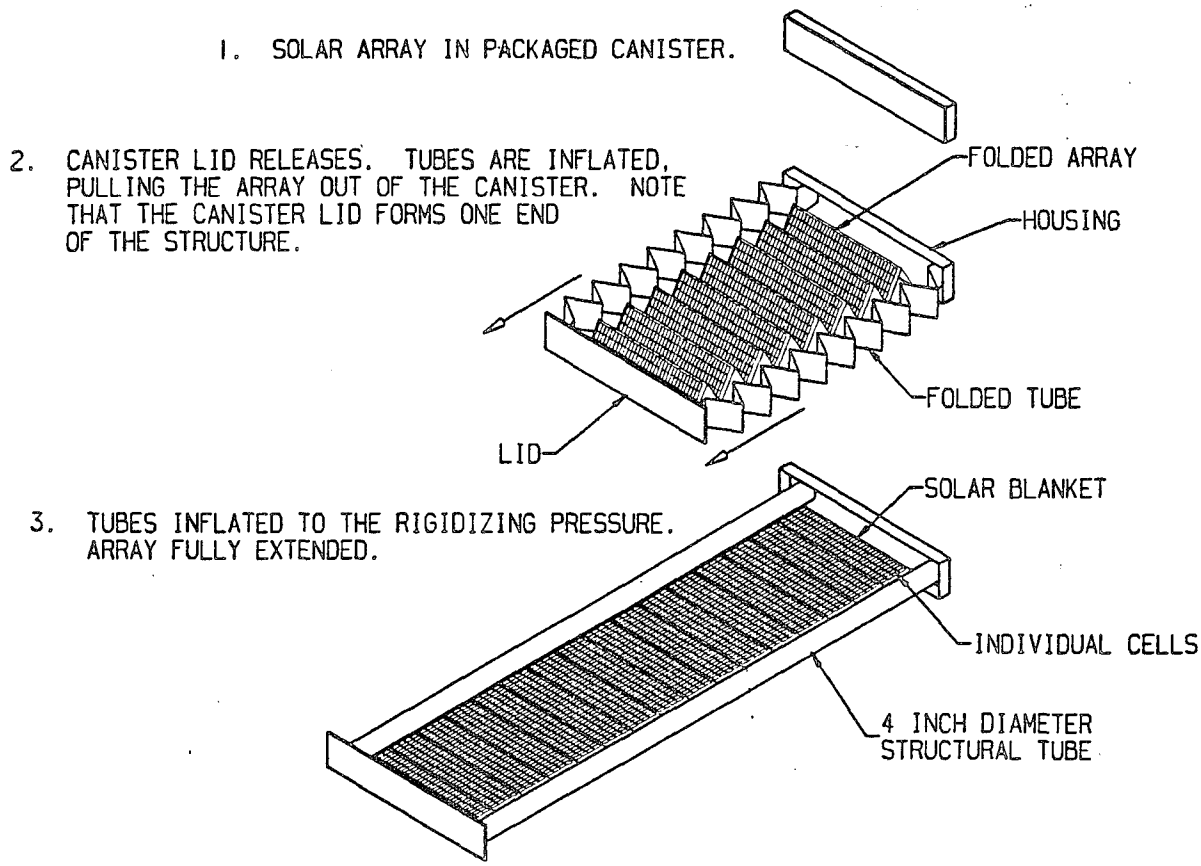

Figure 3. The ITSAT solar array.

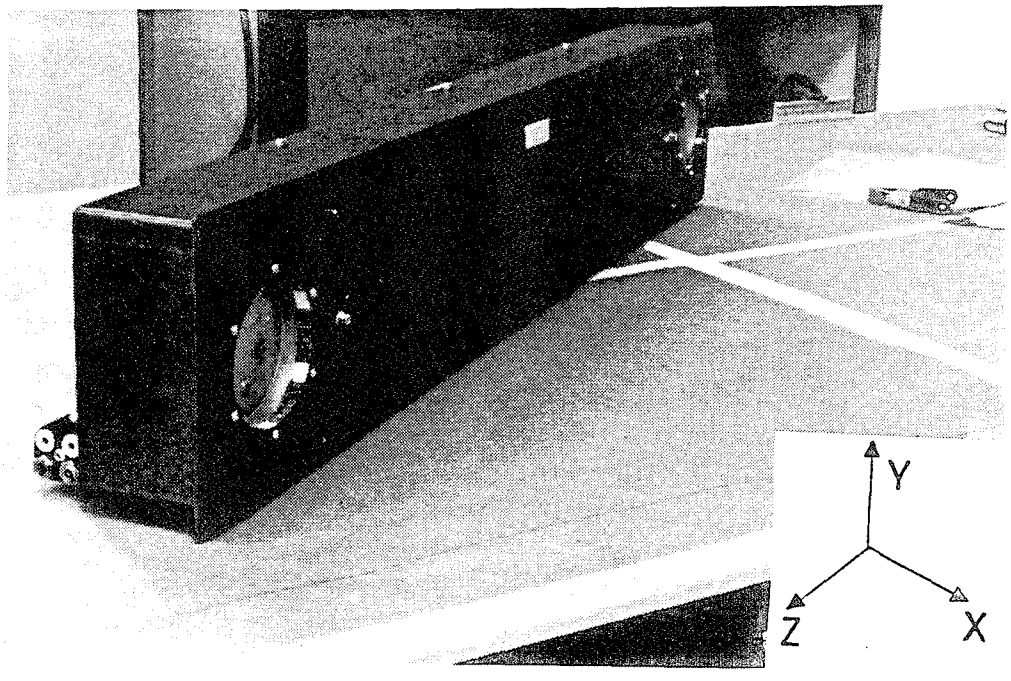

Figure 4. The ITSAT array - packaged.

Table 3. Cell population summary.

TYPE	QUANTITY	THICKNESS	DESCRIPTION
Cells	31	2 mil	2.2 mil cells with 2.9 mil covers
Cells	186	8 mil	8 mil cells with 2.9 mil covers
Simulator	1550	6 mil	Aluminum simulators, black anodized
Simulator	421	6 mil	CMZ Glass
Simulator	44	8 mil	Two 2.9-mil layers of glass bonded w/DC93500 (simulating a working solar cell assembly)

The majority of the working solar cells are 8 mils thick. One row of 2 mil cells is included to simulate the fragility of these more desirable thin cells. The 6-mil glass and the 8-mil glass/glass assemblies are made to simulate the fragility of actual solar cells. Our flight article includes all the interconnections necessary for a fully populated array; continuity and power output can be checked before and after deployment tests on the ground and in space.

2.2 PERFORMANCE REQUIREMENTS

The ITSAT performance requirements and goals are presented in Table 1. These requirements and goals are derived from the Phase II Statement of Work and an ARPA and Phillips Laboratory approved ITSAT requirements document (Ref. 1). The system requirements are identified with an [R] and the goals are identified with a [G]. Also given in this table is the "protoflight" and the "production flight design". The lighter weight production flight design uses information gained from building the protoflight unit fabrication and testing. Several simple modifications to the structure are planned to raise the power density. These are (1) incorporate lightening holes into the housing and lid; (2) use 2.5-in diameter tubes (instead of the current 4 in tubes); (3) use thinner padding for the packaged array; and (4) redesign the tube end caps to mount outside the housing and lid.

These modifications are simple extrapolations of the current hardware and are considered low risk with only minor structural verification testing required.

2.3 LAUNCH VEHICLES

The ITSAT is designed to fit into any of four launchers: Delta II, Titan II, Pegasus and Taurus SSLV. The Pegasus gives the tightest packaging requirement, with a maximum diameter of 46 in. The payload envelope is shown in Figure 5.

The packaged canister has been designed to the worst-case vibration, pyroshock, and thermal environments of the four launch vehicles. The available environmental data on these boost vehicles are given in Figures 6-8.

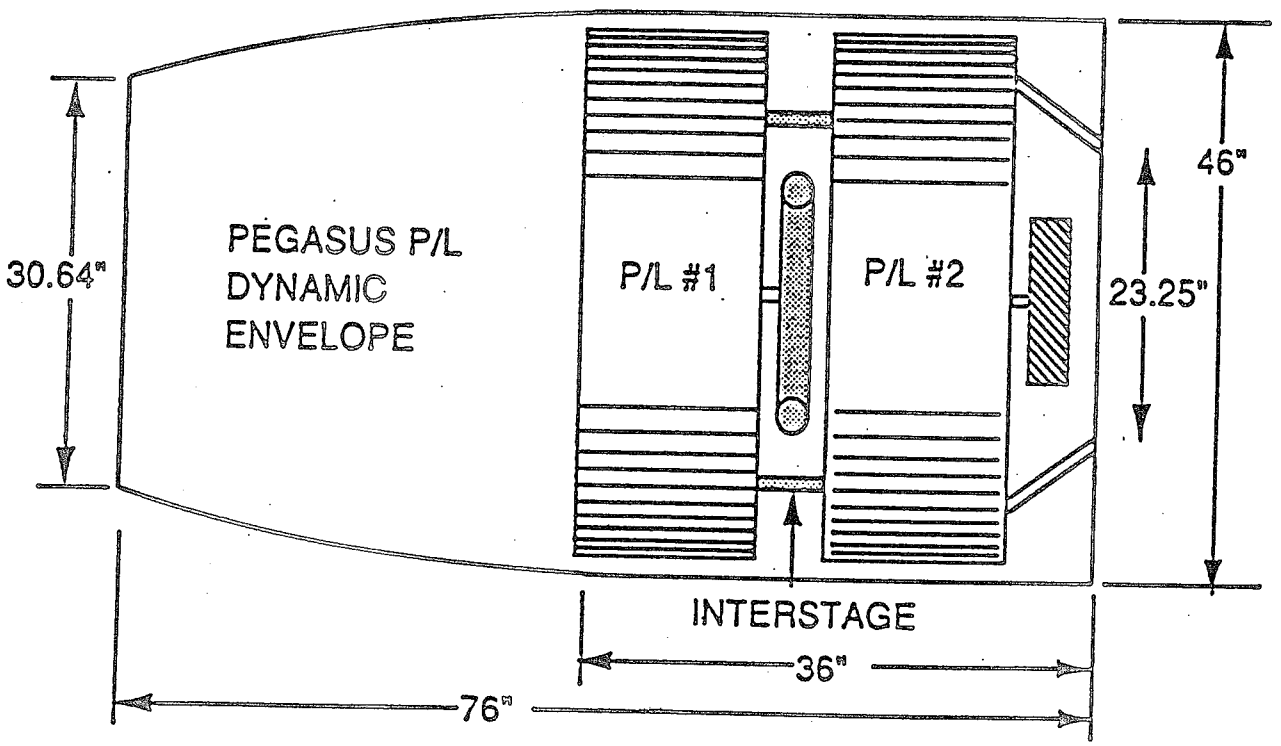

Figure 5. Pegasus payload envelope.

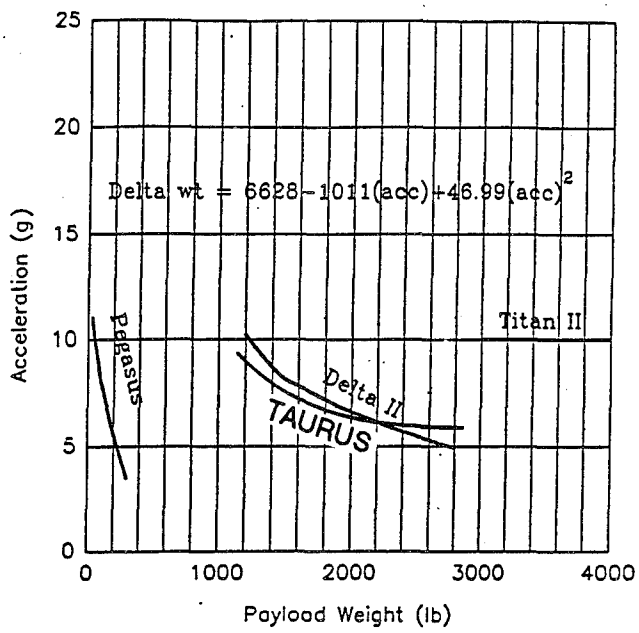

Figure 6. Payload acceleration design environment.

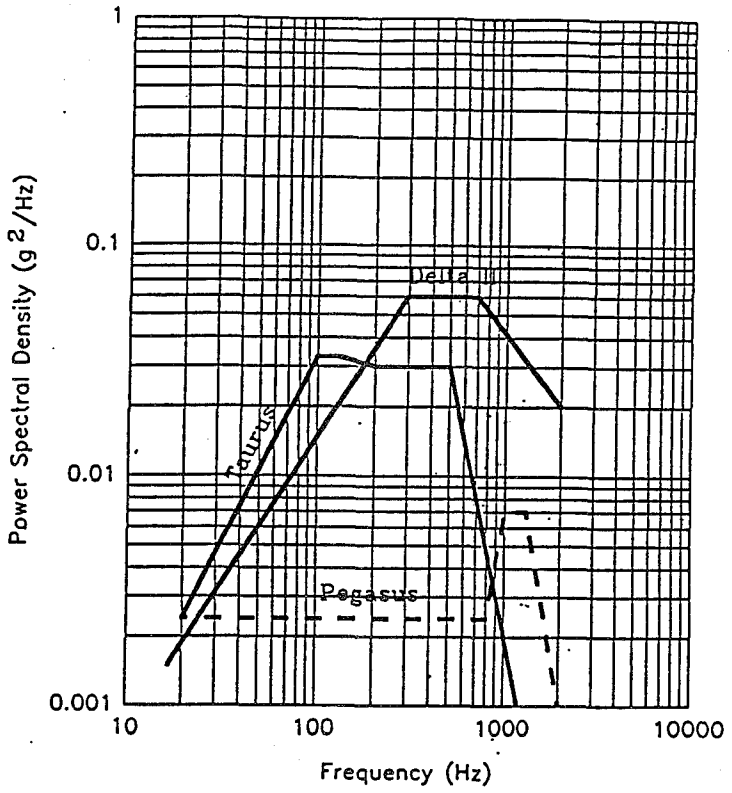

Figure 7. Random vibration design environment.

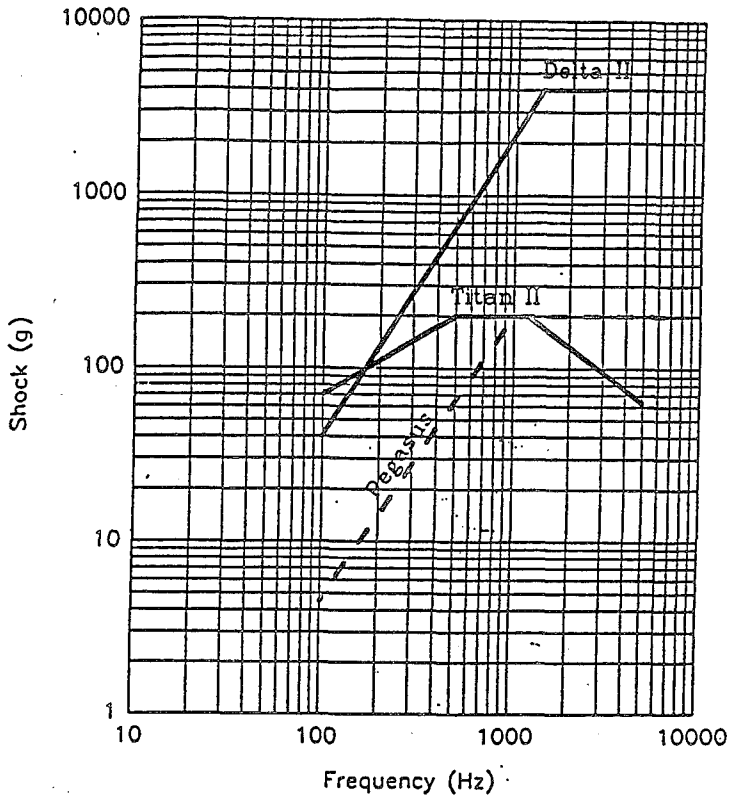

Figure 8. Payload shock design environment.

3.0 DESIGN/ANALYSIS

As power density of the ITSAT was the main driver of this program, a significant effort was spent optimizing the design to reduce weight. All parts were analyzed in detail to extract any unnecessary weight. This section is an update to an earlier report "ITSAT Design Calculations" (Ref. 2) reflecting the final design.

First, the data for the ITSAT as a system are given (mass properties and a thermal analysis). The subsequent section covers the structure; i.e., tubes, housing, lid, and inflation system. This includes everything but the solar blanket. Subsection 3.3 discusses the solar blanket.

3.1 SYSTEM

The following two subsections present the design calculations performed on the ITSAT as a system. The first gives the mass breakdown and the calculation of power density; the second describes a thermal analysis that was performed on the ITSAT as a packaged assembly.

3.1.1 Mass Properties

A detailed breakdown of the mass for the 200-W ITSAT protoflight unit is given in Table 4. This is an output from L'Garde's solar array optimization code, which estimates performance and mass properties for arrays of varying sizes. Shown in Figure 9 is a graphical breakdown by percentage of the solar array masses. The following points should be noted:

- These component masses are for the actual (protoflight) unit tested during Phase II, except that the mass of the blanket is based on a full population of 2.2-mil cells.

- Several improvements can be made (as given in Subsection 5.3) based on information gained from ITSAT Phase II.

Table 4. Mass breakdown for protoflight unit.

COMPONENT	MASS (lb)	MASS (kg)
TUBES AND CAPS		
Tubes	2.062	0.936
Bladders	0.136	0.062
Tube Clamp Rings	0.104	0.047
Tube End Caps	0.291	0.132
Subtotal	2.592	1.177
ENCLOSURE		
Housing	1.220	0.554
Lid	0.628	0.285
Cable Cutters	0.125	0.057
Holddown Cables	0.012	0.005
Subtotal	1.985	0.901
INFLATION SYSTEM		
Puncture Cutter (for tank)	0.154	0.070
Pyro Valve Manifold	0.262	0.119
Diaphram	0.022	0.010
Inflatant Tank	1.154	0.524
Vent Piston	0.002	0.001
Fill Valve	0.019	0.009
Tubing	0.035	0.016
Inflatant	0.221	0.100
Gas generator initiator	0.000	0.000
Subtotal	1.869	0.849

COMPONENT	MASS (lb)	MASS (kg)
MISCELLANEOUS		
Interleaving foam pads	0.340	0.154
End Pads	0.075	0.034
Drive system	0	0.000
Miscellaneous	0.905	0.411
Subtotal	1.320	0.599
SOLAR BLANKET		
Blanket Mass	2.418	1.098
Total Non-Blanket Mass	7.766	3.526
TOTAL MASS	10.184	4.624
Structure % of Mass	76 %	

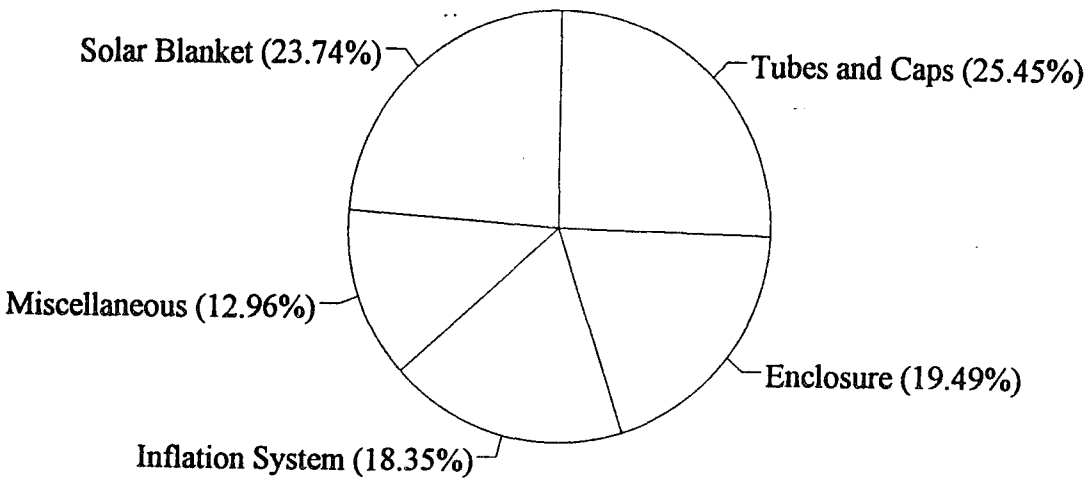

Figure 9. Mass breakdown, protoflight unit.

3.1.1.1 Power Density. By dividing the Beginning of Life (BOL) power output of the array (given in Subsection 3.3.11) by the system mass, the power density of the array was obtained in Watts per kilogram. This is given in Subsection 5.1.

3.1.1.2 Moment of Inertia. The moment of inertia about the x-axis of the array (parallel to the tube axes) is 1670 lb-in^2. This array must rotate about this axis when pointing toward the sun.

3.1.2 Thermal Analysis of Packaged Housing

This subsection presents the results of the thermal analysis of the packaged ITSAT. A complete description of the analysis may be found in Reference 3. A first-order thermal analysis of the ITSAT was performed to predict the approximate temperature of the structure during and after deployment. This was done for a number of reasons:

- To predict the rigidizing pressure of the tubes (directly dependent on temperature - ideal gas properties were assumed for this analysis).

- To find the temperature difference between the sunlit and dark sides of the tube (this determines the "bow" in the tube).

- To find the efficiency of the solar cells which is temperature dependent

The ITSAT enclosure was analyzed using the heat transfer analysis package of the NISA® Finite Element Model Program (Ref. 4). Figures 10 and 11 depict the geometry assumed for the canister. The model developed was one dimensional and incorporated data from various sources. *, **

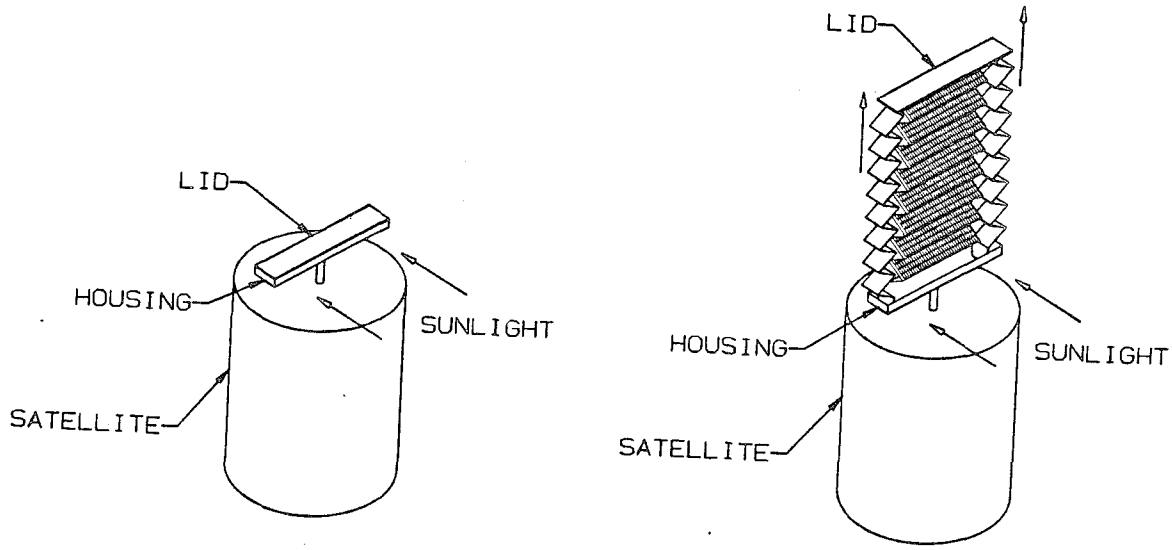

Figure 10. Geometry for canister thermal model.

Table 5 presents the constants and the material properties used for the thermal analysis of the ITSAT canister. Two separate cases were run for configurations with and without multilayer insulation (MLI). Figures 12 and 13 give the initial variation of the canister temperature with time as the canister travels in and out of eclipse. Eventually, the

*Telecon T011193A, "Satellite Temperatures," Geoff Williams to Tricia Tiernan and Larry Crawford, January 11, 1993.

**Telecon, "Satellite Temperatures," Geoff Williams to Dave Gilmore, Aerospace Corporation, February 1, 1993.

temperature of the canister reaches a steady state. Figures 14 and 15 show the steady-state oscillation for cases with and without MLI. The steady-state temperatures were fed in as initial conditions to the tube thermal model of Subsection 3.2.1.

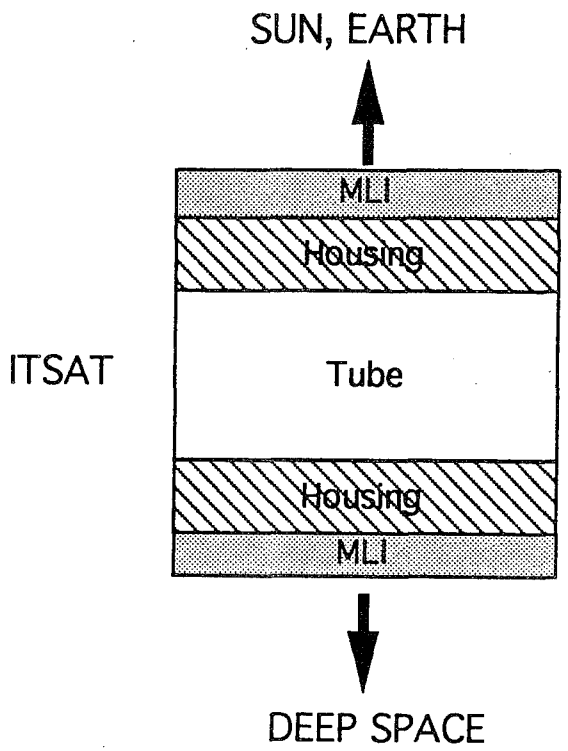

Figure 11. Canister thermal model.

Table 5. Constants and materials properties for canister thermal analysis.

MATERIAL	DENSITY (kg/m^3)	CONDUCTIVITY (W/m.K)	SPECIFIC HEAT (J/kg/K)	THICKNESS (m)
Multilayer Insulation	185.2	0.0014	1090	0.00178
Tube	852.8	67.5	950	0.15951
Housing	1633.1	45.0	600	0.000508[a]

[a] Thickness of Honeycomb Ignored
Emissivity, MLI = 0.05
Emissivity, Housing = 0.95
Absorptivity, MLI = 0.15
Absorptivity, Housing = 0.96

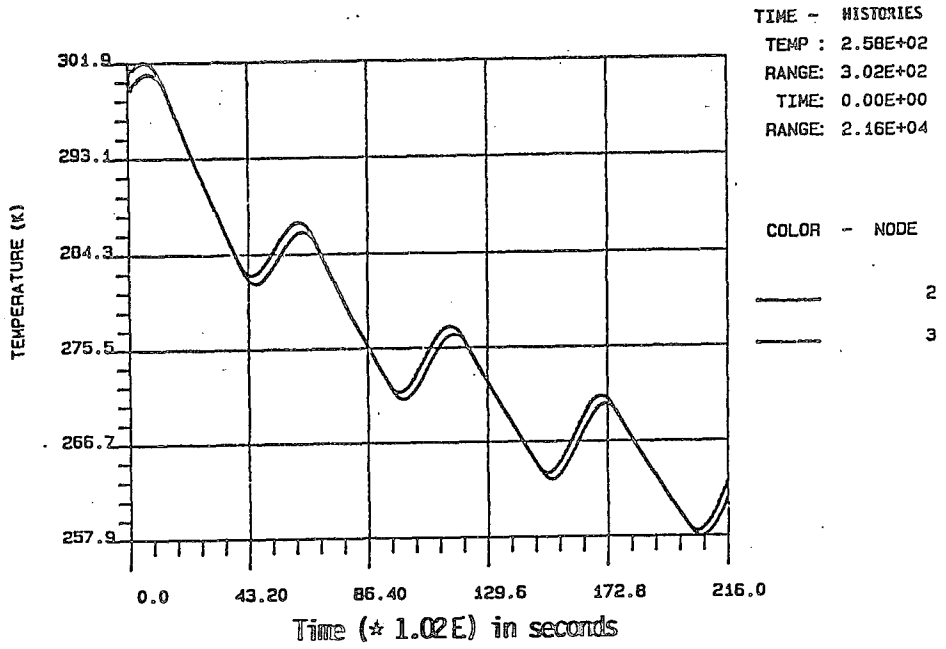

Figure 12. Canister temperature, without MLI.

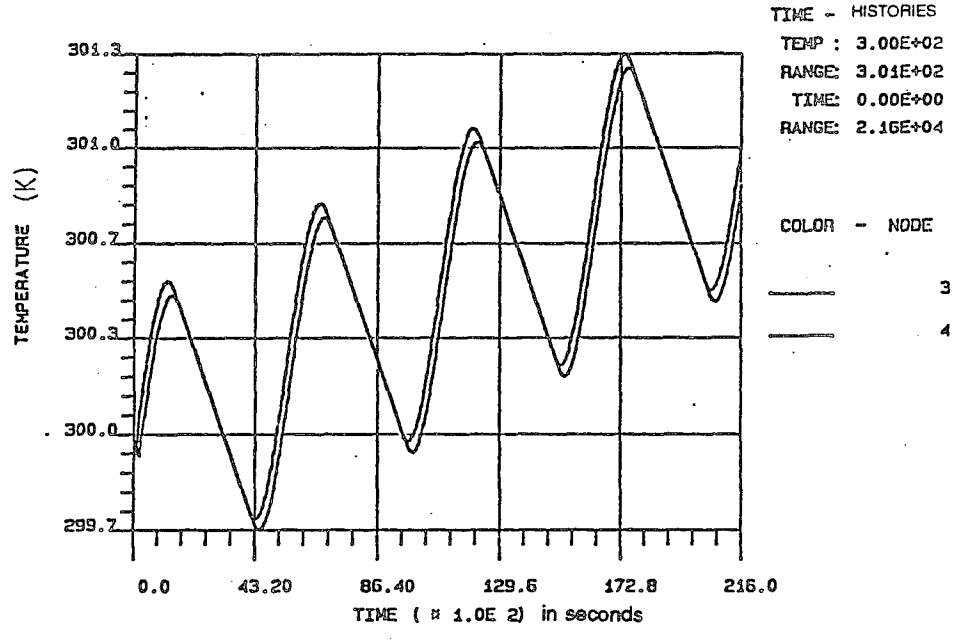

Figure 13. Canister temperature, with MLI.

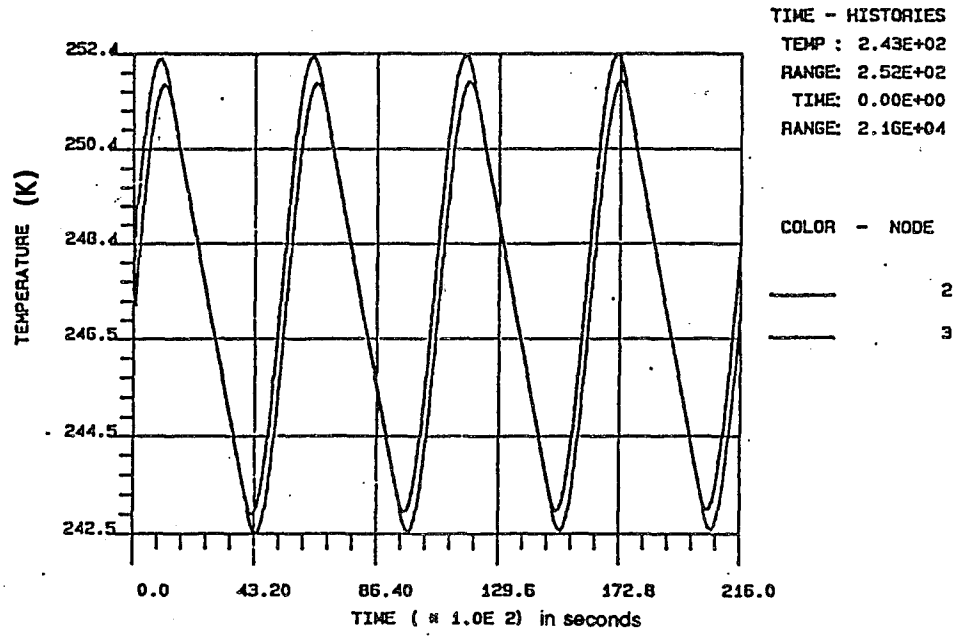

Figure 14. Canister quasi-steady-state temperature, without MLI.

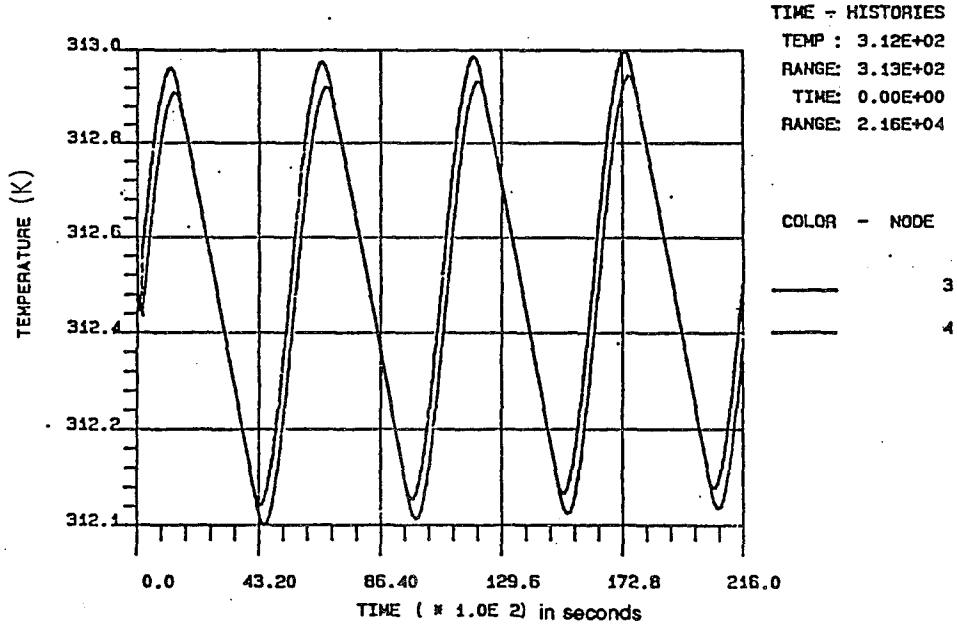

Figure 15. Canister quasi-steady-state temperature, with MLI.

From the analysis conducted for the enclosure, it was determined that MLI be included in the ITSAT design. The MLI should completely cover the ITSAT housing to provide excellent thermal control of the ITSAT. In this way, effects of sunlight and eclipse can be minimized. The MLI was used during the qualification testing at NRL (Subsection 4.7.2).

3.2 STRUCTURE

The structure refers to all the elements used to support the solar blanket when attached to the satellite. This consists of the following components: (1) tubes (on either side of the blanket); (2) inflation system (for inflating the tubes); and (3) enclosure, which is used not only for packaging the array, but also as two of the four sides of the supporting rectangle when deployed. Each of these is discussed in more detail.

3.2.1 Tubes

(P) The tubes are a monocoque cylinder design made from a three-layer laminate. The laminate is aluminum foil sandwiched between two layers of thin plastic. The plastic film is used to hold the pressure when inflating by increasing the tear resistance; otherwise the soft foldable aluminum would tear very easily, allowing large leak paths. Numerous laminate combinations were fabricated and tested in Phase I, including three different alloys of aluminum (5052-O, 1145-O, and 3003-O), and several varieties of reinforced and nonreinforced plastic. During Phase II, differences between reinforced and nonreinforced plastic films were reexamined more closely. Of particular concern is that all materials be space-qualified against the moderately harsh environment of AO and other factors (i.e., low outgassing, brittleness, etc.).

(P) The optimum laminate selection for this application is 3-mil aluminum between two layers of reinforced 1/2 mil Kapton® (Fig. 16). The reinforcement in the Kapton® is made of nylon yarn. The adhesive selected for making the seams is silicon-based and space-qualified and was chosen for its previous space environment qualification. The coating selected for the Kapton® is Indium-Tin-Oxide (ITO), selected not only for its AO resistance, but also for a surface conductivity which is sufficient to prevent static charge buildup. If minor cracks occur

in the coating, they are of minimal concern since the booms are not intended to hold pressure for the duration of the mission; the AO protection is there rather to prevent large chips from peeling and landing on top of active solar cells or other spacecraft components.

The following subsection describes the matrix of materials tested and the space environment that L'Garde considered when selecting the final laminate.

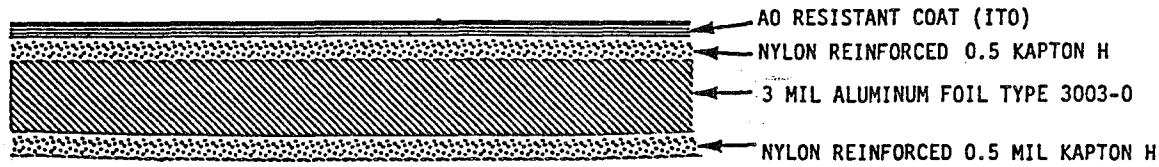

Figure 16. (P) Laminate cross-section.

3.2.1.1 Laminate Requirements. The laminate material must be designed to meet the following criteria:

- Flexible and foldable (capable of becoming an inflatable membrane)
- Rigidizable (after unfolding) by inflation pressure
- Strength - Rigidized 4 in tubes should withstand 12 (0 margin) lb total compressive force
- Minimum practical weight and volume (less than 15 oz/sq yard and 20 mil thick)
- Stand up to space hazards (AO, UV, radiation, etc.)

- Meet NASA standard SP-R-0022A for outgassing

- Can be manufactured in large quantities and pieces

The dominant hazards at the 600-800 km orbit are AO and ionizing radiation. Each of these is discussed further in this section.

The first objective is to estimate the fluence of the particles, then determine the damage to the Kapton® film. The AO will degrade the Kapton® on the tubes.

The fluence is not a constant value, rather it varies according to the solar flare cycle. Table 6 shows the fluence and surface recession of bare Kapton® as a function of duration. For example, if the ITSAT is flown at 600 km on a 3-year mission occurring from 1996-1999, this is a period of low solar activity, making the bare Kapton® only recede by 0.08 mil. However, during a period of high solar activity, the Kapton® will recede by 2.08 mil, which is greater than the 0.5-mil thickness of the material used on the tubes and also greater than the 2-mil solar blanket substrate. These data are given graphically in Figure 17. Note that lowering the altitude greatly increases the damage to the Kapton®.

Table 6. Atomic oxygen fluence predictions.

MISSION DURATION	ORBITAL ALTITUDE, km	SOLAR CONDITIONS	AO FLUENCE[a] ATOMS/cm^2	KAPTON® SURFACE[b] RECESSION, cm (mil)
1996 - 1999	600	Low Activity	6.42×10^{19}	1.92×10^{-4} (0.08)
1997 - 2000	600	Nominal Activity	4.03×10^{20}	1.22×10^{-3} (.48)
1999 - 2002	600	High Activity	1.77×10^{21}	5.31×10^{-3} (2.09)
1996 - 1999	800	Low Activity	1.93×10^{18}	4.91×10^{-6} (2.28×10^{-3})
1997 - 2000	800	Nominal Activity	3.10×10^{19}	9.26×10^{-5} (0.035)
1999 - 2002	800	High Activity	1.78×10^{20}	5.34×10^{-4} (0.21)

[a] Based on NASA/JSC Computational Model (J. Visentine) - 3 years Fluence

[b] Calculated based on Re = 3.0×10^{-24} cm^3/atom for Kapton® and Predicted Fluences by NASA/JSC

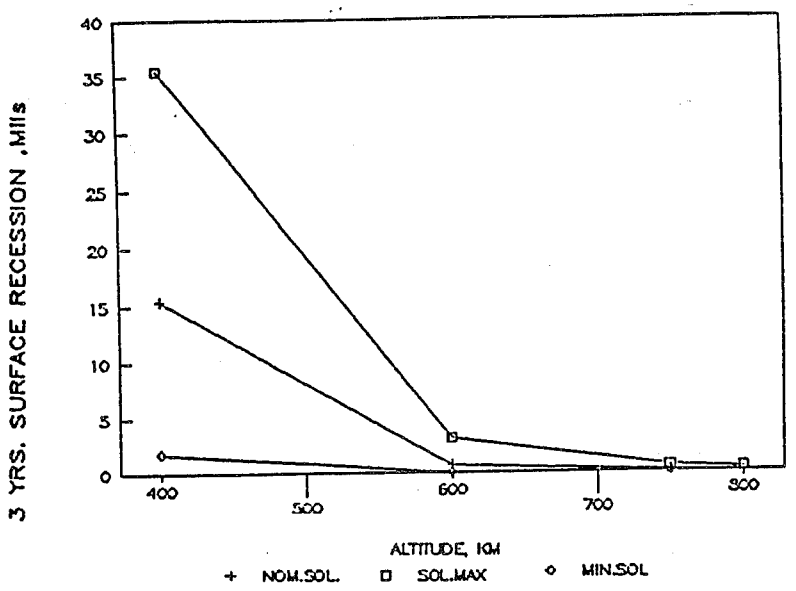

Figure 17. Damage to Kapton® by AO - RAM exposure.

These calculations are for the uncoated (bare) Kapton®. The inclusion of the ITO coating on the tubes increases its durability as detailed later in this subsection.

Table 7 gives the annual fluence level of charged particle radiation for both extremes (0 and 90 deg inclination) and 50-60 deg where fluence level is highest at both orbits (Ref. 5). The last column in Table 7 gives the calculated radiation dosage at 1-mil depth of Kapton film for a 3-year period. Figure 18 shows the effect of Kapton film thickness on estimated absorbed radiation dose for 0 and 90 deg orbit. Under worst radiation conditions (i.e., 800-km altitude and 50-60 deg inclination) the Kapton carrier will be subjected to 1.59×10^{10} rad. Kapton retains 80-100 percent of its tensile strength at 5×10^{9} rad (Ref. 6). Under worst conditions Kapton still retains about 50 percent of its tensile strength after a 3-year exposure to the ionizing radiation and should still have adequate mechanical properties. The Kapton layer acts as a partial radiation shield as well. As the particles strike the film, the dose decreases as shown in Figure 18.

Table 7. Fluence level for charged particle radiation - 3-year surface dosage. (Annual equivalent 1 MeV electron fluence from trapped electrons and protons)

ALTITUDE (km	INCLINATION (deg)	ELECTRONS	PROTONS	ELECTRONS + PROTONS	3 YEAR DOSAGE x1/R, (rad)
800	0	4.40E+09	9.50E+10	9.94E+10	1.32E+06
800	50-60	8.03E+11	1.19E+15	1.19E+15	1.59E+10
800	90	7.20E+11	7.40E+14	7.41E+14	9.87E+09
600	0	1.10E+08	1.04E+02	1.10E+08	1.47E+03
600	50-60	4.91E+11	4.60E+14	4.60E+14	6.13E+09
600	90	4.60E+11	2.40E+14	2.40E+14	3.20E+09

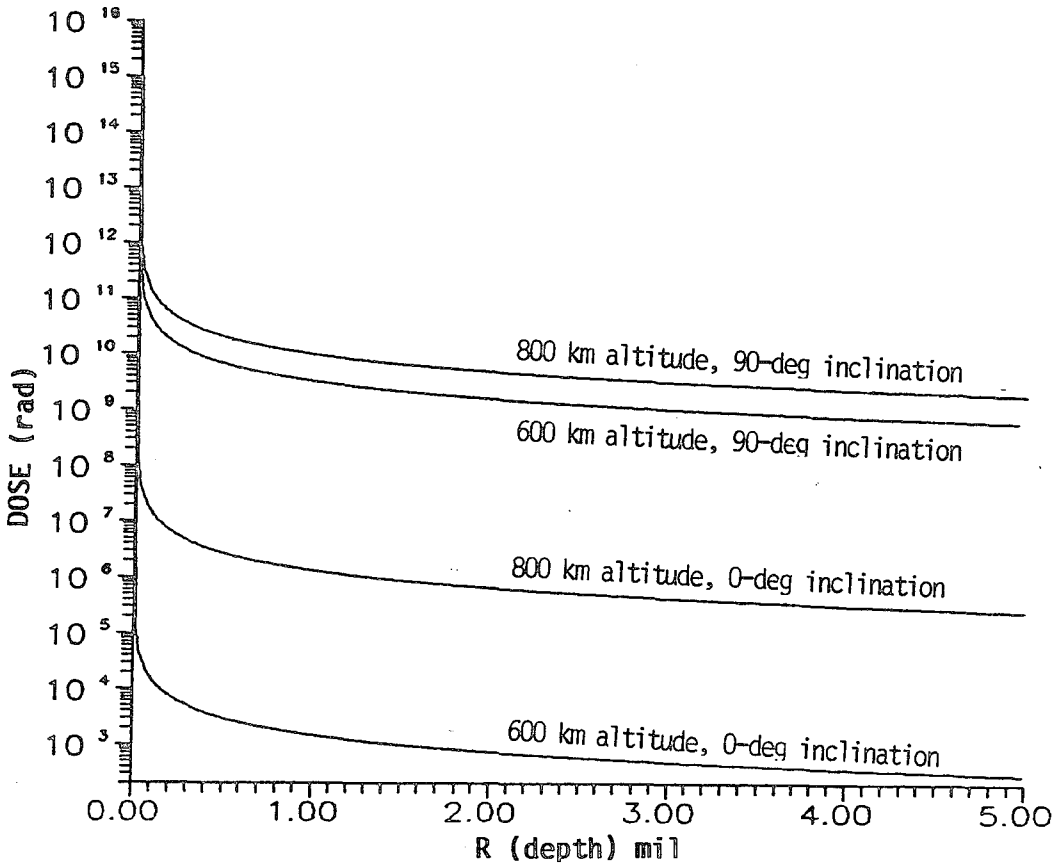

Figure 18. Estimated absorbed radiation doses for Kapton®.

After deployment and rigidization of torus, the plastic layer reinforcement is not critical to the performance of the torus. The main reason to protect this layer is to reduce the possibility of contamination of the solar array. Such contamination may occur by deposition of reaction products of AO with the plastic cover of the laminate.

As a result a coating is necessary for protection of the torus from AO. After an extensive selection process, ITO was specified for the ITSAT tubes due to the following reasons:

- ITO provides an effective barrier against AO. Figure 19* compares different inorganic coatings which are known to shield organic-based plastic films against AO in space environment. As is seen, application of ITO provides a considerable protection against AO in comparison where no coat is applied at all. Although SiO_2 and SiO_x provide more effective protection, ITO was preferred because of its other advantages described here:

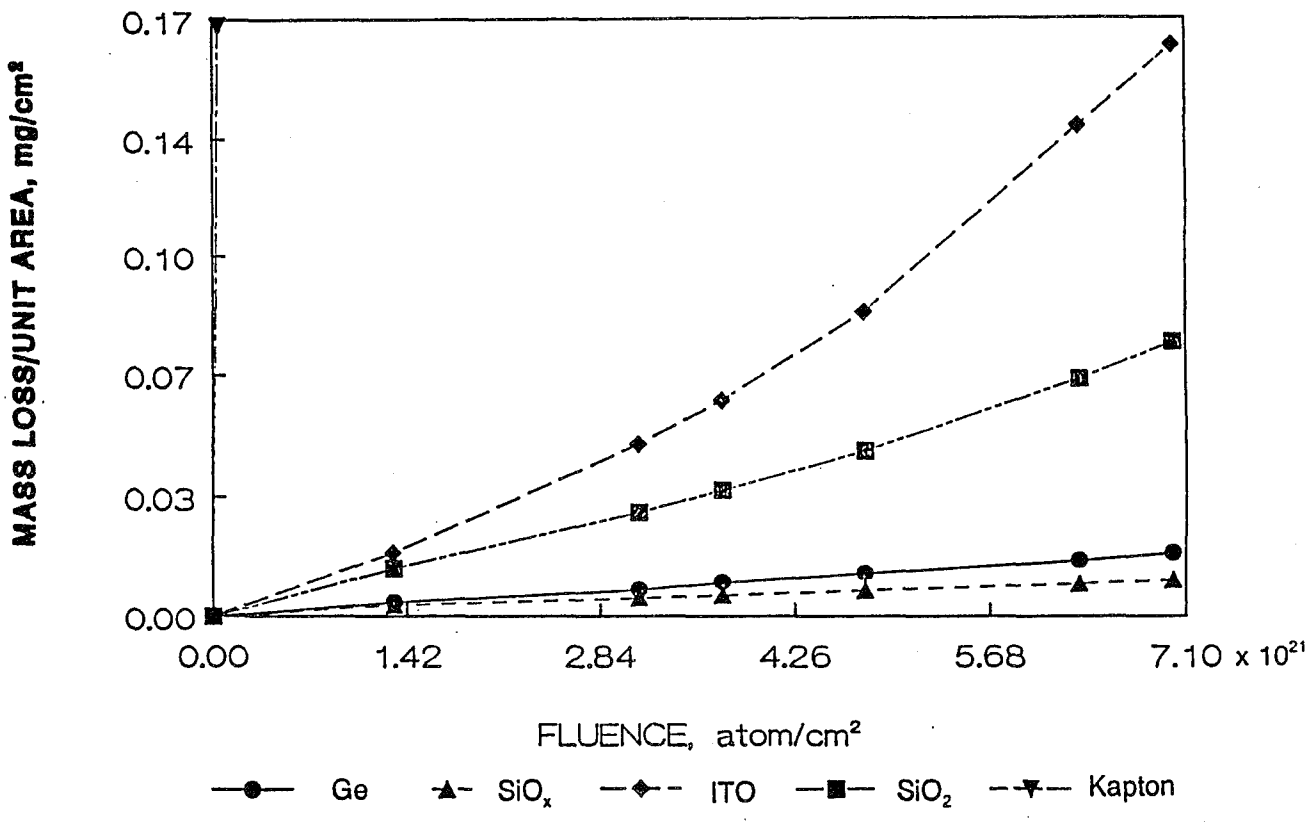

Figure 19. Comparison of different organic coatings.

*Private communication with Bruce Banks of NASA Lewis on 6/29/92.

- ITO provides surface conductivity against static charges. Figure 20 shows surface resistance of Kapton film coated with ITO under different AO fluences. Such a level of conductivity exhibited by ITO is a major advantage over other coats (i.e,. SiO_2 and SiO_x.

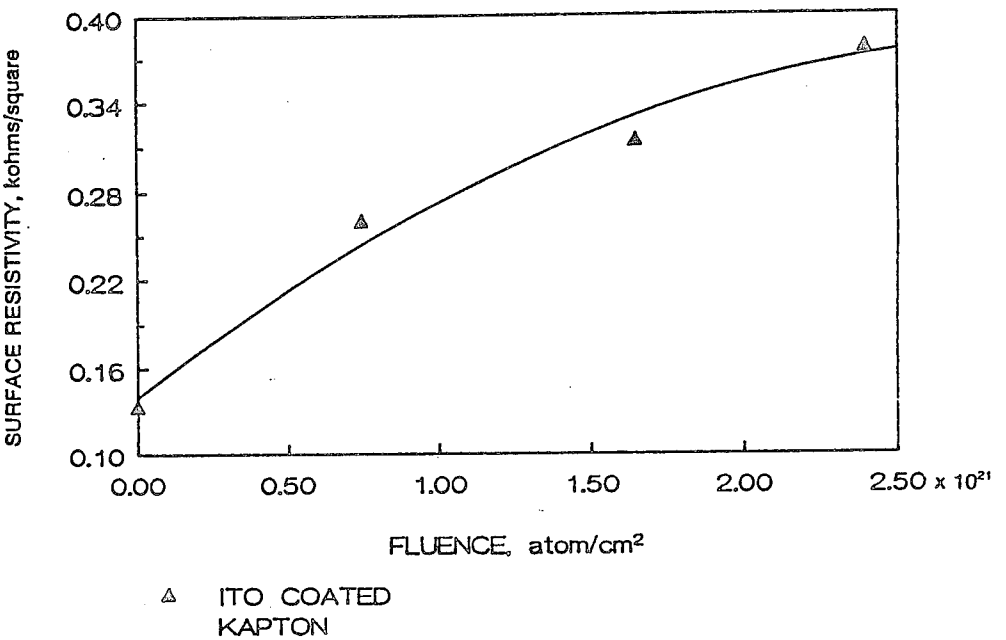

Figure 20. Surface resistance of Kapton® film.

- ITO is commercially available within reasonable cost

- Its performance was recently tested and verified by the Soviet MIR Spacestation (joint French/Soviet Program) - specimen supplied by American companies (Ref. 7). The ITO has been widely investigated, approved, and used by NASA for space applications.

In summary, the exact recession of the Kapton film due to AO is difficult to predict with the ITO coating. While Figure 19 shows a relative decrease in mass loss by inclusion of the ITO, the effect of cracks in the coatings due to tube folding cannot be estimated at this time. All that can be said is that the ITO coating decreases the surface recession, and is the best available for this application at this time.

3.2.1.2 Strength Calculations. The ITSAT requirements call for a 0.03-g acceleration in any direction. The assumption used was that the satellite would be accelerated in two directions simultaneously to create the worst loading (Fig. 21). The loads on the tubes have been determined using this information.

Acceleration α_1 causes a straight compressive load in each tube due to the outboard mass of

1. 1/2 of lid
2. 1/2 of blanket
3. one tube's end cap
4. one tube's clamp ring
5. one tube's mass
6. one tube's inflatant
7. one tube's bladder

For the ITSAT array design, these masses and their corresponding loads on each tube are given in Table 8.

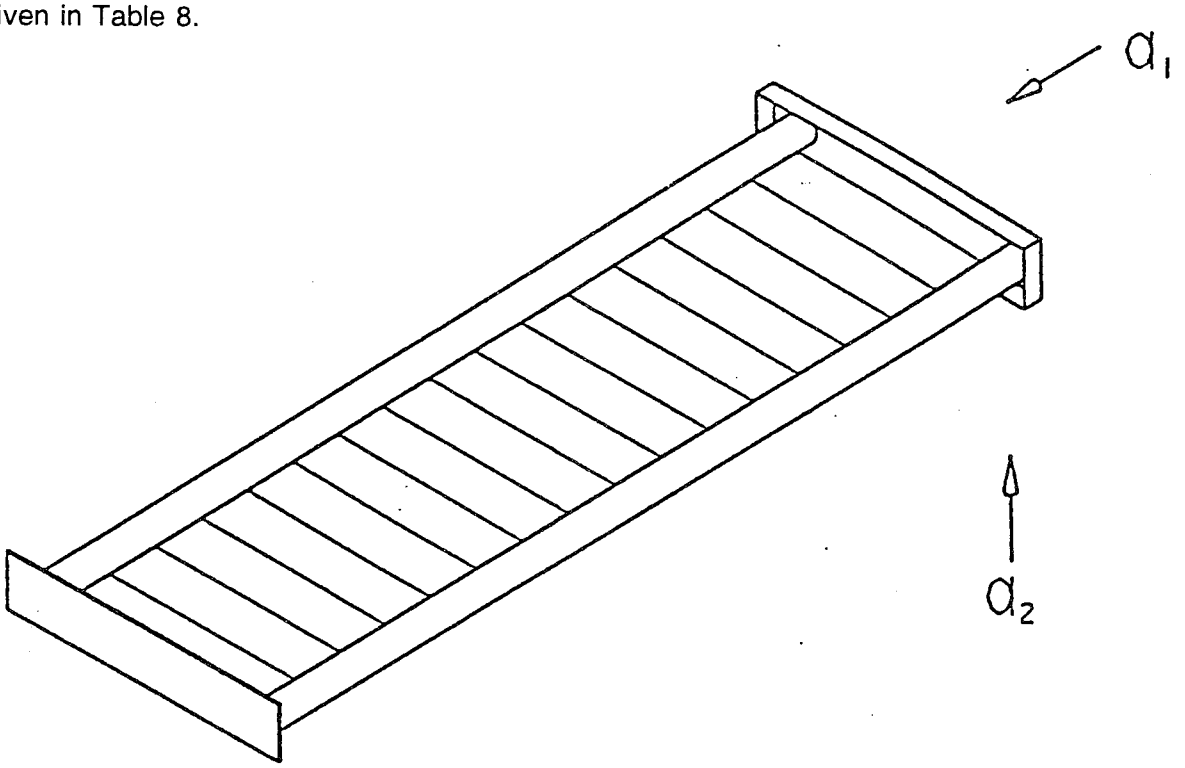

Figure 21. Acceleration loading on ITSAT.

Table 8. Compressive loads.

INERTIAL FORCES DUE TO:	MASS (lbm)	RESULTING COMPRESSIVE FORCE IN TUBE (lbf)
One Tube Mass	1.031	0.0309
One Tube's Bladder	0.068	0.0020
One Tube's Inflatant	0.100	0.0030
1/2 of Blanket	1.209	0.0363
1/2 of Lid	0.314	0.0094
One Tube's Clamp Ring	0.026	0.0008
One Tube's End Cap	0.073	0.0022
TOTAL	2.821	0.085

In addition to the inertial loads, the tensioned solar blanket creates a load in the tubes of 2.60 lb or 1.30 per side. Therefore, the total load in each tube is 0.085 lbf + 1.30 = 1.38 lb. The compressive stress in each tube is the load on each divided by the cross-sectional area of the tube.

$$\sigma_c = \frac{C_\ell}{2\pi rt} = \frac{1.38}{2\pi(2.00)(0.003)} = 36.7 \text{ psi} \quad (1)$$

The maximum bending moment in each tube occurs at the housing end and is calculated by modeling the inertial forces due to the tubes, tube bladders, inflatant, blanket, and the harness as evenly distributed loads over the entire length of the tube, while the lid, tube end caps, and the clamp rings are modeled as concentrated loads at the end of the tube. The uniform distributed loads create a bending moment at the housing of

$$M = \frac{WL}{2} \quad (2)$$

The point loads create a bending moment at the housing of

$$M = WL \quad (3)$$

A summary is given in Table 9.

Table 9. Bending loads.

BENDING MOMENT DUE TO:	MASS (lbm)	LOADING TYPE	RESULTING MOMENT IN-TUBE (in-lbf)
One Tube Mass	1.031	Distributed	2.161
One Tube's Bladder, etc.	0.068	Distributed	0.142
One Tube's Inflatant	0.100	Distributed	0.211
1/2 of Blanket	1.209	Distributed	2.534
1/2 of Lid	0.314	Point	1.316
One Tube's Clamp Ring	0.026	Point	0.109
One Tube's End Cap	0.073	Point	0.305
TOTAL	2.821		6.777

The maximum bending stress is given by

$$\sigma = \frac{Mc}{I} \tag{4}$$

where

$I = \pi t r^3$

c = radius of the tube

then

$$\sigma = \frac{(6.777)(2.00)}{\pi(0.003)(2.00)^3} = 180 \text{ psi} \tag{5}$$

The axial stress and the maximum bending stress are added together to get the maximum stress in the tube. This should not exceed the yield stress of the aluminum.

$$\sigma_{max} = 36.7 + 180 = 217 \text{ psi} \tag{6}$$

For 3003 - 0 aluminum, the yield stress is 6000 psi. Therefore, the factor of safety in this mode is 27.6 psi.

The calculation of critical buckling loads on extremely thin-walled tubes has been investigated by the aerospace industry for quite some time. In particular, this study can draw from test data from three different sources:

- General Dynamics (GD), long column buckling (Ref. 8).
- McDonnell Douglas (MDAC), long column buckling (Ref. 9).
- National Aeronautics and Space Administration (NASA), local buckling (Ref. 10).

Long column buckling causes the entire boom to bend and permanently distort when its length exceeds a critical dimension. This is a macroscopic effect. The data from References 8 and 9 are examples of these, since the tube length is taken into account.

Local buckling occurs at a smaller level, as the thin-walled tube buckles in a sinusoidal waveform similar to flat plate buckling. Data from Reference 10 are examples of this. The length of the cylinder is not taken into account here since the effect is local to the material.

The reasons for comparing all three sources stem mainly from the fact that they are all based on rather limited test data. Large portions of the curves or ranges are extrapolated from just a few data points and a small representation of materials. The method used for this calculation is to compare all three references and use the worst case. Thus, the ITSAT tubes were designed with a high degree of confidence and subsequently tested to validate the approach.

The design of thin cylinders by GD is based on two design curves from Reference 8, given here as Figure 22 (for axial compression) and Figure 23 (for bending). Both these design curves are for unpressurized cylinders, germane to this study since our tubes are a rigidizing design, requiring no permanent inflation pressure.

Test data from MDAC are given in the form of equations rather than curves. Here, the critical axial load is given by

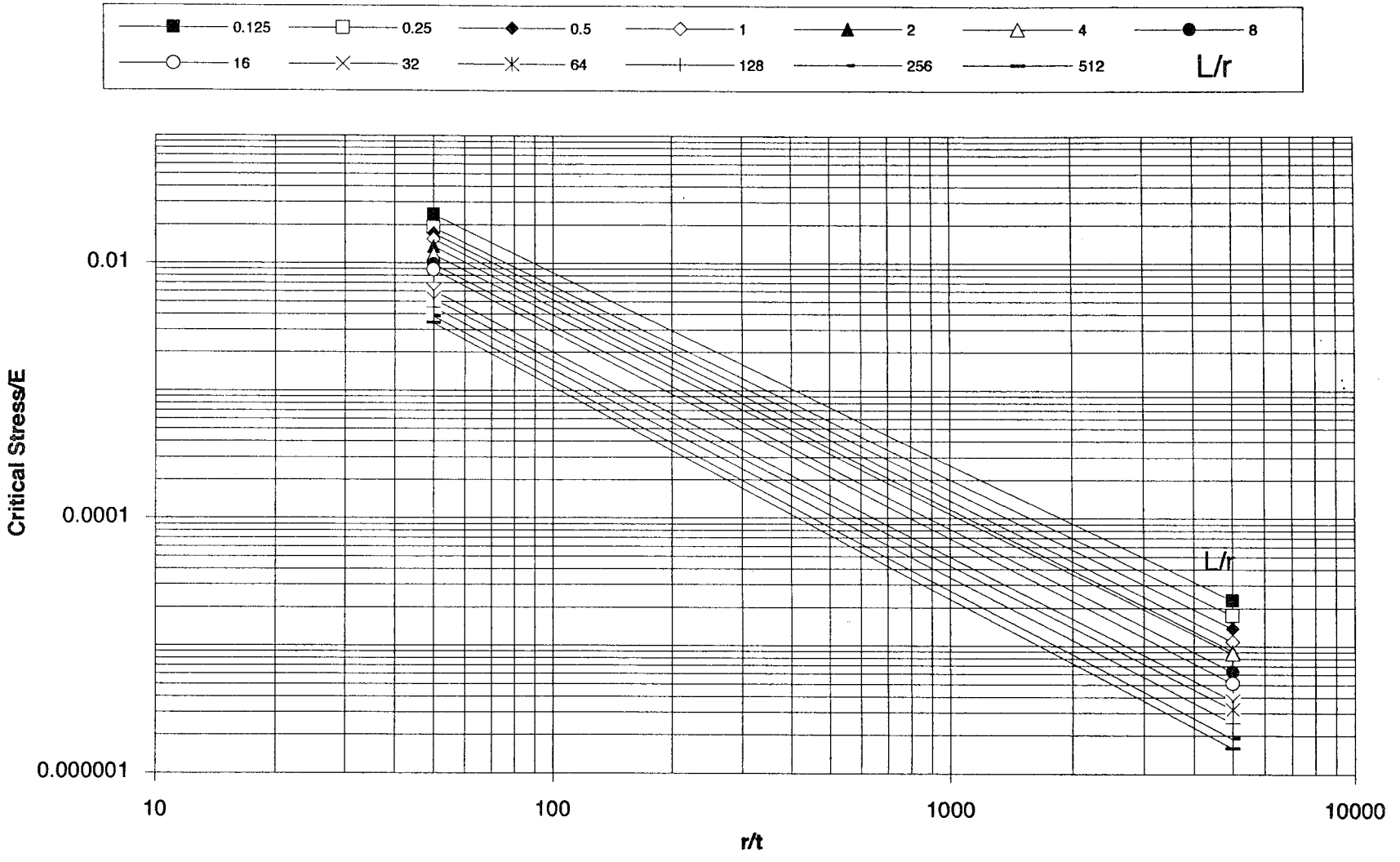

Figure 22. Unpressurized, unstiffened, circular cylinders in axial compression (clamped ends).

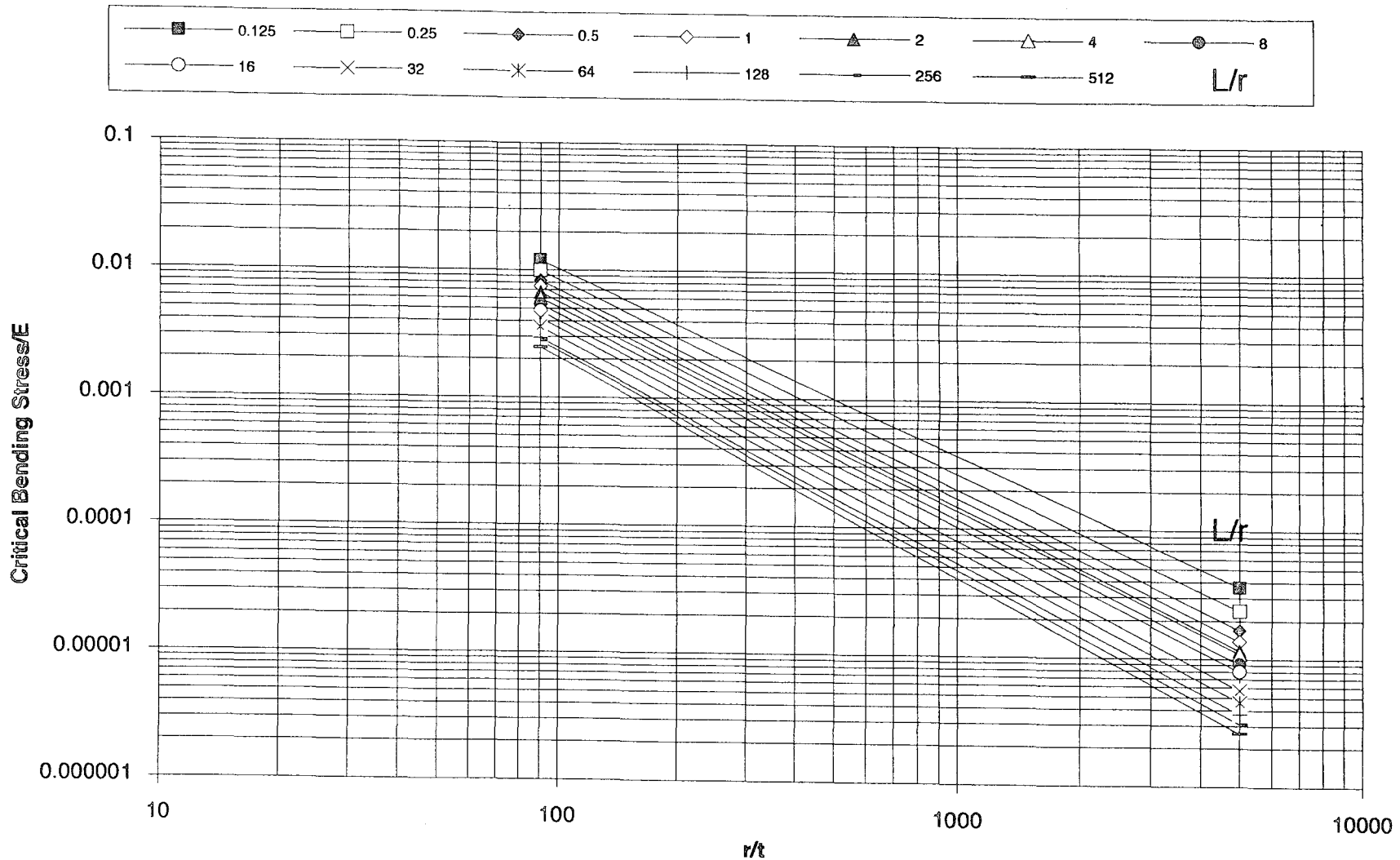

Figure 23. Unpressurized, unstiffened, circular cylinders in bending.

$$P = \frac{0.9038\ Et^3}{L^2}\ (2\pi r\ K_c) \tag{7}$$

where

$$K_c = 1.1605\ C_c\ Z_L \qquad (K_c \text{ must be } \geq 2.5) \tag{8}$$

$$C_c = 0.9048 - 0.1107\ \ell n\ \frac{r}{t} \qquad (C_c \text{ must be } \leq 0.605) \tag{9}$$

$$Z_L = \frac{0.95342\ L^2}{tr} \tag{10}$$

r, L, E, and t are the same as given in Figure 22.

The following equations for critical buckling load come from NASA (Ref. 10). For loading in axial compression, the critical stress is given by

$$\sigma_c,\ crit = \frac{\gamma_1 E}{\sqrt{3(1 - \mu^2)}}\ \frac{t}{r} \quad \text{for} \quad \frac{r}{t} < 1500 \tag{11}$$

where

μ = Poisson's ratio

γ_1 = correction factor given by

$$\gamma_1 = 1 - 0.901(1 - e^{\phi}) \tag{12}$$

(r, t, and E are again the same as in Figure 22).

with

$$\phi = \frac{1}{16}\ \sqrt{\frac{r}{t}} \tag{13}$$

Note that the allowable stress is increased proportionally with increasing t and with decreasing r: i.e., if the radius is increased, the allowable stress decreases. Thus for a flat sheet ($r = \infty$), $\sigma_{crit} = 0$ which makes sense since the plate has very little rigidity to out-of-plane bending and buckles easily. There is a limit to decreasing the radius of the cylinder since the stress will increase to a point equal to the yield stress of the aluminum laminate.

For loading in pure bending, the critical stress to resist buckling is given by

$$\sigma_{b,\,crit} = \frac{\gamma_2 E}{\sqrt{3(1-\mu^2)}} \frac{t}{r} \tag{14}$$

where γ_2 is the correction factor given for bending as

$$\gamma_2 = 1 - 0.731\,(1 - e^{-\phi}) \tag{15}$$

and ϕ is given by Equation 13.

Since the tubes will be subjected to both compression and bending, the combination of both must be considered. The stresses are not simply additive, but rather depend on the interaction equation

$$R_c + R_b = 1 \tag{16}$$

where R_c and R_b are the compressive and bending load ratios, respectively:

$$R_c = \frac{\sigma_c}{\sigma_{c,\,crit}} \tag{17}$$

$$R_b = \frac{\sigma_b}{\sigma_{b,\,crit}} \tag{18}$$

(i.e., local buckling occurs when the sum of R_c and R_b is equal to one)

The above analysis is used to determine the end load at failure and can be compared to test data. "End Load" refers to a load applied perpendicular to the tube axis at the end of a cantilever mounted tube. The data given in Table 10 are input into a parametric study to determine the failure point as a function of tube diameter. The results are given in Figure 24. The four failure theories (three buckling and one yield) are compared to the test point from Reference 11. In this case a full length tube (139.73 in) was folded, inflated to various pressures, and vented to 0 psi. At this point the bending strength was measured. For a 17-psi inflation pressure (the lowest expected pressure during flight), the end load at failure was 0.59 lb. Note that the tube performed much better than predicted by any of the buckling theories. This could be due to (1) the stiffening effect of the Kapton® layers and (2) the conservative approach of the NASA, MDAC, and GD engineers.

Table 10. Data for tube strength predictions.

VARIABLE	SYMBOL	VALUE	UNITS
Tube Length	l	139.73	In
Aluminum Wall Thickness	t	0.003	In
Poisson's Ratio	μ	0.30	------
Elastic Modules	E	2.34×10^{6}[a]	psi
Yield Strength	δ_y	4300	psi

[a] Tested value of bare aluminum

Correction factors were applied to the buckling results to get updated results for use on future arrays. These are shown in Table 11. When these factors are applied, the end load at failure versus tube diameter now looks like Figure 25. These correction factors are based on the test after inflation at 17 psi. Testing of another full length tube rigidized at 22 psi was performed earlier in the program. It buckled at an end load of 0.75 lb. However, data from the 17-psi case were used since this is the pressure expected in flight.

Since it is not customary to use two data points to establish a statistical distribution, further testing should be performed at the expected rigidization pressure to increase the confidence in using these correction factors.

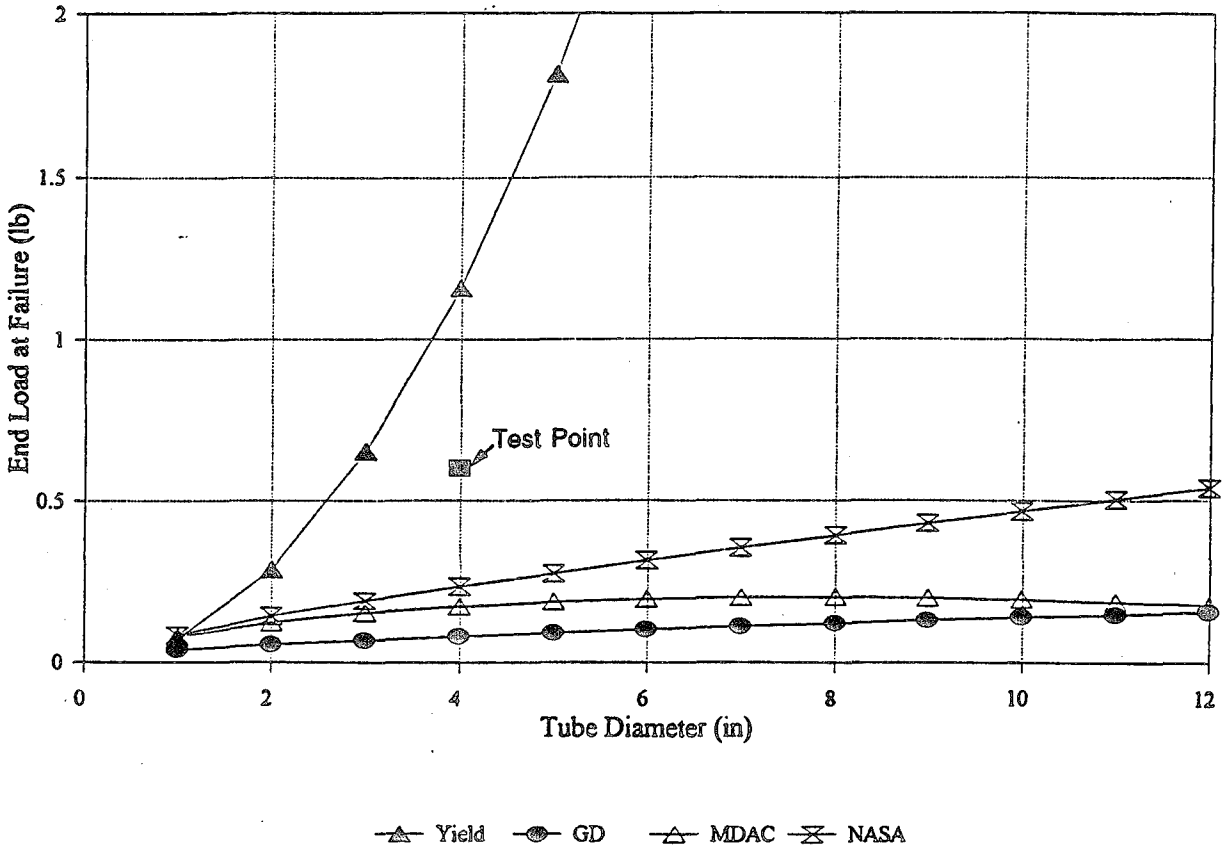

Figure 24. End load at failure versus tube diameter.

Table 11. Correction factors.

BUCKLING THEORY	USE CORRECTION FACTOR OF
General Dynamics	7.33
McDonnell Douglas	3.42
NASA	2.52

3.2.1.3 Thermal Analysis. When the tubes are packaged prior to deployment, they will be at near constant temperature due to the MLI on the enclosure (Subsection 3.1.2). However, as soon as the lid opens, the tubes will immediately radiate their heat to space and to the Earth. If deployment occurs in sunlight, one side will be heated by Earth.

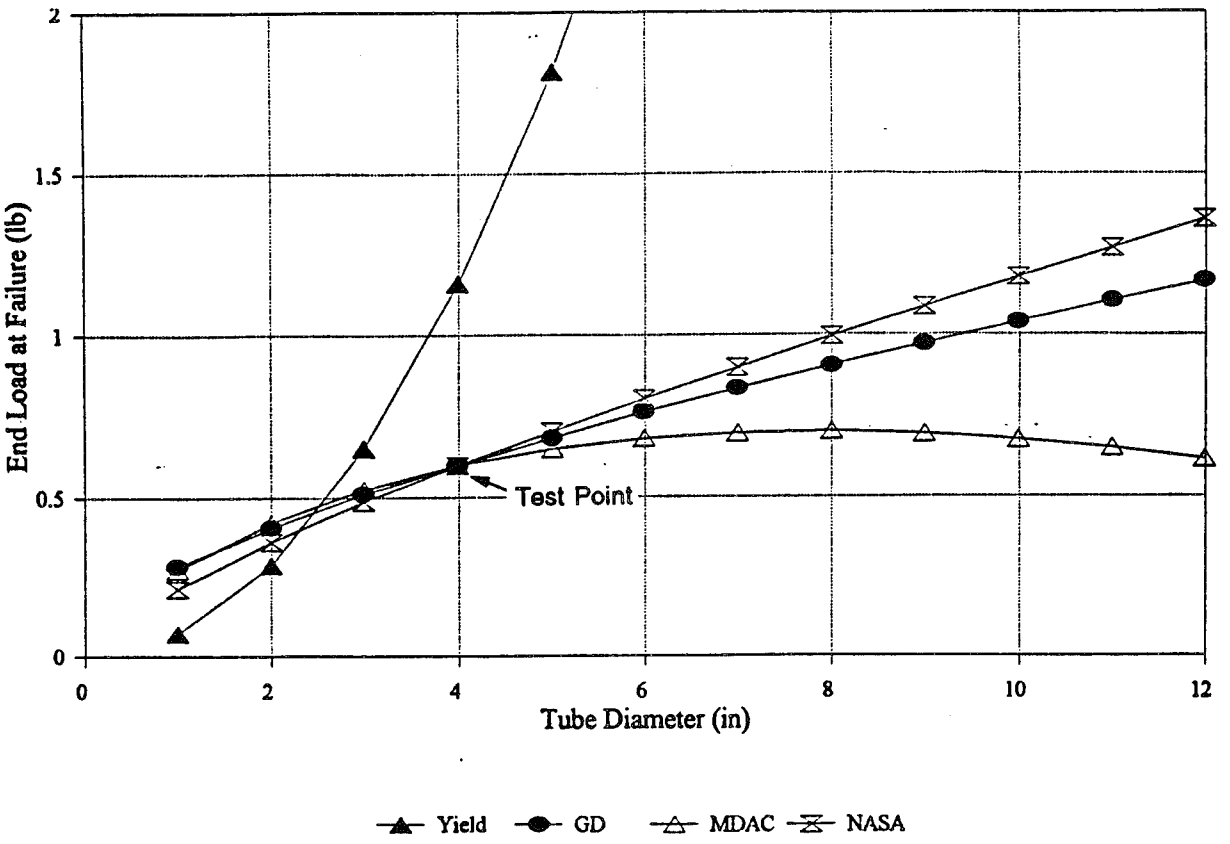

Figure 25. End load at failure versus tube diameter with correction factor.

The most important issue is the rigidizing pressure of the tubes. As the tubes cool during inflation the gas will contract, lowering the pressure. This section presents the results of the thermal analysis of the inflatable tubes. The theory is first presented, followed by the results of the analysis.

The analysis of the inflatable tubes is similar to that used for the light panels on an upcoming IN-STEP Flight Experiment administered by the Jet Propulsion Laboratory (JPL) entitled "Inflatable Antenna Experiment" designed and built by L'Garde (Ref. 12). Figure 26 shows the thermal model of the tubes, which is modeled as two infinite slabs. Heat conduction along and through the tubes is neglected since the Biot Number is $<<$ 1 (Ref. 3). Given the initial conditions (area, temperature, mass, etc.), the temperature of the tube can be calculated as a function of time.

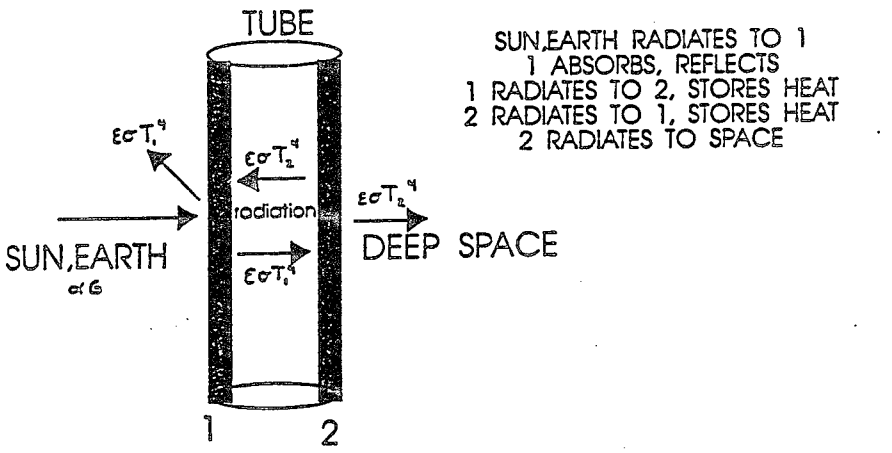

Energy Balance

In = Out + Stored (during time Δt)

SLAB 1:

$$A\Delta t(\alpha G + \epsilon\sigma T_2^4) = (2\epsilon\sigma AT_1^4)\Delta t + Mc\Delta T_1$$

SLAB 2:

$$A\Delta t(\epsilon\sigma T_1^4) = (2\epsilon\sigma AT_2^4)\Delta t + Mc\Delta T_2$$

where:

A = cross-sectional area

Δt = time increment

α = absorptivity

G = power from Sun or Earth

ϵ = emissivity

σ = Stefan Boltzman constant

M = thermal mass

c = specific heat

Figure 26. Inflatable tube thermal model.

Table 12 presents the constants and material properties used for the thermal analysis of the inflatable tubes. For this analysis, the seam mass was assumed to be negligible. Two different starting temperatures were assumed, provided by the results of Subsection 3.1.2 for canisters with and without MLI. The results of the analysis are given in Figures 27-30.

Table 12. Constants and material properties for inflatable tube thermal analysis.

VARIABLE	VALUE
Cross-Sectional Area	1.0 m^2
Time Increment	0.001 s
Absorptivity	0.395
Power from Sun (Earth)	1353 (200) Wm^{-2}
Emissivity	0.78
Stefan Boltzman Constant	5.67×10^{-8} $Wm^{-2}K^{-4}$
Thermal Mass (No seams included)	0.3206 kg
Specific Heat	950 $J\ kg^{-1}K^{-1}$

The next step is to use the tube temperature drop to investigate its effect on the gas pressure in the tubes.

The following two possible deployment scenarios were used for the analysis:

- Assume deployment in eclipse, where radiation from the Earth is 200 W/m^2.*
- Assume deployment in sunlight (the radiation input is the solar constant, 1353 W/m^2)

Using these resulting temperatures, the rigidization pressures (shown in Fig. 31) were calculated. Using different rigidizing pressures, the safety factor of the tubes and the expected natural frequency of the array were determined based on test results from Reference 11.

*L'Garde also performed the analysis assuming no heat input from Earthshine (Ref. 3) as a worst-case. The results were slightly worse and are shown in Table 11.

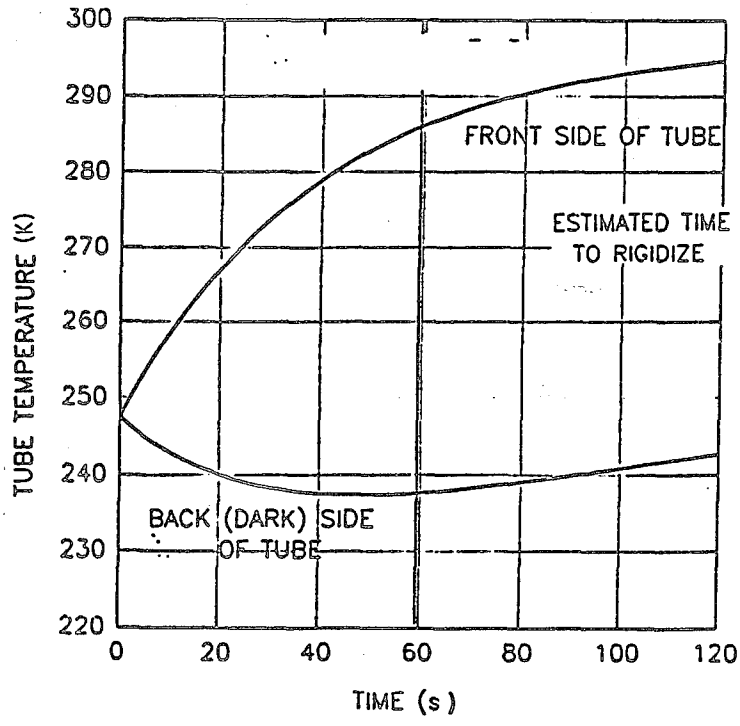

Figure 27. Tube temperature, no MLI, radiated by sun.

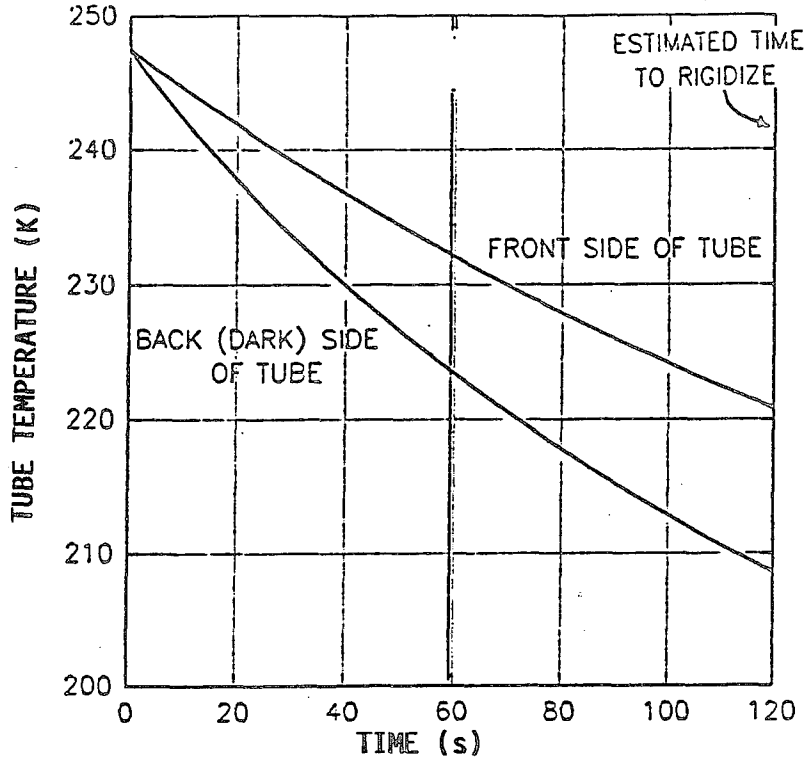

Figure 28. Tube temperature, no MLI, radiated by earth.

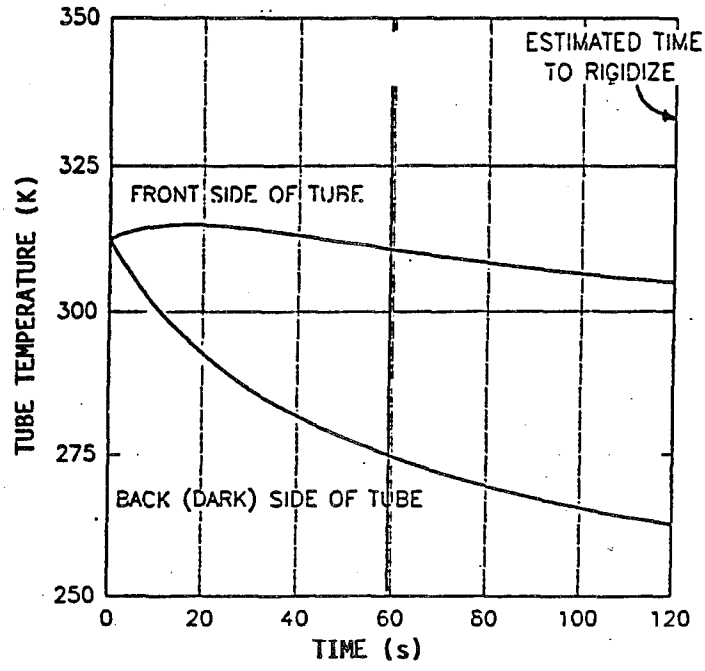

Figure 29. Tube temperature, with MLI, radiated by sun.

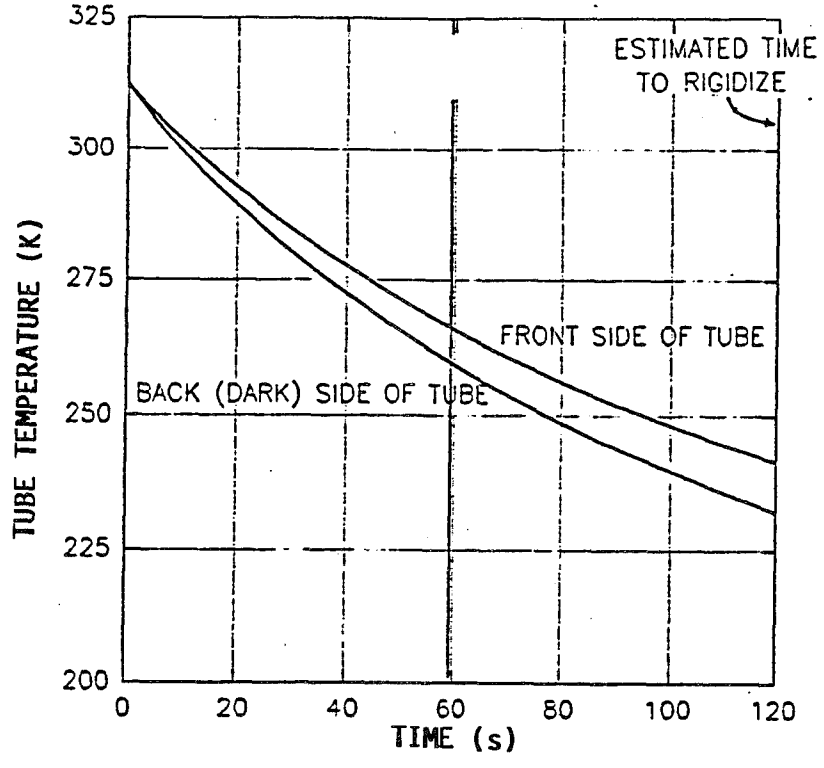

Figure 30. Tube temperature, with MLI, radiated by earth.

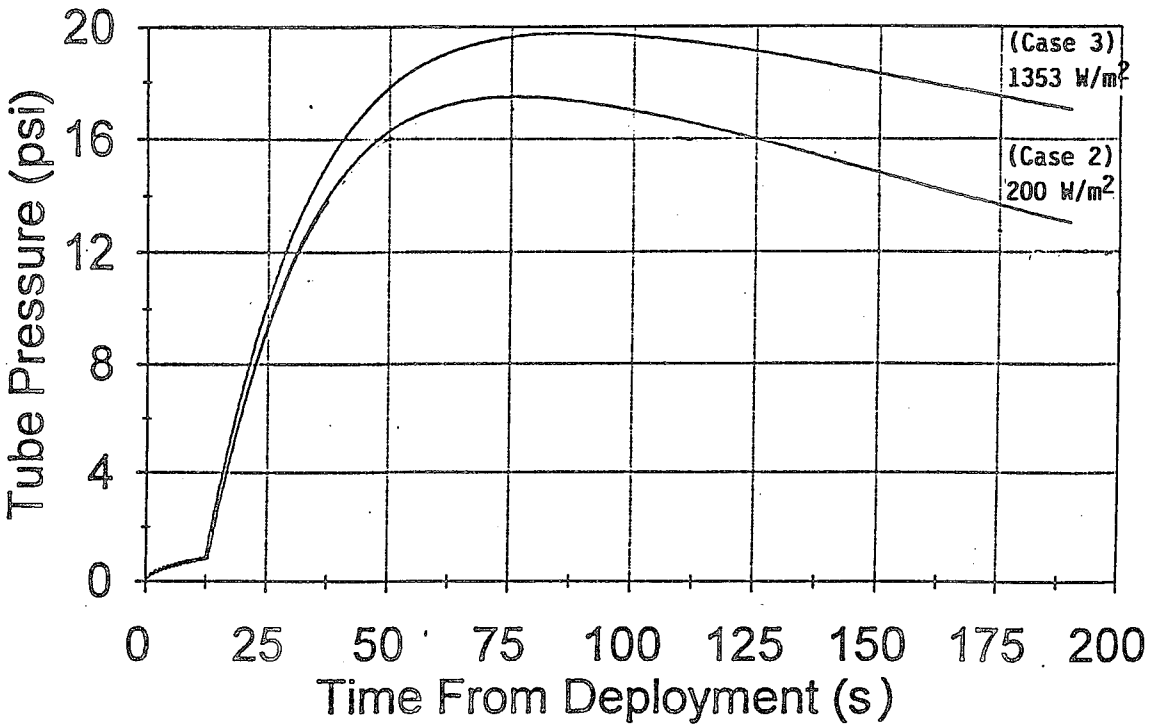

Figure 31. Rigidization pressure.

At the worst-case deployment scenario, the tube still has a safety factor of 10.26 in bending, and the natural frequency will be 1.039 Hz.

The temperature profiles of the previous analysis were inserted into a L'Garde deployment and inflation code. This code calculates the dynamics of the deploying tube (correlated with experimental results) and includes models for the flow restrictors, leaks in the tube, and variable temperature between the tank and tubes. It is a first-order analysis intended to give approximate estimates of tube temperature.

The following assumptions were used in this analysis:

- The tank stays at 312 K assuming an ideal gas. The actual temperature difference was measured at 30°C. Using the ideal gas relations the pressure changes only about 10 percent.

The blowdown from the inflation tank into the struts occurs with constant enthalpy. The resulting temperature change is then determined from the Joule-Thompson coefficient, $\mu = (\partial T/\partial P)_H$. The analysis of this subsection assumed gas for which the Joule-Thompson coefficient is zero. However, nitrogen is not a perfect gas. The maximum gas temperature change was estimated from data for μ for air; μ varies from 0.479 to 0.146°F/atm at a 32°F as the pressure ranges from 1 to 220 atm. For ITSAT, the blowdown was from 205 atm to 1.16 atm. For this change the ΔT was calculated to be about 66°F or 36°C. The actual temperature change should be less than this because of heat transfer from the pressure vessel to the gas, and the test data bear this out.

- The temperature of the gas in the tube is halfway between the front side and back side temperatures. The gas temperature is assumed to follow the tube temperature since it has a thermal mass that is only 10 percent of the thermal mass of the tube. In effect, the thermal condition of the gas is dictated by the tube thermal condition. This assumption has been previously used and validated on many L'Garde programs.

- The leak rate in the tube is the same as that of the ambient test unit (Subsection 4.6).

Figure 31 shows the expected pressure profiles for both cases.

The question now is "What pressure is required to rigidize the tube?" A pressure of 22 psi was originally specified, with a minimum level of 20 psi. This was based on test data early in the program. These data showed that 20 psi was required to completely remove all the wrinkles in the tube. While this was a good indicator of strength of the tube, it was actually an overly conservative approach.

The 20-psi requirement was assumed throughout most of the program until bending tests of a tube that was rigidized at several different pressures, then vented; 5, 8, 11, 14, 17, 20, and 22 psi pressures were used. This determined that the minimum rigidization pressure is 11 psi. The results are contained in Subsection 4.3.1.

Combining the previous results with those of Subsection 4.3.1, Table 13 summarizes both deployment scenarios plus the absolute worst-case scenario where no heat is input from Earthshine during eclipse.

The following results indicate that failure due to bending strength is not a problem; all scenarios result in a factor of safety above 10. In all cases the natural frequency is above the 1-Hz requirement set forth in Reference 1.

This section calculates the "bow" in the ITSAT tubes during three scenarios; eclipse, sunlight, and during the deployment test at NRL. From the thermal analysis, the expected temperatures for the tube are listed in Table 14.

Table 13. Summary of deployment scenarios.

CASE	SCENARIO	RIGIDIZATION PRESSURE EXPECTED	FACTOR OF SAFETY IN BENDING	EXPECTED NATURAL FREQUENCY[a]	FACTOR OF SAFETY TO BURST
1	Earthshine	17.5	10.29	1.042	2.46
2	Sunshine	19.7	10.41	1.054	2.18
-	No Heat Input	17.0	10.26	1.039	2.53

[a] Based on the ambient deployment unit. Qual unit testing showed higher natural frequency (1.04 Hz)

The last case has a zero delta temperature between the front and back side, thus no bow in the tubes. The calculation of the bow in the tube is straightforward. The difference in tube length between the front and back side is equal to

$$\Delta L = (L)(CTE)(\Delta T) \qquad (19)$$

Table 14. Expected tube temperature[a].

CONDITION	FRONT SIDE TEMPERATURE (°C)	BACK SIDE TEMPERATURE (°C)
Eclipse	-85	-113
Sunlight	+27	- 21
NRL Test (cold)	-85	-123
NRL Test (hot)	+70	+ 70

[a] L'Garde Procedure #21231 for the ITSAT thermal vacuum deployment test, dated Oct. 1993

where

L = the length of the tube (139.73 in)

CTE = the coefficient of thermal expansion (1.1×10^{-4}/°C, Ref. 13)

ΔT = the temperature difference, front to back (°C).

The radius of curvature of the tube is then calculated. Looking at Figure 32 the following equations apply:

$$L = R_1 \theta \tag{20}$$

$$L - \Delta L = R_2 \theta \tag{21}$$

$$R_1 = R_2 + d \tag{22}$$

where d is the diameter of the tube (4 in). Combining Equations 20-22, the following relation is obtained for radius of curvature to the near side of the tube:

$$R_2 = \frac{dL}{\Delta L} - d \tag{23}$$

The bow is calculated similarly. Looking at Figure 33

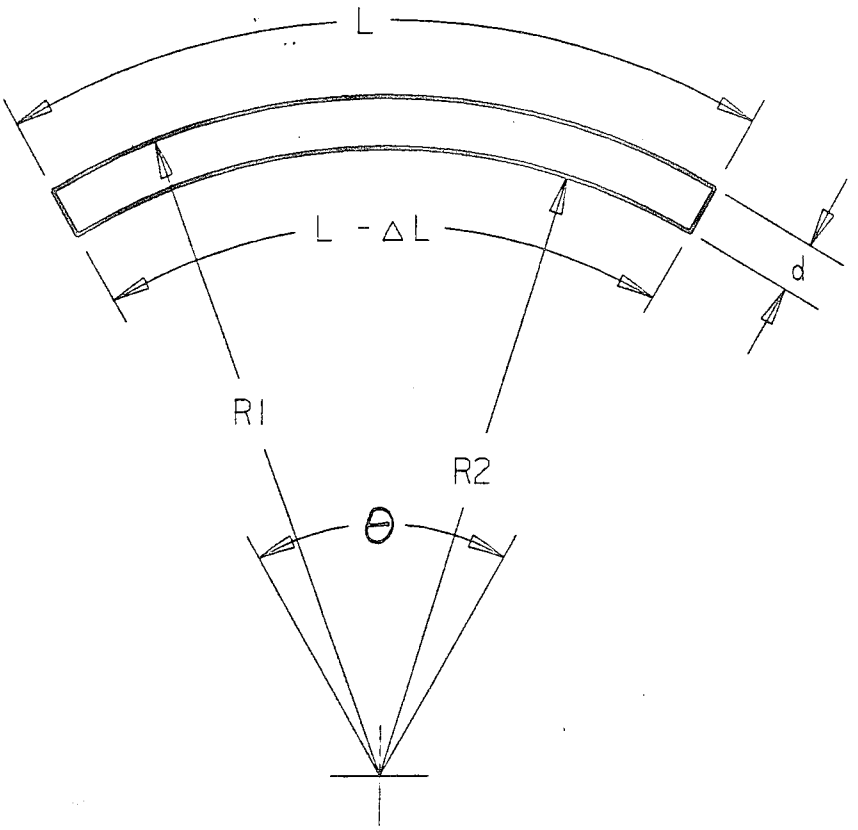

Figure 32. Calculating radius of curvature.

$$x = R_2 - R_2 \cos \frac{\theta}{2} \tag{24}$$

Using the temperature data and the equations, the resulting bow in the tube is now determined for each of the nontrivial situations. The results are shown in Table 15.

During sunlit conditions (the only time the solar cells are generating power) the array will bend away from the sun. Assuming the "housing" end of the array is pointed directly at the sun, the outboard solar cells will be at a 2.62-deg. angle to the sun, making a small cosine loss of 0.1 percent.

Another concern with the ITSAT design is the fatigue of the tube material as the array cycles between eclipse and sunlight conditions. The following analysis shows the tube material will last beyond its 3-year design lifetime.

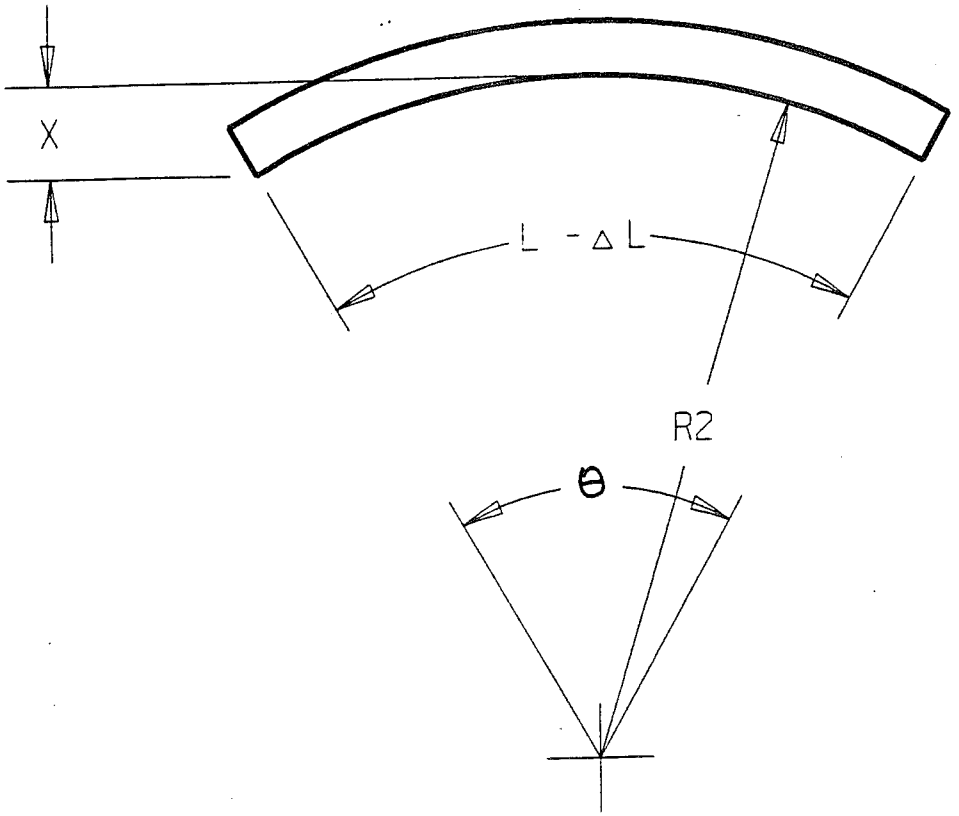

Figure 33. Bow in tube.

Table 15. Expected bow in the ITSAT tubes.

CONDITION	FRONT SIDE TEMPERATURE (°C)	BACK SIDE TEMPERATURE (°C)	ΔL (in)	RADIUS OF CURVATURE (in)	BOW (in)
Eclipse	-85	-113	0.430	1295	1.87
Sunlight	27	- 21	0.738	754	3.20
NRL Test (cold)	-85	-123	0.584	953	2.54

Figure 34 shows a small portion of the tube. In this analysis it is assumed that the entire top half of the tube lies at temperature T_1 and the entire bottom half lies at temperature T_2. Figure 35 shows the interface between the two where the maximum stress exists due to a sudden

temperature transition. The hotter part of the material wants to expand, and the cooler part wants to contract. If the two were not connected the strain would be

$$\epsilon = (CTE)\ (\Delta T)$$

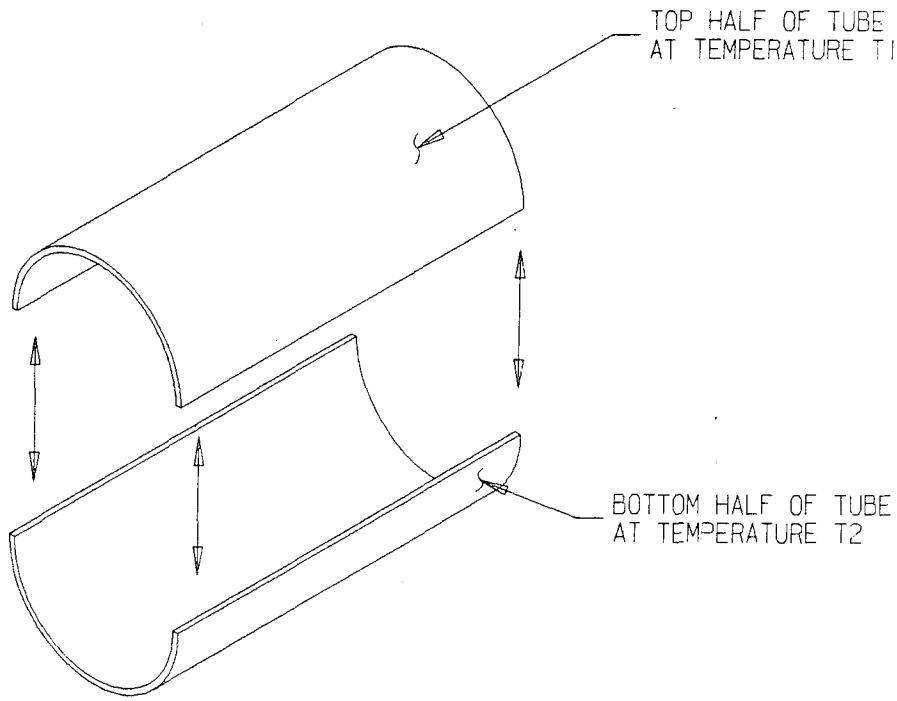

Figure 34. Tube temperature difference.

The stress required to bring the two halves to the same length (since they are connected) is

$$\sigma = E\epsilon = E\ (CTE)\ (\Delta T)$$

Where E is the elastic modulus of the material. Using the tested value of E, 2.34 x 10^6 psi; the CTE noted previously (1.1 x 10^{-4}/°C); and a maximum temperature difference during sunlit conditions of 48°C; the stress due to thermal expansion is 12,400 psi or 78 percent of its 16,000 psi ultimate tensile strength.

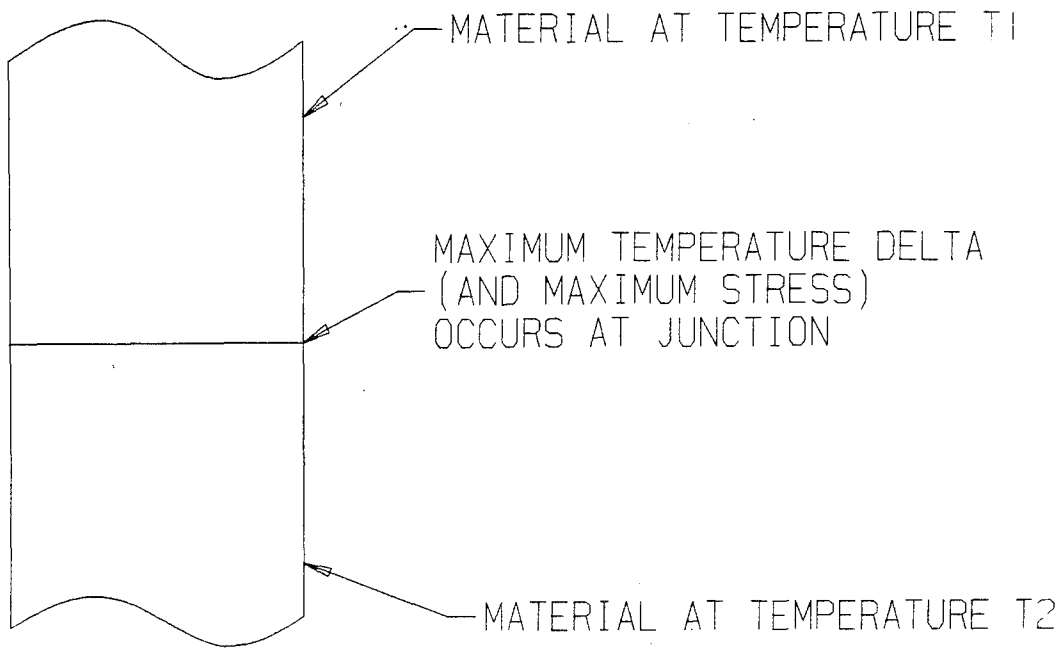

Figure 35. Transition between hot and cold sections of tube.

Since 3003-0 alloy is not typically used as a structural material, no data could be found for its fatigue strength. Figure 36 (Ref. 8) shows the Load-N curve for 2024-T3 aluminum. Reference 8 also states that lower strength materials perform better in fatigue loading situations than the high strength alloys. By conservatively using this curve for the higher strength 2024-T3, we find that the material could fail at 40,000 cycles. Assuming a 90-minute orbit, this equates to 6.8 years of service, a factor of 2.3 over the design life of the 3 years. Failure due to fatigue is not a problem.

3.2.1.4 Leak Rate in Vacuum. Initial design of the inflation system provides for a 22-psi final pressure in the tubes. This design, however, does not take into account leaks in the tubes during inflation. Large leak rates will prevent full rigidization and compromise the integrity of the ITSAT.

Most of the leak testing for the ITSAT tubes was performed in ambient (1 atm) conditions. An analysis is required to relate these data to the leak rate in space for prediction purposes.

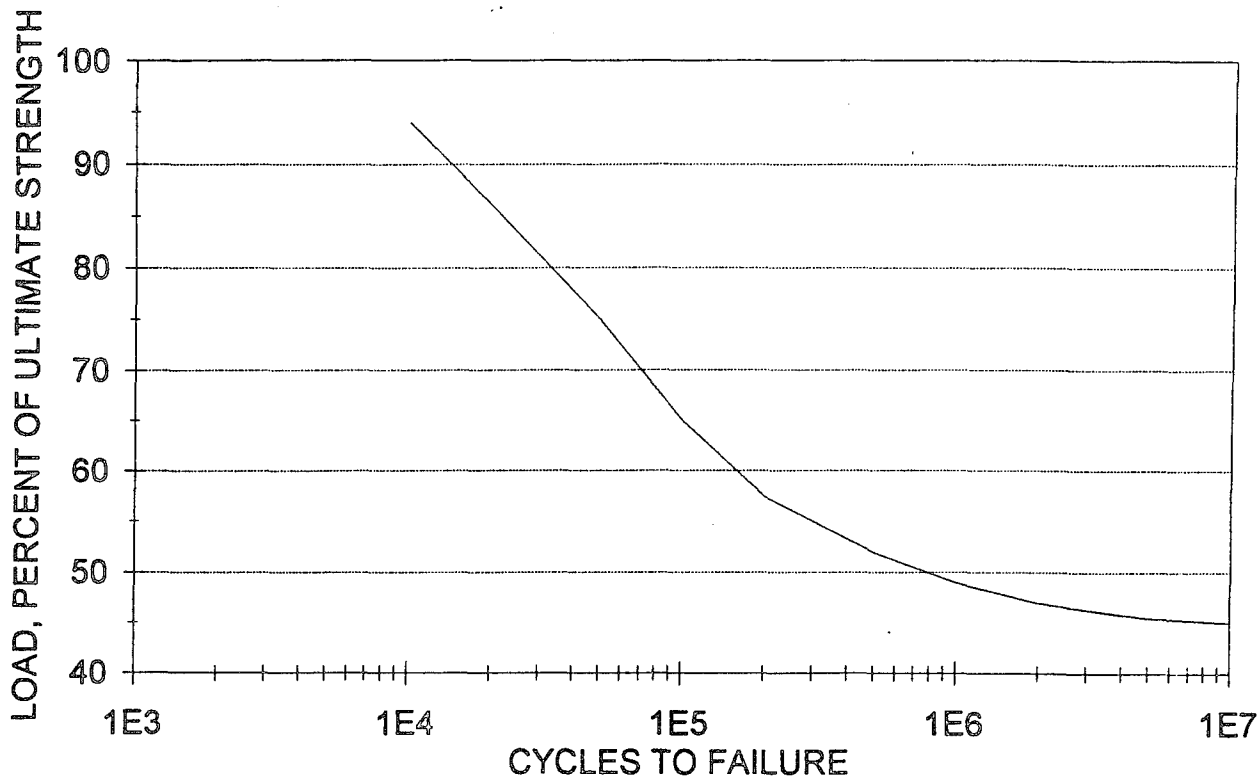

Figure 36. Load-N curve for 2024-T3 aluminum.

Reference 14 details the analytical models and calculations used to determine the effects of leak rates of the ITSAT tubes. An example is given here.

During development testing, one of the ITSAT tubes was leak rate tested in atmospheric conditions. Using the theory from Reference 14, Figure 37 shows the theoretical pressure profile for vacuum conditions, along with the test data for atmospheric conditions. As expected, the leak rate is much slower in vacuum than atmosphere. It should be noted that these data were for a nonbladder tube, which explains the high leak rate. Using the theory, the leak rate of the inflatable in space (vacuum) can be extrapolated from atmospheric leak testing.

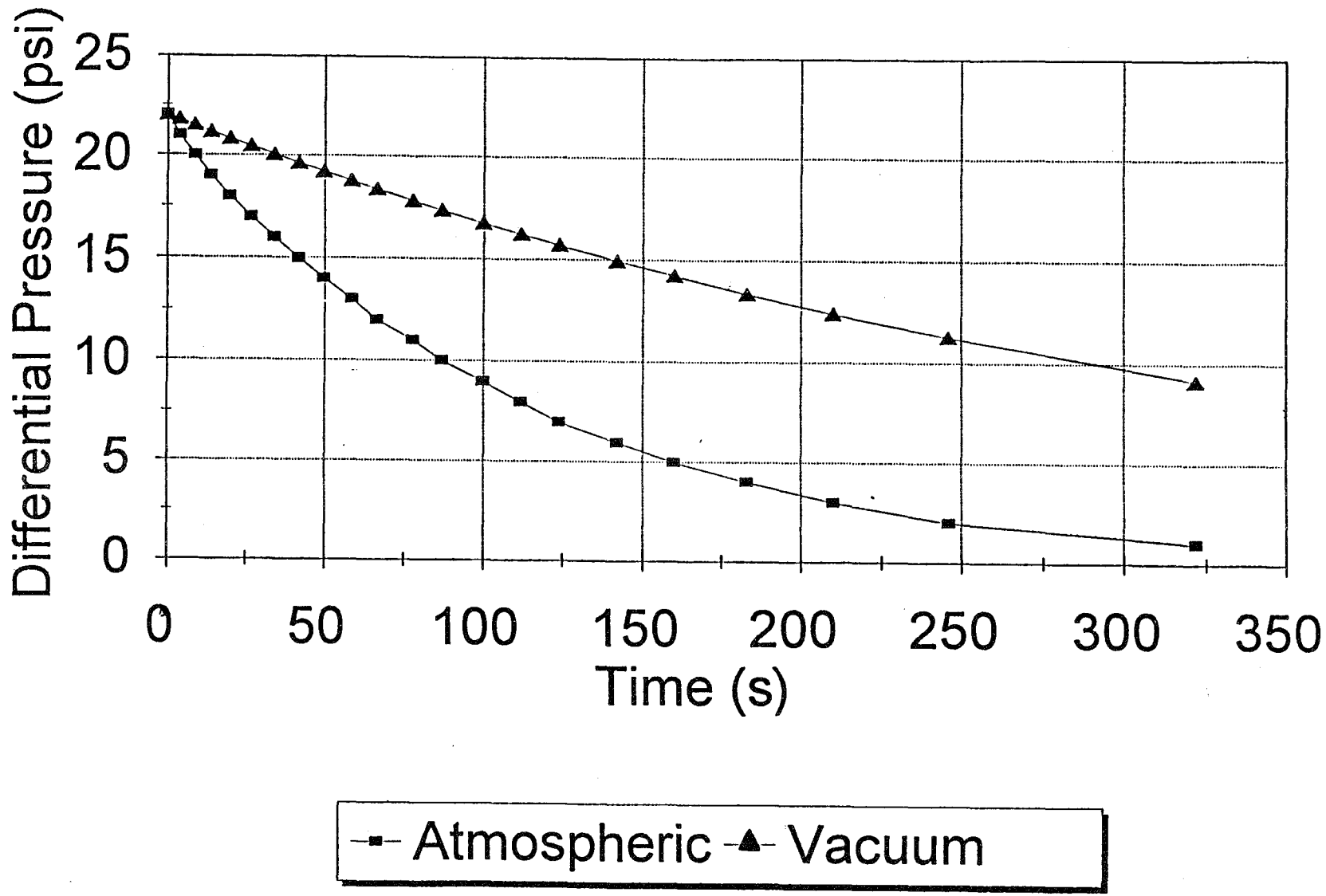

Figure 37. Pressure profiles for vacuum (calculated) and atmosphere (test data).

3.2.1.5 End Caps. The pressurized torus tubes must be capped at each end by a lightweight cap that provides a completely leakproof seal. This is done using a thin spherical end cap clamped by a thin flanged ring (Fig. 38).

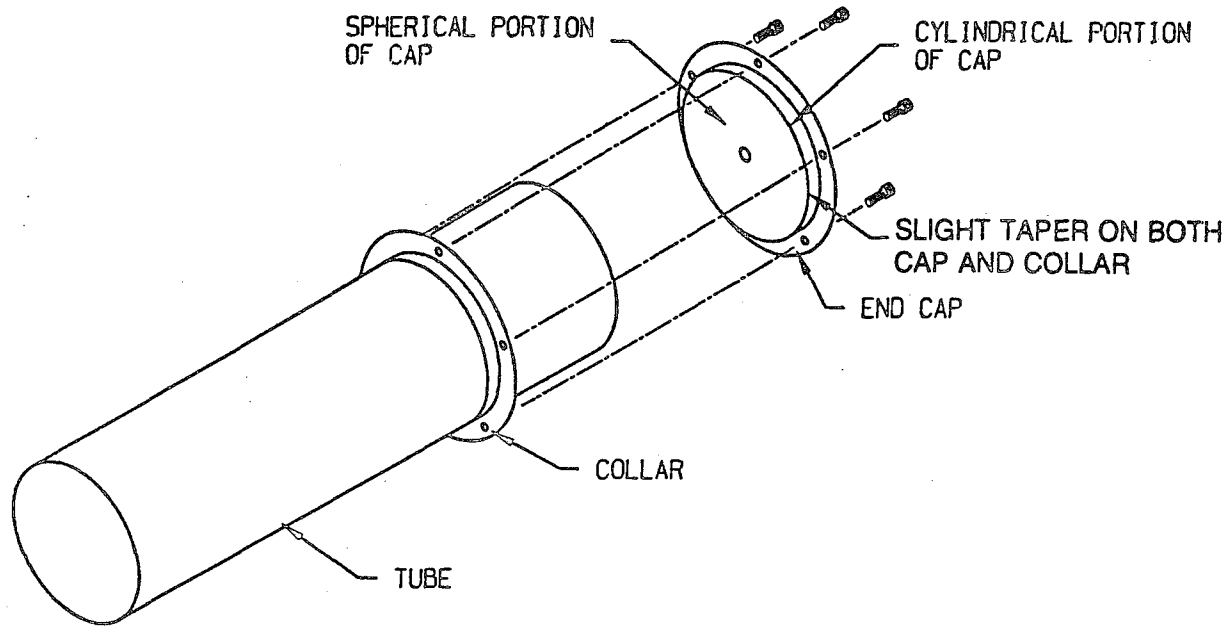

Figure 38. End cap and collar.

The actual end cap and collar is shown in Figure 39.

The analysis to be performed here is on the

(1) Spherical portion of the end cap (make sure it does not blow out) and (2) cylindrical portion of the end cap (make sure it does not buckle). To analyze the spherical portion, use Table 29, Case 3 in Reference 15. This is a spherical shell subjected to an internal pressure (Fig. 40).

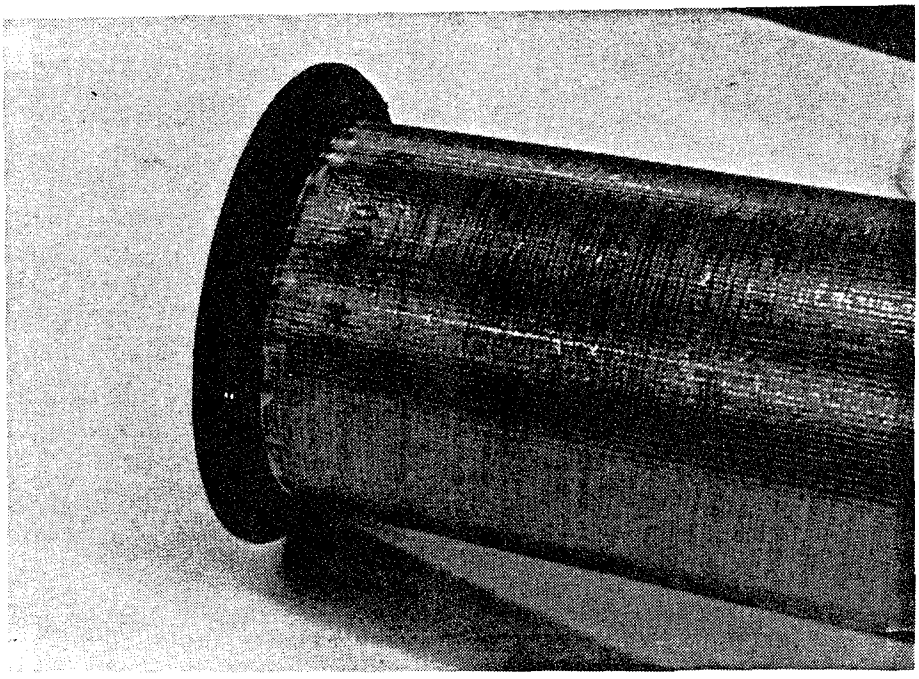

Figure 39. The ITSAT end cap and collar.

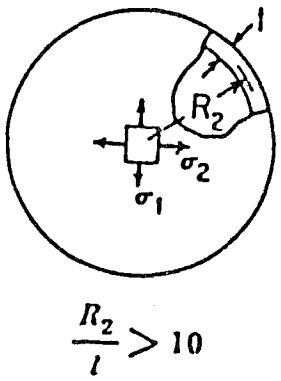

(a) Vessel shape.

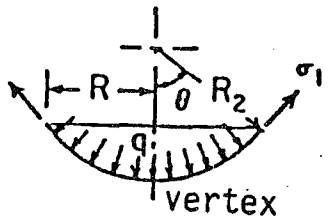

(b) Loading and nomenclature.

Figure 40. Spherical pressure vessel.

For this vessel and loading, the deflection of the vertex of the shell is given by

$$\Delta y = \frac{PR_2^2 (1 - \mu)(1 - \cos\theta)}{2Et} \tag{25}$$

where

Δy = the deflection

P = the inflation pressure = 20 psi

R_2 = the radius of curvature = 5 in

μ = Poisson's Ratio = 0.3

E = the Elastic Modules = 10×10^6 psi

t = the material thickness = 0.031 in

The hoop and longitudinal stresses, σ_1 and σ_2, are equal due to the spherical shape and are given by

$$\sigma_1 = \sigma_2 = \frac{PR_2}{2t} \tag{26}$$

which will be transferred to the cylindrical portion of the cap.

First find the value of θ, knowing R_2 and R = 2 in (half the tube diameter).

$$\sin\theta = \frac{R}{R_2} \tag{27}$$

$$\theta = \sin^{-1} \frac{2}{5} = 0.412 \text{ rad}$$

Now substitute values into Equation 25.

$$\Delta y = \frac{(22)(5)^2(1 - 0.3)(1 - \cos(0.412))}{2(10 \times 10^6)(0.031)} = 0.000052 \text{ in} \quad (28)$$

which is obviously tolerable. The stress in the aluminum skin is

$$\sigma_1 = \sigma_2 = \frac{(22)(5)}{2(.031)} = 1760 \text{ psi} \quad (29)$$

For 6061-T6 aluminum, with a yield stress of 40,000 psi, the safety factor is 40,000/1760 = 22.7.

The cylindrical portion is subjected to two loadings, both of which are transferred from the spherical end cap portion. See Figure 41 which shows the loading broken up into (1) inward loading and (2) axial loading.

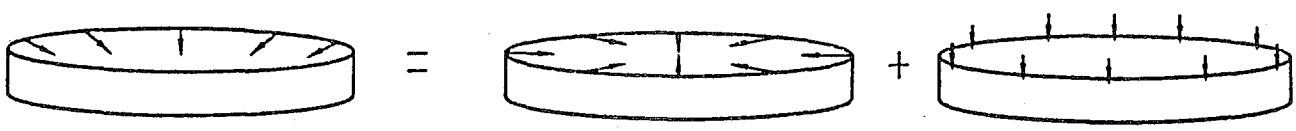

Figure 41. Forces on cylindrical portion of end caps.

First look at the inward loading by using the applicable formula from Reference 15. The loading and shape are given in Figure 42.

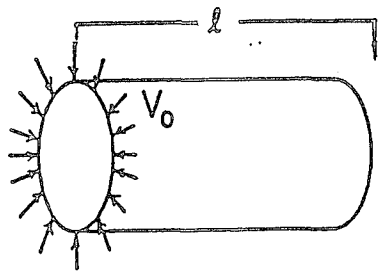

For $\lambda\ell < 6$

Figure 42. Inward load on a cylindrical tube.

The radial deflection is given by

$$y_A = \frac{-V_o C_{13}}{2D\lambda^3 C_{11}} \tag{30}$$

where V_o is the line load in pounds per inch and C_{11}, C_{13}, D, and λ are constants given by

$$C_{11} = \text{Sinh}^2\lambda l - \sin^2\lambda l$$

$$C_{12} = \text{Cosh}\lambda l \, \text{Sinh}\lambda l - \cos\lambda l \sin \lambda l$$

$$D = \frac{Et^3}{12(1 - \mu^2)} \tag{31}$$

$$\lambda = \frac{3(1 - \mu^2)}{R^2t^2}^{1/4} \tag{32}$$

The inward load V_o is the inward component of the spherical shell stress, or

$$V_o = (\sigma_{inward})(t) = (\sigma_1)(t) \cos\theta \tag{33}$$

For our numbers

$$V_o = (1760)(0.031)(\cos.412)$$

$$= 50.0 \text{ lb/in}$$

$$D = \frac{(10 \times 10^6)(0.031)^3}{12(1 - 0.3^2)} = 27.95 \quad (34)$$

$$\lambda = \left[\frac{3(1 - 0.3^2)}{(2)^2 (0.031)^2}\right]^{1/4} = 5.142 \quad (35)$$

$$\lambda \ell = (5.142)(0.562) = 2.89 \quad (36)$$

which is less than 6; this case is valid.

$$C_{11} = \text{Sinh}^2 (2.89) - \text{Sin}^2 (2.89) = 80.73 \quad (37)$$

$$C_{13} = \text{Cosh} (2.89)\ \text{Sinh} (2.89) - \cos (2.89)\ \sin (2.89) = 81.53 \quad (38)$$

which gives a radial deflection of

$$Y_A = \frac{-(50.0)}{2(27.95)(5.142)^3} \cdot \frac{81.53}{80.73} = -0.0066 \text{ in} \quad (39)$$

The circumferential stress is given simply by

$$\sigma_2 = \frac{y_A E}{R} = \frac{(0.0061)(10 \times 10^6)}{2} = 30{,}500 \text{ psi} \quad (40)$$

which gives a safety factor of 40,000/30,500 = 1.31; not a huge margin, but remember that this analysis does not account for the stiffening effect of the attached spherical portion; it assumes the loaded end of the cylinder is free.

The third and final check is the axial force on the cylindrical part of the end cap. Since it is such a short cylinder, buckling can be ignored and only a simple check is made that the axial stress does not exceed the yield point.

$$\sigma_{axial} = \sigma_1 \sin\theta$$
$$= (1760)\sin(0.412) \qquad (41)$$
$$= 705 \text{ psi}$$

making a safety factor of 40,000/705 = 56.8

Some of the safety factors calculated in the previous analysis are rather high for conservatism; a thinner material conceivably could be used. Future ITSAT designs may investigate use of a thinner material to decrease the system mass.

3.2.2 Inflation System

The inflation system is shown schematically in Figure 43. Upon command from the controller unit (i.e., satellite command), a pyrotechnic puncture cutter pierces an aluminum diaphragm to let the gas flow from the inflatant tank. There it flows through the primary restrictor which allows only a very slow flow rate. This restriction is absolutely necessary to assure that the boom deploys slowly and controllably. The last component of the inflation valve assembly is a vent valve, which allows the trapped air in the packaged booms to vent during ascent in the launch vehicle; thereby avoiding premature inflation. Prior to releasing the gas, the vent is open to atmosphere. Upon initiation, the vent closes due to the pressure of the gas.

The actual ITSAT inflation system is shown in Figure 44. The remainder of this section will discuss the individual components of the inflation system.

3.2.2.1 Inflatant Tank. The inflatant tank holds the pressurized gas until the structure is ready for deployment/rigidization. L'Garde investigated using standard inflatant tanks and found they were far too heavy for the weight critical ITSAT; in addition, they were large in diameter (2-in or more) making them difficult to package.

It was decided to design a tank that would be as light and small in diameter as possible. The following section gives the analysis of the tank. Subsection 4.4.3 gives a description of the tank proof/burst testing. Two elements of the tank are analyzed here (the tubing and the two

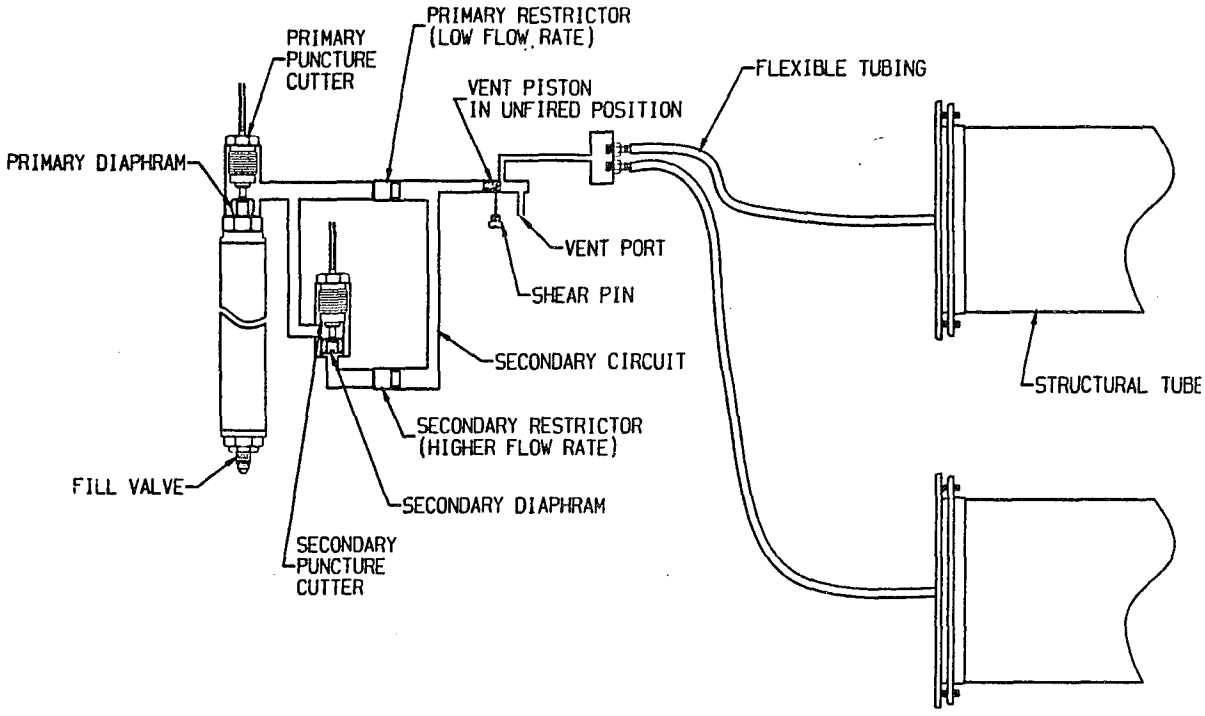

Figure 43. Inflation system schematic.

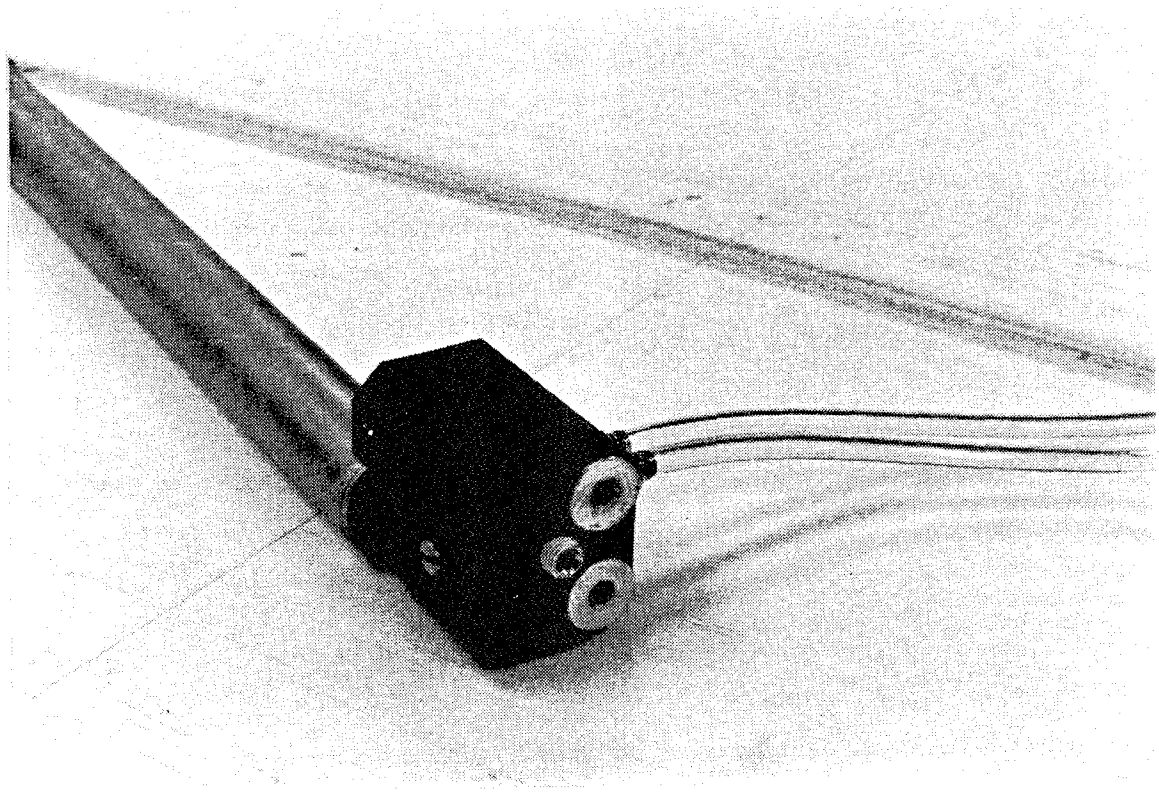

Figure 44. Inflation system with tank.

end caps) to assure that the tank will hold the operating pressure for launch, qualification, and acceptance tests.

The calculations for the tubing are based on the stress formulas for a pressurized cylinder:

$$\text{hoop stress, } \sigma_h = \frac{Pr}{t} \tag{42}$$

$$\text{longitudinal stress, } \sigma_\ell = \frac{Pr}{2t} \tag{43}$$

where P is the inflation pressure in the tank, r is the inside radius, and t is the wall thickness.

Under a given pressure for the above relations, the hoop stress is the limiting factor so it will be used for these design calculations.

The volume of the tank is

$$V = \pi r^2 L \tag{44}$$

where L is the inside length of the tank.

The pressure required to fulfill the inflatant mass requirements is found by the Ideal Gas Law, solved for P;

$$P = \frac{mRT}{V} \tag{45}$$

where m is the mass of inflatant required, R is the gas constant, and T is the temperature of the gas.

These equations were solved using r and L and different materials as variables to find the lightest tank. Following the trade studies, it was determined that a high strength alloy steel would provide the lightest tank.

The end caps are contoured disks that are welded to each end of the tubing. They are analyzed as round flat plates with clamped edges, subjected to a uniform pressure on one side. The stress and deflection are given in Reference 15 (Fig. 45).

Uniformly distributed load from r_o to r, with fixed edges

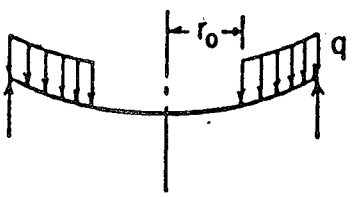

Figure 45. Pressure loading on a circular plate.

Here, the deflection at the center of the plate is given by

$$y_c = \frac{-Pr^4}{2D}(L_{14} - 2L_{11}) \tag{46}$$

the bending moment at the center is

$$M_c = Pr^2(1 + \mu)L_{14} \tag{47}$$

and the bending moment at the edge is

$$M_r = \frac{-P}{8r^2}(r^2 - r_o^2)^2 \tag{48}$$

where in our case

$r_o = 0$

r = plate radius

P = tank pressure

D, L_{11}, and L_{14} are constants given by

$$D = Eb^3/12(1 - \mu^2). \tag{49}$$

$$L_{11} = \frac{1}{64}\left\{1 + 4\left(\frac{r_o}{r}\right)^2 - 5\left(\frac{r_o}{r}\right)^4 - 4\left(\frac{r_o}{r}\right)^2\left[2 + \left(\frac{r_o}{r}\right)^2\right]\ln\frac{r}{r_o}\right\} \tag{50}$$

$$L_{14} = \frac{1}{16}\left[1 - \left(\frac{r_o}{r}\right)^4 - 4\left(\frac{r_o}{r}\right)^2 \ln\frac{r}{r_o}\right] \tag{51}$$

To convert the bending moments (Eqs. 47 and 48) to bending stresses, the following equation is used

$$\sigma = 6M/t^2 \tag{52}$$

As stated previously, a thorough optimization was performed on different materials, tank diameters, and lengths to come up with the optimum design. The final design is shown in Table 16.

Material used is 4130 alloy steel heat treated to a MINIMUM yield strength of 185,000 psi.

Table 16. Final tank design.

VARIABLE	DESCRIPTION	VALUE	UNITS
r	Inside Tank Radius	0.472	in
L	Inside Tank Length	38.75	in
t	Tank Wall Thickness	0.028	in
b	Tank End Cap Thickness	0.25	in
R	Gas Constant for Nitrogen	55.15	$\frac{ft\ lb_f}{lb_m\ °R}$
T	Temperature of Gas in Cylinder	528	°R
σ_y	Yield Strength	185,000	psi
ρ	Material Density	0.29	lb/in^3
μ	Poisson's Ratio	0.3	
E	Elastic Modulus	30×10^6	psi

First the volume of the tank is calculated by Equation 44.

$$V = \pi(0.472)^2(38.75) = 27.12\ in^3 \tag{53}$$

and the pressure to hold the required inflatant is (using Eq. 45).

$$P = \frac{(.221\ lb_m)(55.15\ ft\ lb_f)(528°R)}{lb_m°R\ (27.12\ in^3)} \cdot 12\ \frac{in}{ft} = 2870\ psi \tag{54}$$

This makes a hoop stress in the tubing of

$$\sigma_h = \frac{(2870)(0.472)}{0.028} = 48{,}400 \text{ psi} \tag{55}$$

which is a factor of 3.82 under the yield stress of the material.

Now analyze the end caps using Equations 46-52. The constants are calculated to be

$$D = \frac{(30 \times 10^6)(0.25)^3}{12\,(1 - 0.3^2)} = 42{,}900$$

$$L_{11} = \frac{1}{64}$$

$$L_{14} = \frac{1}{16} \tag{56}$$

Therefore, the deflection at the center of the cap is

$$y_c = -\frac{(2870)(0.472)^4}{2\,(42900)}\,[1/16 - 2(1/64)]$$

$$y_c = 0.000052 \text{ in (adequate margin)} \tag{57}$$

The bending moment at the center is (using Eq. 47)

$$M_c = (2870)(0.472)^2(1 + 0.3)(1/16) = 52.0 \text{ in lb} \tag{58}$$

creating a stress of

$$\sigma = \frac{6\,(49.5)}{(0.25)^2} = 4990 \text{ psi} \qquad \text{(safety factor = 37)} \tag{59}$$

The bending moment at the edge is

$$M_r = -\frac{(2870)(0.472)^2}{8} = 79.9 \text{ in-lb.} \quad (60)$$

$$\sigma = \frac{6\,(76.3)}{(0.25)^2} = 7670 \text{ psi} \quad \text{(safety factor = 24)} \quad (61)$$

The large safety factors on the end caps would lead one to believe that the thickness could be less. However, both ends are ported to accept AN-type fittings, and a minimum thread engagement of 0.25 in is required.

The safety factor of 3.82 is actually higher than necessary; DOD-Handbook-343 gives a requirement of 2.0 safety factor for pneumatic vessels as shown in Table 17. The next generation of ITSAT type arrays could have increased power densities by using a lighter weight tank.

3.2.2.2 Diaphragm Stress. The burst diaphragm (P/N 18112) must also resist the gas pressure when the tank is pressurized. Referring to Figure 46, critical failure will occur when the pressure causes the diaphragm to "punch out" a hole at the diaphragm end.

The force necessary is the sheared area times the ultimate shear stress of the material, or

$$F = (\sigma_{us})\,(A_s) \quad (62)$$

The pressure necessary to cause this to happen is

$$P = \frac{F}{A_D} \quad (63)$$

Where A_D is the area that is exposed to the pressure. Combining Equations 62 and 63 yields the pressure necessary for bursting the diaphragm:

Table 17. Pressurized components factors of safety.
(from DOD-HDBK-343 [USAF])

Component c/	Design Ultimate	Acceptance (Proof)	Qualification
Solid Rocket Motor Cases b/	1.25	1.10 a/	1.25 a/
Pneumatic Vessels b/	2.00	1.50 a/	2.00 a/
Lines, Fittings, and Hoses			
Less than 3.81 cm dia. d/	4.00	2.00 a/	4.00 a/
3.81 cm dia. and larger d/	1.50	1.10 a/	1.50 a/
Other Pressurized Components	2.50	2.00 a/	2.50 a/

Notes:

a/ No yielding permitted at acceptance (proof) test pressure, and no rupture at qualification pressure.

b/ Factors of safety shown are minimum values applicable to metallic pressure vessels for which ductile fracture mode is predicted via a combination of stress and fracture mechanics analyses. Design of metallic pressure vessels for which brittle fracture mode is predicted by these analyses shall be in accordance with fracture mechanics methodology wherein the proof factor as well as the design ultimate factor of safety shall be established to provide a minimum of four times the specified service life against mission requirements. In addition, a fracture control program shall be established to prevent structural failure due to the initiation or propagation of flaws or crack-like defects during fabrication, testing, and service life.

c/ All pressure vessels, sealed containers, lines, fittings, and other pressurized components of equipment to be launched in the STS shall be designed to meet the applicable safety requirements of NHB 1700.7 (NASA) and SAMTO HB S-100 (designated by NASA as KHB 1700.7).

d/ 3.81 cm diameter is equivalent to 1.5 inches diameter.

$$P = \frac{\sigma_{us} A_s}{A_D} \tag{64}$$

The yield shearing stress is generally 50 percent of the tensile yield stress, and the ultimate shearing stress is generally 75 percent of the ultimate tensile stress. For aluminum alloy 2024-T4:

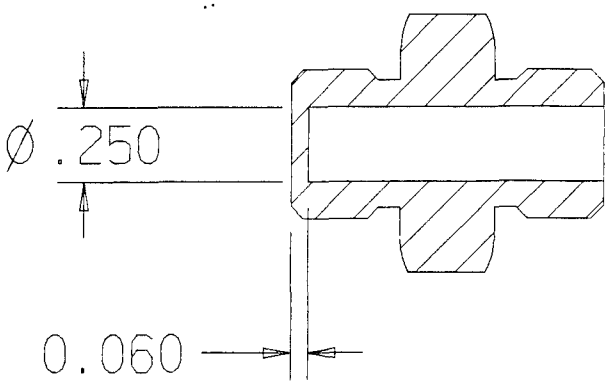

Figure 46. Diaphragm cross-section.

	Value
Yield stress (psi)	47000
Yield shearing stress (psi)	23500
Ultimate tensile stress (psi)	68000
Ultimate shearing stress (psi)	51000

Using the above values in Equation 64, the diaphragm will yield at

$$P = \frac{(23500)(\pi)(0.250)(0.06)}{\pi/4\ (0.250)^2} = 22{,}600 \text{ psi} \qquad (65)$$

Likewise, the diaphragm will not burst until its ultimate shearing stress is reached, at a pressure of 49,000 psi.

3.2.2.3 Tank Thread Pull-Out Strength. Will the diaphragm pull out of its threads? The following analysis shows that the threads will not pull out.

Referring to Reference 16, first analyze the load necessary to break the threaded portion of a screw, then find the length of engaged threads necessary to equal this load. The breaking load of any thread is given by

$$F = \sigma A_t \tag{66}$$

Where A_t is the tensile stress area of the thread, and σ can be either the yield or ultimate stress (both are given below). The necessary length of thread engagement is given by

$$L_e = \frac{2 \times A_t}{3.1416\, K_\eta max[½ + 0.57735\eta(E_s min - K_\eta max)]} \tag{67}$$

In this formula, the factor of 2 means that it is assumed that the area in shear of the screw must be twice the tensile stress area to develop the full strength of the screw (this value is slightly larger than required, thus providing a small factor of safety against stripping); L_e is the length of engagement, in inches; η is the number of threads per inch; $K_\eta max$ is the maximum minor diameter of internal thread; $E_s min$ is the minimum pitch diameter of external thread for the class of thread specified; and A_t is the tensile stress area of screw thread given by thread tables.

For a ½-20 UNF thread,

$K_\eta max = 0.4459$
$E_s min = 0.4675$
$\eta = 20$

which gives an L_e value of 0.3046 in. Our thread engagement for the diaphragm is only about 0.25 in, so the equivalent breaking load given by Equation 66 will be reduced by a factor of 0.25/0.3046 = 0.821.

Substituting numbers back into Equation 66 along with this factor gives a yield load of

$$F_y = (0.821)(47000)(0.1599) = 6170 \text{ lb} \tag{68}$$

or an ultimate load of

$$F_u = (0.821)(68000)(0.1599) = 8930 \text{ lb} \tag{69}$$

The pressure necessary to cause these loads is now calculated:

$$P = \frac{F}{A_p} \tag{70}$$

where A_p is the area where the pressure is applied. As a worst case, this may be calculated using the full (major) diameter of the thread.

$$P_y = \frac{6170}{(\pi/4)(0.50)^2} = 31{,}400 \text{ psi} \tag{71}$$

Using the ultimate stress, the burst pressure is then:

$$P_u = \frac{8930}{(\pi/4)(0.50)^2} = 45{,}500 \text{ psi} \tag{72}$$

3.2.2.4 Summary-Tank Design. Table 18 gives a summary of the above calculations

Table 18. Tank analysis summary.

FAILURE MODE	PRESSURE NECESSARY TO YIELD (psi)	F.S. BASED ON YIELD	PRESSURE NECESSARY TO BURST (psi)	F.S. BASED ON ULTIMATE
Tank Hoop Stress	11000	3.82	11900	4.13
Diaphragm Stress	22600	7.86	49000	17.1
Thread Pull-Out Strength	31400	10.9	45500	15.9

3.2.2.5 Puncture Cutter. This design has been previously used by L'Garde on the Red Tigress I and II Programs. The same puncture cutter and diaphragm are exactly the same as before, both of which were extensively tested during development of the Red Tigress payloads. A short analysis is given here.

The puncture cutter is made by ICI Aerospace, Model #1SE311. A data sheet is shown in Figure 47 which shows that the cutter will reliably puncture a 0.035-in thick AMS 6350 steel diaphragm hardened to R_c 26-32. This material has an ultimate stress of 120,000 psi. Since

the diaphragm is constructed from aluminum alloy 2024-T4 (yield stress = 68,000 psi), the cutter should be able to puncture a thickness which is indirectly proportional to the ratio of the tensile strengths.

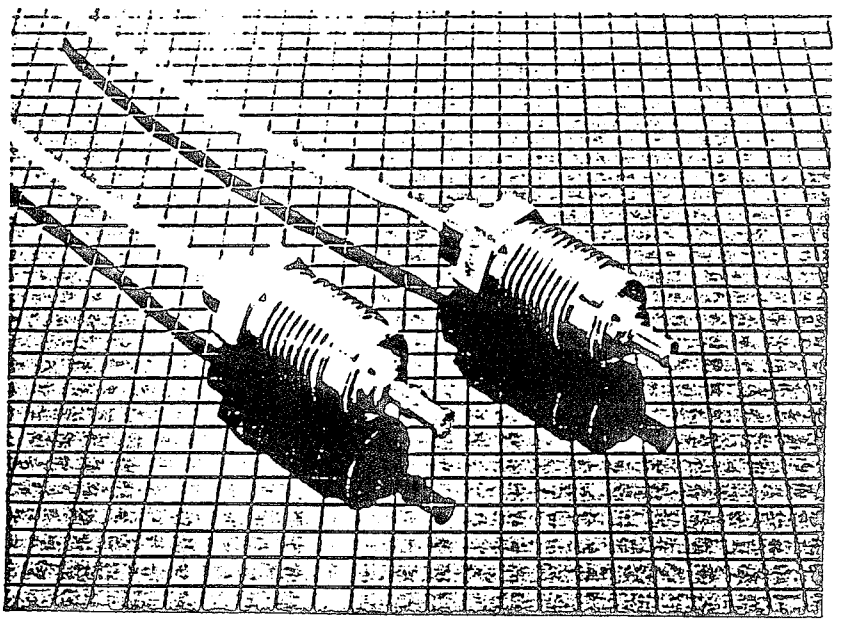

Grid Scale: Actual Size = ½".

Characteristics

Some of the characteristics listed here are nominal; others are levels to which the units have been tested. They are not limits on design capabilities. Please consult an ICI Aerospace representative before using this data as a specification.

Electrical

Bridge resistance @ 76°F (24°C):
0.8 - 1.5 ohm

All-fire current @ -65°F (-54°C):
4.0 amp, .025 s

No-fire current @ 165°F (74°C):
1.0 amp, 5 min

Insulation resistance:
Before fire: Greater than 1.0 megohm with 50 Vdc, leads to case

After fire: Greater than 100 ohm with 50 Vdc, .05 to 120 s

Static resistance:
25 kW discharge from a 500 pF capacitor applied through a 5000 ohm series resistor

Mechanical

Size:
See drawing

Lead length:
25" (640 mm)

Weight:
35 gm

Stroke:
Punctures a .035" (.889 mm) thick AMS 6370 steel diaphragm hardened to R_c 26-32. After puncture, a minimum flow area of .003 in^2 (.790 mm^2) is maintained for 120 sec Min.

Function time:
25 ms Max.

Figure 47. Data sheet for puncture cutter.

Max Diaphragm thickness = $(0.035)\frac{120{,}000}{68{,}000} = 0.062$ in

Our diaphragm thickness is just under this, at 0.060 in, so it will be OK.

3.2.2.6 Vent Valve Shear Pin. The vent valve is basically a piston in a cylinder with a pin protruding through the cylinder wall into one side of the piston. Gas pressure forces the piston down and shears the pin. The following analysis assures that the shear pin is sized correctly such that it will shear when pressurized and will not shear when exposed to steady-state acceleration and vibration loads.

First analyze the piston when pressurized. The piston and shear pin setup is shown in Figure 48. The force pushing down on the piston is

$$F_p = \frac{P\pi D_p^2}{4} \tag{73}$$

where D_p is the diameter of the piston

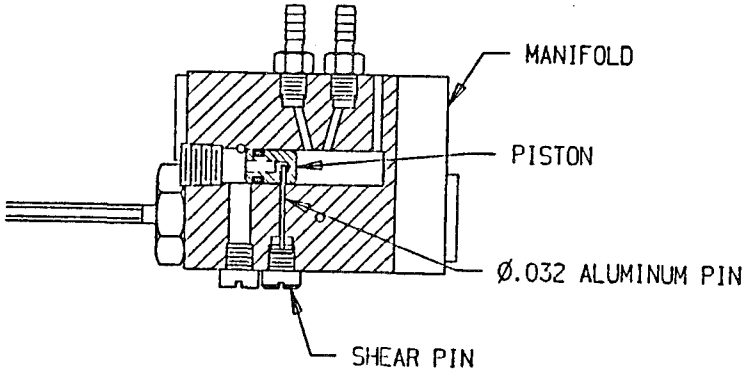

Figure 48. Vent piston and shear pin.

Shearing of the pin occurs when this force causes the shear stress in the pin to exceed the material's shear strength.

$$F_s = \frac{\sigma_{us}\ \pi\ D_s^2}{4} \tag{74}$$

where D_s is the diameter of the shear pin, and σ_{us} is the ultimate shear stress of the material. Equating Equations 73 and 74 and solving for the pressure yield

$$P = \frac{\sigma_{us}\ D_s^2}{D_p^2} \tag{75}$$

which gives the pressure at which shearing of the pin will occur. The ultimate shear stress is given below. For the material chosen (Aluminum 6061-T6) these numbers are

	Strength (psi)	Approximate Shear Strength (psi)
Yield	40,000	20,000
Ultimate Tensile	45,000	33,750

Using Equation 75 the pressure is then

$$P = 33750 \cdot \frac{(0.032)^2}{(0.250)^2} = 553 \text{ psi} \tag{76}$$

The nominal tank pressure is 2870 psi. Shearing of the pin will occur by a margin of 5.2.

Next make sure that the pin will not shear prematurely due to environmental loading. The force on the piston is simply its mass times the acceleration, where the mass is

$$m = \pi \frac{D_p^{\ 2}}{4}\ L_p\ \rho \tag{77}$$

where L_p is the length of the piston. For our values,

$$m = \frac{\pi(250)^2}{4}(0.375)(0.0975) = 0.0179 \text{ lb}$$

and the acceleration of 12 g gives a force of 0.215 lb. This results in a shear stress in the pin of

$$\sigma = \frac{0.215 \text{ lb}}{\frac{\pi}{4}(0.032)^2 \text{ in}^2} = 267 \text{ psi} \qquad (79)$$

making a safety factor of 20,000/223 or 75 (based on yield shear stress).

3.2.2.7 Inflation Rates. An analytical model was developed for the ITSAT program which calculates the dynamics of the inflation. Included in this model are flow rate calculations and calculations for the deployment dynamics (acceleration, velocity, etc.). This section details the setup of the theoretical model and presents results of the current ITSAT design.

The ITSAT inflation system is shown in Figure 43. Upon initiation, the first puncture cutter is activated, puncturing the diaphragm. Gas then travels through a low flow rate restrictor and then to the structural tubes. The restrictor prevents the structure from inflating too quickly, which could lead to high accelerations and stresses on the tubes and blanket. After the structure is fully deployed, a second diaphragm is punctured, and flow then flows through a high flow rate restrictor. This allows the structure to reach rigidization pressure in a reasonable time. The analytical model equations model two phenomena; the flow through the restrictors and the dynamic motion of the structure. Each section is presented.

The restrictors used for ITSAT are purchased items. Referring to Figure 49

$$Q = 3.06 \times C \times F \times P1/(\text{LOHMS} \times \text{SQRT}(T1)) \qquad (80)$$

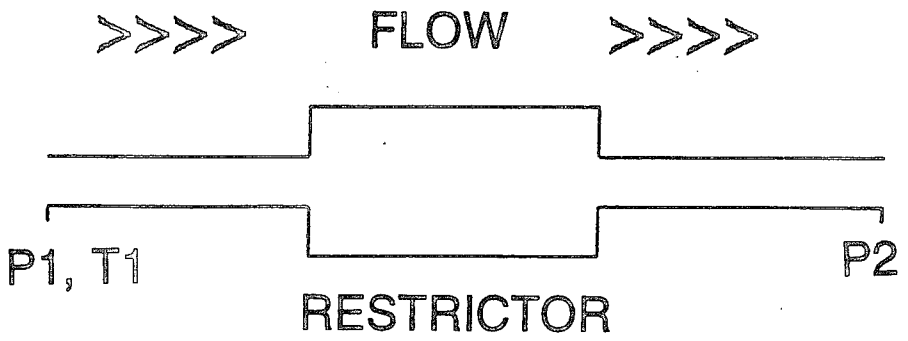

Figure 49. Flow through restrictor.

where

Q	=	Flow rate in standard liters/minute
C	=	Gas correction factor = 224 for Nitrogen
F	=	Pressure ratio factor
P1	=	Upstream pressure in Kilopascals
LOHMS	=	Lohm rate for a single orifice restrictor
T1	=	Upstream temperature in degrees Kelvin

$$F = 3.86\sqrt{\left(\frac{P_2}{P_1}\right)^{1.429} - \left(\frac{P_2}{P_1}\right)^{1.714}} \quad \text{for } \frac{P_1}{P_2} - 1 < 1 \tag{81}$$

$$F = 1.0 \quad \text{for } \frac{P_1}{P_2} - 1 > 1 \tag{82}$$

To convert the following rate into kilograms per second:

$$FLOW = Q * FAC/(60.*1000) \tag{83}$$

where

FAC = 1.185 g per standard liter for Nitrogen

The flow rate model used in the ITSAT inflation model was supplied by the flow restrictor manufacturer. This model has been validated by the manufacturer during its 40-year history in designing and developing miniature fluid control components for aerospace and other industries. The manufacturer developed the equations used in the ITSAT model from laboratory testing and computer modeling of flow-fields, pressure distributions, flow forces, and stability and transient responses.

These equations give the flow rate through the restrictor. Using a finite difference approximation and the Ideal Gas Law, the new pressures can be determined.

NEW MASS IN TANK = OLD MASS IN TANK - (FLOW RATE * TIME INCREMENT) (84)

NEW MASS IN BLANKET = OLD MASS + (FLOW RATE * TIME INCREMENT) (85)

NEW PRESSURE = NEW MASS * GAS CONSTANT * TEMP/VOLUME (86)

The above equations do not account for losses due to other flow restrictions such as bends in tubing, boundary layer losses in the tubing, or puncture cutter orifice losses. These losses will decrease the flow rate, which will influence the deployment characteristics and the pressurization profile. However, the time to deploy and time to inflate are not critical for ITSAT; in fact, the goal is for a slow deployment and subsequent inflation. Therefore, disregarding losses will give a worst-case scenario. If the blanket survives worst-case, the actual deployment will also be survivable.

The solar blanket and tubes are deployed by the pressure force acting on the tubes. The force acting on the tubes can be described as

FORCE = CRED * PRESSURE * AREA + SPRING FORCE (87)

where

FORCE	=	force acting to deploy blanket
CRED	=	force reduction coefficient (described below)
PRESSURE	=	pressure in the tubes
AREA	=	cross-sectional area of tubes (where pressure force is acting)
SPRING FORCE	=	term which represents "springiness" of tube material

The force acts on the mass on the blanket that has not been deployed.

$$MASS = BLKMAS * [1 - (BLKLEN/BLKLNF)] + BLKZ \quad (88)$$

where

MASS	=	mass of blanket under force
BLKMAS	=	total mass of blanket minus the lid mass
BLKLEN	=	length of blanket deployed
BLKLNF	=	total length of blanket
BLKZ	=	mass of lid

Thus, when the blanket is stowed, the force acts on the total mass. When the blanket is fully deployed, the force only acts on the lid mass.

Knowing the force and the mass, the acceleration of the blanket can be calculated. Then, using a finite difference approximation, the velocity and position of the blanket can easily be determined. After solving for the new deployed distance, the tube volume must be increased to account for the newly deployed portion. Once this is determined, the process can be repeated.

Equation 87 contains a force reduction coefficient. This coefficient takes into account force losses from friction and the unfolding and expansion of the tubes as they deploy. Although approximate values of this coefficient can be discovered through theoretical analysis, the best

method to determine this coefficient is through testing. By matching theoretical results (with the correct force reduction coefficient) to test results, the model can then be used for future test predictions.

The ITSAT deployment model was initially correlated to the test results of a 5-ft tube deployed in L'Garde's vacuum chamber (Subsection 4.4.4). Figure 50 shows the match between test and theory for this case. The force reduction coefficient which produced this match was then used for full-scale tube deployment predictions. Although the correlation to test data is somewhat limited, the model was used for accurately predicting pressure profiles during the thermal vacuum test (Subsection 4.7.2).

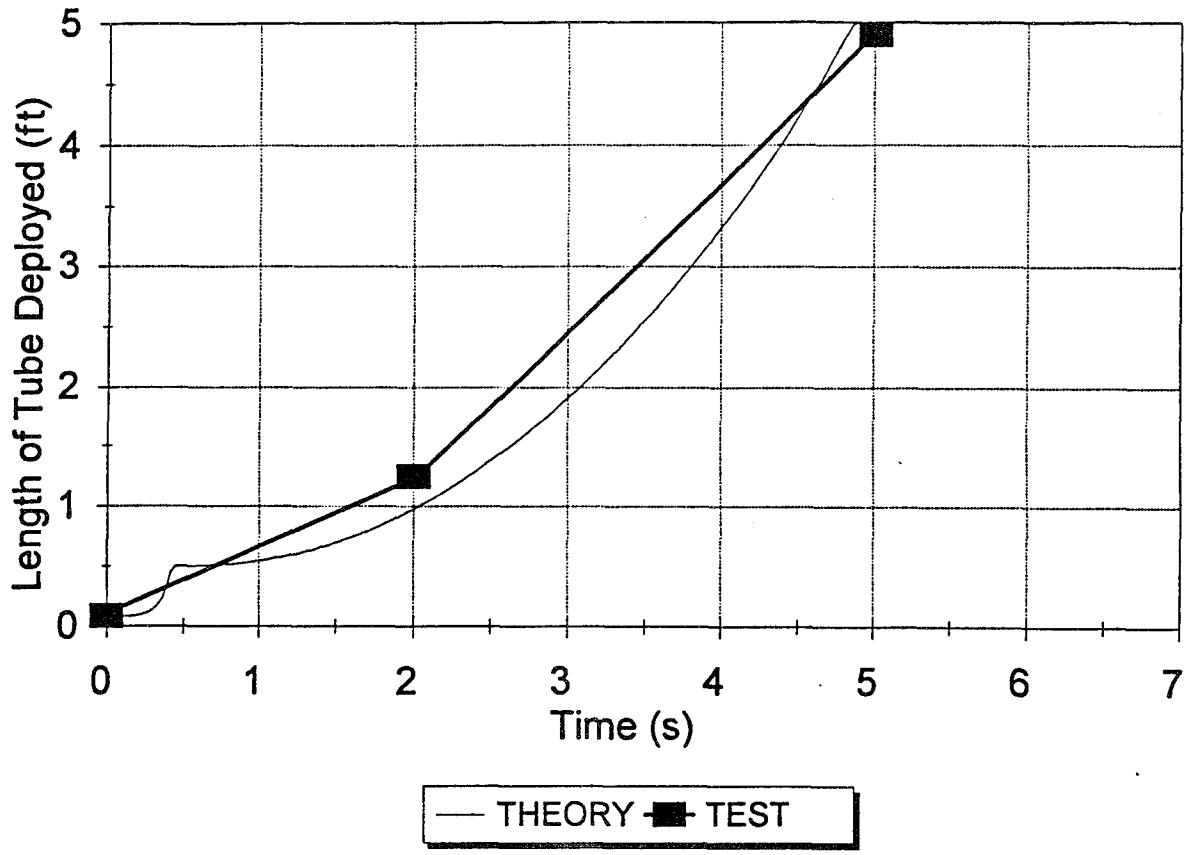

Figure 50. Correlation between theoretical model and 5-ft tube deployment test results.

The input parameters for the deployment simulation are shown in Figure 51. The corresponding deployment parameters (pressure, acceleration, velocity, position) are given in Figures 52 to 55. As can be seen from these figures, the blanket deploys in ~15 s and reaches full pressure in about 75 s. The maximum acceleration acting on the blanket is <13- f/s^2.

TANK PRESSURE IN PSI
2870.

TANK VOLUME IN IN^3
27.3

TANK TEMPERATURE IN DEGREES F
70

CATALOG VISCO JET #1 LOHM RATE
73000.

CATALOG VISCO JET #2 LOHM RATE
5000.

CROSS-SECTIONAL AREA OF BLANKET TUBES (BOTH) IN^2
25.1328

INITIAL LENGTH OF BLANKET (IN)
5.

FULLY DEPLOYED BLANKET LENGTH (IN)
139.73

TOTAL WEIGHT OF DEPLOYABLE STRUCTURE - END WT (LB)
3.5

TOTAL WEIGHT OF END STRUCTURE (LB)
0.7

Figure 51. Input parameters.

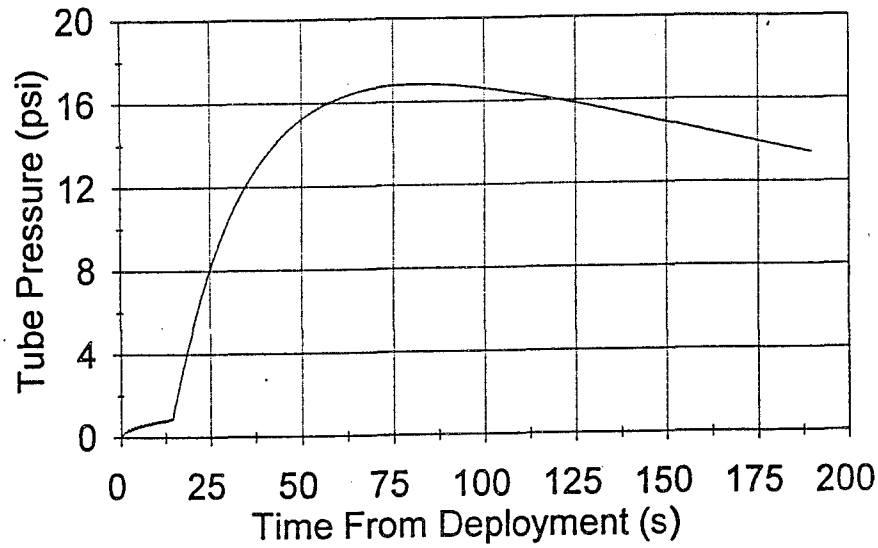

Figure 52. Tube pressure.

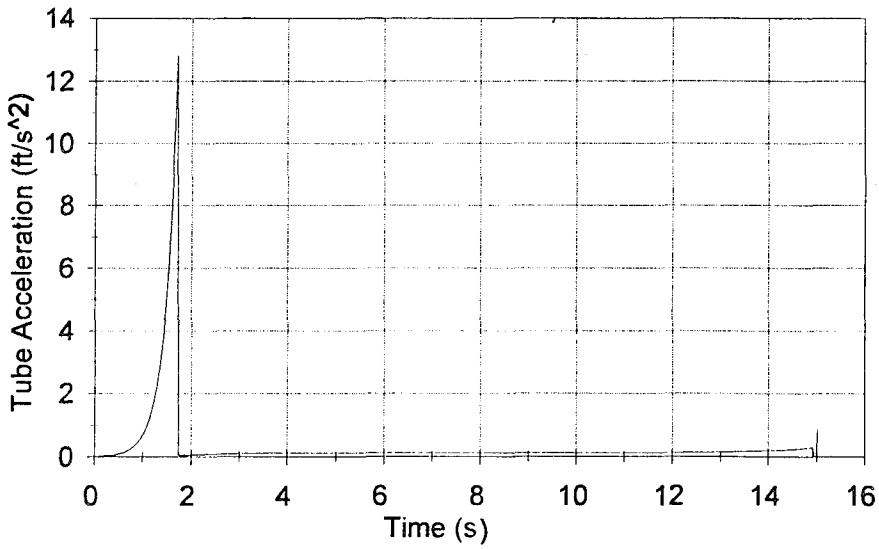

Figure 53. Blanket acceleration.

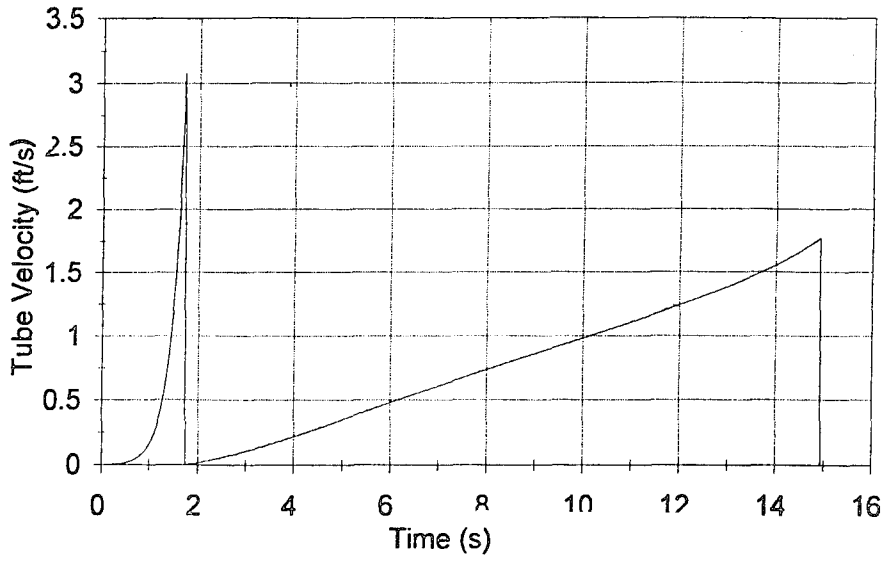

Figure 54. Blanket velocity.

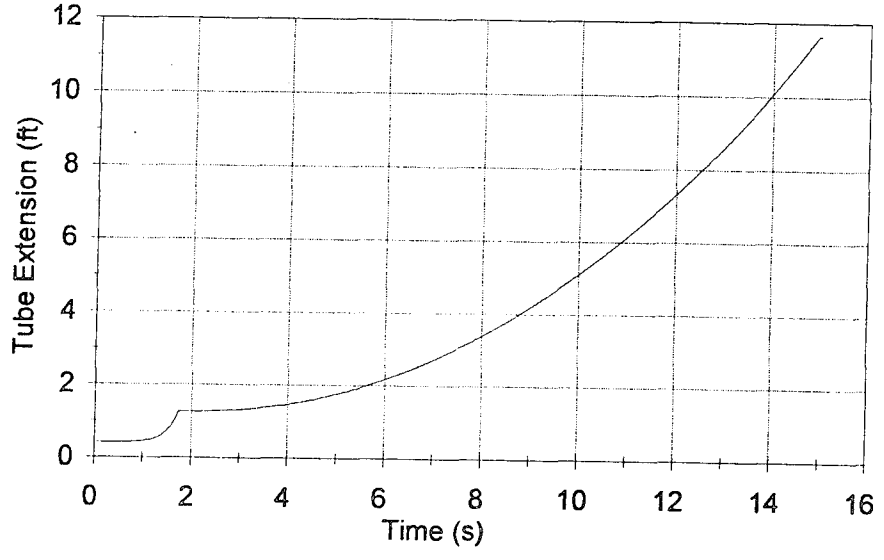

Figure 55. Extended blanket length.

3.2.3 Enclosure

The ITSAT system is enclosed in a rectangular box which contains the folded structural tubes, folded solar blanket, inflation system, and miscellaneous components. When deployed, the lid and housing act as two opposite sides of the rectangle which surrounds the solar blanket; the structural tubes form the other two sides.

The bare housing and lid from the ITSAT program are shown in Figure 56. These are constructed from vented Nomex honeycomb, encased on either side by 6-mil graphite-epoxy facesheets, making an extremely stiff and strong enclosure. The housing and lid are held together with two holddown cables located inward of the two tubes. The mounting for these is shown in Figure 57.

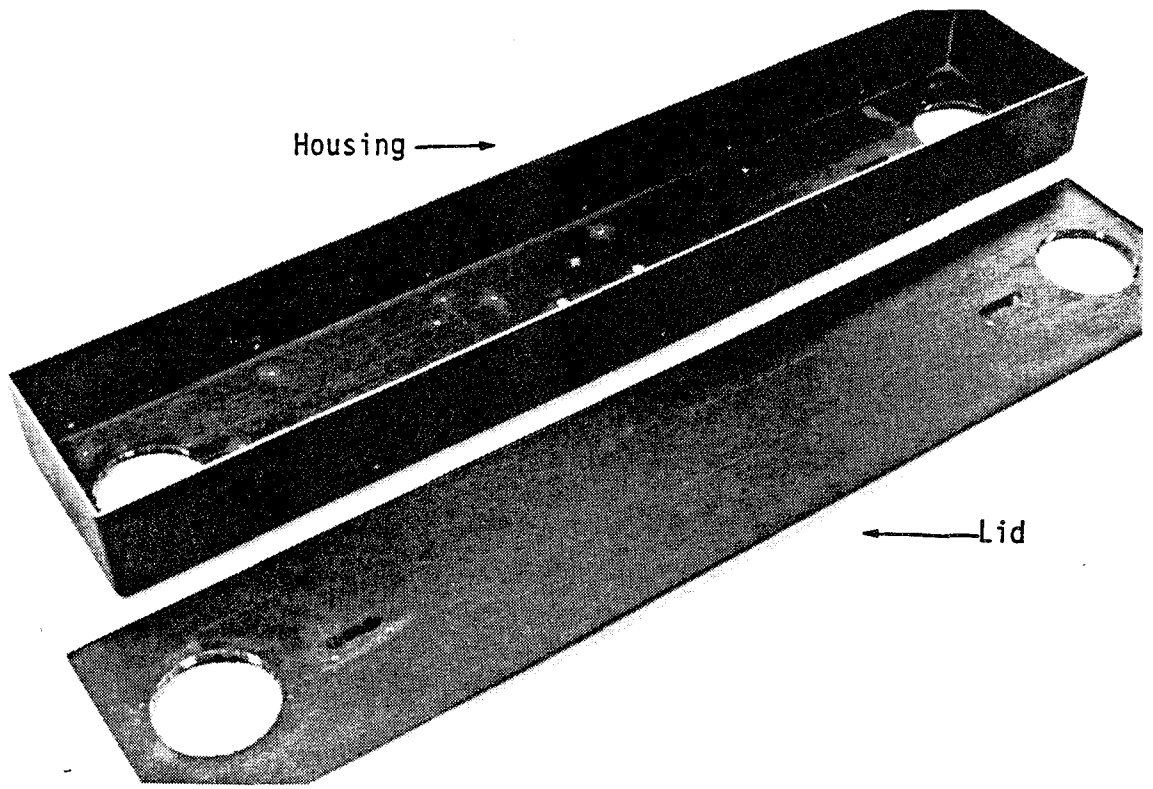

Figure 56. Housing and lid (ITSAT).

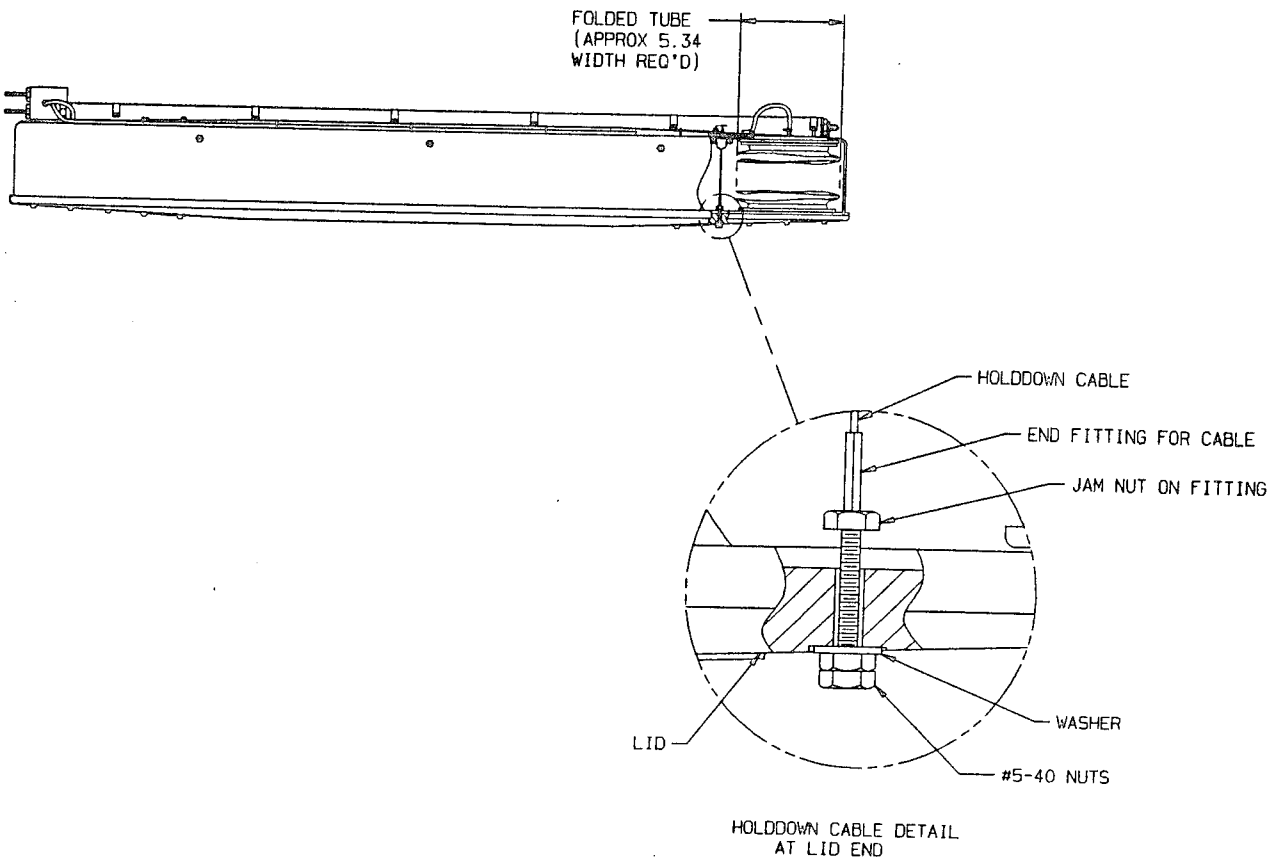

Figure 57. Holddown cable method.

A pyrotechnic cable cutter shears the cable to enable the lid to open. The Data Sheet for the cable cutters is shown in Figure 58.

3.2.3.1 Blanket Padding. When folded and stowed, the solar blanket and cells must be protected from the harsh launch environments. Interleaving pads protect the blanket panels from damage (Fig. 59). These are made from 0.25-in thick polyamide foam, covered by 0.5-mil Kapton® facesheets. The Kapton® protects the polyamide from UV damage. One-fourth inch thick pads of the same construction are also used at each end of the folded blanket. Figure 60 shows the housing end of the ITSAT solar array with the padding installed.

TECHNICAL DATA SHEET
HOLEX SERIES 5800 GUILLOTINES

DESCRIPTION

The HOLEX 5800 Series Guillotines were designed to incorporate the one amp-one watt No Fire characteristic in the versatile 2800 Series Guillotines. Additional handling safety is provided while retaining all the reliable operating characteristics of the 2800 Series. The 5800 Series Guillotines are classified as "Class C" Explosives and may be shipped by air or surface transport.

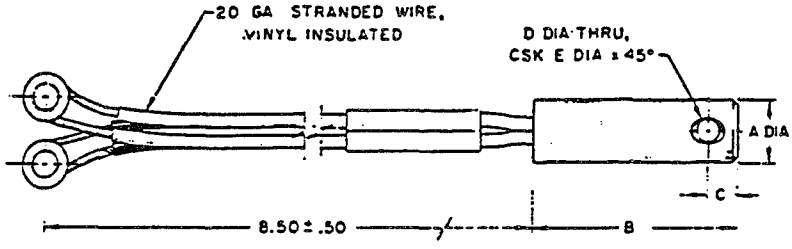

APPLICATION DATA

The 5800 series guillotines have been extensively tested for operation over a temperature range of −65°F to +160°F and are designed to meet most current military environmental specifications.

These guillotines will cut the following specific cables:
MODEL 5800—3/32 Dia 7 x 7 Cres Cable per MIL-C-5424
MODEL 5801—3/16 Dia 7 x 19 Cres Cable per MIL-C-5424
MODEL 5802—3/8 Dia 7 x 19 Cres Cable per MIL-C-5424
MODEL 5803—7/16 Dia 7 x 19 Cres Cable per MIL-C-5424
1/2 Dia 6 x 19 Galv Stl Commercial Cable

For applications involving other sizes and materials please contact HOLEX incorporated

HOLEX PART NO.	DIA A ± .005	DIM. B ± .035	DIM. C ± .025	DRILL D DIA	CSK E DIA	UNIT WT (OZ)
5800	.375	1.490	.200	#30 (.1285)	.188	7/8
5801	.500	2.01	.375	1/4 (.2500)	11/32	1
5802	.875	3.120	.870	7/16 (.4375)	5/8	3-1/2
5803	1.125	3.500	.800	9/16 (.5625)	7/8	6

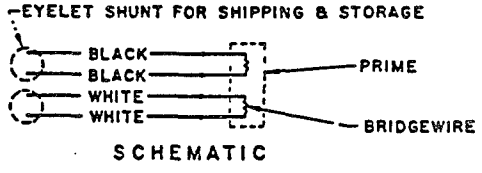

SCHEMATIC

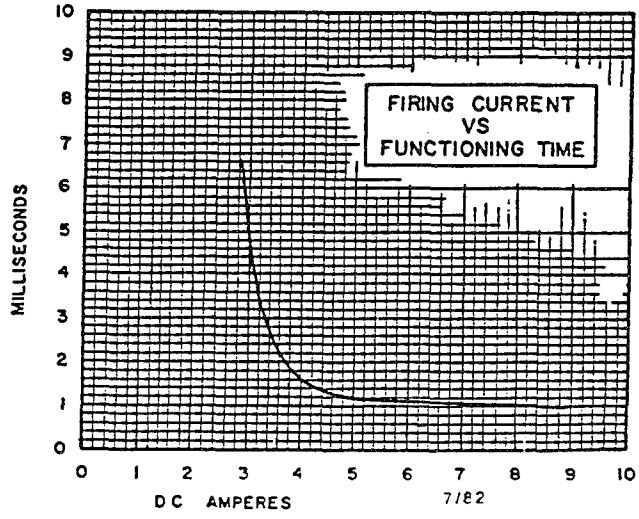

FIRING CHARACTERISTICS

NO-FIRE CURRENT — 1.0 AMP FOR 1 MINUTE
ALL-FIRE CURRENT — 4.5 AMPERES
RECOMMENDED ALL-FIRE CURRENT — 5.0 AMPERES
BRIDGEWIRE RESISTANCE — 1.0 ± 0.1 OHM
PIN-TO-CASE RESISTANCE — 2 MEGOHMS AT 500 VDC
PIN-TO-CASE NO-FIRE — 100 VAC RMS

Figure 58. Data sheet for ITSAT cable cutter.

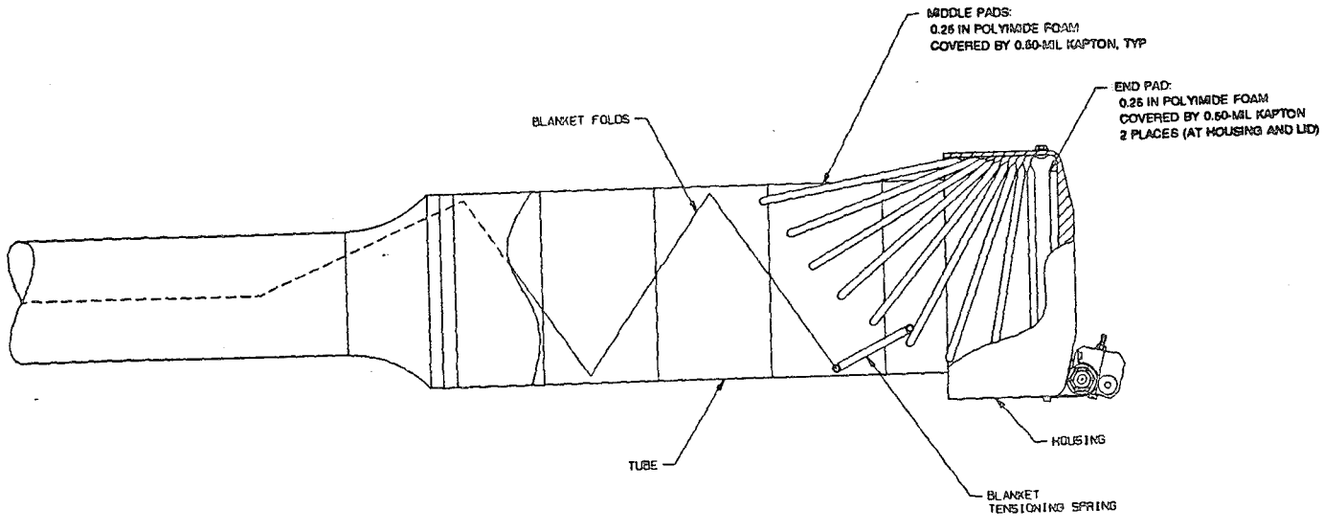

Figure 59. Blanket padding concept.

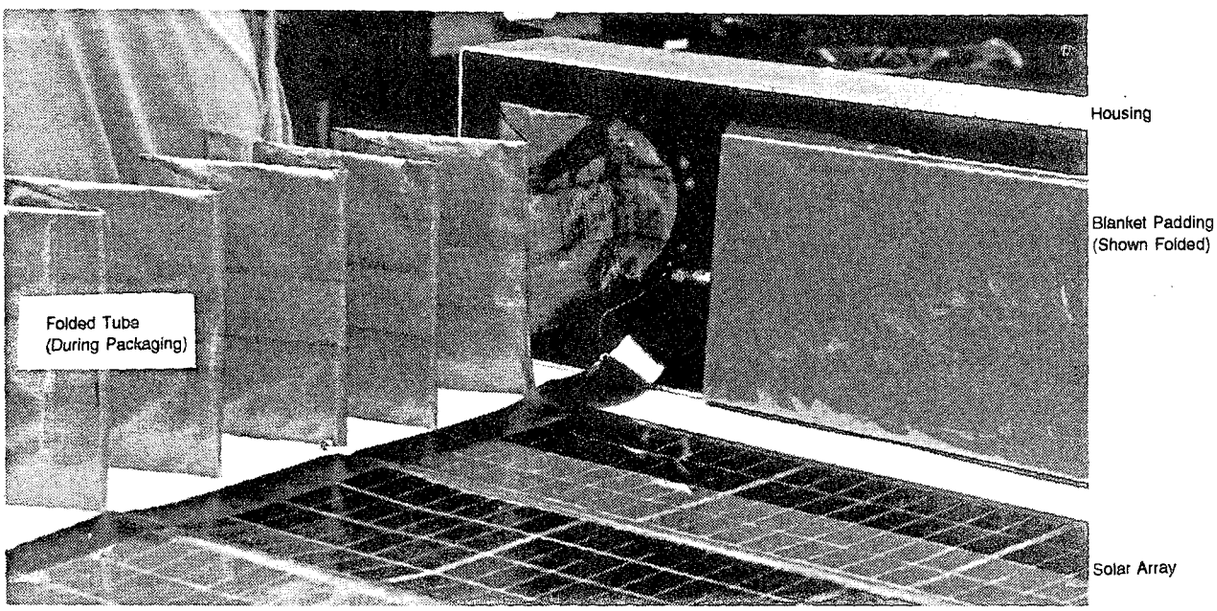

Figure 60. Blanket padding - ITSAT.

The force required to compress the foam layers was determined during packaging tests to be ~10 lb. In addition, the force required to compress each torus tube into the housing was determined empirically to be 10.3 lb. The packaged blanket and the folded tubes must be resisted entirely by the two holddown rods shown in a free body diagram in Figure 61.

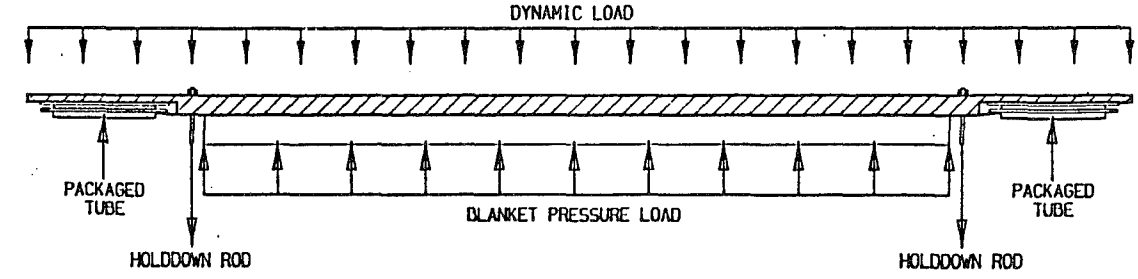

(a). Lid

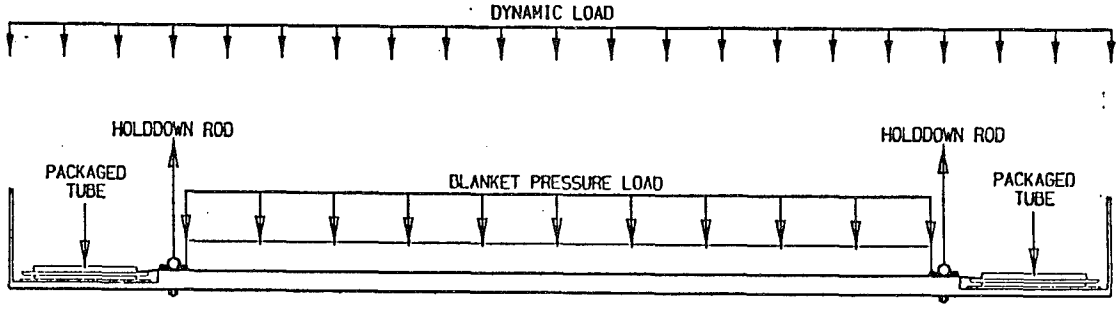

(b) Housing

Figure 61. Packaged forces.

The total static tensile load in each rod is then

$$\frac{10}{2} + 10.3 = 15.3 \text{ lb} \tag{89}$$

3.2.3.2 Housing. The housing can be analyzed as a beam, and only half of it needs analysis due to symmetry. The free body diagram is given in Figure 62. Both static forces and dynamic forces are analyzed at the same time. A summary of the loads is given in Table 19.

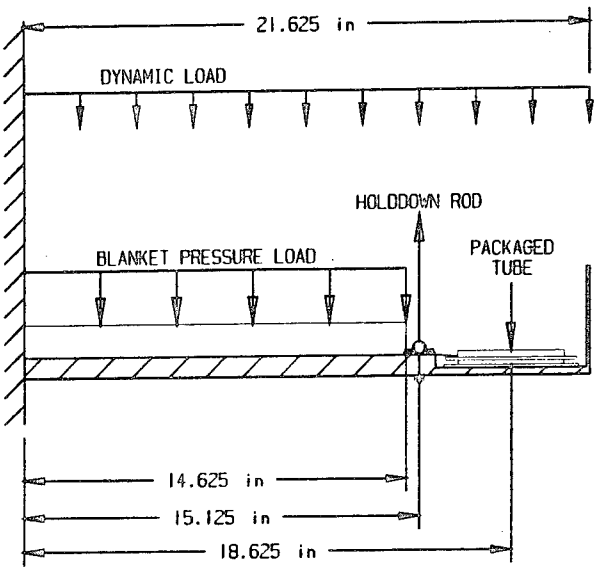

Figure 62. Free body diagram of housing.

Table 19. Loads on housing.

LOADINGS	TYPE	STATIC OR DYNAMIC	POSITION OF LOADING (in)	VALUE	UNITS
Blanket Pressure	Uniform	Static	0 to 14.625	0.342	lb/in
Holddown Rod	Point	Static	15.125	30.445	lb
Tube Package Pressure	Point	Static	18.625	10.300	lb
Inertial Loading	Uniform	Dynamic	0 to 21.625	2.826	lb/in

The uniform line load caused by the blanket is simply the areal force (10 lb) divided by its length (29.25 in) or 0.342 lb/in. A shear and moment diagram are drawn in Figure 63, where the maximum moment exists at mid-span with a value of 658 in/lb. The stress at this point is given by

$$\sigma = \frac{Mc}{I} \tag{90}$$

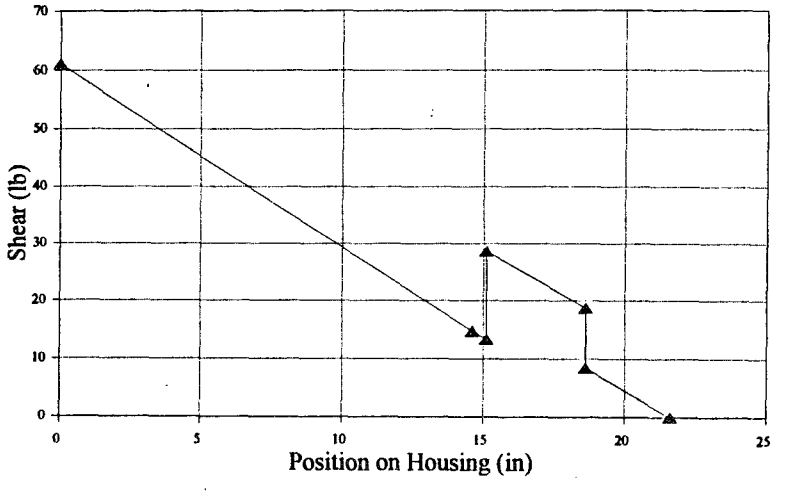

(a) Shear diagram.

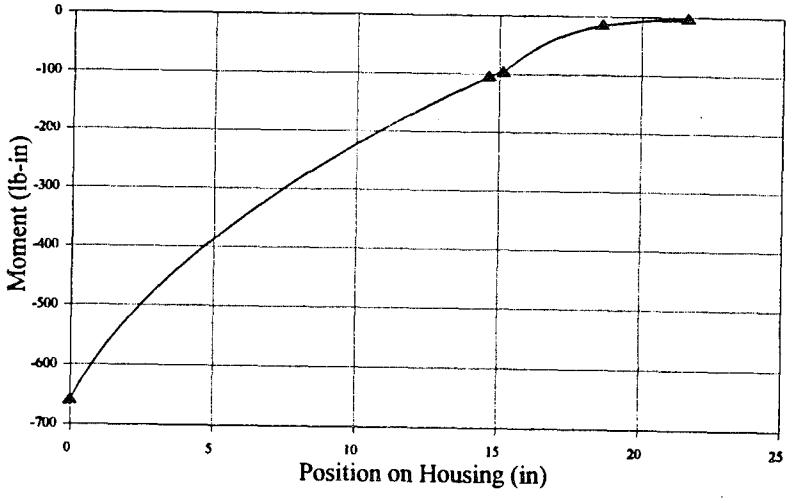

(b) Moment diagram.

Figure 63. Shear and moment diagrams of housing.

where the moment of inertia and distance to the outermost fiber are found by examining the cross section of the housing (Fig. 64).

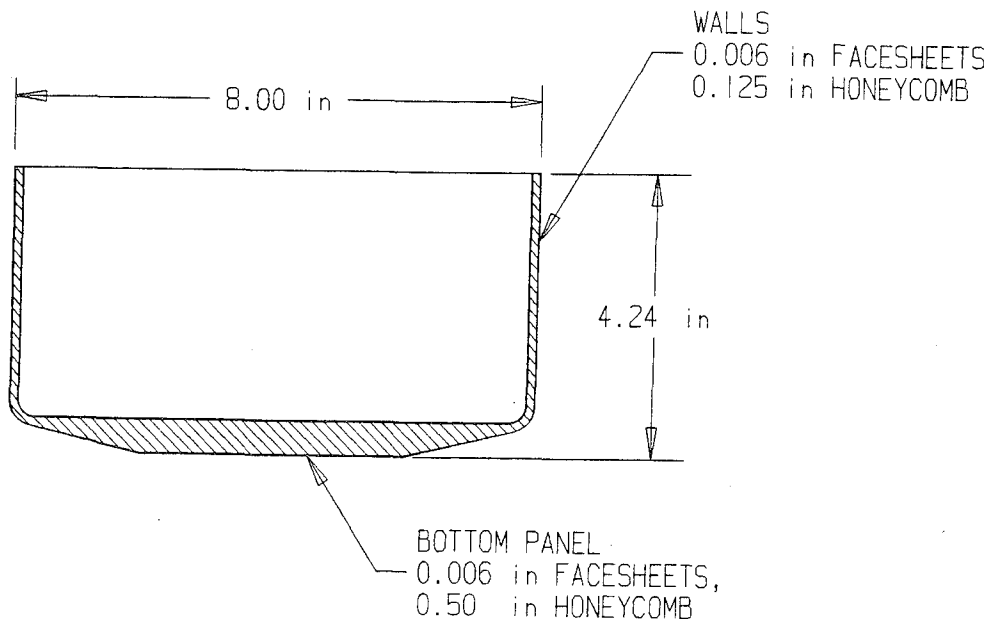

Figure 64. Cross-section of housing.

The section analysis is given in Table 20. For simplicity ignore the chamfers on either corner of the box and consider the entire bottom panel to be 0.5 in thick. The stress in the outermost fiber (at the rim of the box) is then

$$\sigma = \frac{(658)(2.961)}{0.318} = 6125 \text{ psi} \qquad (91)$$

which is below the compressive yield strength of the graphite/epoxy honeycomb (21,000 psi) by a safety factor of 3.43.

For deflection of the box, the principle of superposition and standard equations from Reference 15 are used. The result is given in Figure 65.

Table 20. Section analysis of housing.

	# OF SECTIONS	REDUCTION FACTOR DUE TO TAPERING	WIDTH, b (in)	HEIGHT, h (in)	HOLES IN SECTION (%)	CROSS SECTIONAL AREA (in^2)	MASS (lb)	Y BAR (in)	A * Y BAR (in^3)	OFFSET d (in)	MOI OF SECTION (in^4)
1) Bottom Skin	1	1	8.000	0.006	0	0.048	0.151	0.003	0.000	1.276	0.078
2) Core	1	0.75	8.000	0.500	0	0.000	0.135	0.000	0.000	0.000	0.000
3) Top Skin of Base	1	1	8.000	0.006	0	0.048	0.151	0.509	0.024	0.770	0.028
4) Inside Skin of Sides	2	1	0.006	3.728	0	0.045	0.141	2.376	0.106	1.097	0.106
5) Core of Sides	2	1	0.125	3.728	0	0.000	0.042	0.000	0.000	0.000	0.000
6) Outside Skin of Sides	2	1	0.006	3.728	0	0.045	0.141	2.376	0.106	1.097	0.106
7) Bead at Top	2	1	0.000	0.000	0	0.000	0.000	4.240	0.000	2.961	0.000
Totals				4.24		0.185	0.761		0.237		0.318

Total Y bar = 1.279 in
Distance to outermost fiber, c = 2.961 in

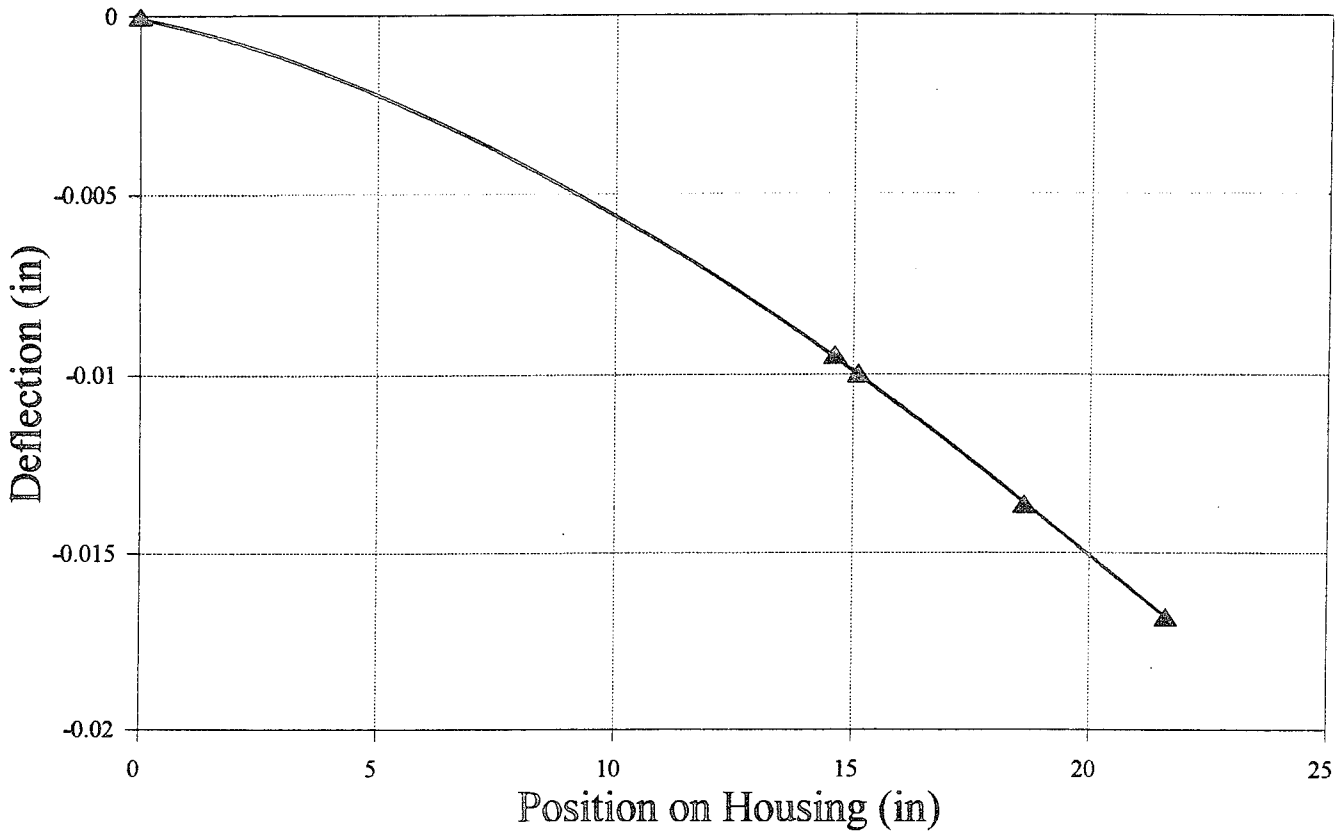

Figure 65. Deflection of housing.

The mass of the housing listed in Table 20 does not include (1) foam potting around all holes, (2) foam potting around the rim, and (3) threaded inserts. By adding all these components, the total housing mass is 1.22 lb.

The ITSAT assembly must not resonate at a frequency near the natural frequencies of the spacecraft. Natural modes of vibration below 50 Hz are most damaging; this analysis shows that the fundamental (or lowest) frequency of the housing alone is 105 Hz. The stiffening effects of adding the lid, inflatant tank, and other miscellaneous components will increase the frequency even higher.

By inspection, the lowest mode will be looking at the long side of the housing, with the mounting flange at the center. By symmetry, only half of the housing needs to be analyzed.

This is similar to the previous method of stress calculation. (See Fig. 62 where the center of the housing can be considered to be attached to a "wall".) The solution of the natural frequency for this type of clamped-free beam has been performed in Reference 17; only the results will be presented here. The natural frequencies are given by

$$\omega_n = (\beta_n l)^2 \sqrt{\frac{EIg_c}{\rho l^4}} \tag{92}$$

where the number β_n depends on the boundary conditions of the problem. For the cantilever case

$$(\beta_1 l)^2 = 3.52$$

$$(\beta_2 l)^2 = 22.0$$

$$(\beta_3 l)^2 = 61.7 \tag{93}$$

E, I, and l have been discussed previously and ρ is the mass per unit length:

$$\rho = \frac{10.18\ lb_m}{43.25\ in} = 0.235\ lb_m/in \tag{94}$$

The first mode natural frequency is then given by

$$\omega_1 = (3.52)\sqrt{\frac{(14,800,000)(0.318)(386)}{(0.235)(21.62)^4}} = 662\ \frac{rad}{s} \tag{95}$$

or 105 Hz. The second and third natural frequencies are found similarly:

ω_2 = 658 Hz

ω_3 = 1845 Hz

3.2.3.3. Lid. The lid is constructed similarly to the housing (honeycomb w/facesheets) shown in Figure 56. As with the housing, the ends are tapered to lighten it up. There are small flanges that overhang the housing on all sides. The lid can also be modeled as half of a simple beam. The loading is given in Figure 66.

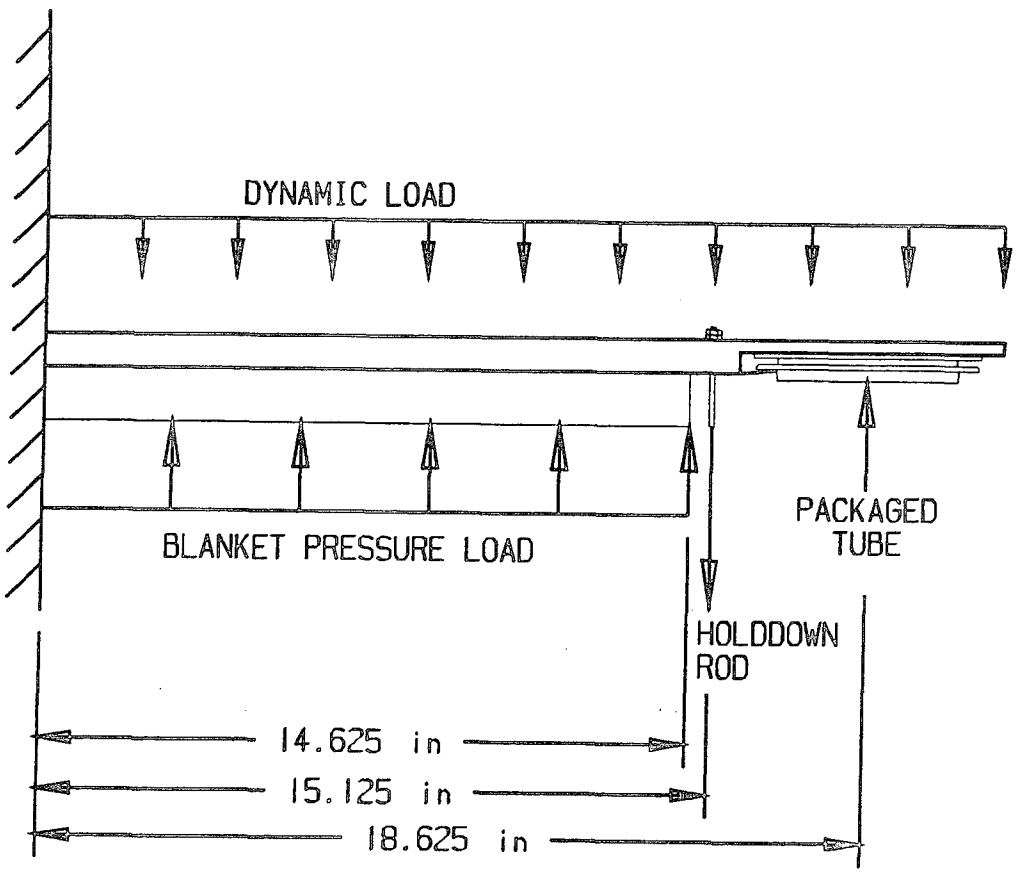

Figure 66. Free body diagram of lid.

Both static forces and dynamic forces are analyzed at the same time. A summary of the loads is given in Table 21.

Table 21. Loads on lid.

LOADINGS	TYPE	STATIC OR DYNAMIC	POSITION OF LOADING (in)	VALUE	UNITS
Blanket Pressure	Uniform	Static	0 to 14.625	0.342	lb/in
Holddown Rod	Point	Static	15.125	15.300	lb
Tube Package Pressure	Point	Static	18.625	10.300	lb
Inertial Loading	Uniform	Dynamic	0 to 21.625	1.352	lb/in

This is almost the same as the loading for the housing except for the inertial loading value. For the case of the lid, the inertial force due to the mass of the housing and inflatant tank can be removed since these are fixed to the spacecraft.

A shear and moment diagram are drawn in Figure 67 where the maximum moment occurs at mid-span with a value of 319 in-lb. The stress here is given by Mc/I. As with the housing, the cross-sectional moment of inertia of the lid must be determined. The section analysis of the lid is given in Table 22.

The stress in the outermost fiber (at the bottom of the lid facing the solar array) is then

$$\sigma = \frac{(319)(0.384)}{0.0235} = 8475 \text{ psi} \qquad (96)$$

As with the housing, this is below the compressive yield strength of the graphite/epoxy honeycomb (21,000 psi) by a factor of 2.48.

For deflection of the lid, the principle of superposition is again used. The results are given in Figure 68. Equations are similar to those used for the housing.

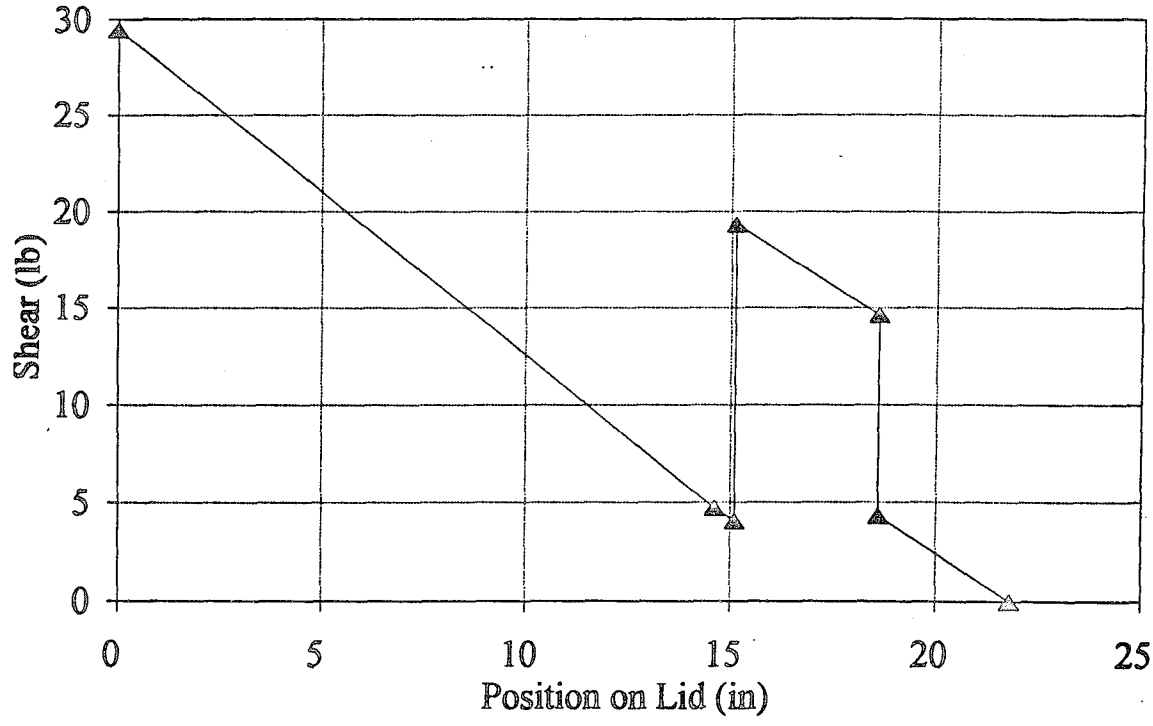

(a). Shear diagram.

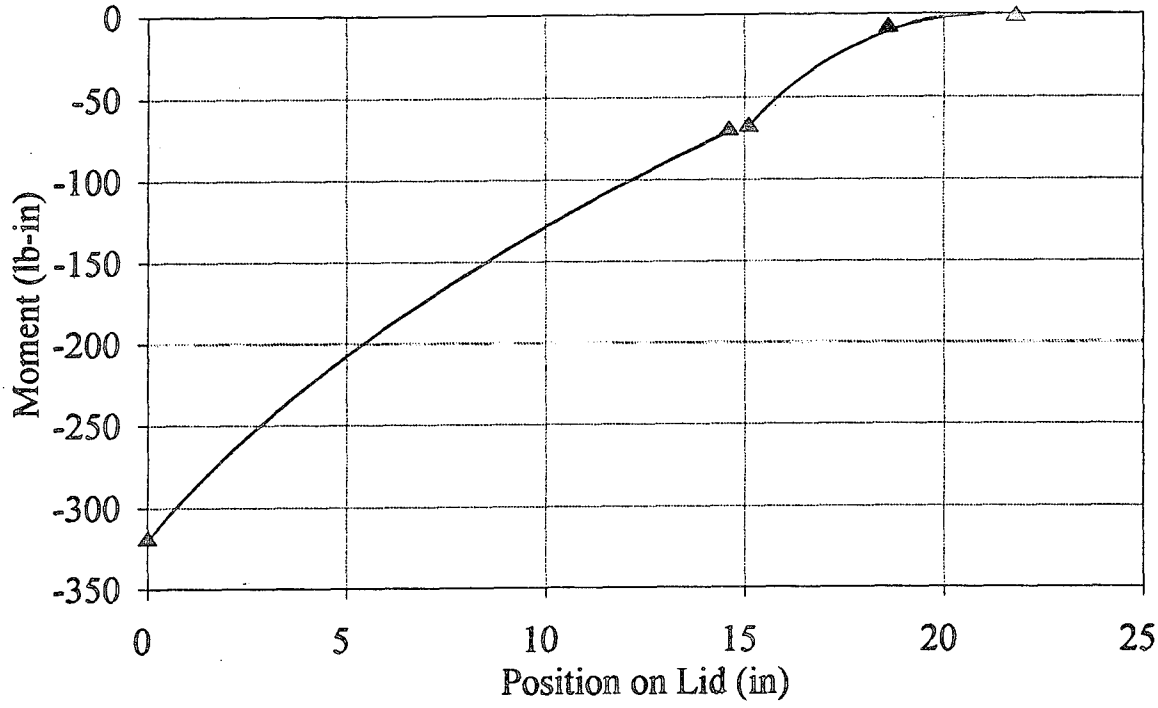

(b). Moment diagram.

Figure 67. Shear and moment diagrams of lid.

Table 22. Section analysis of lid.

	# OF SECTIONS	REDUCTION FACTOR DUE TO TAPERING	WIDTH, b (in)	HEIGHT, h (in)	HOLES IN SECTION (%)	CROSS SECTIONAL AREA (in^2)	MASS (lb)	Y BAR (in)	A * Y BAR (in^3)	OFFSET d (in)	MOI OF SECTION (in^4)
1) Top Skin	1	1.000	8.375	0.006	0	0.050	0.160	0.003	0.000	0.375	0.007
2) Core	1	0.667	8.375	0.750	0	0.000	0.190	0.000	0.000	0.000	0.000
3) Bottom Skin	1	1.000	8.375	0.006	0	0.050	0.160	0.759	0.038	0.381	0.007
4) Sides & Flange	2	1.000	0.006	0.375	0	0.005	0.014	0.313	0.001	0.066	0.000
Totals				0.762		0.105	0.524		0.040		0.01443

Total Y bar 0.3781 in
Distance to outermost Fiber, c = 0.3839 in

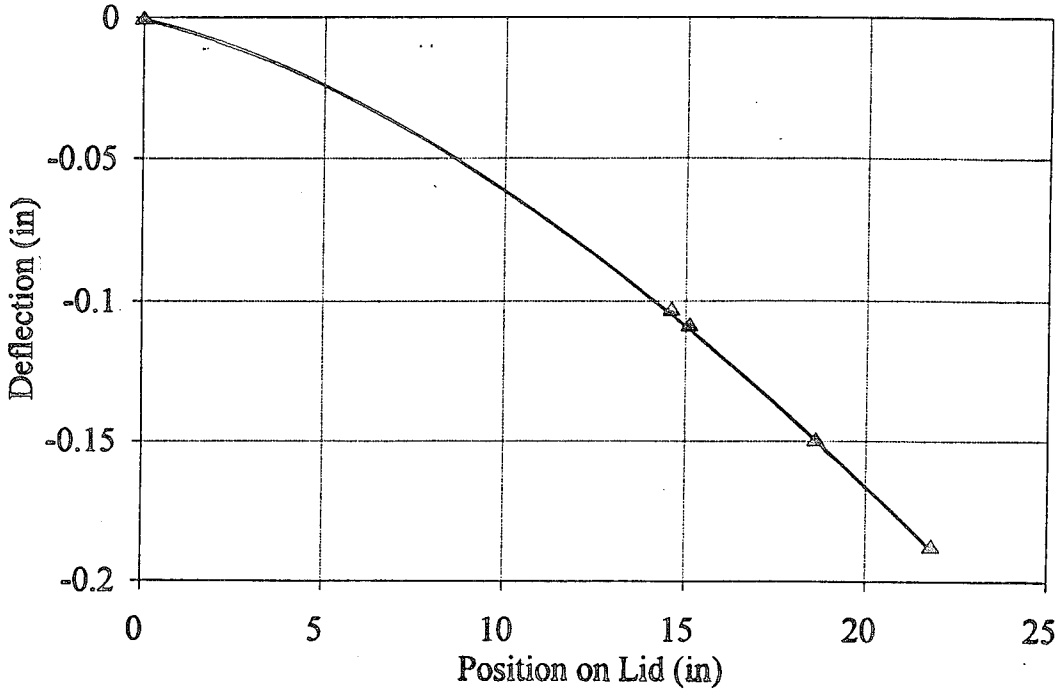

Figure 68. Deflection of lid.

The materials for the lid are the same as for the housing, and a complete summary is given in Table 22. With the potting and inserts added in, the total mass is 0.626 lb.

3.3 SOLAR BLANKET

3.3.1 Overall Description

The ITSAT solar blanket is shown in Figure 69. Thin crystalline silicon solar cells are bonded to a flexible Kapton® film substrate. The substrate is coated with SiOx to resist AO degradation in the LEO environment as discussed in Subsection 3.2.1.

The blanket layout is given in Figure 70. The blanket consists of six individual solar panel assemblies, each of which has three subpanels with foldlines between them for packaging. The panels are connected together with graphite epoxy hinge pins with eyelets on the side of the pins for attachment to the tubes.

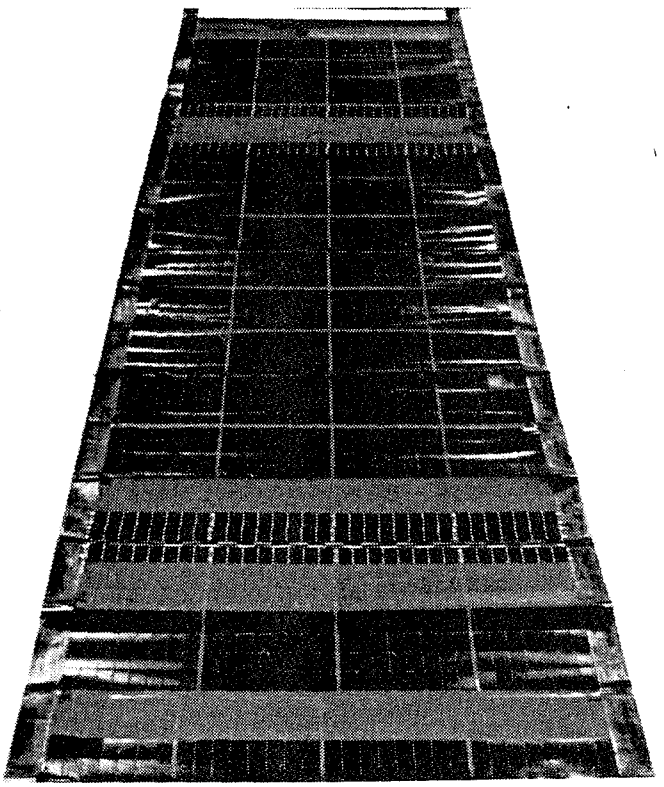

Figure 69. The ITSAT solar blanket.

The blanket is separated into six subpanels for ease of manufacturing. These smaller sections can be more easily assembled and in the event of major breakage of the cells during handling (i.e., enough breakage to warrant panel replacement rather than individual cell replacement), it is possible to replace one panel rather than the entire blanket.

Each subpanel consists of 4 rows of 31 cells connected in series. Each string in the current design is separated electrically, although later designs could use multiple strings to increase the output voltage. At either end of the string, the output power is routed back to the satellite via two flat cable wiring harnesses.

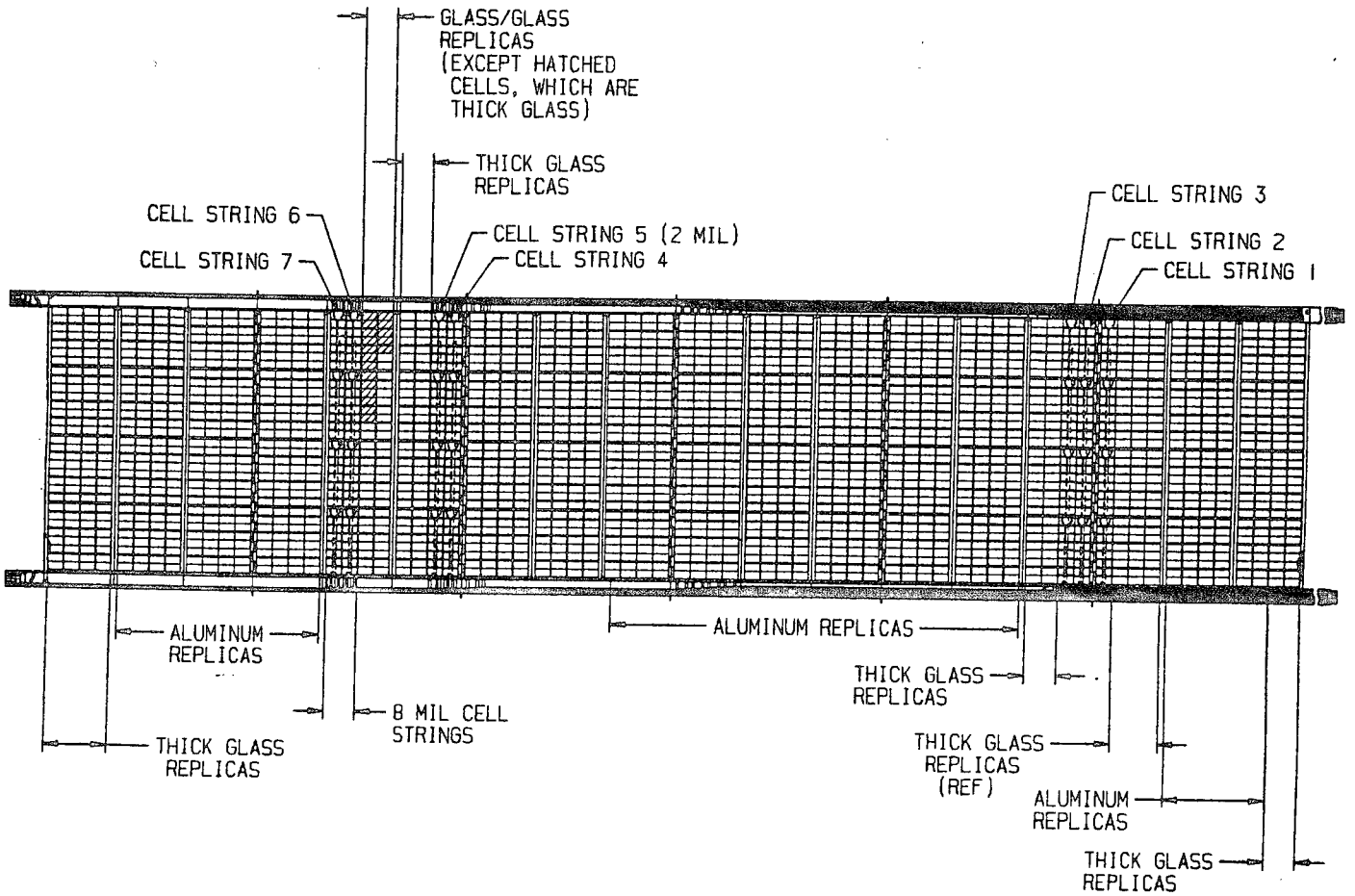

Figure 70. Solar blanket layout.

3.3.2 Cell Types Used

As a cost saving measure, the blanket is only partially populated by working solar cells (7 strings or about 10 percent). While thin silicon cells (2.2-mil) were desired for the blanket, it was prohibitive to populate even 10 percent with these cells. Instead, only one string was made up of 2.2-mil cells, while the other six working strings were 8-mil cells. All solar cells were purchased from Applied Solar Energy Corporation (ASEC). The other 90 percent of the blanket was populated with various simulated solar cells. A summary of the cells and the simulators is given in Table 23.

Table 23. Solar blanket population summary.

TYPE	THICKNESS (mils)	COVER GLASS THICKNESS (mils)	NUMBER ON BLANKET	PERCENTAGE OF TOTAL	PURPOSE
Silicon Solar Cell	8	2.9	186	8.3%	Actual Cell
Silicon Solar Cell	2.2	2.9	31	1.4%	Actual Cell
Glass Simulator	6	---	421	18.9%	Fragility, Mass Simulator
Two Ply Glass/	2.9	2.9	44	2.0%	Fragility, Mass Simulator
Glass Simulator	----	---	-----	------	-----
Aluminum Simulator	6	---	1550	69.4%	Mass Simulator
TOTAL			2232	100%	

3.3.3 Resistance Temperature Devices (RTDs)

Resistance Temperature Devices are mounted on the back side of 14 of the working solar cells (Fig. 71). These are used to monitor the temperature of the cell during electrical testing, for general information during the qualification testing at NRL and for flight testing.

3.3.4 Bypass Diodes

Bypass diodes were included on the blanket to protect the blanket from cell damage and partial shading. The 31-cell string was divided into 4 substrings (3 substrings of 8 cells each, and 1 substring of 7 cells). L'Garde investigated using flat diodes (Ref. 18) and while this method of packaging would lead to a more compact folded blanket, these types of diodes were not available from any sources. Figure 72 shows a "simulated" flat diode and how it would be incorporated on the solar blanket.

(P) A conventional round diode was used instead. This is shown in Figure 73. Etched copper strips were bonded to the back side of the blanket to provide the bypass circuit (Fig. 71).

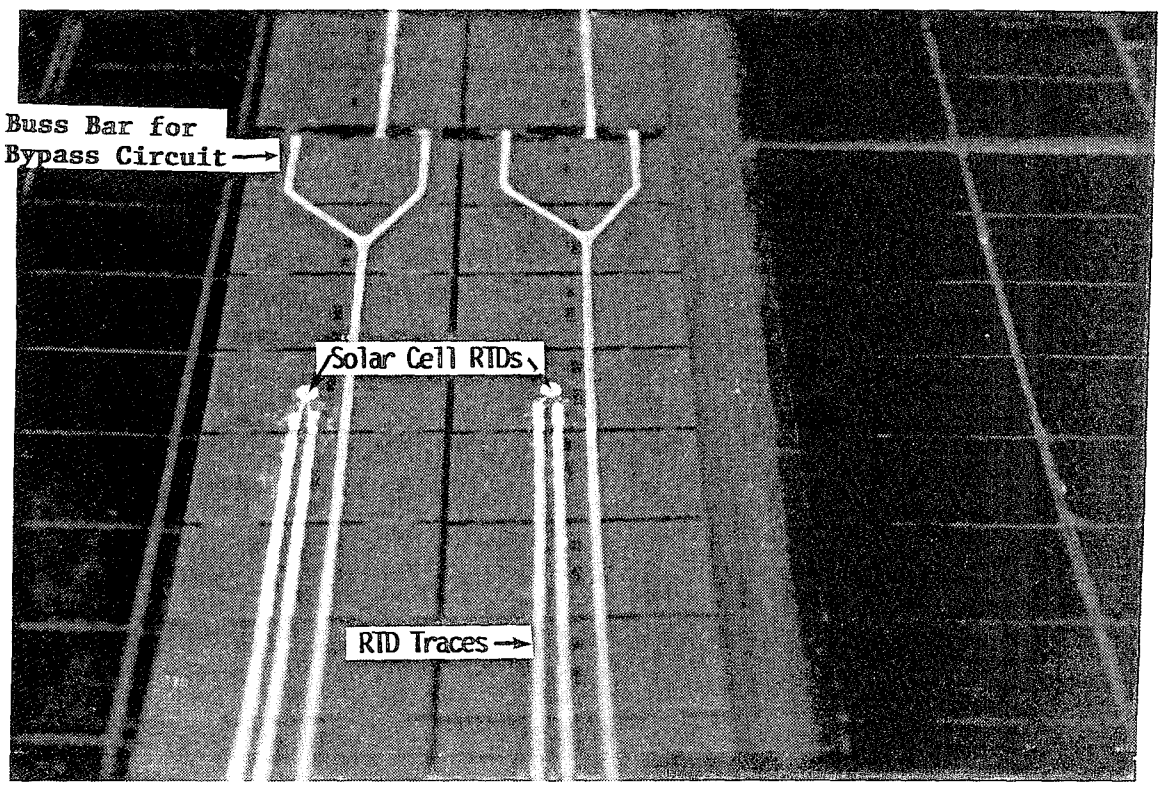

Figure 71. (P) The RTD and bypass circuits for diodes.

3.3.5 Wiring Harness

Flat cables run down each side of the blanket to route the power from the solar cell strings back to the housing (Fig. 74). The wiring harness is folded at each solar blanket hinge as shown in Figure 75. The harness is slightly longer than the solar blanket to keep the harness from taking any load when the blanket is tensioned.

The copper conductors used in the ITSAT design were sized so that only a maximum of 2.3 percent power is lost through the longest conductor.

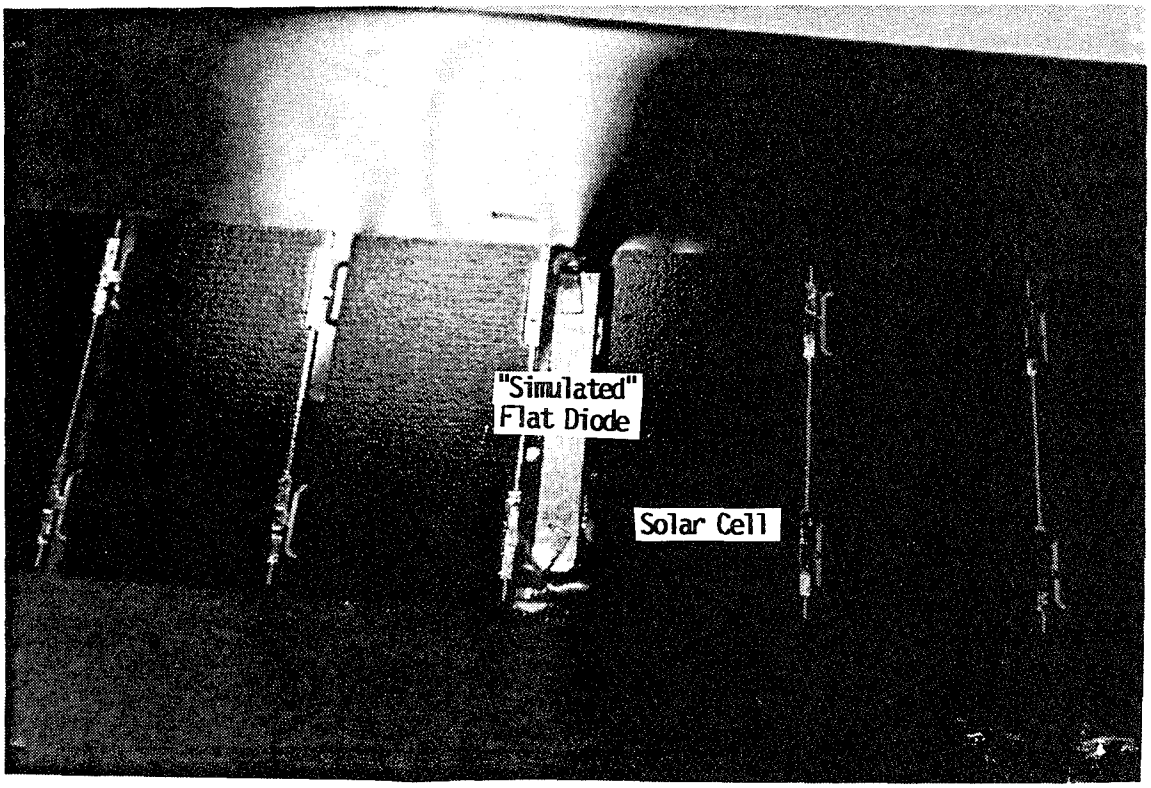

Figure 72. Flat diode on blanket.

3.3.6 Substrate Material

The solar cells are bonded to a flexible film substrate. The material is a Kapton® sheet coated with SiOx to resist AO degradation in the LEO specified in Table 1.

The film is coated on both sides with SiOx to provide a pinhole and crack-free coat with a specified surface resistance. The surface resistivity must be high enough to avoid excessive current leakage through the blanket surface. On rigid solar panels (where Kapton® is present only for its insulating properties) a coating is unnecessary, and the bare Kapton® provides good insulation allowing very little possibility of current leakage.

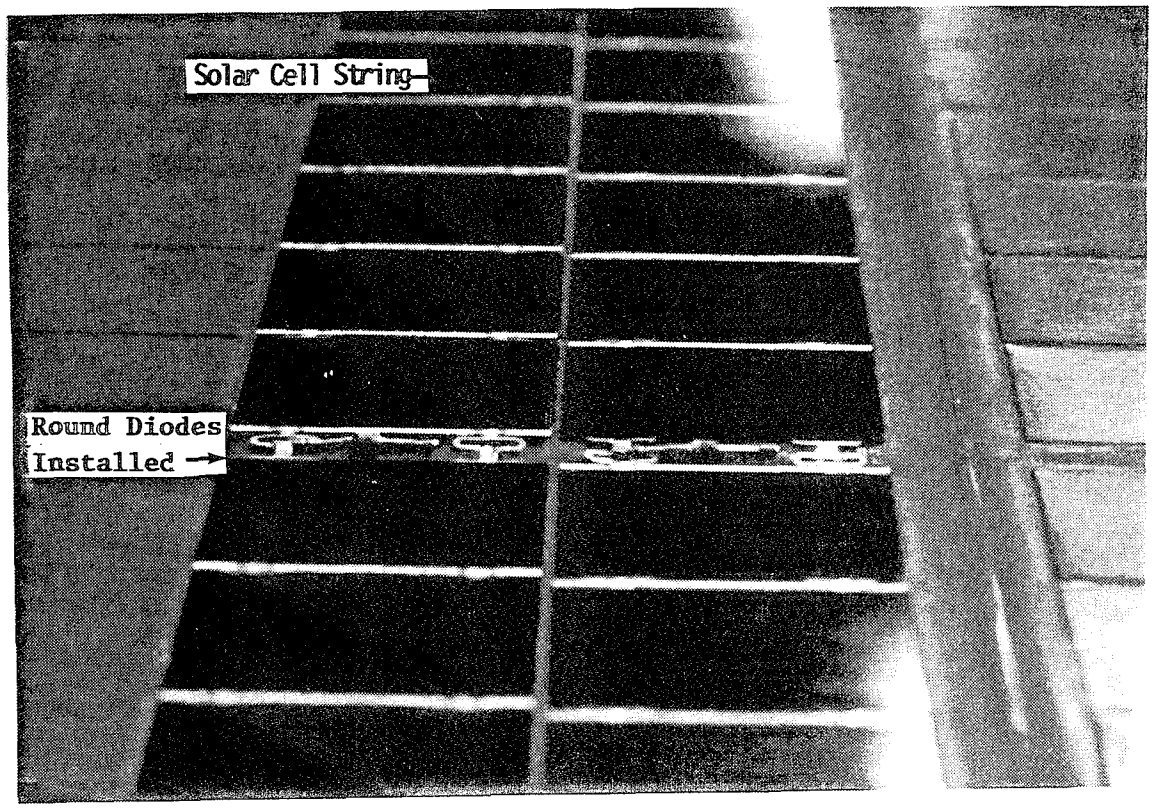

Figure 73. (P) Bypass diodes.

The ITSAT array is of the flexible blanket type. The substrate material is under tension to reduce billowing of the blanket during satellite maneuvers. Therefore, it is essential that the substrate maintain its structural strength during the entire mission. The coating must provide a good resistivity to reduce the current paths and must not reduce the tensile strength of the Kapton®.

Problem: Knowing the resistivity of the surface, the voltage difference between adjacent cells, and the distance between the cells; find the loss of power due to surface conductance.

Solution: Refer to Figure 76 which gives the parameters mentioned above. The maximum loss will be between cells of adjacent strings due to the higher voltage difference between them. While no requirement exists, the customary standard is to limit the surface conductance losses to 0.1 percent of the total power.

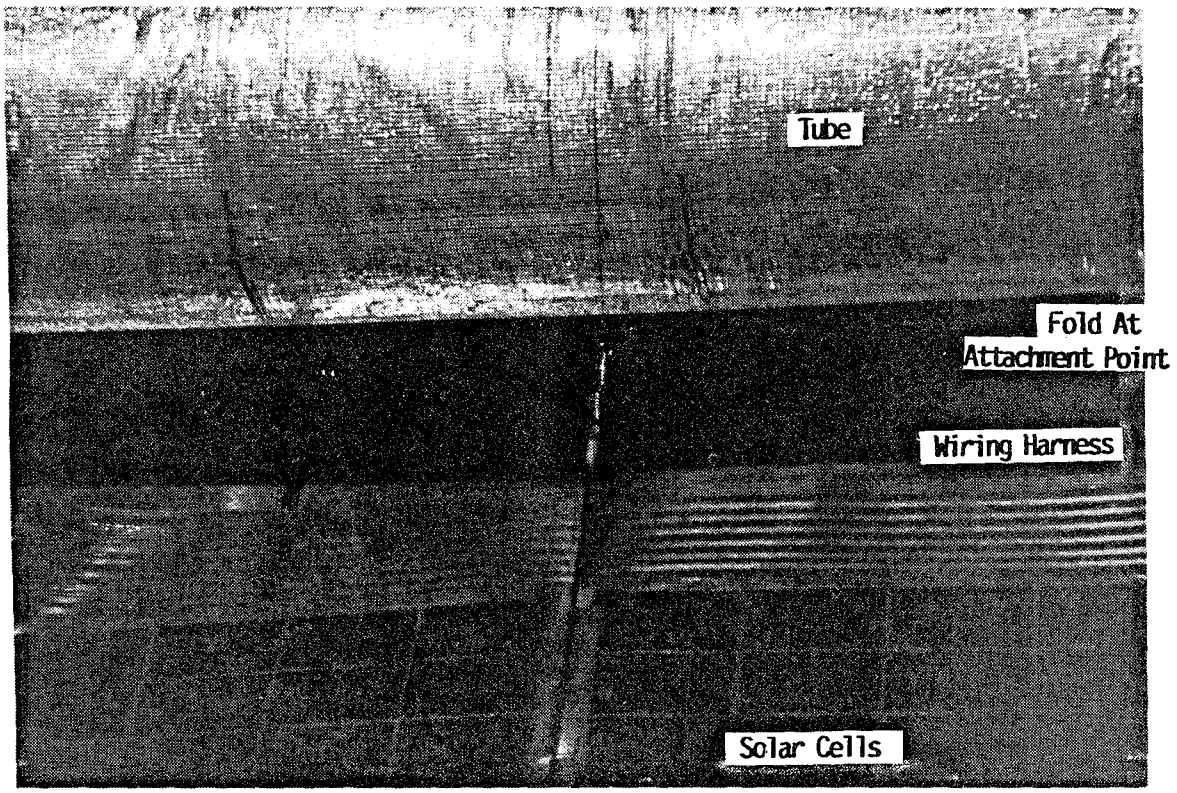

Figure 74. Wiring harness.

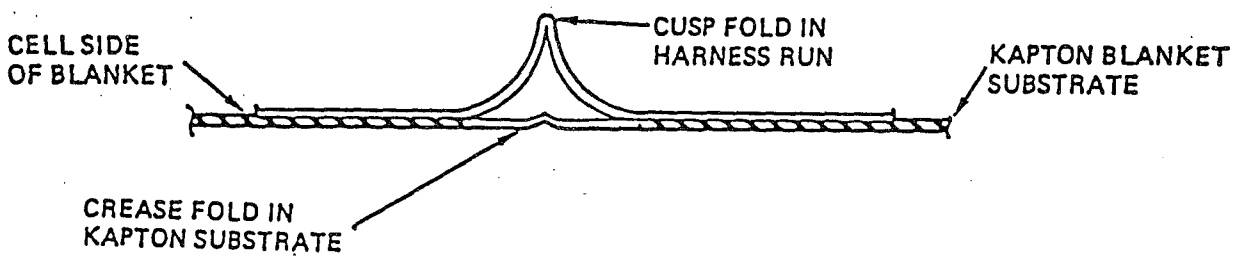

Figure 75. Cusp folds in wiring harness.

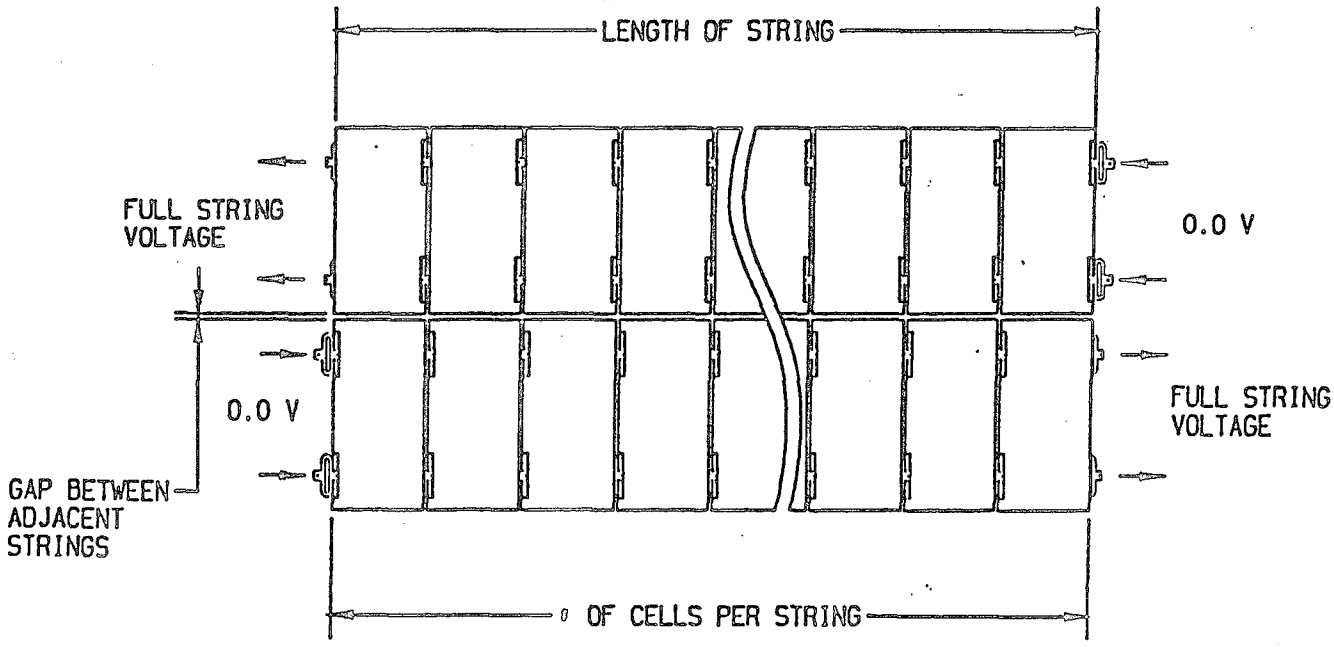

Figure 76. Nomenclature.

The resistance of the gap between the cell strings is calculated by

$$R_g = R_s (d/l) \tag{97}$$

where

R_s = Surface resistivity of the material (ohm/sq)

d = distance between cell strings (in)

l = length of the solar cell string (in)

The current flow between the cell strings is calculated by

$$I = V_{avg}/R_g \tag{98}$$

where V_{avg} is the average voltage between adjacent cells, which is only half of the full string voltage since the cells in the exact middle of the string see no voltage at all, while the end cells see a full string voltage difference.

The power loss (in watts) between cell strings is then

$$P_{loss} = V_{avg} * I \quad (99)$$

The above calculation method can be used to determine the exact resistivity requirements. For our ITSAT design, a surface resistivity of >4 x 10^6 ohms/sq was required to limit the conductance losses to <0.1 percent. We actually specified a resistivity of 10 x 10^6 ohms/sq to be conservative.

3.3.7 Interconnects

The interconnect joins the cells into strings. Two interconnects per cell are used for redundancy. They must be large enough to carry the current through the strings. The following analysis calculates the fusing current of the flat interconnect and the voltage drop through the copper material.

Fusing Current - Reference 19 gives the current carrying capacity of a round wire of diameter d:

$$I = kd^{3/2} \quad (100)$$

where

I = fusing current in amperes

k = constant for the material (10,244 for copper)

d = wire diameter in inches

For the current design, the width of the interconnect at the narrowest point is 0.030 in, with a 1-mil thickness. There are two parallel paths, however, so the total cross-sectional area is (2) (0.030) (0.001) = 0.00006 in^2, making an equivalent round wire diameter of 0.0087 in. Using Equation 100, the fusing current of the interconnect is

$$I = (10244)\ (0.0087)^{3/2} = 8.37\ A \tag{101}$$

For the expected cell output of 0.290 A, the safety factor is 29. Since round wire has the minimum surface for a given cross-section and current flows on surface, this is conservative.

Voltage Drop - The voltage drop is proportional to the length of the conductor and inversely proportional to the cross-sectional area, or

$$V_{drop} = KI/A \tag{102}$$

where

K = the conductivity of the material
I = the length of the conductor
A = the cross-sectional area of the conductor

K was determined experically to be 1.53×10^{-7} V-in. The expected drop will be 0.00074 V, which is only 0.19 percent of the 0.392 EOL voltage of the cell.

3.3.8 Cover Glass

The cover glass is Pilkington's CMZ Cerium-doped borosilicate. A magnesium fluoride antireflective coating is applied to the cover to increase solar absorption. This is a standard item, used on most Cell-Interconnect-Cover (CIC) glass assemblies.

An adhesive layer bonds the cover glass to the solar cell. A Dow Corning DC 93500 which is also an industry standard was used.

3.3.9 Summary Cell Stack

The cell stack dimensions are given in Table 24.

Table 24. Cell stack.

ITEM	FOR THIN CELLS	FOR THICK CELLS
Cover Glass	0.0029	0.0029
Adhesive	0.0015	0.0015
Interconnect	0.001[a]	0.001[a]
Solar Cell	0.0022	0.008
Adhesive (to substrate)	0.002	0.002
Kapton® Substrate	0.002	0.002
TOTAL	**0.0106**	**0.0164**

[a] Not included in cell stack thickness.

3.3.10 Solar Cell Efficiency Degradation

3.3.10.1 Cell BOL Efficiency. For the standard silicon space solar cells with back surface field (BSF) and back surface reflector (BSR), the starting efficiency is 13.8 percent. The 8-mil cells from ASEC, however, are BSR but not BSF. Their efficiency is 12.0 percent. In the cell efficiency summary given at the end of this section, both cases will be compared.

The above efficiency is a rather theoretical value since it is given for a single cell at a datum temperature of 28°C. Cells are most widely used in strings to get to the proper voltage and can get to a temperature higher than 28°C due to the heating from less than perfect conversion of sunlight to electricity. Both of these aspects will be discussed in the following sections.

Array assembly losses occur not on a cell level but on a cell string/array level. Data are modeled from Reference 20 due to similarity in design. Losses come from three sources: (1) installation mismatch, (2) diode losses, and (3) harness losses.

Installation mismatch losses occur since cells cannot be matched perfectly by output into strings. A higher producing cell is somewhat blocked by a lower producing cell when connected in series. The value to be used here is a standard number, 0.985, based on experience.

The diode losses come from the forward dropping voltage of the blocking diodes. The bypass diodes should not affect the efficiency as long as the cell substrings they are protecting are in working order. Wiring harness losses occur due to the resistance of the thin copper conductors in the wiring harness. The diode and harness losses are combined into a standard degradation factor of 0.977, again drawing data from Reference 20.

Solar cell efficiencies are given at a standard temperature of 28°C. Temperatures higher than this cause a lower efficiency by an amount proportional to the temperature proportional to the temperature degradation coefficient:

$$TDF = 1 - \left|k\,(T_{op} - T_{ref})\right| \qquad (103)$$

where

TDF = Temperature degradation factor
T_{op} = Operating temperature of cell
T_{ref} = Reference temperature, 28°C
k = Temperature degradation coefficient

The value of k is derived from testing* to be 0.45 percent/°C at BOL and 0.42 percent/°C at EOL. An average value of 0.435 percent/°C is used in this analysis. The operating temperature at BOL is determined to empirically be 60.9°C*. This is based on the particular substrate, cell, coatings, etc. These numbers are estimated based on the best available data. Until a more thorough analysis is performed, the 60.9°C temperature will be used in these calculations. Substituting numbers into Equation 103 yields

*George Vendura, telephone call to Mark Kruer, TRW, May 20, 1992.

$$TDF = [1 - (60.9-28)(0.00435)] = 0.857 \quad (104)$$

Note that this represents a significant inefficiency. All methods used to keep the cell cool serve to increase array efficiency.

3.3.10.2 Cell EOL Efficiency. Several factors influence the EOL efficiency; they are given next.

Array assembly losses due to mismatch and diode/harness are the same as BOL, 0.985 and 0.977, respectively.

As at BOL, a higher temperature than 28°C will cause a reduction in efficiency. The case at EOL is worse due to the lower output. More of the incoming sunlight is converted to heat instead of useful energy. The temperature at EOL is 65.4°C* making a temperature degradation factor (TDF) of 0.837.

Radiation losses result from continuous omnidirectional proton and electron bombardment in the space environment. However, such bombardment is attenuated by the presence of any shielding materials on front and back surfaces. In general, the thicker and more massive the material, the greater the shielding effect. For this reason, cover glasses of various thicknesses are routinely added to the cell's front surfaces, depending on the environment and desired EOL output. The rear surface of the cell is shielded partially by the Kapton® substrate and adhesive.

The shielding effect has been widely studied for solar cells. Data are given in Reference 5 for the fluence of particles reaching the cell surface versus the cover glass thickness and the altitude and inclination of the mission. These tables are given for the case of infinite backshielding, which is not the case here. The ITSAT back surface is shielded somewhat by the Kapton®, but it certainly is not infinite.

Separate tables are given for protons and electrons, so the procedure is

*George Vendura, telephone call to Mark Kruer, TRW, May 20, 1992

1. Start with the front surface. Find the equivalent fused silica cover glass thickness. For materials other than fused silica, the equivalent thickness is in direct proportion to its density relative to fused silica, i.e., a 2-mil thick material with a density twice that of fused silica would have an equivalent thickness of 4-mil. Account for the adhesive the same way and add to the cover thickness.

2. Look in the table for electrons and find the annual fluence for this thickness, the spacecraft's inclination and the spacecraft's altitude. For ITSAT, both 600- and 800-km altitudes (the extremes) need to be calculated at each of the 10 inclinations (see Table 25).

3. Do the same for the protons (Table 26).

4. Now analyze the back surface in the same manner. Again, the Kapton® and adhesive both count, so find their equivalent fused silica thicknesses and add together.

5. Add the electron and proton fluences in steps 2 and 3.

6. For each combination of altitude and inclination, add the equivalent 1-MeV electron fluence from protons and electrons, front and back side (four combinations).

7. Take the worst case from step 6. This is the fluence for 1 year only. Multiply this number by the mission lifetime (3 years in this case) to find the total fluence.

8. Now use this number in the figures for P_{max} degradation versus fluence (also from Ref. 5). Make sure to choose the correct figure as these are given for various type cells, thicknesses, etc.

The values for altitude and inclination are chosen here to be the worst case. So while the calculation method is being demonstrated, the most conservative fluence number will also be calculated. This occurs at an altitude of 800 km and an inclination of 50 deg. The numbers

Table 25. Annual equivalent 1-MeV electron fluence from trapped electrons, 50-deg inclination-infinite backshielding (from Ref. 5).

ELECTRONS - ISC, VOC, AND PMAX

EQUIV. 1 MEV ELECTRON FLUENCE FOR ISC - CIRCULAR ORBIT
DUE TO GEOMAGNETICALLY TRAPPED ELECTRONS - MODELS AE6MAX, AEI7LO

INCLINATION = 50 DEGREES.

ALTITUDE (N.M.)	ALTITUDE (KM)	SHIELD THICKNESS, CM (MILS) 0 (0)	2.54E-3 (1)	7.64E-3 (3)	1.52E-2 (6)	3.05E-2 (12)	5.09E-2 (20)	7.64E-2 (30)	1.52E-1 (60)
150	277	8.96+10	7.94+10	6.84+10	5.83+10	4.59+10	3.59+10	2.77+10	1.44+10
250	463	2.04+11	1.76+11	1.47+11	1.22+11	9.36+10	7.18+10	5.47+10	2.79+10
300	555	2.94+11	2.51+11	2.07+11	1.69+11	1.27+11	9.66+10	7.31+10	3.69+10
450	833	7.33+11	6.03+11	4.77+11	3.73+11	2.64+11	1.93+11	1.42+11	6.92+10
600	1111	1.69+12	1.35+12	1.03+12	7.71+11	5.15+11	3.59+11	2.57+11	1.20+11
800	1481	4.91+12	3.85+12	2.84+12	2.05+12	1.29+12	8.54+11	5.89+11	2.62+11
1000	1852	1.17+13	9.13+12	6.69+12	4.76+12	2.94+12	1.91+12	1.29+12	5.56+11
1250	2315	2.31+13	1.81+13	1.33+13	9.50+12	5.90+12	3.84+12	2.60+12	1.11+12
1500	2778	3.31+13	2.58+13	1.89+13	1.34+13	8.26+12	5.32+12	3.58+12	1.53+12
1750	3241	4.19+13	3.24+13	2.34+13	1.63+13	9.68+12	6.01+12	3.94+12	1.65+12
2000	3704	4.83+13	3.70+13	2.64+13	1.80+13	1.02+13	6.03+12	3.80+12	1.53+12
2250	4167	5.22+13	3.97+13	2.80+13	1.87+13	1.02+13	5.78+12	3.50+12	1.38+12
2500	4630	5.36+13	4.07+13	2.85+13	1.90+13	1.02+13	5.62+12	3.35+12	1.33+12
2750	5093	5.22+13	3.97+13	2.79+13	1.86+13	1.00+13	5.54+12	3.31+12	1.36+12
3000	5556	4.86+13	3.71+13	2.64+13	1.79+13	9.96+12	5.73+12	3.57+12	1.55+12
3500	6482	4.06+13	3.17+13	2.34+13	1.67+13	1.03+13	6.68+12	4.57+12	2.17+12
4000	7408	3.64+13	2.95+13	2.28+13	1.73+13	1.18+13	8.24+12	5.95+12	2.92+12
4500	8334	3.65+13	3.07+13	2.49+13	1.98+13	1.43+13	1.04+13	7.68+12	3.79+12
5000	9260	3.77+13	3.29+13	2.78+13	2.31+13	1.74+13	1.31+13	9.72+12	4.79+12
5500	10186	4.03+13	3.61+13	3.13+13	2.67+13	2.08+13	1.59+13	1.19+13	5.90+12
6000	11112	4.56+13	4.14+13	3.66+13	3.18+13	2.53+13	1.97+13	1.51+13	7.59+12
7000	12964	6.05+13	5.57+13	4.97+13	4.36+13	3.53+13	2.79+13	2.16+13	1.11+13
8000	14816	7.14+13	6.58+13	5.89+13	5.17+13	4.19+13	3.31+13	2.56+13	1.31+13
9000	16668	8.30+13	7.65+13	6.84+13	6.00+13	4.85+13	3.83+13	2.95+13	1.49+13
10000	18520	9.10+13	8.38+13	7.48+13	5.54+13	5.25+13	4.11+13	3.13+13	1.53+13
11000	20372	8.69+13	7.99+13	7.12+13	6.20+13	4.95+13	3.83+13	2.88+13	1.35+13
12000	22224	7.53+13	6.91+13	6.13+13	5.32+13	4.22+13	3.23+13	2.40+13	1.10+13
13000	24076	6.77+13	6.19+13	5.47+13	4.72+13	3.70+13	2.81+13	2.07+13	9.18+12
14000	25928	5.33+13	4.84+13	4.24+13	3.62+13	2.80+13	2.09+13	1.51+13	6.50+12
15000	27780	3.76+13	3.38+13	2.92+13	2.46+13	1.86+13	1.36+13	9.58+12	3.91+12
16000	29632	3.04+13	2.71+13	2.32+13	1.93+13	1.43+13	1.02+13	7.10+12	2.75+12
17000	31484	2.40+13	2.12+13	1.79+13	1.47+13	1.06+13	7.42+12	5.02+12	1.83+12
18000	33336	1.78+13	1.55+13	1.29+13	1.03+13	7.29+12	4.95+12	3.24+12	1.09+12
19327	35793	1.00+13	8.52+12	6.90+12	5.41+12	3.67+12	2.39+12	1.50+12	4.54+11

Table 26. Annual equivalent 1-MeV electron fluence from trapped protons (Voc, Pmax), 50-deg inclination-infinite backshielding (from Ref. 5).

PROTONS - VOC AND PMAX

EQUIV. 1 MEV ELECTRON FLUENCE FOR VOC AND PMAX CIRCULAR ORBIT DUE TO GEOMAGNETICALLY TRAPPED PROTONS, MODEL AP8MAX

INCLINATION = 60 DEGREES.

ALTITUDE (N.M.)	ALTITUDE (KM)	SHIELD THICKNESS, CM (MILS) 0 (0)	2.54E-3 (1)	7.64E-3 (3)	1.52E-2 (6)	3.05E-2 (12)	5.09E-2 (20)	7.64E-2 (30)	1.52E-1 (60)
150	277	1.28+13	1.12+12	5.29+11	3.17+11	1.90+11	1.38+11	1.14+11	8.89+10
250	463	7.96+13	8.94+12	4.40+12	2.61+12	1.52+12	1.05+12	8.42+11	6.27+11
300	555	1.63+14	2.04+13	9.85+12	5.71+12	3.25+12	2.22+12	1.77+12	1.31+12
450	833	8.14+14	9.38+13	4.55+13	2.65+13	1.50+13	9.99+12	7.77+12	5.51+12
600	1111	2.28+15	2.53+14	1.26+14	7.57+13	4.40+13	2.88+13	2.20+13	1.50+13
800	1481	6.27+15	6.94+14	3.76+14	2.43+14	1.52+14	1.02+14	7.75+13	5.13+13
1000	1852	1.73+16	1.88+15	1.05+15	6.98+14	4.39+14	2.82+14	2.07+14	1.28+14
1250	2315	4.40+16	5.42+15	3.11+15	2.09+15	1.29+15	7.61+14	5.19+14	2.79+14
1500	2778	8.44+16	1.26+16	7.42+15	5.01+15	3.00+15	1.63+15	1.02+15	4.60+14
1750	3241	1.44+17	2.45+16	1.47+16	9.91+15	5.76+15	2.95+15	1.71+15	6.41+14
2000	3704	2.24+17	4.22+16	2.49+16	1.62+16	8.81+15	4.17+15	2.26+15	7.33+14
2250	4167	3.41+17	7.15+16	4.02+16	2.43+16	1.19+16	5.06+15	2.63+15	7.29+14
2500	4630	4.94+17	1.05+17	5.61+16	3.18+16	1.40+16	5.47+15	2.56+15	6.80+14
2750	5093	7.02+17	1.46+17	7.33+16	3.85+16	1.53+16	5.48+15	2.42+15	5.98+14
3000	5556	9.32+17	1.81+17	8.47+16	4.13+16	1.49+16	5.03+15	2.14+15	5.02+14
3500	6482	1.65+18	2.61+17	1.01+17	4.05+16	1.15+16	3.65+15	1.47+15	3.20+14
4000	7408	2.62+18	3.21+17	1.04+17	3.54+16	8.11+15	2.36+15	9.03+14	1.87+14
4500	8334	3.76+18	3.56+17	9.75+16	2.87+16	5.41+15	1.43+15	5.13+14	1.00+14
5000	9260	5.11+18	3.73+17	8.49+16	2.13+16	3.27+15	7.93+14	2.69+14	4.90+13
5500	10186	6.77+18	3.88+17	7.33+16	1.54+16	1.90+15	4.39+14	1.42+14	2.31+13
6000	11112	7.56+18	3.30+17	5.24+16	9.52+15	9.69+14	2.00+14	5.94+13	8.46+12
7000	12964	8.51+18	1.94+17	2.10+16	2.75+15	1.78+14	2.82+13	6.82+12	7.08+11
8000	14816	7.14+18	8.23+16	6.03+15	6.80+14	2.47+13	2.93+12	5.67+11	4.35+10
9000	16668	4.62+18	2.39+16	1.04+15	6.70+13	1.66+12	1.52+11	3.03+10	5.23+09
10000	18520	2.78+18	5.02+15	1.26+14	5.59+12	1.90+10	1.83-03	0.00	0.00
11000	20372	1.80+18	1.02+15	8.15+12	2.36+11	8.49+08	1.83-03	0.00	0.00
12000	22224	1.22+18	1.83+14	9.90+10	9.63-03	0.00	0.00	0.00	0.00
13000	24076	9.23+17	2.69+13	1.25+07	0.00	0.00	0.00	0.00	0.00
14000	25928	6.25+17	3.94+12	6.20+06	0.00	0.00	0.00	0.00	0.00
15000	27780	3.74+17	7.85+11	3.41+06	0.00	0.00	0.00	0.00	0.00
16000	29632	2.74+17	8.18+09	0.00	0.00	0.00	0.00	0.00	0.00
17000	31484	1.96+17	6.17+09	0.00	0.00	0.00	0.00	0.00	0.00
18000	33336	1.30+17	4.88+09	0.00	0.00	0.00	0.00	0.00	0.00
19327	35793	3.58+16	3.11+09	0.00	0.00	0.00	0.00	0.00	0.00

used for the cell stack are the numbers for the extrapolated BSR BSF cells with 2-mil cover glass (see Table 27).

Table 27. Equivalent thickness calculations.

ITEM	DENSITY THICKNESS (in)	EQUIVALENT ($lb/1n^3$)	ρ/ρ^a_{fs}	THICKNESS (in)
Front				
Cover Glass	0.002	0.0935	1.176	0.00235
Cover Glass Adhesive	0.0015	0.042	0.528	0.00079
Total Front Surface Shielding				0.00314
Back				
Cell to Substrate Adhesive	0.002	0.0355	0.447	0.00089
Substrate	0.002	0.0505	0.635	0.00127
Total Back Surface Shielding				0.00216

[a] Fused silica density is 0.0795 lb/in^3.

Now look at Tables 6.21 and 6.22 in Reference 5, given here as Tables 25 and 26. First do the front side. Interpolation is required for both the shield thickness and altitude. The fluence behaves approximately linearly for shield thickness, but for altitude the fluence behaves logarithmically. Therefore, the procedure is to find the $\log_{10}$ of the fluence for each entry in the table and interpolate using these numbers. An interpolated table is given as Table 28. From this table, the fluence of electrons and protons for the front and back sides is given below:

Side	Particles	Fluence
Front	Electrons	4.28×10^{11}
Front	Protons	3.72×10^{13}
Back	Electrons	4.79×10^{11}
Back	Protons	5.48×10^{13}
TOTAL		9.29×10^{13}

For a 3-year exposure, the fluence is three times this number, or 2.79×10^{14}.

Table 28. Fluence tables for 50-deg inclination.
(from Ref. 5, with modifications)

		SHIELD THICKNESS (mil)											
	ALTITUDE (km)	0	log f	1	log f	2.164	3	log f	3.136	6	log f	12	log f
Electrons (table 6.21)	277	9.0E+10	10.952	7.94E+10	10.900	7.30E+10	6.84E+10	10.835	6.79E+10	5.83E+10	10.766	4.59E+10	10.662
	400	1.5E+11	11.189	1.34E+11	11.128	1.22E+11	1.13E+11	11.055	1.13E+11	9.50E+10	10.978	7.35E+10	10.866
	463	2.0E+11	11.310	1.76E+11	11.246	1.59E+11	1.47E+11	11.167	1.46E+11	1.22E+11	11.086	9.36E+10	10.971
	555	2.9E+11	11.468	2.51E+11	11.400	2.25E+11	2.07E+11	11.316	2.05E+11	1.69E+11	11.228	1.27E+11	11.104
	600	3.4E+11	11.533	2.89E+11	11.461	2.59E+11	2.37E+11	11.375	2.35E+11	1.92E+11	11.284	1.43E+11	11.155
	750	5.6E+11	11.747	4.64E+11	11.667	4.10E+11	3.72E+11	11.570	3.68E+11	2.94E+11	11.469	2.12E+11	11.327
	800	6.6E+11	11.818	5.43E+11	11.735	4.79E+11	4.32E+11	11.635	4.28E+11	3.40E+11	11.531	2.42E+11	11.384
	833	7.3E+11	11.865	6.03E+11	11.780	5.30E+11	4.77E+11	11.679	4.72E+11	3.73E+11	11.572	2.64E+11	11.422
	1111	1.7E+12	12.228	1.35E+12	12.130	1.16E+12	1.03E+12	12.013	1.02E+12	7.71E+11	11.887	5.15E+11	11.712
Protons (table 6.22)	277	1.3E+13	13.107	1.12E+12	12.049	7.76E+11	5.29E+11	11.723	5.19E+11	3.17E+11	11.501	1.90E+11	11.279
	400	4.3E+13	13.632	4.42E+12	12.646	3.10E+12	2.15E+12	12.332	2.11E+12	1.28E+12	12.107	7.52E+11	11.876
	463	8.0E+13	13.901	8.94E+12	12.951	6.30E+12	4.40E+12	12.643	4.32E+12	2.61E+12	12.417	1.52E+12	12.182
	555	1.6E+14	14.212	2.04E+13	13.310	1.43E+13	9.85E+12	12.993	9.66E+12	5.71E+12	12.757	3.25E+12	12.512
	600	2.1E+14	14.325	2.61E+13	13.417	1.83E+13	1.26E+13	13.101	1.24E+13	7.32E+12	12.865	4.16E+12	12.619
	750	5.0E+14	14.702	5.95E+13	13.774	4.16E+13	2.88E+13	13.460	2.83E+13	1.68E+13	13.224	9.50E+12	12.978
	800	6.7E+14	14.828	7.83E+13	13.894	5.48E+13	3.79E+13	13.579	3.72E+13	2.21E+13	13.344	1.25E+13	13.097
	833	8.1E+14	14.911	9.38E+13	13.972	6.57E+13	4.55E+13	13.658	4.46E+13	2.65E+13	13.423	1.50E+13	13.176
	1111	2.3E+15	15.358	2.53E+14	14.403	1.79E+14	1.26E+14	14.100	1.24E+14	7.57E+13	13.879	4.40E+13	13.643

Note: Light shading indicates the interpolated rows and columns
Dark shading indicates the fluence numbers used

Refer to Reference 5 and find the figure which describes the cell best (given here as Fig. 77). For a fluence of 2.79×10^{14}, the maximum power is degraded by a factor of 0.872.

For miscellaneous losses, included here are UV degradation; temperature cycle fatigue; cover glass darkening; and adhesive darkening. Each of these is described in more detail next.

Ultraviolet degradation is caused by UV light impinging on the cell. Our factor here is based on Reference 20 (Fig. 78) which shows that the degradation occurs rapidly in the first year, then levels off to a value of 0.98.

Temperature cycling is due to eclipsing the array every orbit. The result is an increase in resistance of the solder joints and a corresponding decrease in cell string power. As with UV degradation, the damage is done in the first year, degrading to a value of 0.98.

Again, cover glass darkening occurs in the first year then levels off to a value of 0.99.

Adhesive darkening degrades the cell by a factor of 0.994 and also occurs most rapidly in the first year.

Table 29 shows the cell degradation effects at BOL and EOL; Figures 79 and 80 show the data pictorially. Note that the highest contributor is temperature degradation in both cases. Any way to limit the cell temperature is welcome. This table is for the extrapolated 2-mil BSR, BSF cell. For the actual 8-mil BSR cell, the degradation factors are given in Table 30.

3.3.11 Overall Blanket Power

For our solar blanket with 6 panels (18 subpanels), 4 rows per subpanel, 31 cells per row, the total number of cells is 2232. The overall blanket power for a full population is then given by Table 31.

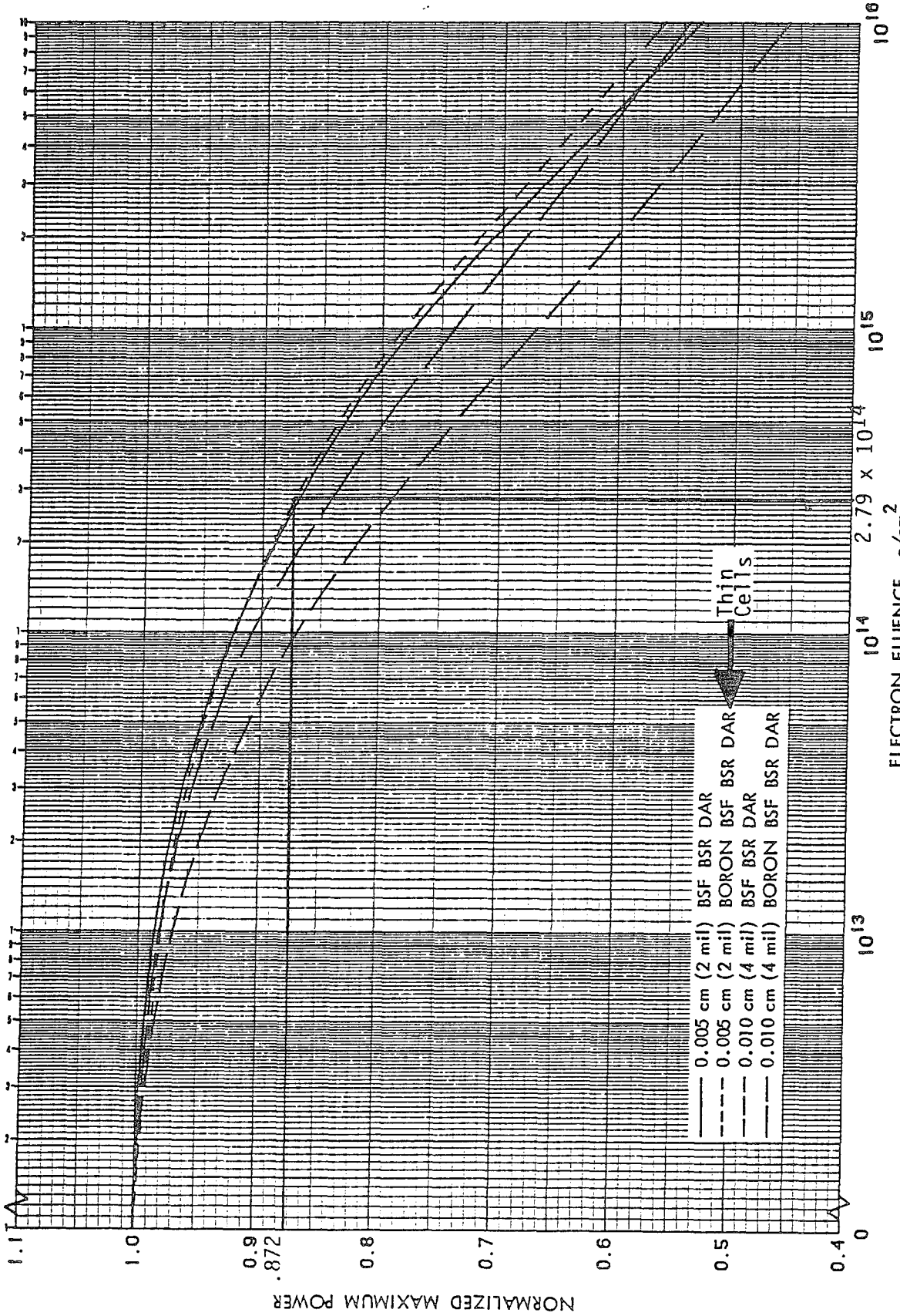

Figure 77. Normalized P_{max} versus 1 MeV electron fluence for 10 Ohm-cm n/p BSF thin silicon cells with BSR (from Ref. 5).

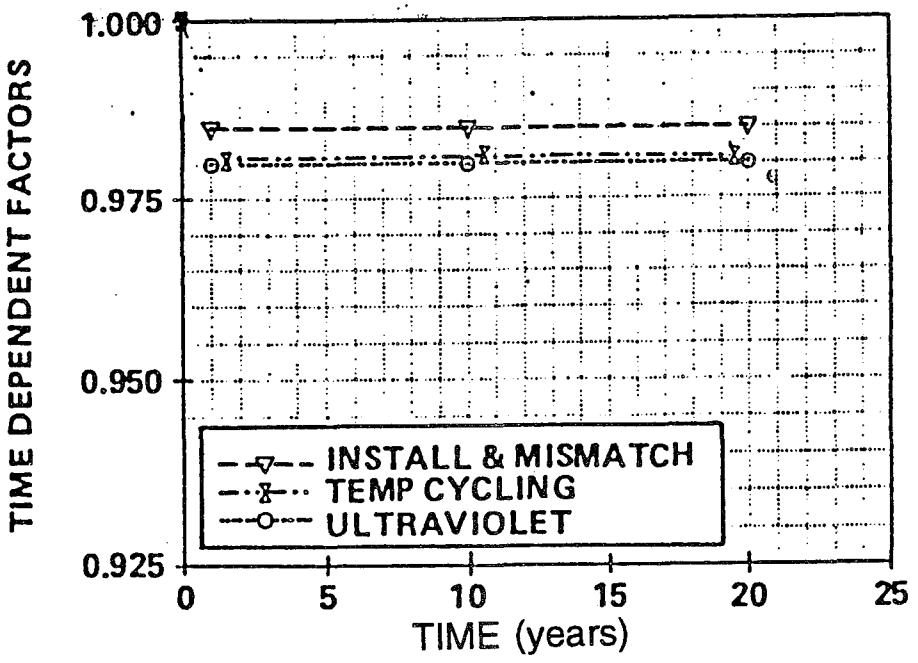

Figure 78. Key array sizing factors.

3.3.12 Blanket Tension

To keep the blanket from fluttering excessively, it must be tensioned at each end. The blanket is suspended by each corner, and the cables are each tensioned to 1.30 lb.

3.3.13 Cell Outputs and Sorting

Electrical outputs were supplied with all of the 8 mil cells that were purchased from ASEC (Ref. 21)*. To provide the maximum power from the array, L'Garde sorted the cells in descending order of efficiency. The highest efficiency cells were grouped as one string, the next most efficient cells were grouped as another, and so on. The results are given in Appendix A.

No electrical output was available for the individual 2.2-mil cells. Of the 40 cells that were purchased, 31 of the "best-looking" cells were chosen for cover glassing and inclusion on the solar blanket as cell string #5.

*Memo LM-93-GW-083, CIC Data Sheet, dated March 17, 1993.

Table 29. Degradation factors for thin cell.

BASIC CELL EFFICIENCY - 13.8 PERCENT

BOL	LOSS
Installation Mismatch	0.985
Diode/Line Loss	0.977
Temperature (60.9°C)	0.857
Total BOL Losses	0.825
Overall BOL Cell Efficiency	11.380%
Individual BOL Cell Output	0.123W

EOL	
Installation Mismatch	0.985
Diode/Line Loss	0.977
Temperature (65.4°C)	0.837
Radiation Damage	0.872
UV Degradation	0.980
Temperature Cycling	0.980
Cover Glass Darkening	0.990
Adhesive Darkening	0.994
Total EOL Losses	0.664
Overall EOL Cell Efficiency	9.164%
Individual EOL Cell Output	0.099W

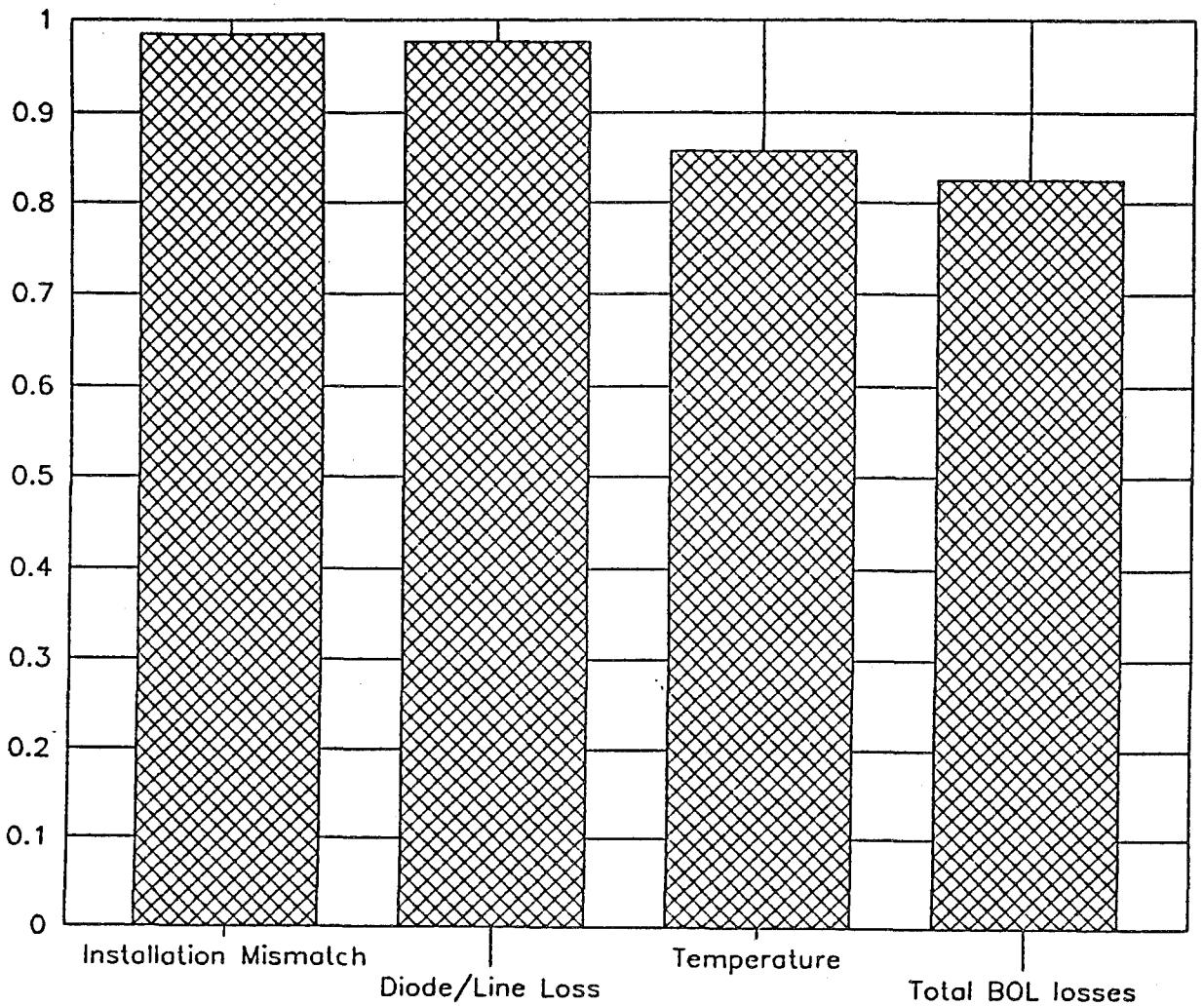

Figure 79. The BOL losses for thin cell.

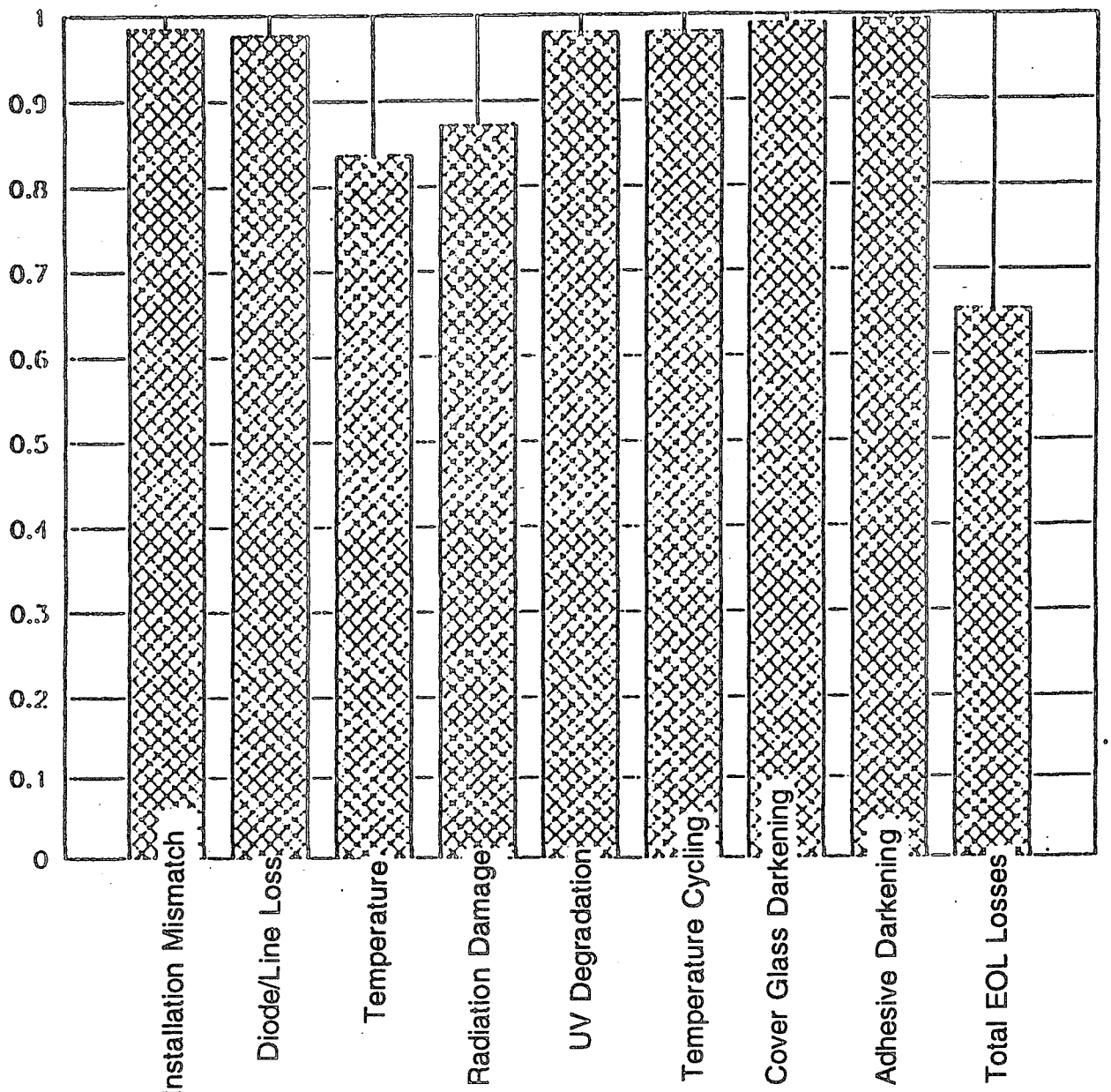

Figure 80. The EOL losses for thin cells.

Table 30. Degradation factors for ASEC cell.

BASIC CELL EFFICIENCY - 12.0 PERCENT

BOL	LOSS
Installation Mismatch	0.985
Diode/Line Loss	0.977
Temperature (60.9°C)	0.857
Total BOL Losses	0.825
Overall BOL Cell Efficiency	9.895%
Individual BOL Cell Output	0.107W

EOL	
Installation Mismatch	0.985
Diode/Line Loss	0.977
Temperature (65.4°C)	0.837
Radiation Damage	0.878
UV Degradation	0.980
Temperature Cycling	0.980
Cover Glass Darkening	0.990
Adhesive Darkening	0.994
Total EOL Losses	0.669
Overall EOL Cell Efficiency	8.024%
Individual EOL Cell Output	0.087W

Table 31. Blanket power.

CELL TYPE	TIME OF MISSION	BLANKET POWER (W)
2 mil BSR, BSF	BOL	274
2 mil BSR, BSF	EOL	221
8 mil BSR	BOL	239
8 mil BSR	EOL	194

4.0 DEVELOPMENT TESTING

Prior to system testing, each of the component subsystems were subjected to functional tests. This section describes the testing performed. When selecting the laminate used for the tubes, L'Garde performed a series of coupon level tests to select the laminate for the tubes. These included strength/Modules tests, peel tests, and outgassing tests. After the laminate was selected, short length tubes were first constructed for foldability, strength, leak, and burst testing. The next step was to make full length tubes (roughly 12-ft long) for bending strength and stiffness, leak, and deployment testing.

The blowdown inflation system design needed proving out. A series of tests were performed to assure (1) the inflation rates were correct, (2) the folded tubes would vent fast enough during ascent, and (3) the inflatant tank was sufficiently strong.

The solar array design was based primarily on the L'Garde Solar Array Program. Two additional tests were performed which are described in Subsection 4.5

After all the component testing, the final test was to deploy the solar array as a system in ambient conditions. This is described in Subsection 4.6. A complete test matrix is given in Table 32.

4.1 LAMINATE TESTS

Flat coupons were constructed and tested for tensile strength, modulus, and outgassing. The outgassing results are given in Table 33. Case 1 shows the results of an unbaked sample subjected to NASA Standard SP-R0022A. It shows that the total mass loss of 1.14 percent is slightly above the 1 percent limit set by the Standard. However, 0.26 percent is due to water vapor (harmless by NASA standards) so the material passes here. The collected volatile condensible material (CVCM) is 0.11 percent, slightly higher than the 0.1 percent limit. The easiest way to lower the CVCM is to use a prebake to remove most of the volatiles before flight.

Table 32. Master test matrix.

TEST PLAN SECTION	CONTRACT SECTION	STATUS	ITEM	TEST	COMPONENT	OBJECTIVE	TEST FACILITY	Procedure No.	REMARKS
3.1	4.2.5.2	Complete Complete Complete	1 2 3	Strength Permeability Pinhole/Leak Tests	Tube Material (Flat Coupons)	Material Selection	L'Garde	N/A N/A N/A	Determine ruggedness of materials
3.2	4.2.5.2	Complete Complete Complete	4 5 6	Packaging Compression Packaging	Sample Tubes (24" Long Tubes)	Material Selection	L'Garde	N/A N/A	Measure packaged height for incorporation into the design.
3.3	4.2.5.2	Complete Complete Complete	7 8 9	Packaging Compression Packaging	Full Length Tubes (Fold to Expected Packaged Size)	Functionality Packaging Techniques	L'Garde	N/A N/A N/A	Begin developing packaging procedure for the ITSAT assembly starting with the tubes Document with video.
3.4	4.2.5.2 4.2.5.4	Complete Complete	10 11	Thermal Vacuum	Sample Blanket (Flight like Cells)	Effect on power output before & after deployment, visual inspection	L'Garde		Being developed under the LSAP program
3.5	4.2.5.2 4.2.5.4	Complete Complete	12 13	Packaging Folding	Replica Blanket (Dummy Cells) &Housing/Lid	Visual Inspection of Cells after Deployment	L'Garde		Further develop the packaging procedure for the assembly, document with video.
3.6	4.2.5.2	Complete Complete	14 15	Folding Packaging	Full Blanket (with Cells) &Housing/Lid	Effect on power output before & after packaging visual inspection	L'Garde		This should use the final draft packaging procedure as developed in sections above, document with video.
3.7	4.2.5.2	Complete	16	Electrical Design	Controller Board Pyro Valve Lid Cable Cutters	Functionality Flow Rates	L'Garde	N/A	Component tests for test equipment detailed procedure optional
3.8	4.2.5.2	Complete	17	Lid Release	Lid/Pyro Cutters	Functionality	L'Garde		Outline Test Procedure acceptable
3.9	4.2.5.2	Complete	18	Pressure Test	Inflantant Tank	Proof Pressure	L'Garde		Outline Test Procedure acceptable
3.10	4.2.5.2	Complete	19	Inflation System	Inflation System	Functionality Flow Rates	L'Garde		Outline Test Procedure acceptable
3.11	4.2.5.2 4.2.5.4	Complete	20	System Deployment @ L'Garde	Flight Hardware W/Flight Blanket	Functionality Packaging Techniques Effect on Power output before & after deployment	L'Garde		Detailed test procedire required will probably use ordnance items and COTR will be present.
4.1	4.2.5.3	Complete Complete Complete Complete Complete Complete Complete Complete	 21 22 23 24 25 26 27	Environmental Tests(a) Functional Test(a) Thermal Cycle Random Vibration Pyro Shock Pressure Leak Thermal Vacuum	Flight Hardware W/Flight Blanket Coupon Level Performed with Actual Hardware Combined with NRL test Combined with NRL test Combined with NRL test	Qualification of flight hardware Environments, Stress Screening	L'Garde		A Detailed functional test procedure will be required, this test procedure will be used throughout the test program and during launch checkout. The environmental test procedures can be outline type procedures that ref the functional procedure.
4.2	4.2.5.3	Complete	28	Fundamental Frequency		Determine Natural Frequency of Packaged and Deployed Assembly	L'Garde		Outline Test Procedure acceptable
4.3	4.2.5.3 4.2.5.4	Complete	29	System Deployment Vacuum Test Thermal Analysis	Flight Hardware W/Flight Blanket	Functionality Temperature Power Output in Chamber (compare to coupon) Effect on Power output before & after deployment	NRL		Detailed test plan AND procedure will be required and submitted to Edwards AFB prior to testing, see schedule for dates.

a. A system functional test will follow each environmental test.
Most packaged environmental tests were deleted due to restructuring of the program in Sept. - Oct. 1993.

Table 33. Outgassing of selected laminates[a].

CASE	SPECIMEN	% TML[b]	% CVCM[c]	% WVR[d]
1	Unbaked	1.14	0.11	0.26
2	Prebaked (75°C/24 hr/2-4 Torr)	0.91	0.12	0.12
3	Prebaked A(75°C/72 hr/1-2 Torr)	1.00	0.12	0.30
4	NASA Standard SP-R0022A (Allowable)	≤1.0	≤0.10	

[a] Test Method: Per NASA Standard - SP-R0022A
[b] TML: Total Mass Loss
[c] CVCM: Collected Volatile Condensible Material
[d] WVR: Water Vapor Recovered

Case 2 shows a 24-hour prebake at 75°C in a vacuum of 2-4 torr. The fact that the CVCM raised slightly to 0.12 percent is due to the accuracy of the test method, not due to the prebake. The same inconsistency is seen on data obtained in Case 3 (higher baking times).

Comparison of test results obtained on prebaked samples (Cases 2 and 3) indicate the large margin of error is associated with the way the test has been conducted. Unexpectedly, the very same material prebaked 72 hr (Case 2) exhibited more percent TML than that prebaked only for 24 hr. The outside vendor who performed the above outgassing tests acknowledged that there is a ±20 percent margin of error with their present CVCM measurements. The error may be even more since these tests have been conducted in a laboratory without ambient control. The NASA outgassing test is performed at 10^{-6} torr. The prebaking pressure (Table 33) was much higher (1-4 torr). L'Garde previous experience has shown that by prebaking the materials at a much higher vacuum (i.e., 10^{-4} to 10^{-6} torr) the material can be brought up to acceptable levels. We are confident that the actual future flight units can be prebaked to meet NASA outgassing standard.

4.2 SHORT TUBE TESTS

To evaluate the strength, foldability, shelf life, and burst pressure of the ITSAT tube design, short length tubes (24 in long) were constructed and tested.

4.2.1 Rigidization/Compression Tests

4.2.1.1 Objectives. The objectives of this test were to

- experimentally determine the rigidization pressure required to remove all wrinkles
- determine the effectiveness of seams and internal sealers
- determine the leak rate before and after rigidization
- measure the compression strength

4.2.1.2 Results. Referring to each of the objectives mentioned, the results are the following:

- Twenty to twenty-two psi is needed to remove the wrinkles in the tube. However, this is not a direct indication of the required pressure for strength purposes. Subsection 4.3.1 shows that a much lower rigidization pressure (11 psi) is all that is required to meet the strength needs of the ITSAT.
- The seams and internal sealer were flexible enough to survive folding and deployment.
- The leak rate before folding was acceptable; the leak rate after folding was not. This led to the development of a bladder to prevent excessive leakage.
- The compression strength of the samples was measured. The results are given in Figures 81 and 82. To rigidize these two samples 22 psi was used. After rigidization the pressure was vented and the test performed.

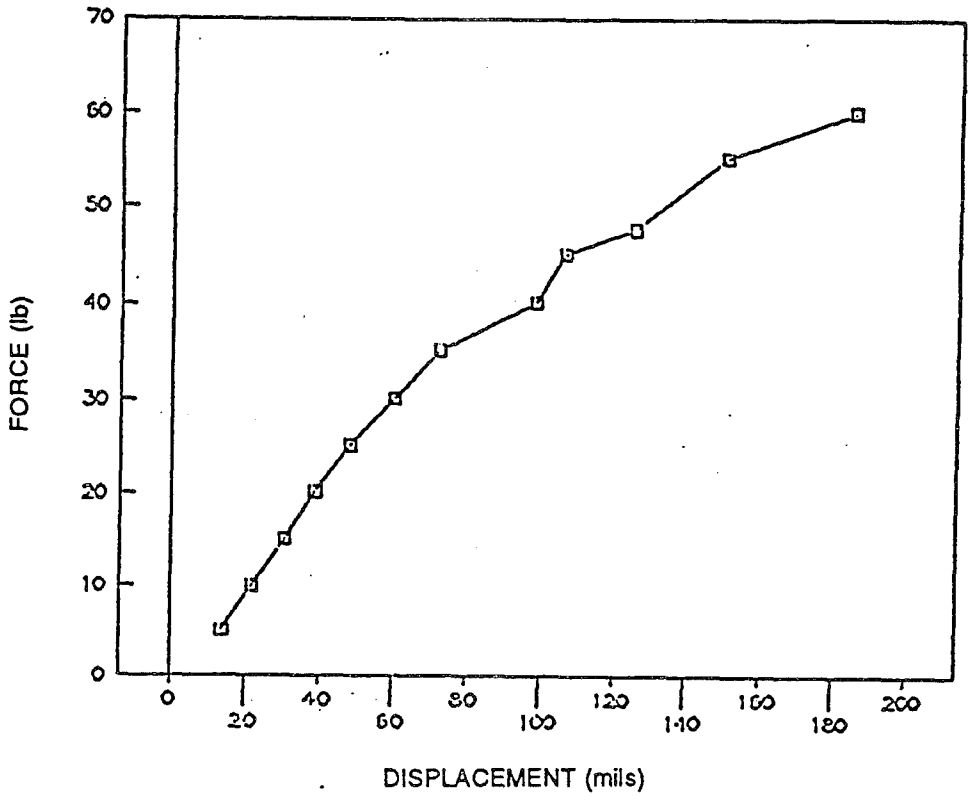

Figure 81. Four-inch tube compression test tested after folding/rigidization (sample #1).

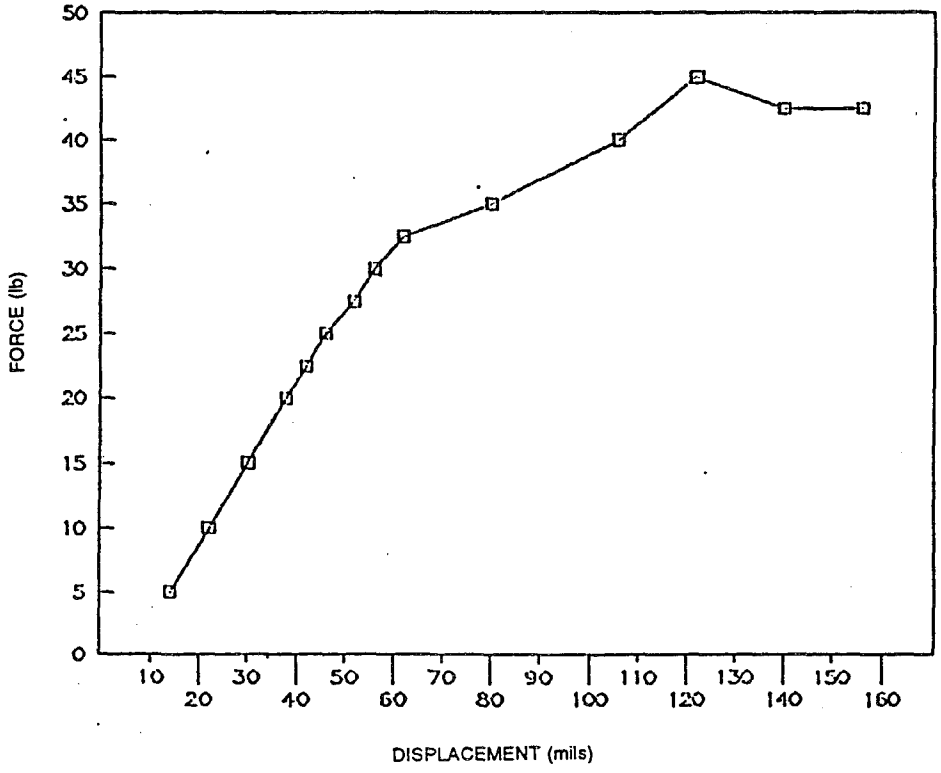

Figure 82. Four-inch tube compression test tested after folding/rigidization (sample #2).

4.2.2 Multiple Folding of Rigidized Tube

The objective of this experiment was to examine the effect of multiple packaging and folding cycles on the compression strength of the rigidized 4-in tubes. The test results will determine if the flight article can be fully ground tested before stowage without a fear of deteriorating the torus.

A 4-in diameter, 2-ft long tube was made. The tube was folded accordion style in ≈4 in wide folds. The tube was unfolded and pressurized (rigidized) to 22 psi and its compression strength was measured.

The test indicated that the ITSAT laminate is capable of being folded numerous times and will still become re-rigidized (Fig. 83). The compression strength of the test tube folded and re-rigidized seven times is still well over the required designed strength of the torus.

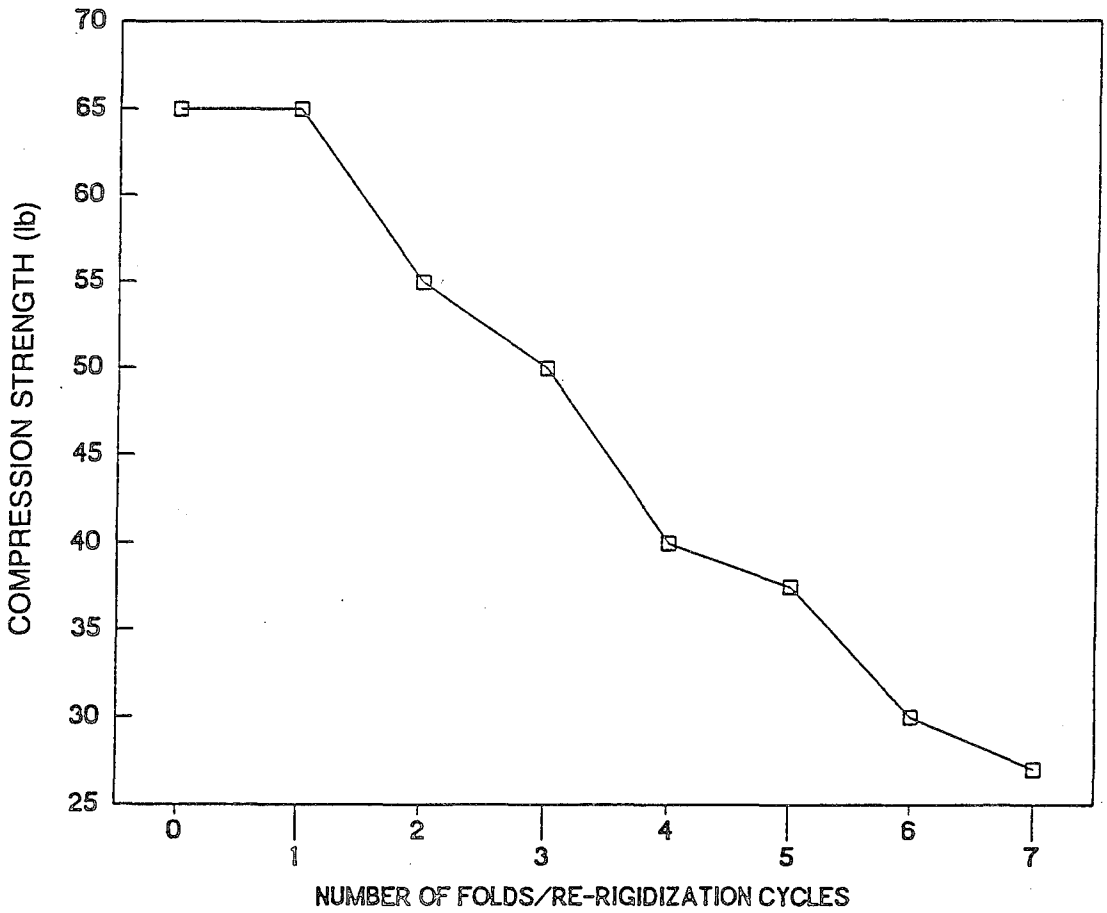

Figure 83. Compression strength versus number of packaging cycles.

Based on this small number of specimens, no loss in compression strength occurred at N = 1 (one folding cycle) indicating a full ground test can be performed on the flight unit without a fear of damaging the torus. However, the recommended safest approach is to replace the tubes after ground testing, using a set of virgin tubes for flight testing.

4.2.3 Shelf Life Test

In any flight application of the ITSAT, the solar array would be stored for a period of time before launch. This may range from a few months to a few years. One concern was that the aluminum would creep over time becoming inflexible and brittle. A test was performed to show that the ITSAT is capable of being stored for long periods without losing its integrity.

Toward the beginning of the program (9 October 1992), a short tube was packaged on 4-in fold lines and was stored in this state. At the end of the program (25 January 1994), the tube was inflated to the design pressure of 22 psi to show that it remains flexible enough to unfold, even after long periods of storage.

No loss in flexibility occurred; the tube achieved its rigidization pressure with no problems. The test can be seen on L'Garde videotape # 159.

4.2.4 Burst Test

A 24-in ITSAT sample tube was pressurized until burst to investigate how much pressure margin there is on the tube inflation pressure. The test setup is shown in Figure 84. The steps involved were

1. Fold the tube along 5.3 in foldlines (same as the ITSAT foldlines).
2. Inflate the tube to 10 psi to deploy it.
3. Turn on the video camera and high speed camera.
4. Turn up the pressure until burst.

The tube was pressurized quickly since there was only 32 s of high-speed film available.

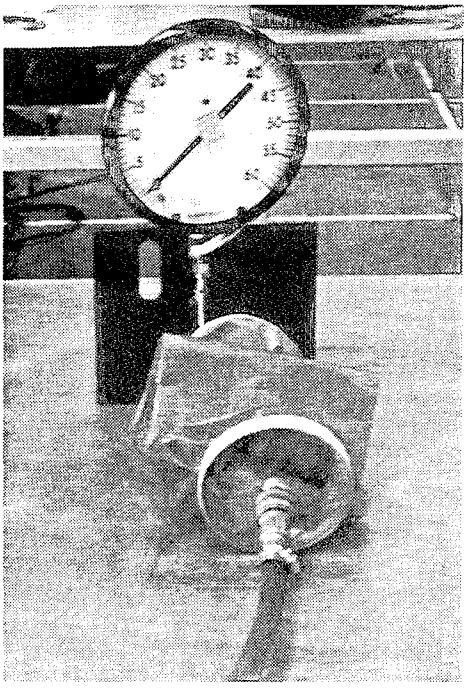

Figure 84. 24-in sample tube test setup.

The burst test can be seen on L'Garde videotapes #V136 and #V153. A photograph of the burst tube is shown in Figure 85. The tube burst at a pressure 43 psi. Based on this test the ITSAT tube has a nominal safety factor to burst of 43/22 or 1.95.

Since the test article was only one-sixth the length of the flight tubes, it is possible that the full length tube will burst at a lower pressure due to a higher probability of defects in the seam and/or material.

The tube was constructed without a bladder, as it was fabricated prior to this design change. The addition of a bladder should not affect the tube strength directly, although there is a small possibility that the bladder can get tangled during inflation. Further testing can determine the burst strength with more confidence. To develop an adequate statistical database, additional tube testing can be done.

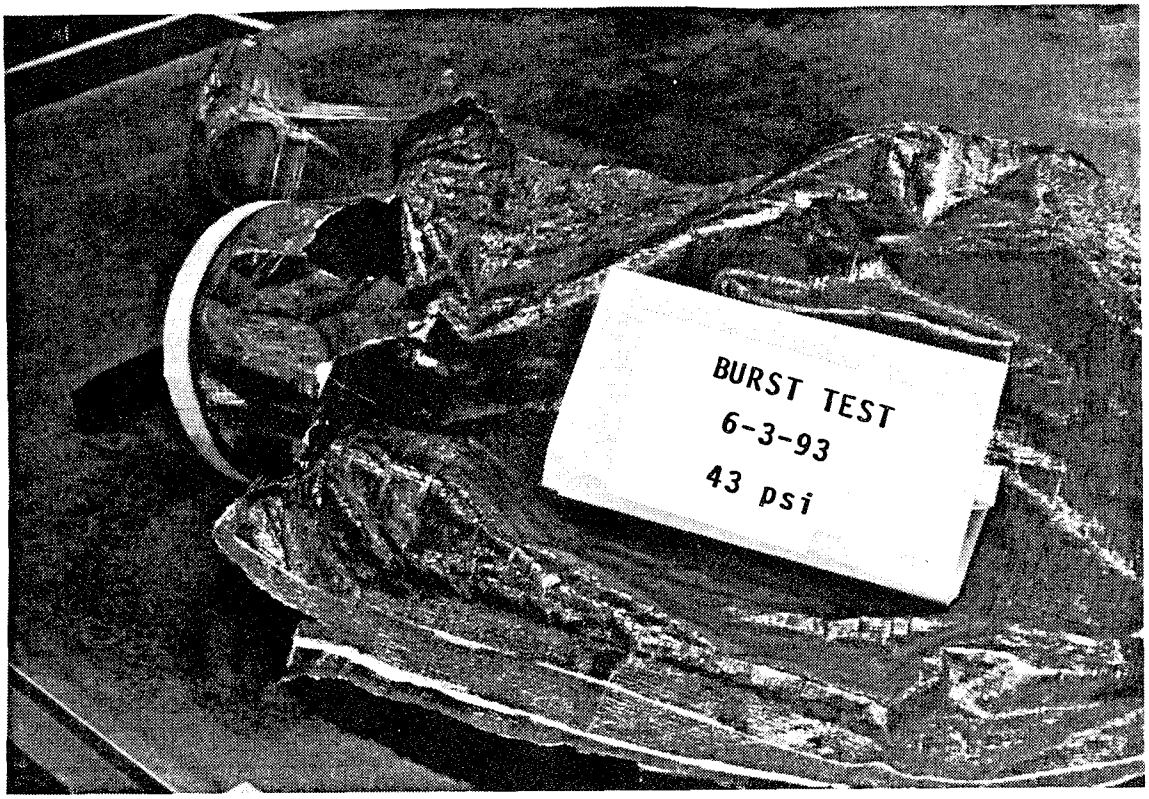

Figure 85. Burst tube.

4.2.5 Thermal Cycle of Tube Materials

Both the laminate and the bladder must be preserved prior to deployment, since deployment subjects the greatest loads to these components. If the laminate debonds, the tear resistance will decrease, making deployment less reliable. Similarly, if the bladder is weakened, subsequent inflation is threatened. To resolve these concerns, a simple test was run to determine the damage caused by thermal cycling at the expected launch temperatures given in Reference 1. The tests showed that the tubes will survive this environment. No degradation in visual appearance or strength was noted in any of the samples. A complete description of the test is given in Reference 22 and the results are given here. A photograph of the samples is shown in Figure 86. A total of 20 thermal cycles were performed from -40 to 150°F (-40 to 65.6°C). No soak time was incorporated at these temperatures. The temperature profile is shown in Appendix B.

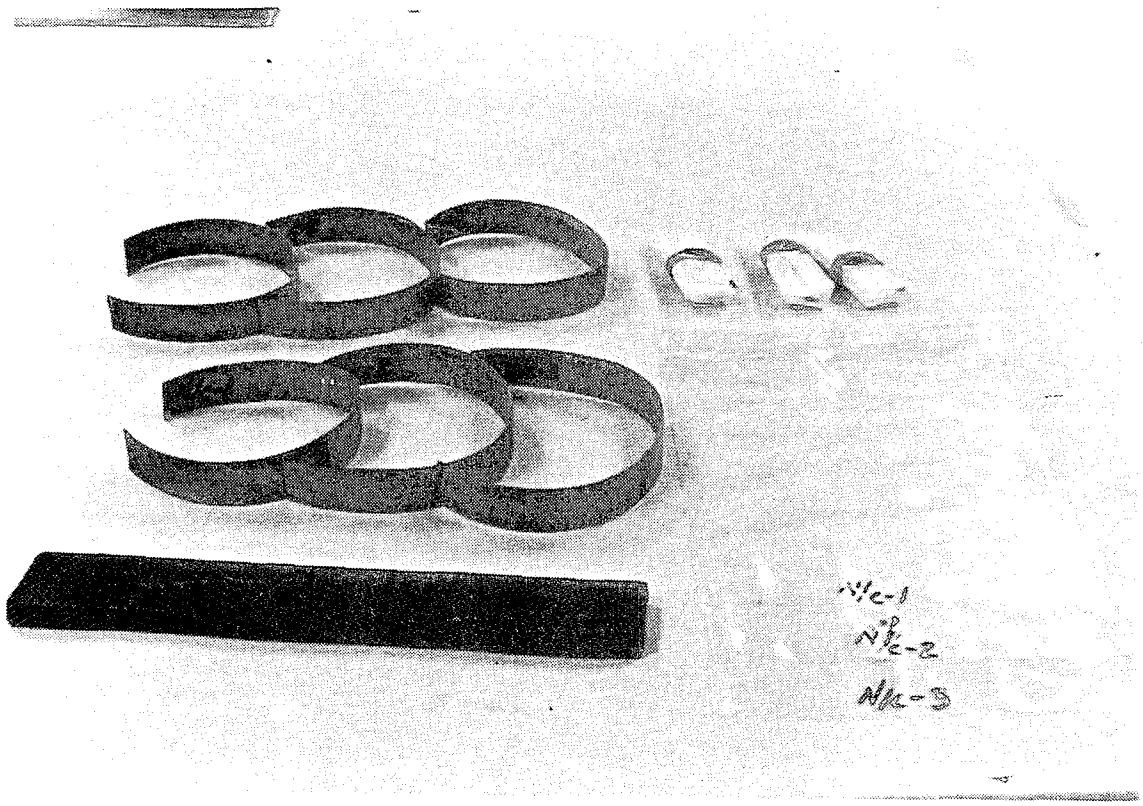

Figure 86. Sample tube materials.

After cycling, the tensile strength and breaking point of all three laminate specimens were compared to three samples that were not cycled. The results are shown in Table 34. There was no apparent degradation of the tube materials due to cycling.

As with the laminate samples, bladder samples that were thermal cycled were compared to samples that were not cycled. The samples were 12 in long by 5.1 in in diameter (same diameter as the ITSAT bladders). Each bladder was destructively tested. The results are shown in Table 35. No difference in the burst pressure was noted due to thermal cycling.

Table 34. Tensiometer results, laminate material.

SAMPLE #	DESCRIPTION	BREAKING STRENGTH (lb)	LOCATION
C-1	Cycled	96.70	Side of seam
C-2	Cycled	88.66	Side of seam
C-3	Cycled	77.45	Side of seam
N/C-1	Not Cycled	90.00	Side of seam
N/C-2	Not Cycled	85.86	Not at seam
N/C-3	Not Cycled	98.56	Center of seam

Table 35. Bladder material tests.

SAMPLE #	BURST LOCATION	PRESSURE (psi)
C-1	At heat seal	1.30
C-2	Down the side (not at seal)	1.40
C-3	Down the side	1.30
N/C-1	Hole in side	1.30
N/C-2	Down the side	1.30
N/C-3	Down the side	1.30

4.3 FULL LENGTH TUBE TESTS

This section presents the test data from the full length tube tests.

4.3.1 Bending Strength/Stiffness Tests at Various Rigidizing Pressures

A series of tests were conducted to investigate the effect of rigidization pressure on bending stiffness and bending strength of the ITSAT tubes.

4.3.1.1 Background. During the initial fabrication and testing of the short tubes, a "goal" rigidizing pressure of 22 psi was established. This was the pressure required to remove all the wrinkles in the laminate material caused by packaging. Initial studies indicated that the tube had to be completely smooth to perform as a thin-walled structural member. This turned out not to be the case. Rather, as this section shows, the strength of the tube changes only slightly if the pressure does not reach the 22-psi value.

Optimizing the baseline rigidizing pressure has several advantages:

- Less gas is needed for inflation, allowing a smaller, lighter inflatant tank to be used.
- Lower inflation pressure means the safety factor for bursting the tube is higher.
- If we can specify a larger acceptable range of pressures required for rigidization, we can be more flexible for inflation conditions, i.e., inflation can occur in eclipse, in sunlight, etc.

4.3.1.2 Removal of Wrinkles. After filling the tube to each pressure, the tube was vented to zero pressure and a photograph was taken. After the photograph, the bending test was performed. Although it is a subjective assessment as to how high the pressure must be taken to remove an adequate amount of wrinkles, it appears that 11 psi removes enough wrinkles to provide a structurally sound tube.

4.3.1.3 Bending Strength Versus Rigidizing Pressure. Table 36 and Figure 87 give the results of the strength test. A description of Figure 87 follows:

- The bottom line is the stress level requirement for the tube which is the expected stress level expected in flight (assuming a maximum load on the satellite of 0.03 g).
- The middle line shows the stress level requirement for the tube which is the expected stress level multiplied by a safety factor of 1.4 (per DOD-HDBK-343).

Table 36. Bending strength results.

RIGIDIZING PRESSURE (psi)	YIELD POINT (lb)	FAILURE POINT (lb)	BENDING MOMENT AT FAILURE (in-lb)	BENDING STRESS AT FAILURE (psi)	BENDING STRESS EXPECTED (psi)	SAFETY FACTOR
11	0.24	0.45	62.88	1668	213.2	7.82
14	0.46	0.55	76.85	2039	213.2	9.56
17	0.51	0.59	82.44	2187	213.2	10.26
20	0.57	0.60	83.84	2224	213.2	10.43
22	0.63	0.63	88.03	2335	213.2	10.95

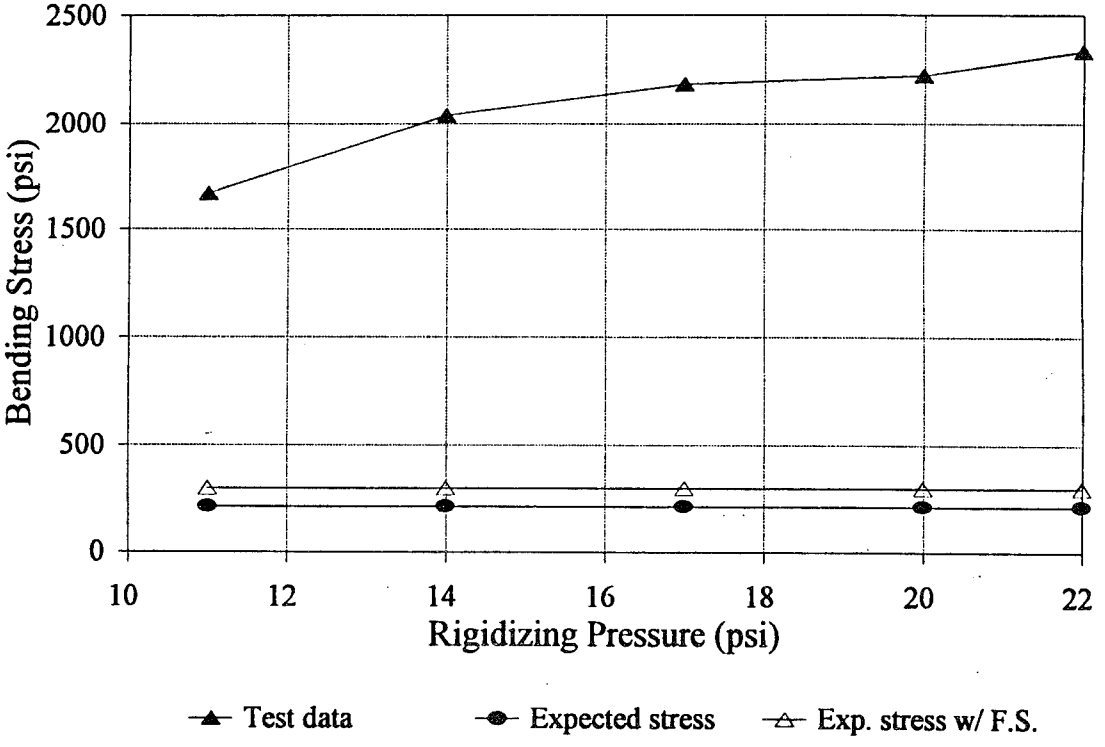

Figure 87. Bending strength versus rigidization pressure.

- The top line of the graph shows the test data, in which we pulled a tube from its outer end and found the stress level in the laminate when the tube buckles at its base. Note that the 5- and 8-psi pressures are not included on the graph since the tube did not rigidize sufficiently at these pressures.

While there were still some wrinkles in the material at these lower pressures, the strength was well above the design requirements in all cases.

These data are compared to the bending strength needed in flight. Refer to Subsection 3.2.1 where the applied bending load to the tube in flight is calculated. The results show that the minimum safety factor (for 11 psi) is still 7.82; failure due to bending strength is no problem. The bending tests showed that the tubes are of a conservative design and can be optimized in later designs to reduce mass and volume.

4.3.1.4 Bending Stiffness Versus Rigidizing Pressure. The stiffness varied with rigidization pressure as shown in Table 37 and Figure 88. The question is "what is the minimum stiffness required?" There was not a direct requirement for stiffness, though we did have a goal for deployed natural frequency which depends on stiffness.

From Subsection 4.7.2 it is seen that the deployed natural frequency was 1.04 Hz about its z-axis (its weakest direction) at a minimum rigidizing pressure of 17.2 psi. Now the natural frequency is calculated for differing tube stiffnesses. In other words, if the pressure is different from the 17.2 psi attained during the test, what will the natural frequency be? The results are given in Table 38 and Figure 89.

Table 37. Bending stiffness results.

RIGIDIZING PRESSURE (psi)	STIFFNESS (lb/in)
11	0.300
14	0.346
17	0.395
20	0.432
22	0.457

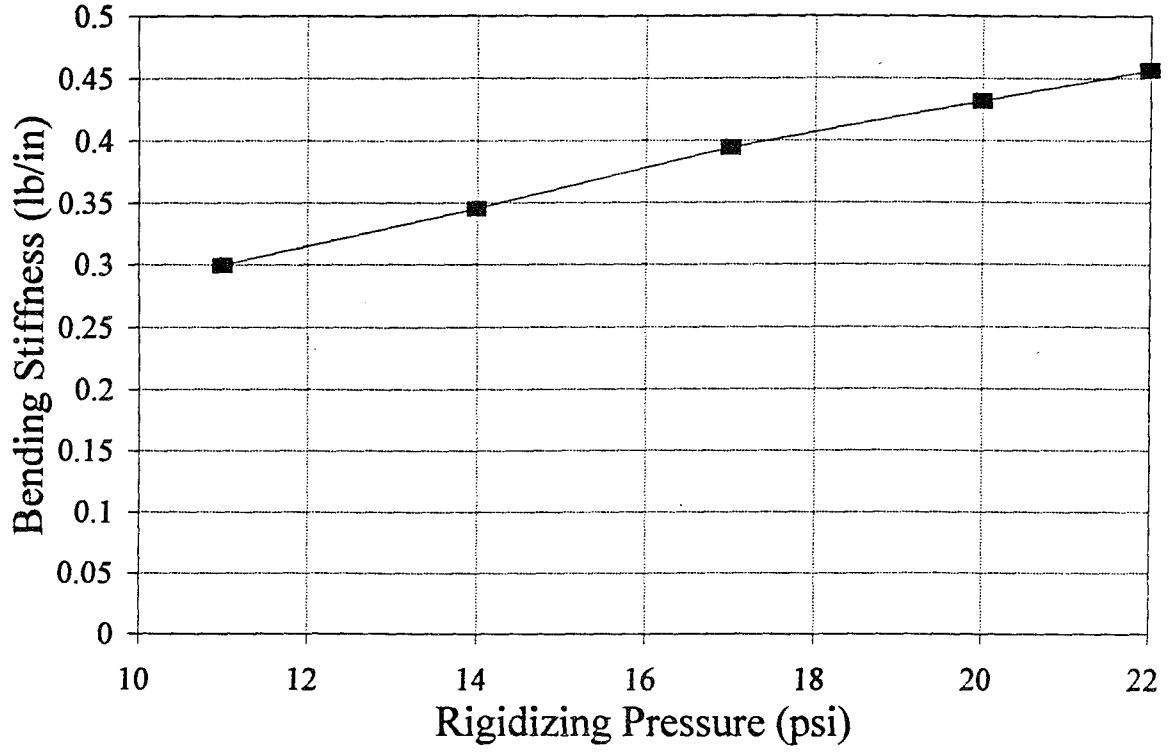

Figure 88. Bending stiffness versus rigidization pressure.

Table 38. Natural frequency versus rigidization pressure.

RIGIDIZING PRESSURE (psi)	TUBE STIFFNESS (lb/in)	ARRAY STIFFNESS (lb/in)	ARRAY NATURAL FREQUENCY ABOUT THE Z-AXIS (Hz)
11	0.300	0.263	0.982
14	0.346	0.280	1.012
17	0.395	0.294	1.039
20	0.432	0.304	1.056
22	0.457	0.310	1.066

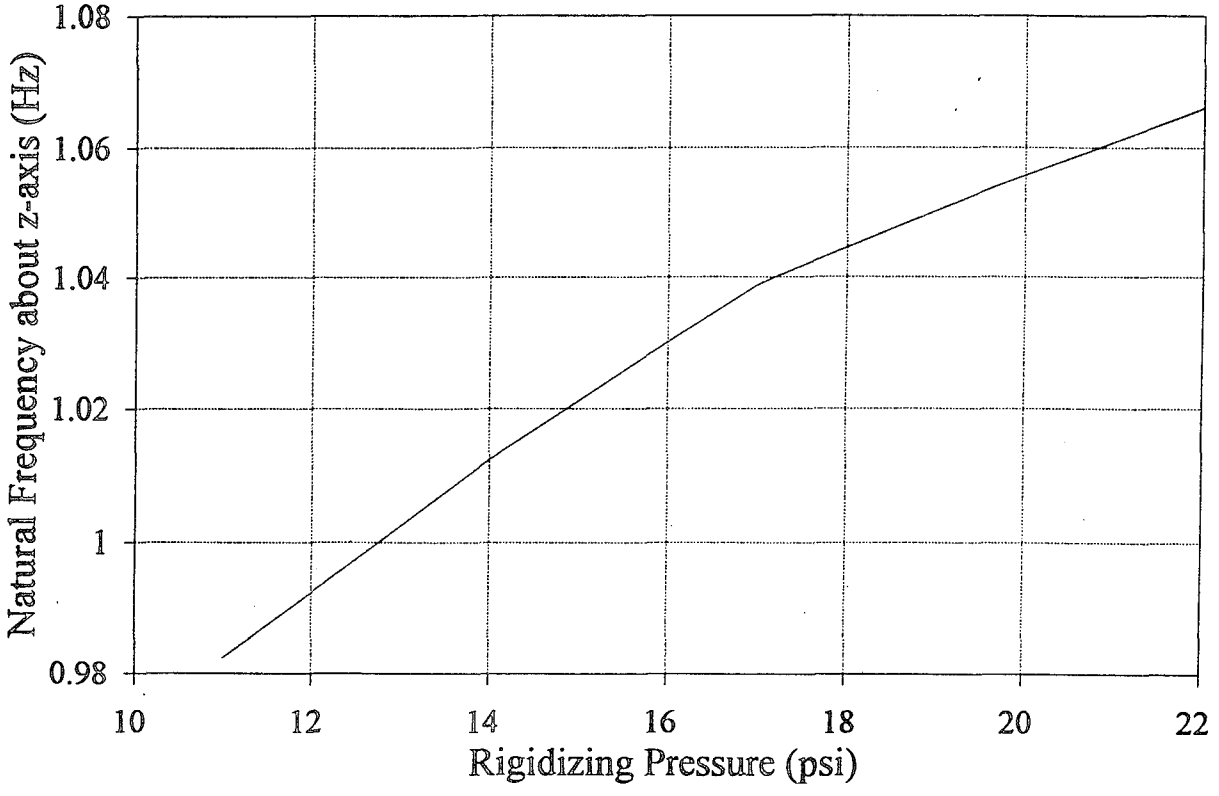

Figure 89. Natural Frequency versus rigidization pressure.

4.3.1.5 Conclusions. This test showed that if 22 psi is not achieved during the vacuum test or in flight, the ITSAT will have adequate integrity due to the tube's large safety factor. The natural frequency will decrease slightly with decreasing rigidization pressure.

To determine the rigidization pressure achieved during flight, we ran an analysis to determine the temperature at deployment and the resulting rigidization pressure. The results of this are contained in Subsection 3.2.1.

4.4 INFLATION SYSTEM TESTS

A number of development tests were performed on the inflation system. The purpose of these was to prove the operation of the components prior to the system tests described in Subsections 4.6 and 4.7.

4.4.1 Fixed Volume Blowdown Test

The object of this test was to measure the following items: (1) verify the proper functioning of the ITSAT II inflation system; (2) measure the gas flow rate from the inflation system; and (3) measure the pressure rise inside the simulated inflatable volumes. A complete test report can be found in Reference 23.

The inflation assembly was connected to two simulated fixed volumes of approximately 1767 in^3 each. These volumes were used to represent the internal volumes of the deployed inflatable(s). Figure 90 shows the inflation assembly connected to the two blowdown volumes, along with a pressure transducer on each blowdown volume to measure the internal pressure rise of the fixed volumes. In addition a flow meter was placed in series with one of the lines to measure gas flow during the test. This entire assembly was placed inside the L'Garde vacuum chamber as shown in Figure 91. The results of the blowdown tests are shown in Figure 92.

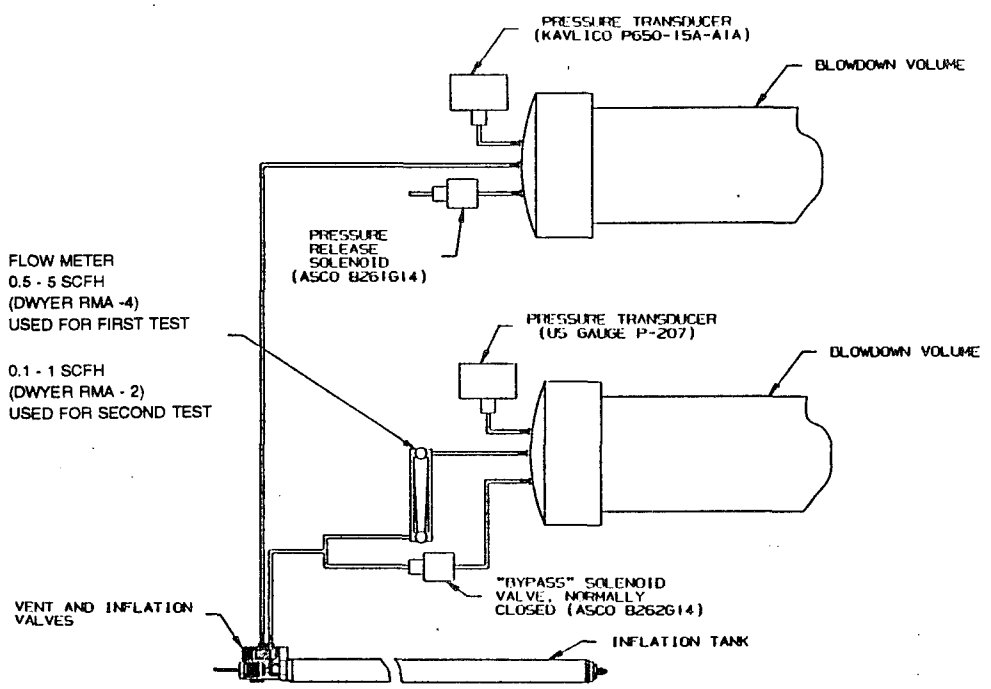

Figure 90. Inflation assembly test setup.

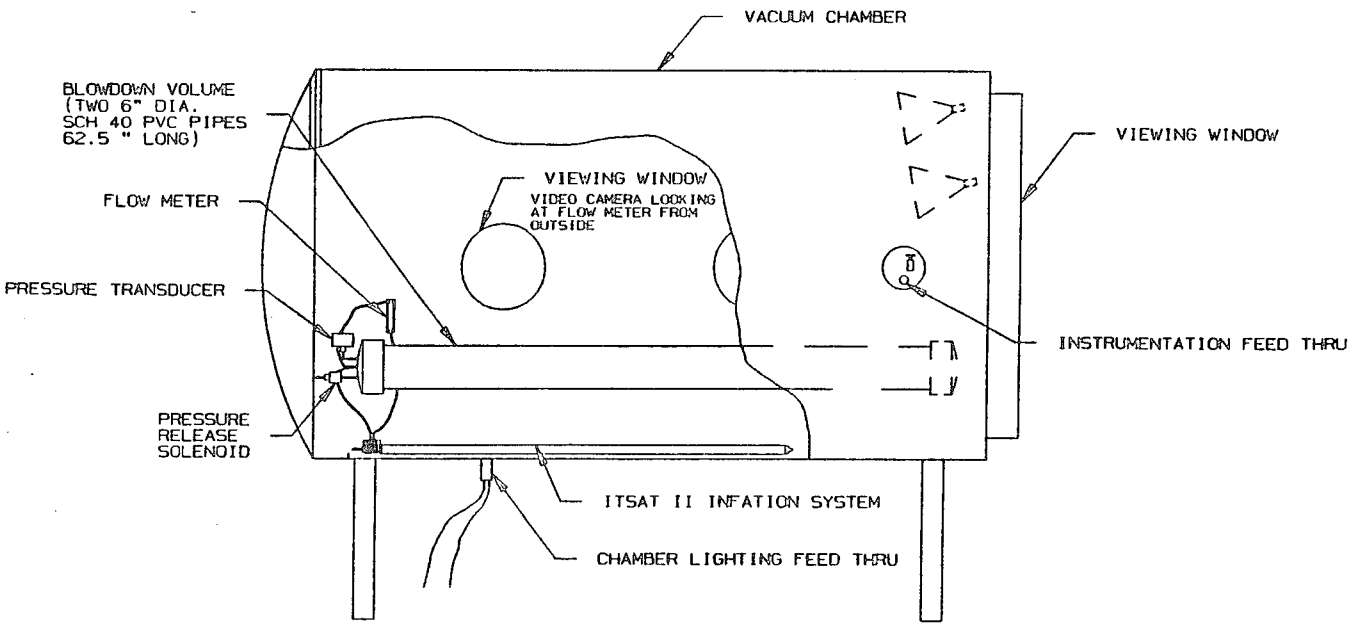

Figure 91. Vacuum chamber test setup.

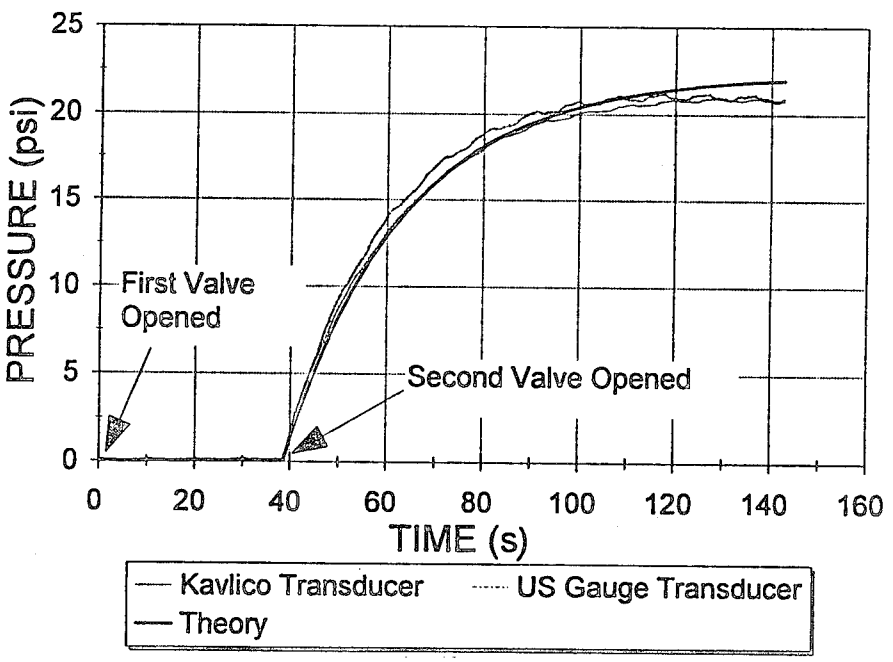

Figure 92. Fixed volume blowdown test results.

The results were as theory predicted. The first inflation valve was opened at T = 0; this slow rise in pressure is used to deploy the inflatable tubes in space. At T = 38 s the second inflation valve was opened to allow the remaining inflation gas to enter into the fixed volumes at the faster rate. The test showed the correct final pressure of approximately 22 psi.

4.4.2 Ascent Venting Test

The object of this test was to determine if the ITSAT II vent valve assembly can adequately vent residual pressure from the inflatable(s) when subjected to a simulated ascent pressure profile (Ref. 24). For this test a simulated volume was used to represent the internal volume occupied by the packaged inflatable tubes.

The vent valve assembly was connected to a simulated vent volume of ~125 in^3. This simulated vent volume was used to represent the approximate internal volume of the packaged inflatable(s). Figure 93 shows the vent valve connected to the simulated vent volume, along with a pressure transducer to measure the internal pressure of the simulated vent volume. This entire assembly was placed inside a small vacuum chamber as shown in Figure 94. Figure 94 also shows the pump and valving system used to produce the required ascent pressure profile.

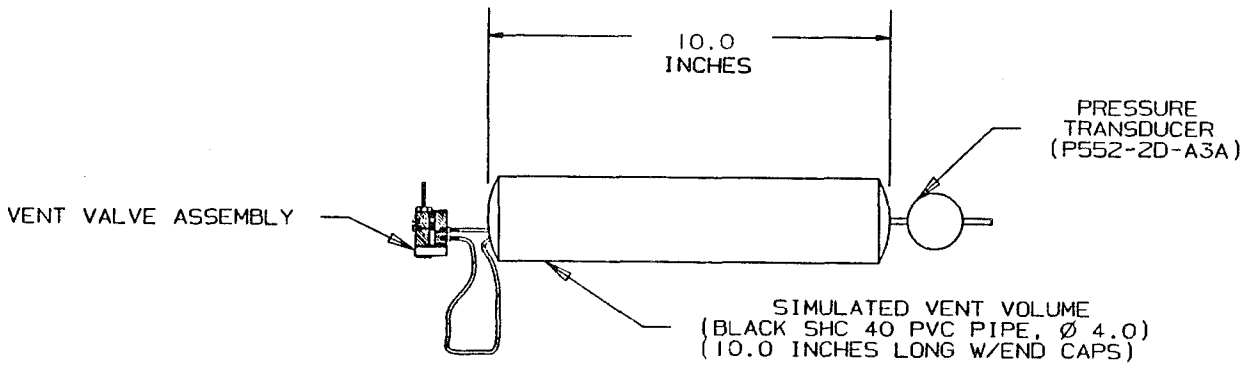

Figure 93. Vent valve, simulated vent volume assembly.

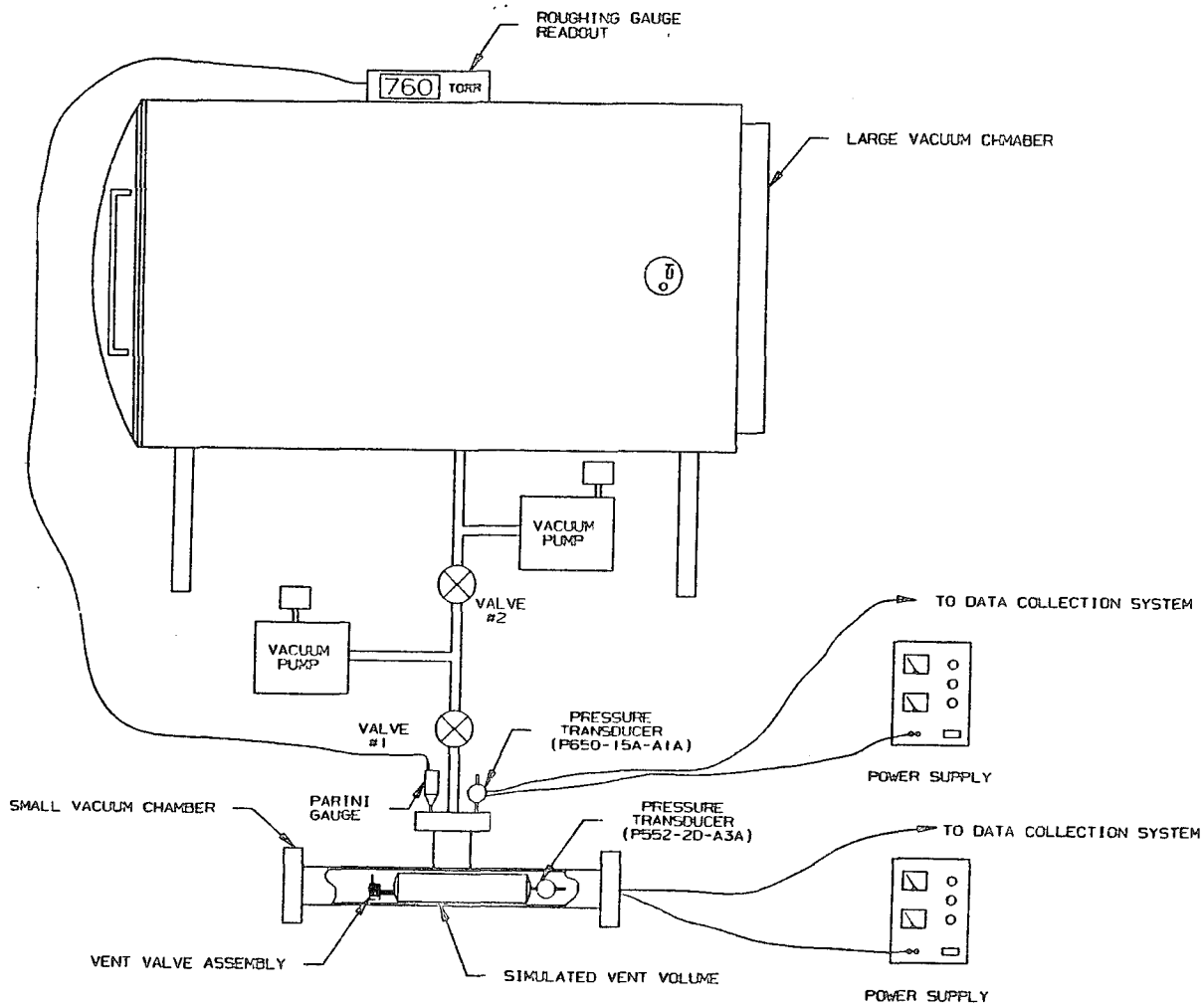

Figure 94. Vent valve test setup.

The venting tests were run as follows. Valve #1 was closed and valve #2 was opened. Both vacuum pumps were turned on and allowed to run for ~4 hr. The cyro-pump was activated to bring the large vacuum chamber pressure as low as possible. Valve #2 was closed and the data collection system was started. Valve #1 was slowly opened to allow the small vacuum chamber to begin to vent. The valve was opened at a rate to roughly follow the pressure profile shown in Figure 95. When valve #1 was fully open and the first vacuum pump could no longer vent at a fast enough rate to match the profile shown in Figure 95, valve #2 was opened to the large evacuated chamber.

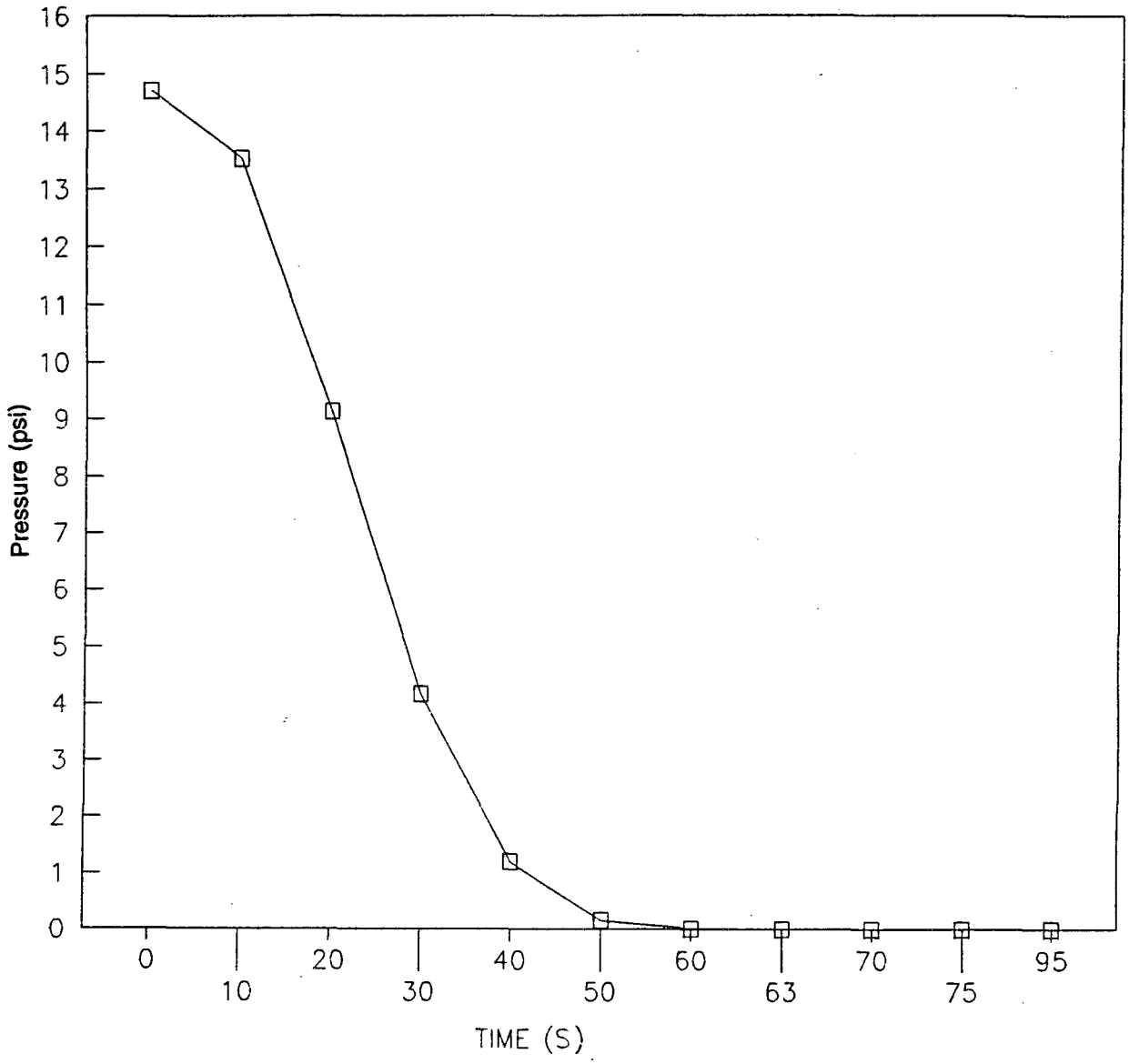

Figure 95. Ascent pressure profile.

The test closely followed the actual ascent venting profile shown in Figure 95. The three curves shown in Figure 96 are (1) the ascent venting profile specification (same curve as shown in Figure 95, (2) the actual test vent profile, and (3) the fixed volume pressure rise. This graph shows a maximum pressure rise inside the fixed volume of 0.65 psi.

The limited pressure rise inside the fixed volume should cause no significant problems to the packaged inflatables during an actual flight test. The test results shown are for the most severe ascent pressure profile the system would ever experience. This test proves the ITSAT II vent valve assembly has adequate capacity to vent the inflatables during flight.

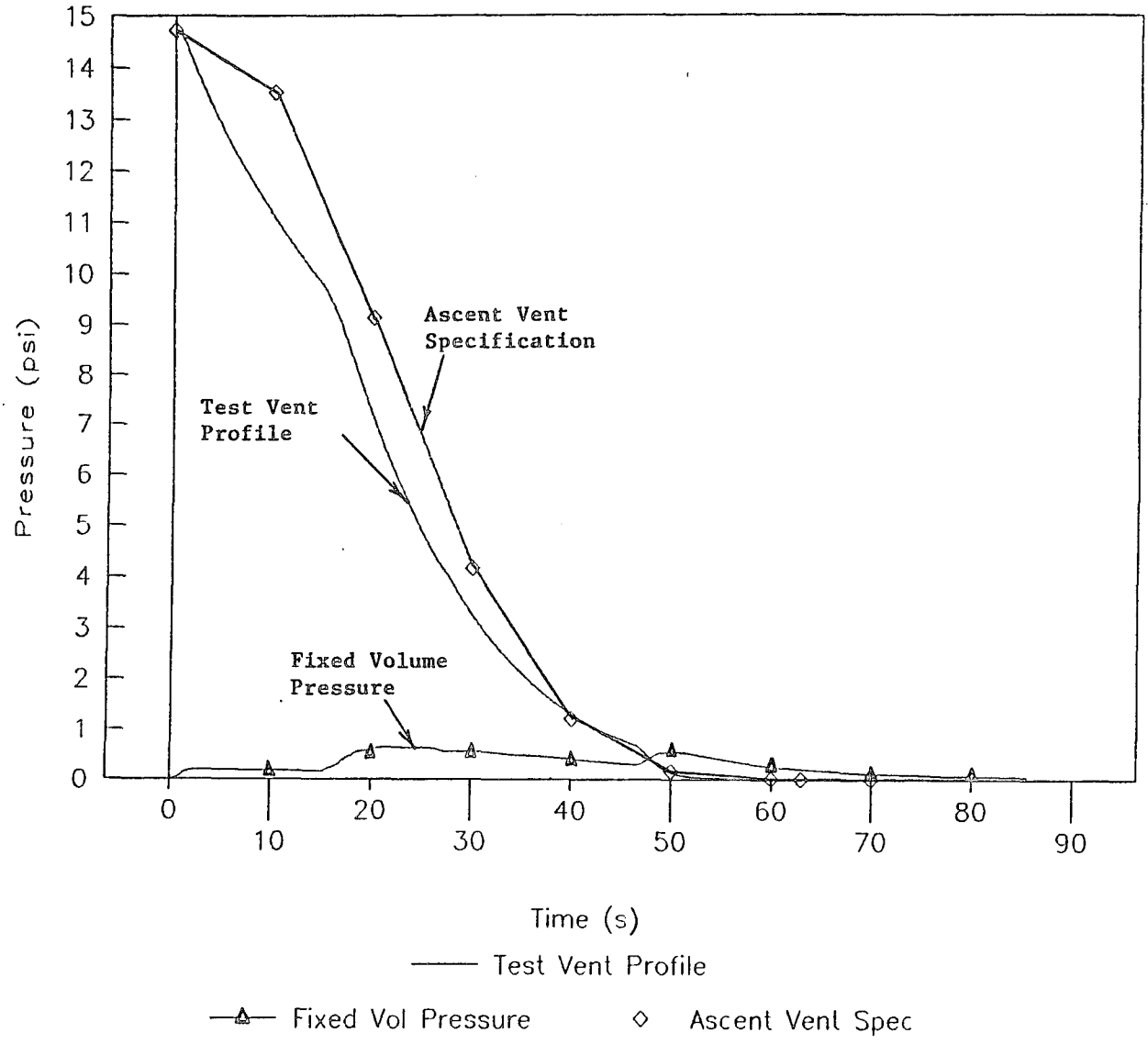

Figure 96. Ascent venting test results.

4.4.3 Inflatant Tank Testing

The object of this test was to "Qualify" the inflation tank. This qualification was done in several steps. The first "test" was a burst test to determine if the tank design would meet the required safety factor. The next two "tests" were proof tests of the actual flight inflation tanks. All testing was done at J.C. Carter Company in Costa Mesa, California.

Figure 97 shows the test setup for proof and burst testing. During testing two videos were created, one monitoring the test article and the other observing the pressure gauge of the system.

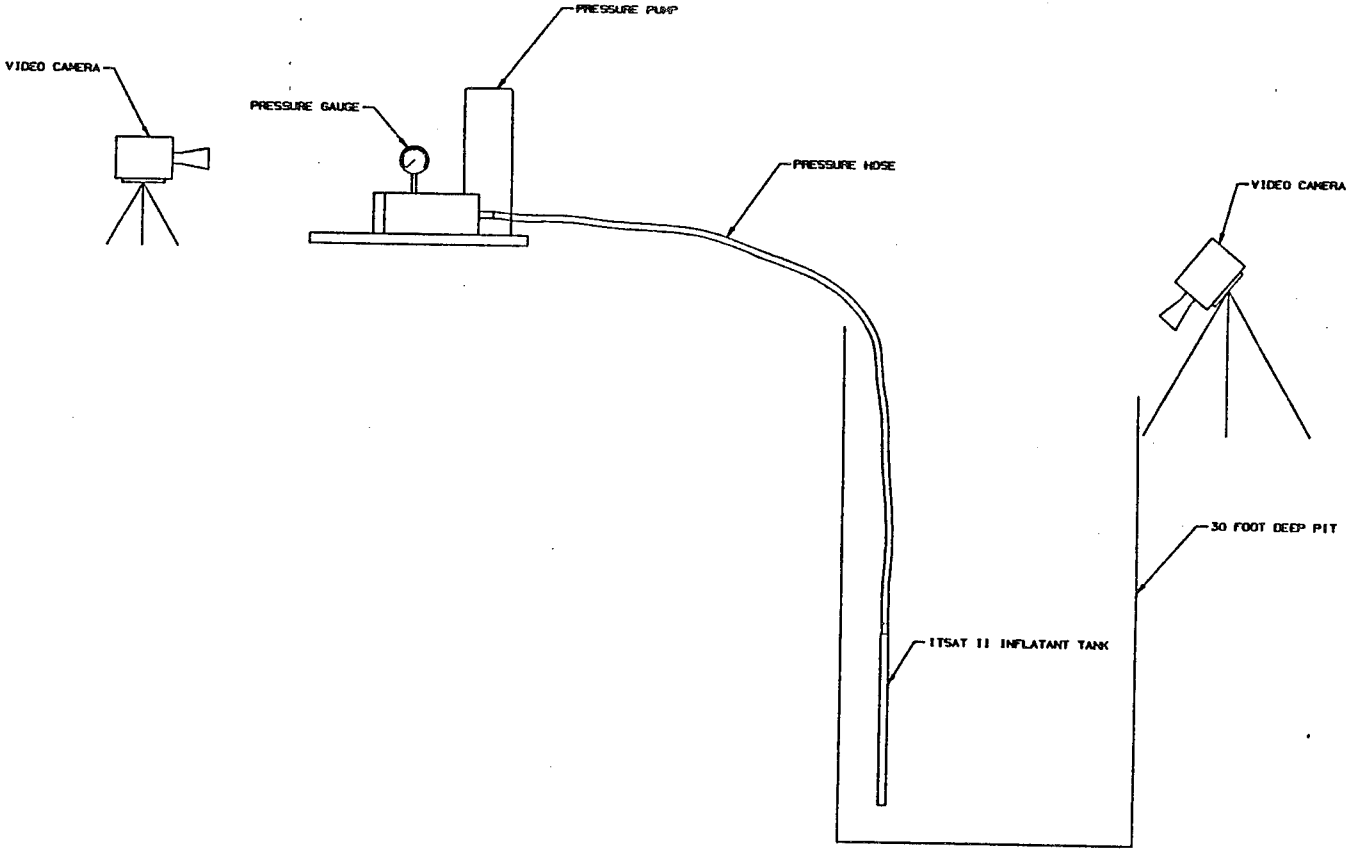

Figure 97. Inflatant tank proof and burst pressure test set up.

Inflatant tank serial number -01 was tested to burst. The burst test was run as follows. The unit was set up as shown in Figures 97 and 98. The tank was pressurized to proof pressure (5500 psi) and allowed to stand for 10 min. No leaks were observed at proof pressure. Next the pressure in the tank was increased in steps of ~500 psi until the unit ruptured at 13,250 psi. Figure 99 shows the ruptured inflation tank. The factor of safety based on this burst pressure is 13,250 psi/2870 psi = 4.62.

Tank serial numbers -02 and -03 are the two flight units which were each proof-tested at a slightly higher pressure (6000 psi) for 10 mins. No leaks were observed during the proof tests. A complete description of the test results is given in Reference 25.

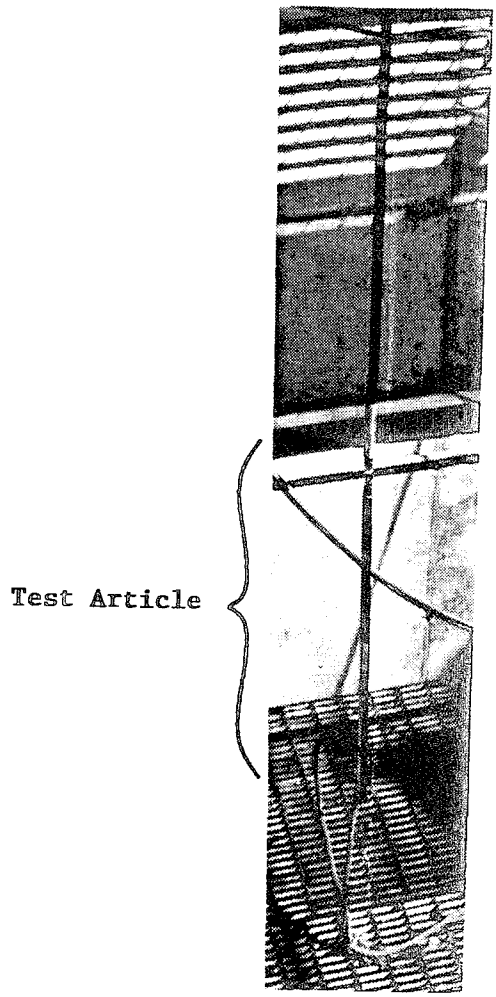

Figure 98. Inflatant tank during testing.

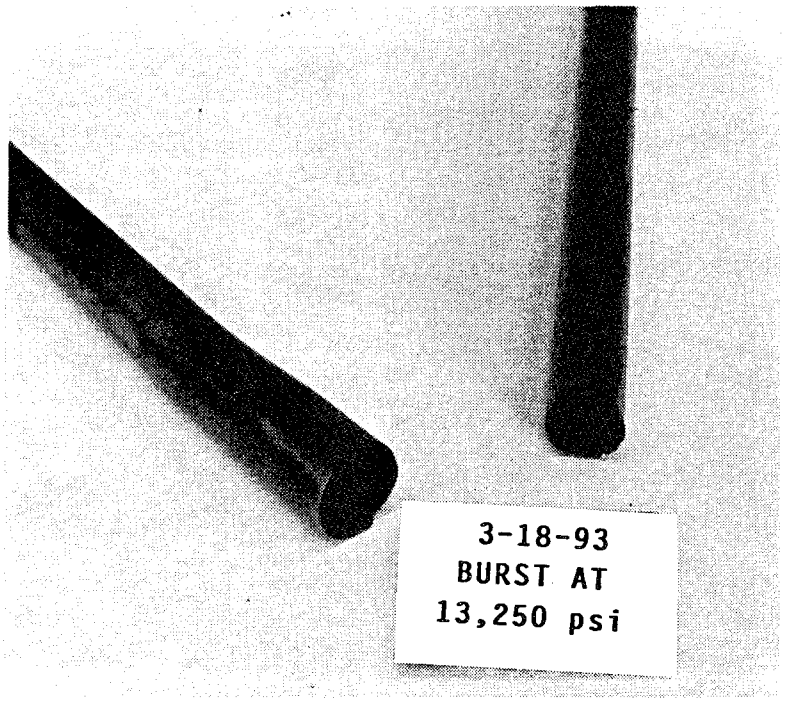

Figure 99. Ruptured inflatant tank.

4.4.4 Five Foot Tube Inflation Test

The object of this test was to deploy a 5-ft long ITSAT II rigidizable tube in vacuum using the actual ITSAT II inflation system hardware (Ref. 26). During the test the following items were measured and observed: (1) verified the proper balloon deployment speed after firing the first of two inflation valves; (2) measured the gas flow rate from the inflation system after firing the first and second inflation valves; (3) measured the pressure rise inside the inflatable tube after firing the first and second inflation valves; and (4) measured the balloon leak rate in vacuum after the tube has been fully pressurized and rigidized.

The ITSAT Inflation Assembly was connected to the packaged 5-ft long ITSAT II inflatable tube. Figure 100 shows the five-foot tube inflation test components test setup. This entire assembly was placed inside the L'Garde vacuum chamber as shown in Figure 101. Figure 101 also shows the "slider plate" on a slight (5 deg) downward slope to more realistically simulate a deployment in zero gravity. The free end of the inflatable tube was allowed to slide on this nearly frictionless surface during the deployment.

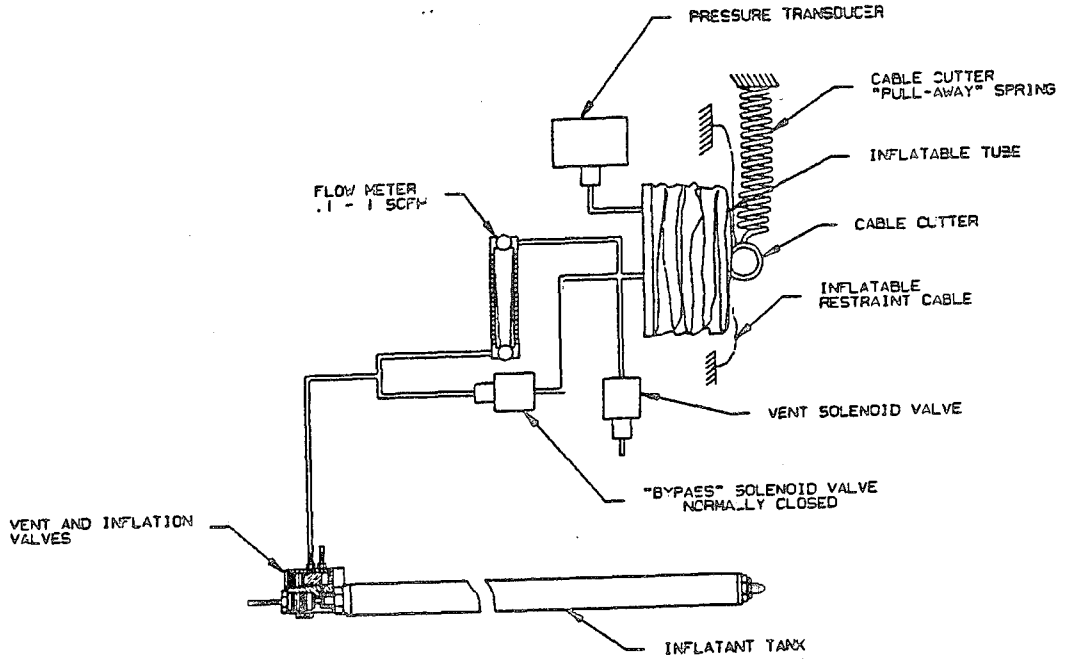

Figure 100. Five-foot tube inflation test components test setup.

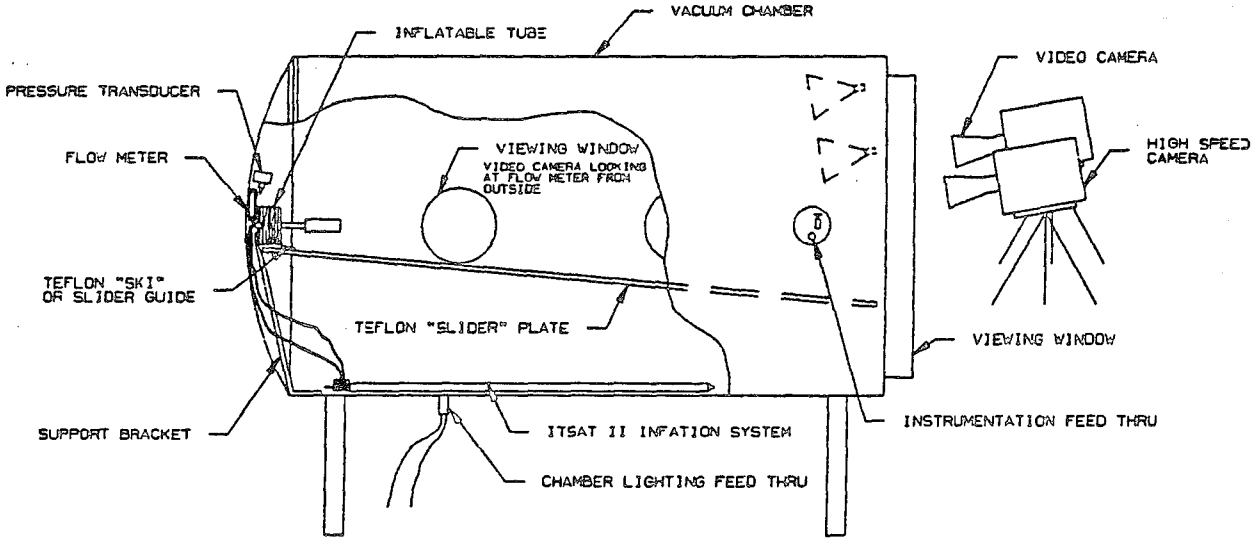

Figure 101. Five-foot tube vacuum chamber test setup.

The tube pressure data from this test were recorded using the L'Garde data collection system. The tube deployment was recorded visually using a Super VHS video camera operating at 30 frames per second at 1/1000-s shutter speed.

The inflation test of the 5-ft long rigidizable tube was conducted three times. The first test determined that the originally selected primary visco-jet was too restrictive. The second test discovered a leak path in the vent valve assembly which caused the tube not to reach full pressure and, thus, not rigidize. The third test was a complete success.

The results of test #3 are given in Figures 102 to 104, Figures 102 and 103 give the results from the "inflation" portion of the test and Figure 104 shows the results from the "leak test" portion of the test. L'Garde video tape number V144 shows the deployment of the tube viewed from outside the vacuum chamber looking through the large window.

Figure 103 shows the pressure rise in the inflatable tube after the first and second inflation valves were opened. The first of the two inflation valves was opened at T = 0.0 s. At T = 5 s the tube was fully extended but still had a slight kink. At T = 27.0 s the kink was removed and the tube was completely deployed. Also, at this time the second inflation valve was fired and the pressure rose to ~22 psi in 70 s. This pressure profile closely resembles the profile required for the deployment and rigidization of the tubes in the actual flight system.

The results of the "leak test" portion of the test can be found in Figure 104. These results were obtained after the inflatable had been folded and deployed one time as it would be in the flight system. The vacuum results were obtained by monitoring the leak rate of the inflatable after pressuring the tube to 22 psia while inside the vacuum chamber. The fuse did not include a bladder since this design change was not incorporated at the time.

4.5 SOLAR ARRAY DEVELOPMENT TESTING

The ITSAT blanket was based on fabrication techniques learned during the L'Garde Solar Array Program. Two of the tests conducted on small scale coupons are discussed here.

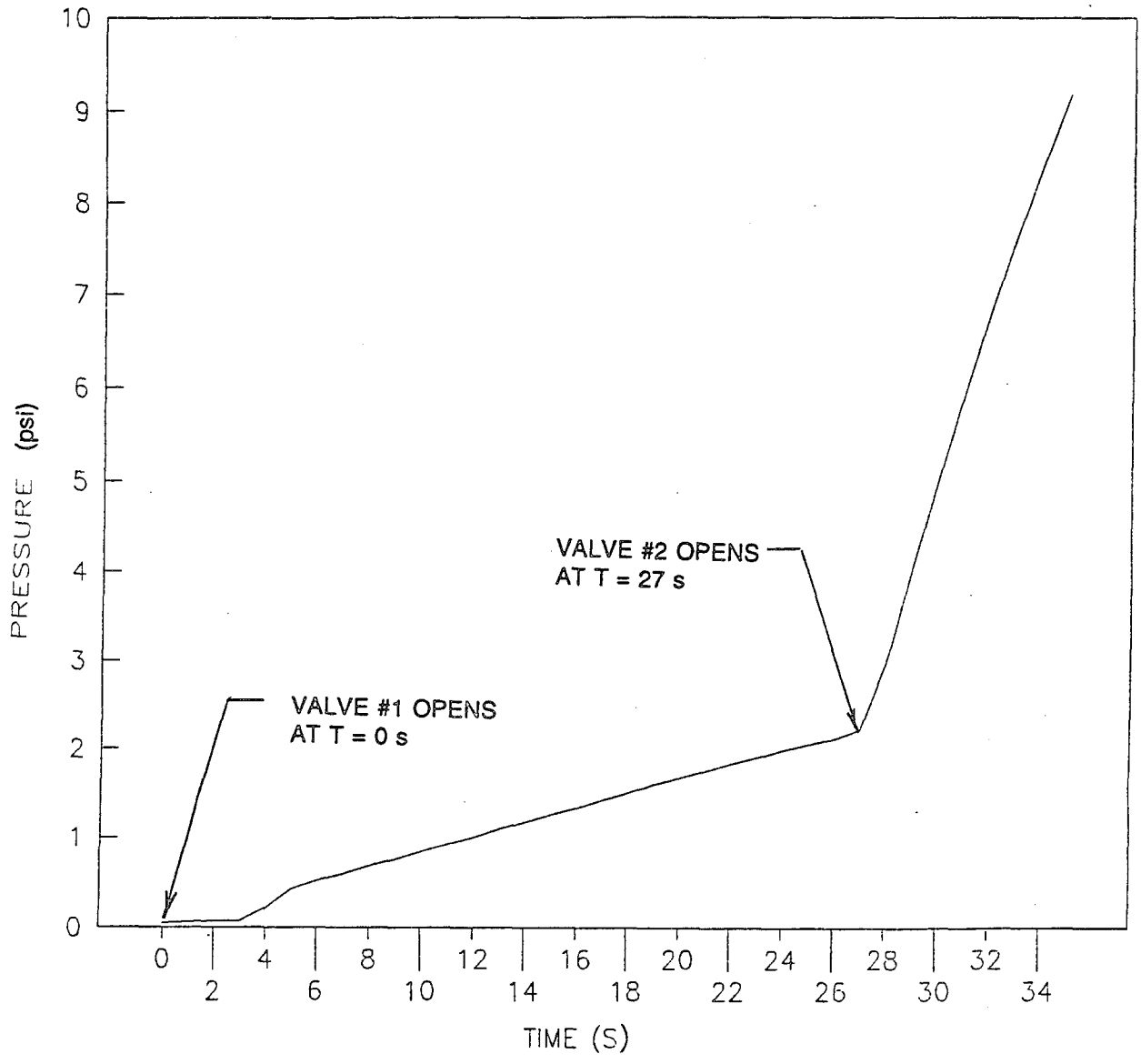

Figure 102. Pressure profile (stage 1).

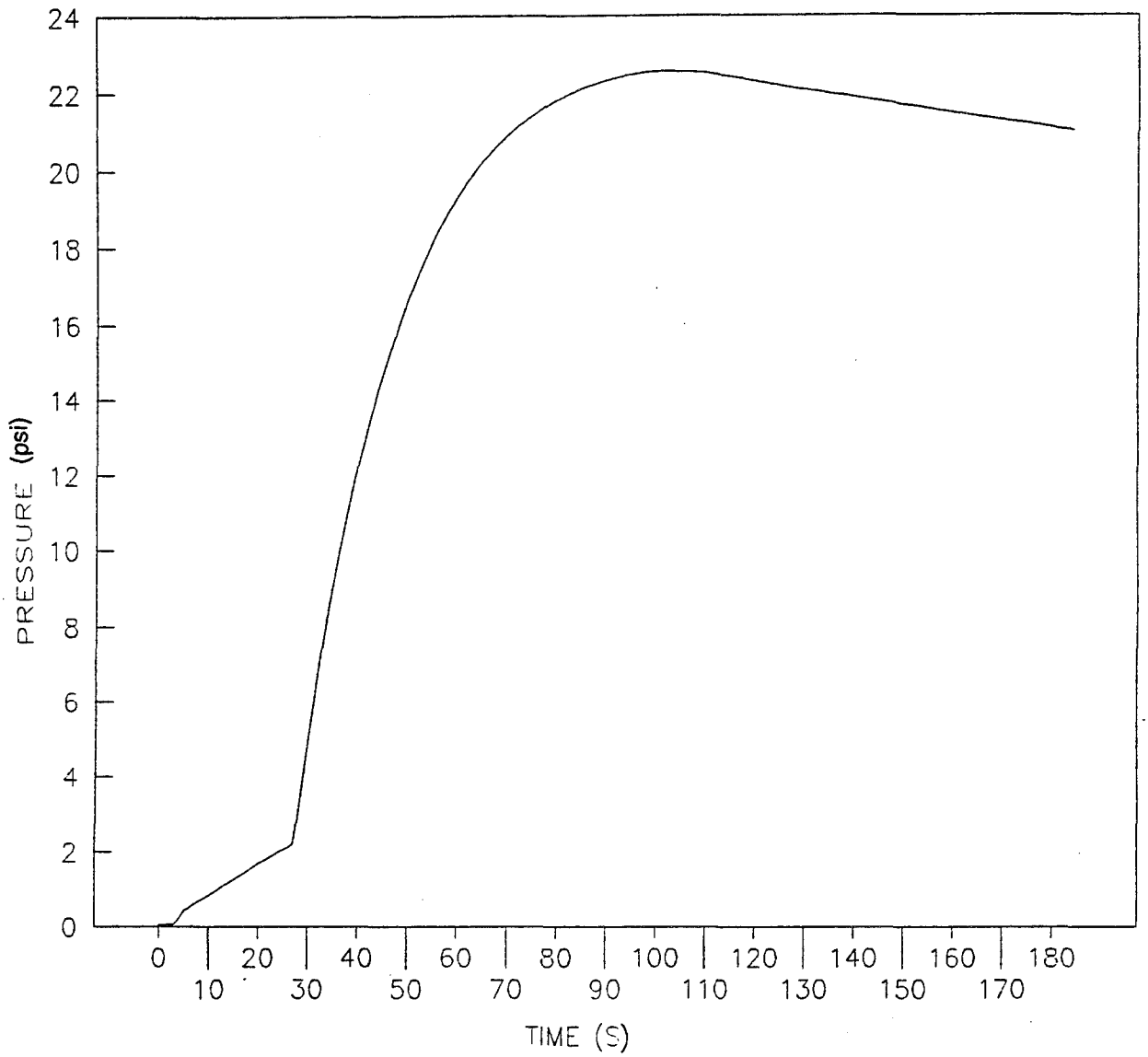

Figure 103. Pressure profile (stage 2).

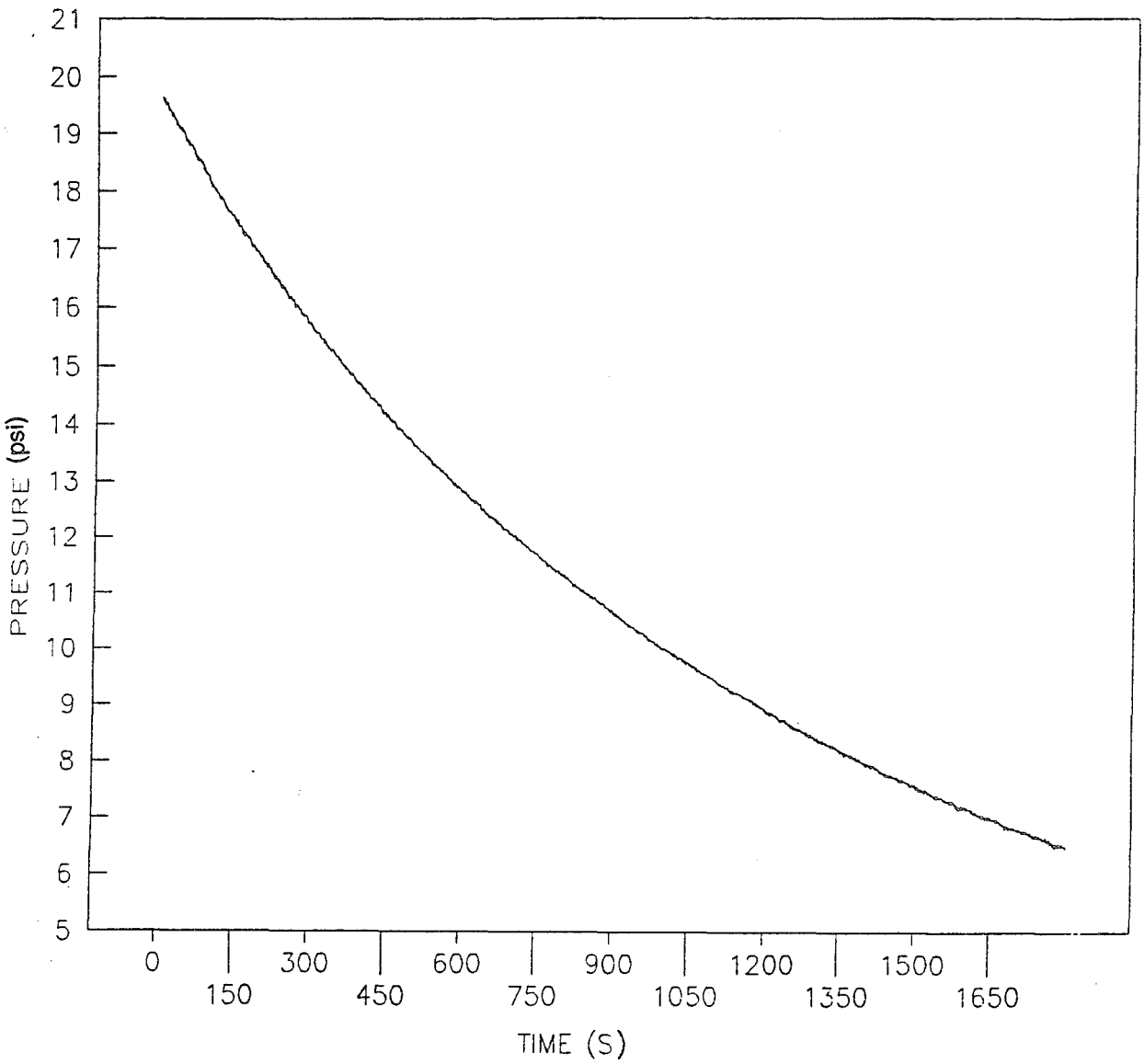

Figure 104. Vacuum leak rate.

4.5.1 Peel Tests of SiOx-Coated Kapton®

The purpose of the test was to see what effect the SiOx coating has on the bonding of the solar cells to the solar blanket substrate. Samples of noncoated Kapton® were tested for comparison. Our tests indicated that the peel strength is improved using the coated Kapton®.

Five samples of each type of Kapton® were tested (5 coated and 5 noncoated). These were bonded to the backs of solar cells with McGhan Nusil CV1-1142 adhesive (same as that used for the ITSAT blanket). The samples mounted on the tensiometer are shown in Figure 105.

Table 39 gives a summary of the results. Coated Sample #4 represented a poor bond rather than a degradation of bond strength due to the coating.

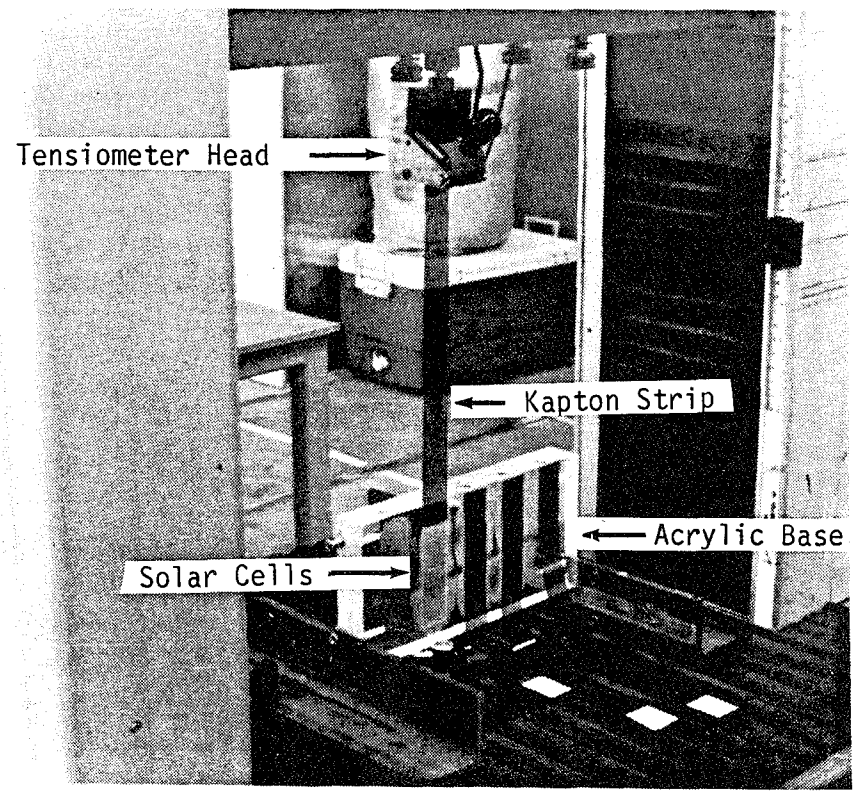

Figure 105. SiOx coated Kapton® test setup.

Table 39. Peel strength results.

TYPE	SAMPLE #	AVERAGE PEEL STRENGTH (lb)
Bare	1	0.05
Bare	2	0.10
Bare	3	0.05
Bare	4	0.04
Bare	5	0.01
Coated	1	0.20
Coated	2	0.20
Coated	3	0.15
Coated	4	0.00
Coated	5	0.10

The data are rather scattered, but, if anything, show an improvement using the coated Kapton®. From this test, it can be concluded that the SiOx coating is as strong as the bond itself.

4.5.2 Thermal Cycling of Solar Blanket Coupon

A subscale solar blanket was made and tested according to L'Garde Procedure No. 21237. The tests were (1) visual inspection before thermal cycling, (2) I-V test before thermal cycling, (3) visual inspection after thermal cycling, and (4) I-V test after thermal cycling. Reference 27 gives a complete discussion of the testing.

The coupon was inspected before thermal cycling. Figure 106 shows a photograph of the front of the coupon. The coupon was tested at NASA-Lewis under the direction of Dave Brinker. The temperature extremes were -100° C and +80° C. L'Garde performed an I-V test before cycling, and NASA performed I-V tests at 0 cycles (before cycling), 1000 cycles, and 2000 cycles. The only visual difference in the coupon is that the exposed portions of the interconnect slightly darkened after cycling.

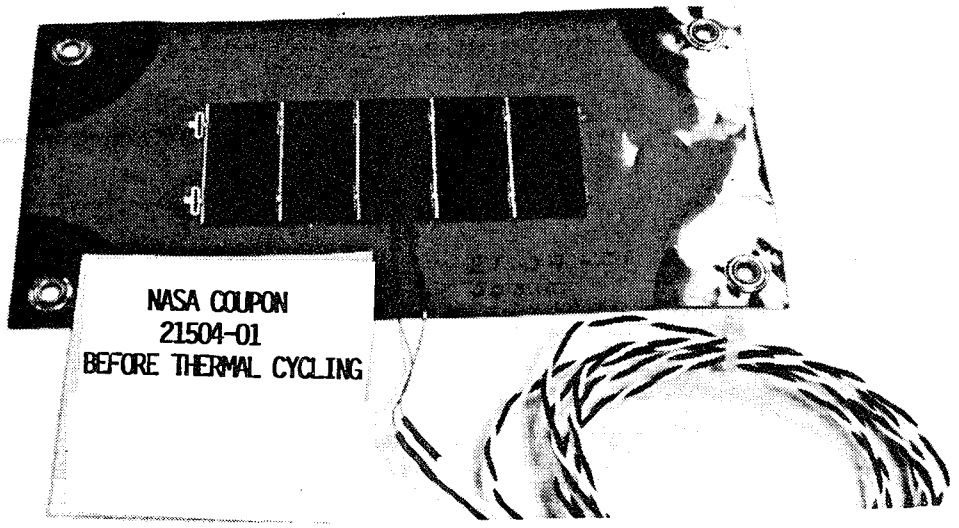

Figure 106. Front of coupon.

Electrically, the coupon performed as shown in Table 40. The test showed no significant electrical degradation of the coupon.

Table 40. Electrical output data.

NUMBER OF CYCLES I-V TESTED BY	0 L'GARDE	0 LEWIS	1000 LEWIS	2000 LEWIS	CHANGE (%) FROM 0 TO 2000 CYCLES (LEWIS DATA)	DIFFERENCE BETWEEN L'GARDE AND LEWIS DATA (at 0 CYCLES)
Isc (mA)	274.30	297.85	298.89	299.33	0.50%	7.9%
Voc (V)	2.68	2.72	2.662	2.685	-1.29%	1.5%
Imax (mA)	250.3	285	279.1	276.6	-2.95%	12.2%
Vmax (V)	2.168	2.265	2.115	2.190	-3.31%	4.3%
Pmax (mW)	539.9	645.6	590.3	605.7	-6.18%	16.4%
Fill Factor	-------	0.796	0.742	0.753	-5.40%	--------
Efficiency	-------	11.76%	10.75%	11.03%	-6.21%	--------

4.6 SYSTEM TESTS

4.6.1 Ambient Deployment Test

This test was performed in the high bay area at L'Garde and consisted of deploying the ITSAT development unit on a slanted surface in a one atmosphere environment. The deployment

surface consisted of a polished aluminum plate surrounded by a structural frame. Teflon® "skis" were mounted to the lid providing vertical support while allowing near frictionless sliding. The little friction there was between the Teflon® and aluminum was negated by the downward slope of the frame.

The configuration of the ITSAT tested here was basically the same as the flight design except for the following features:

- The replica solar blanket was used instead of the actual solar blanket.
- The inflation system was not used. An off-board nitrogen tank was used for inflation.

4.6.1.1 Pretest Vibration. To test the padding concept and the enclosure structure, the packaged ambient unit was tested on the shaker to acceptance and qualification levels in all three axes.

During vibration testing, there was a concern that the blanket would shake around and come loose from the padding. While testing the replica blanket will not determine cell breakage, it would indicate the magnitude of movement of the array under the specified packaging pressure. This did not happen. The padding was still well within the folds of the array.

The vibration of the packaged unit also determined that the housing and lid are adequate to survive the environments.

4.6.1.2 Deployment. Prior to deployment, the frame was set up according to L'Garde Procedure No. 21239. The angle chosen for the test was determined by sliding a piece of Teflon down the plate and adjusting the tilt until the Teflon just barely continued to slide down the plate after an initial push (the initial push is given to negate the static coefficient of friction). This resulted in a deployment angle of 7.98 deg.

The test was a success. The following L'Garde videotapes recorded the deployment test:

V-156 Top view of array.

V-157 Side view of housing and lid separation

V-158 View of pressure gauges (to be compared to the pressure transducers if necessary)

The packaged array is shown mounted in Figure 107. The deployed array is shown in Figures 108 and 109.

4.6.1.3 Deployment Results. The test was designed for a deployment time of 14 s . This was achieved. The tubes were then brought to full pressurization.

The array came out very straight, never touching the sides of the frame at all. After cutting both cables, the lid seems to move out about 3 in to relieve the pressure caused by the compression of the padding. This allows the lid to start out even, before the pressure starts to flow.

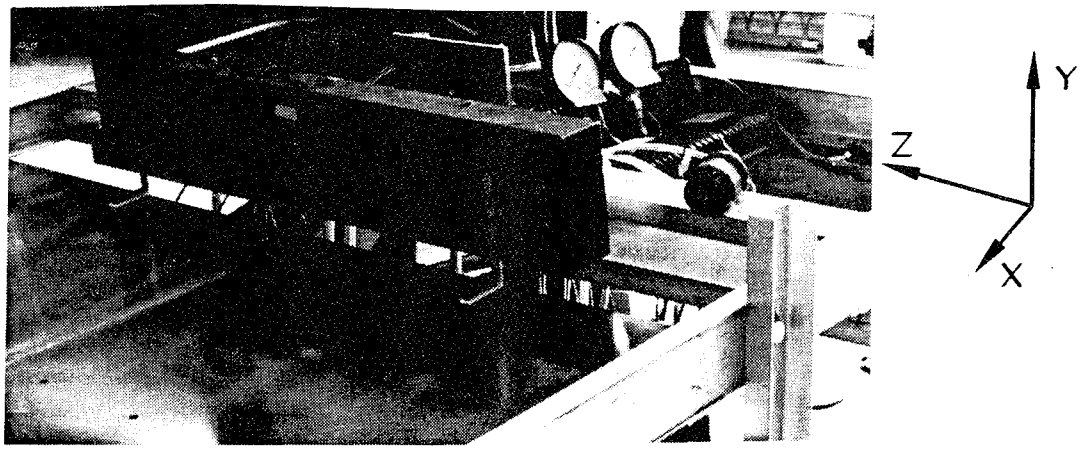

Figure 107. Packaged ITSAT (development unit).

4.6.1.4 Bending Test. The deployed array was tested for its strength in bending about both the y- and z-axis. The test setup for the y-axis case is shown in Figure 110. The ITSAT was then rotated 90 deg and tested about the z-axis.

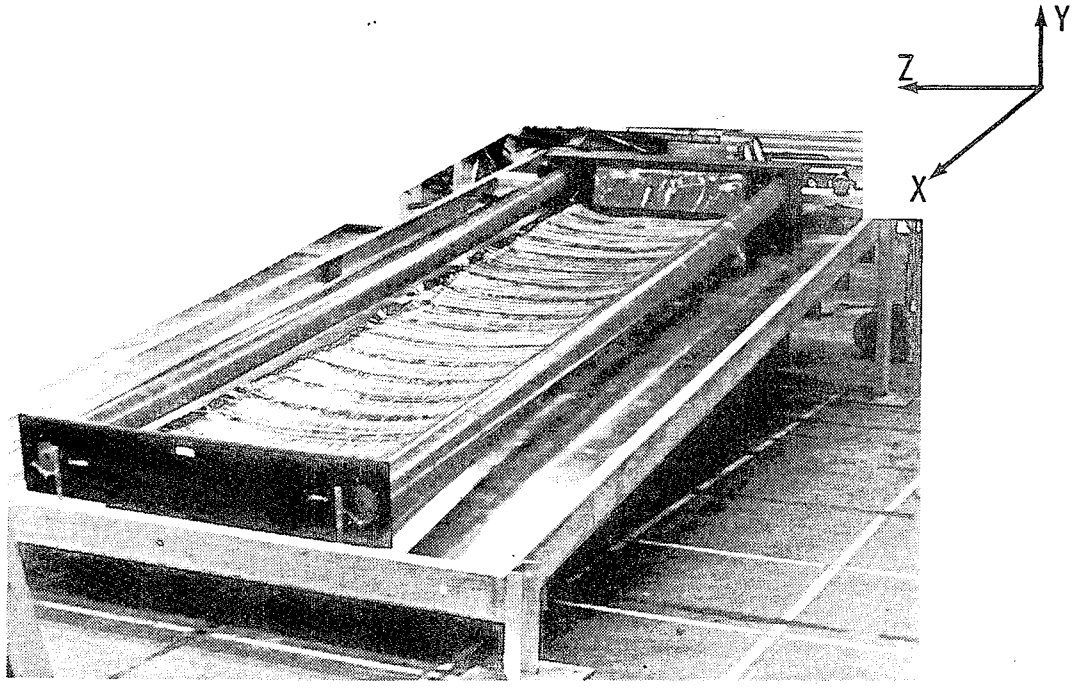

Figure 108. Deployed ITSAT array - oblique view (development unit).

The point of failure for the array structure was the point where the deflection curve deviated from a straight line. This correlated with the point where wrinkles started to appear on the tube. The results are given in Table 41 along with the results from tests for the single tube.

Note that there is more compliance about the z-axis due to the shape of the structure. Also note that the ambient test results are less stiff than the single tube tests. This is due to the mounting of the tubes to the housing, which is not as stiff as the test stand used in the single tube tests. In other words, some of the deflection was caused by the housing.

4.6.1.5 Natural Frequency Test. The natural frequency of the array was also tested about the y- and z-axes. The test method used a video camera looking down at the lid with a grid paper below it (Fig. 111). The video tape was then examined frame by frame to determine the natural frequency of the oscillating array. The resolution is ±1/30 s.

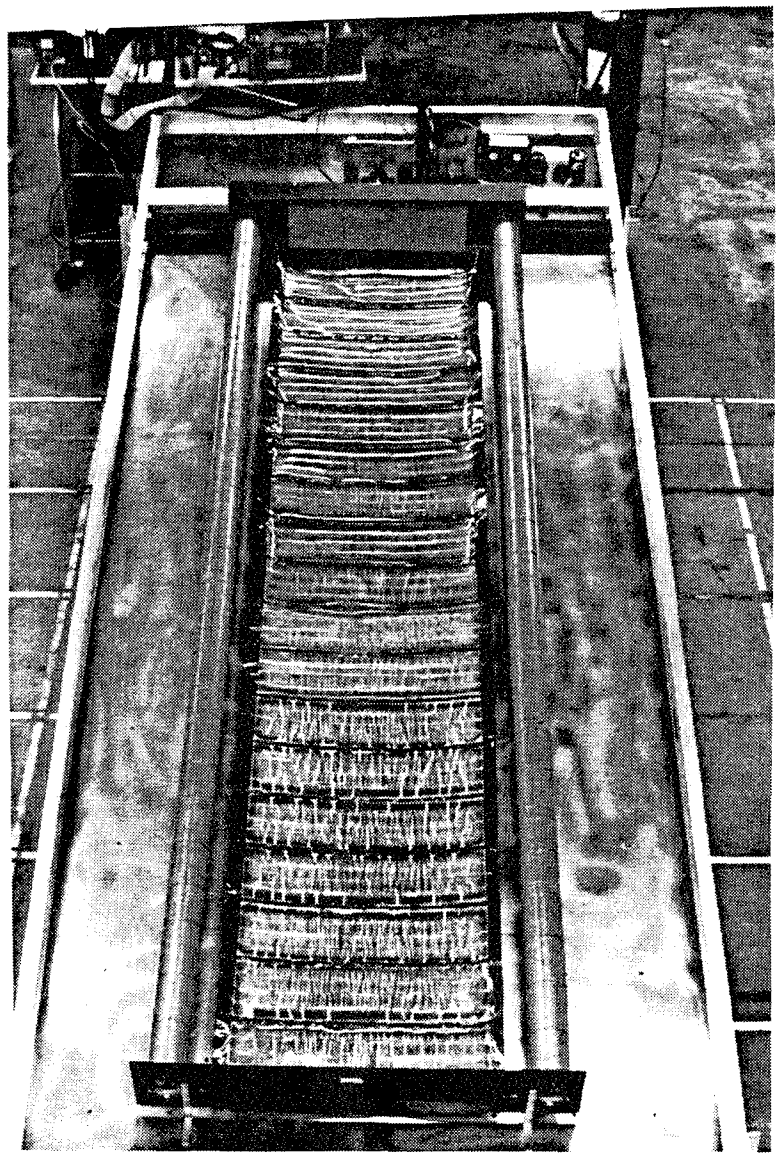

Figure 109. Deployed ITSAT array - top view (development unit).

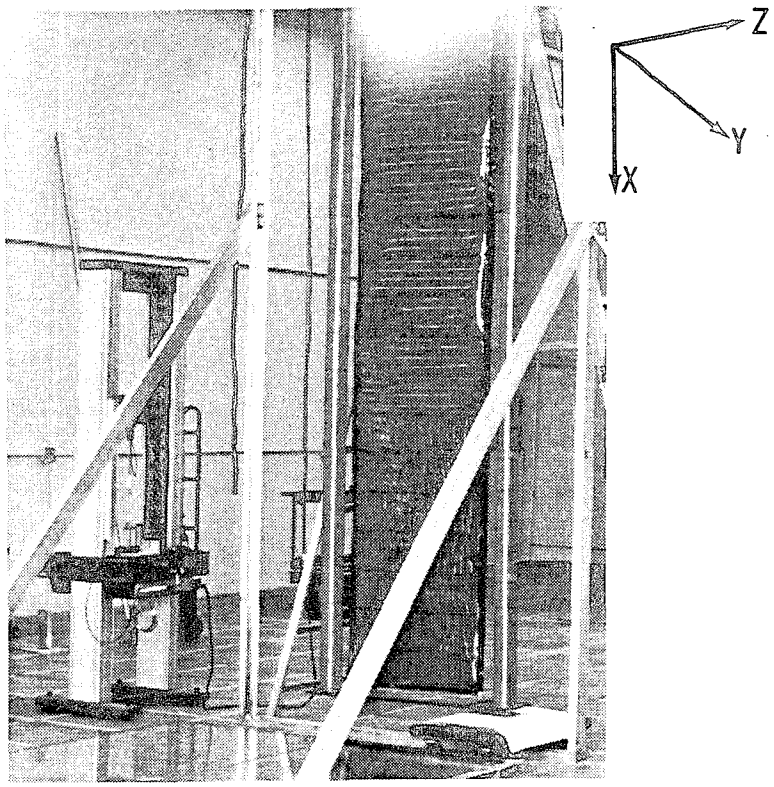

Figure 110. Bending test about the y-axis.

Table 41. Tube strength comparison.

ORIENTATION	FORCE AT FAILURE (lb)	DEFLECTION AT FAILURE (in)	STIFFNESS (lb/in)	SOURCE
About Y-Axis	2.58	5.22	0.494	---
About Z-Axis	1.35	4.36	9.310	---
Single Tube w/o Bladder	0.75	1.05	0.714	Ref. 28
Single Tube w/Bladder	0.90	1.32	0.680	Ref. 29

The test was performed three times in each direction, and an average calculated. The results are presented next:

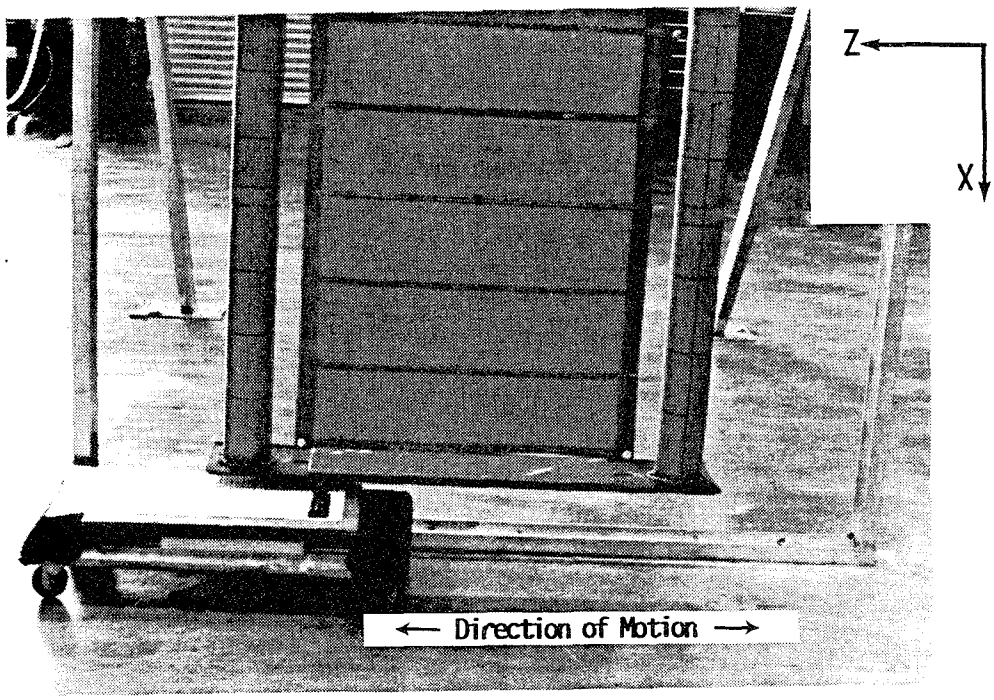

Figure 111. Natural frequency test, parallel to array.

Test #	Rotation Axis	Natural Frequency (Hz)
1	Y	1.4516
2	Y	1.4516
3	Y	1.4674
Average		1.4569
Maximum Deviation From Average		0.72%
1	Z	0.8955
2	Z	0.9091
3	Z	0.8955
Average		0.9000
Maximum Deviation From Average		1.00%

The natural frequency about the z-axis (0.900 Hz) is slightly below the contract goal of 1.0 Hz. These numbers can be compared to predictions from our single tube test results.

Test Description	Natural Frequency (Hz)	Source
w/o Bladder	2.48	Ref. 28
w/Bladder	2.26	Ref. 29

While the single tube tests did use weights on the tube end to simulate the lid mass, etc., the numbers do not agree. This is due to three reasons:

- The single tube was mounted firmly to an aluminum plate, whereas the ambient test tubes were mounted to the housing, which contributed to the compliance of the system.

- The ambient test used the actual case of a stiff tube coupled to a "trampoline" suspended blanket. The addition of this sprung mass lowers the natural frequency.

- This test was performed in ambient conditions; the flat blanket causes a large air drag which decreases the natural frequency. However, preliminary calculations (Ref. 30) show this to be a minor effect. Going to vacuum should only increase the natural frequency from 0.900 to 0.904 Hz in this direction. The test data from NRL determined the natural frequency in vacuum directly (see Subsection 4.7.2).

4.6.1.6 Conclusions. The ambient test met all test objectives. All the needed data were taken and demonstrated that the ITSAT can deploy smoothly and straight.

4.7 QUALIFICATION TESTING

After assembling the ITSAT protoflight unit for qualification testing, it was subjected to the following environmental/functional tests: (1) random vibration in all three axes; (2) testing at NRL; and (3) electrical I-V testing of the solar blanket, before and after deployment. These are described in detail in this section.

4.7.1 Random Vibration

The packaged ITSAT qualification unit was subjected to random vibration testing according to L'Garde Procedure No. 21783. The packaged ITSAT qualification unit is shown attached to the shaker in Figure 112. The ITSAT was vibrated to acceptance and qualification levels in all three axes. Figure 113 shows the response spectrum for the ITSAT at qualification levels in the x-axis.

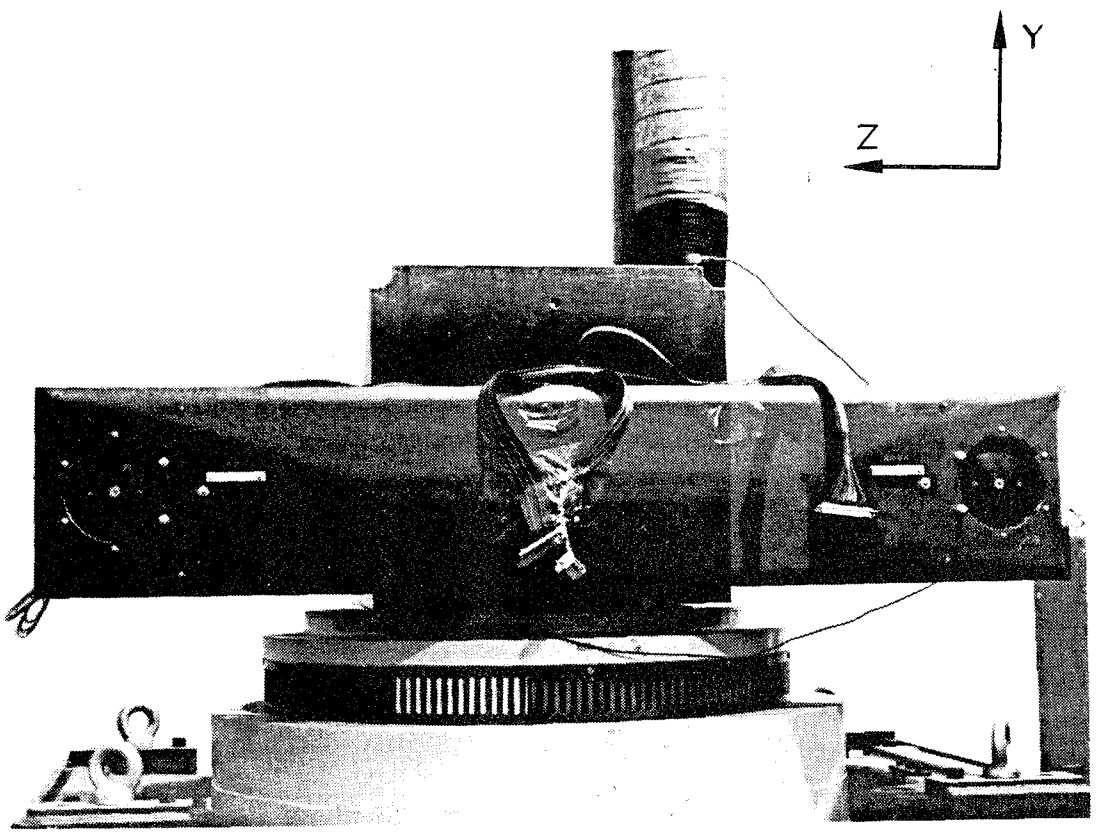

Figure 112. Test article shown mounted for vibration in y-axis.

The test indicated no visual damage to the structure and no degradation in the cell/RTD continuity per the electrical functional test procedure. See Reference 31 for a complete test report.

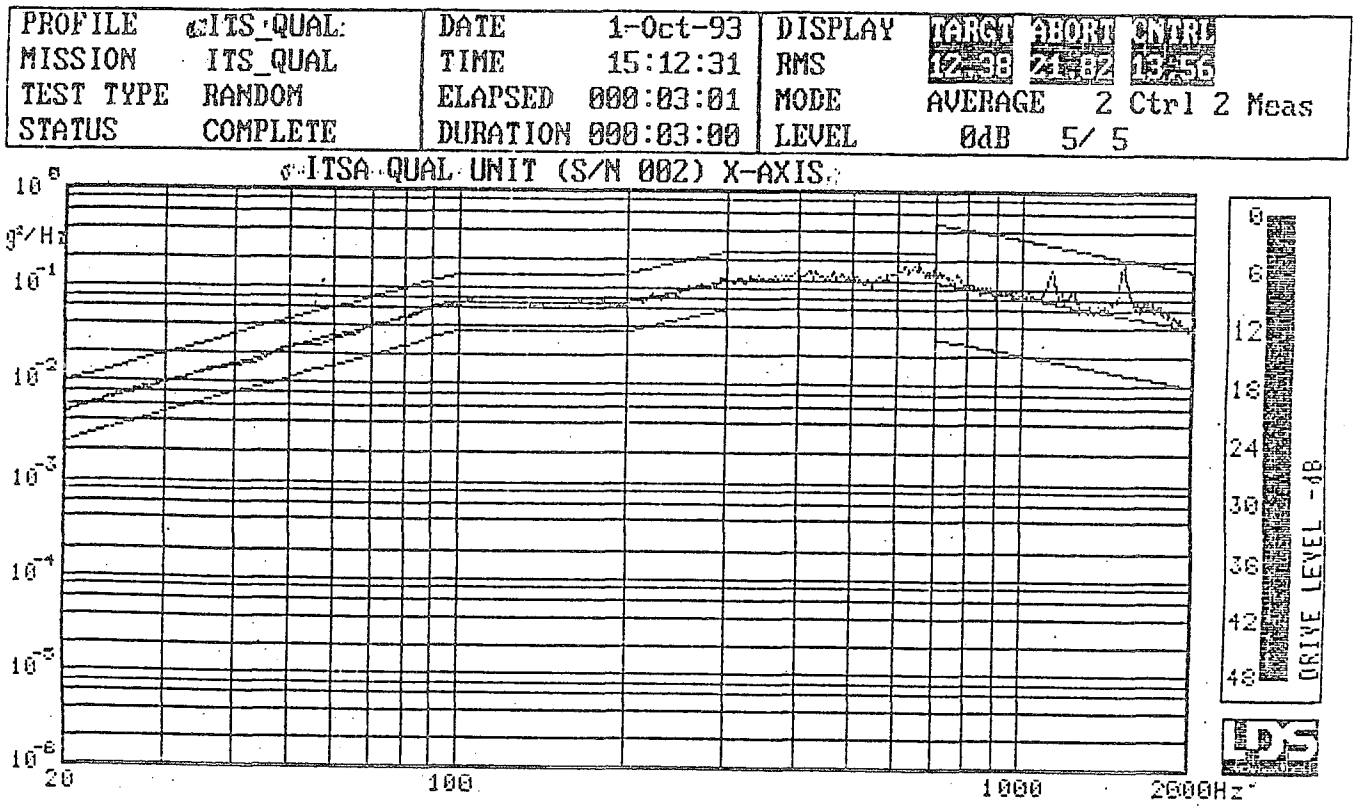

Figure 113. Qualification level, x-axis.

4.7.2 Thermal Vacuum Testing at NRL

This section describes the set of tests performed on the ITSAT qualification test article at NRL. The tests were performed during the period of October 23 through 30, 1993. The tests were performed according to L'Garde Procedure No. 21231.* Each of the three subtests met their objectives.

- During the deployment test, the ITSAT extended straight and achieved a rigidization pressure of between 17.2 and 18.0 psi. There was no physical damage to the solar cells, and only minor breakage to five of the glass simulators. Four of these were located on the last (outboard) subpanel.

*L'Garde Procedure No. 21231 for ITSAT Thermal Vacuum Deployment Test.

- During dynamics testing, the ITSAT showed a natural frequency of 1.04 Hz.

- During thermal cycling, the ITSAT was subjected to five complete cycles between -85 and +70°C, with two soaks at the cold temperature and two soaks at the hot temperature, each of 2-hr duration.

A comprehensive test report is presented in Reference 32. The following is an excerpt from the report.

The tests at NRL consisted of the following three subtests:

1. Deploy the ITSAT on a slight slant using the test support frame. As with the ambient test (Subsection 4.6), the slant was present to eliminate the effects of sliding friction, since we deployed horizontally in the 1-g environment. The outputs of the deployment test were

   a. Document the deployment dynamics

   b. Assess solar cell damage caused by deployment

   c. Measure pressure profile of the tubes during and after deployment for comparison to pretest predictions

   d. Measure temperature profile of the tubes to be compared with pretest predictions

2. Stand up the ITSAT array vertically in the chamber and perform a dynamics test to determine natural frequency of the deployed ITSAT. The outputs of the dynamics test were

   a. Measure natural frequency of the array

   b. Determine damping characteristics of the array

3. Thermal cycle the array in this vertical position. The outputs of this test were

   a. Qualify the array per MIL-STD-1540B

   b. Assess tube deformation due to thermal effects (tube "bow")

The chamber was evacuated before each subtest and evacuated afterward. The test was performed in NRL's 16-ft diameter, 30-ft long Thermal Vacuum Chamber.]

An overall view of the vacuum chamber is given in Figure 114. Shrouds lined the inside of the chamber wall, which could be pumped with liquid nitrogen for the cold cycles and hot dry nitrogen for the hot cycles. Thermocouples were attached to the shroud to monitor its temperature, the output of which was fed to a strip chart recorder. The data were collected using NRL's data acquisition system.

The deployment frame was set up so that a small sample of Teflon would just barely slide down the surface, after a slight push is imparted. Thus, the coefficient of sliding (not static) friction is negated.

For thermal cycling, 4 in wide by 12 ft long cold plates were mounted 2 in away from the back side of the tubes. Liquid nitrogen was pumped through the tubes to achieve the desired cold plate temperature. After each cold cycle, dry nitrogen was circulated through to purge the tubes of the liquid nitrogen.

The purpose of these plates was to bring the back side temperature of the tubes to -123°C (10°C colder than the estimated coldest flight temperature) while the front side temperature was -85°C.

4.7.2.1 Deployment Test. The ITSAT was deployed on Tuesday, October 26th. All equipment and sensors worked perfectly.

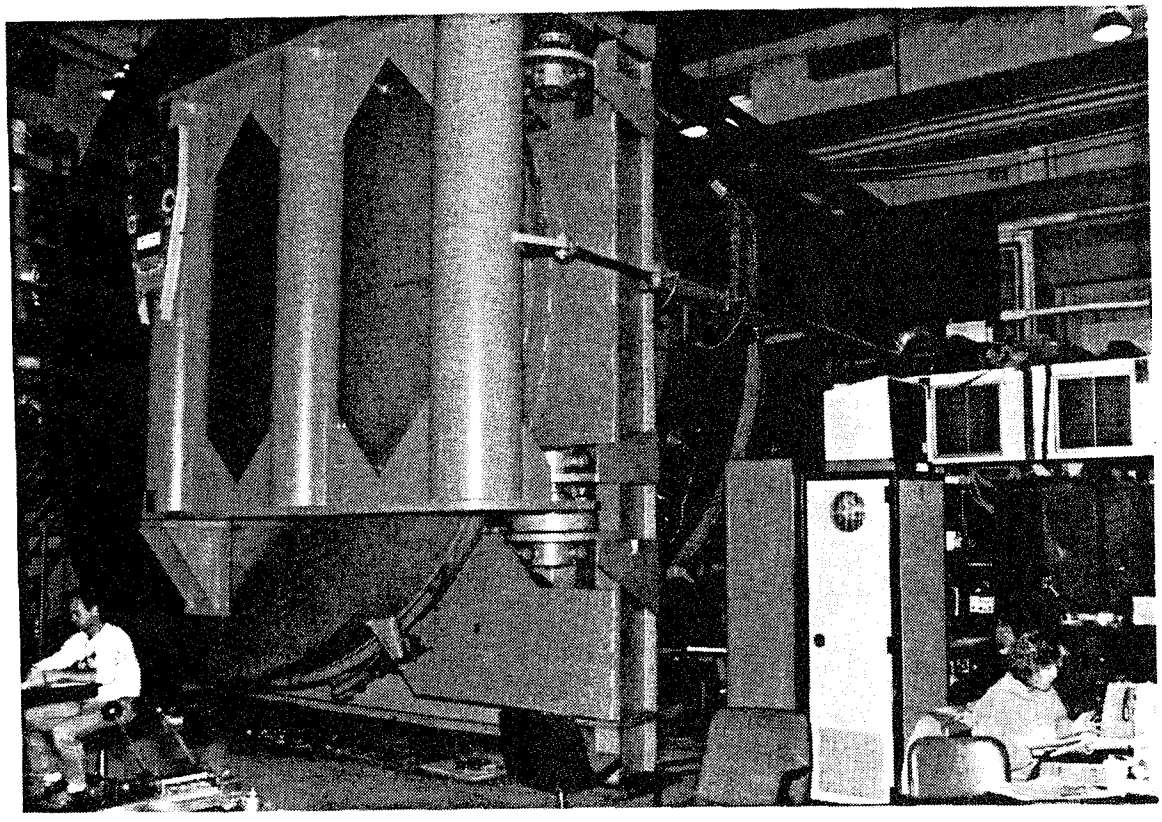

Figure 114. Vacuum chamber - overall view.

The tube pressures are shown in Figures 115 and 116. Figure 115 gives the pressure over a 900-s time period, while Figure 116 shows an enlarged view of the first 200 s of the test.

Also shown in Figure 116 is the pressure profile from our flow model for comparison. At T = 0 the lid was released; note that there is no pressure increase until the primary inflation circuit was opened at T = 5 s. Here we see an almost constant tube pressure as the tube is extending. At about T = 13 s, the tubes are fully extended, and the pressure rises slightly due to the constant volume situation. At T = 30 s, the secondary circuit opens, allowing a faster flow of gas into the tubes.

At T = 78 s, the right tube reached its maximum pressure of 18.0 psi, while the left tube reached its maximum of 17.2 psi at 96 s. The two tubes are tied together with tubing, so

there should not be a drastic difference in pressure. The slight difference (0.8 psi) during rigidization is due to either the difference in conductance of the supply tubes or a slightly larger leak rate from the left tube. A thorough analysis should be performed at a later stage. The pressure equalizes at about T = 110 s.

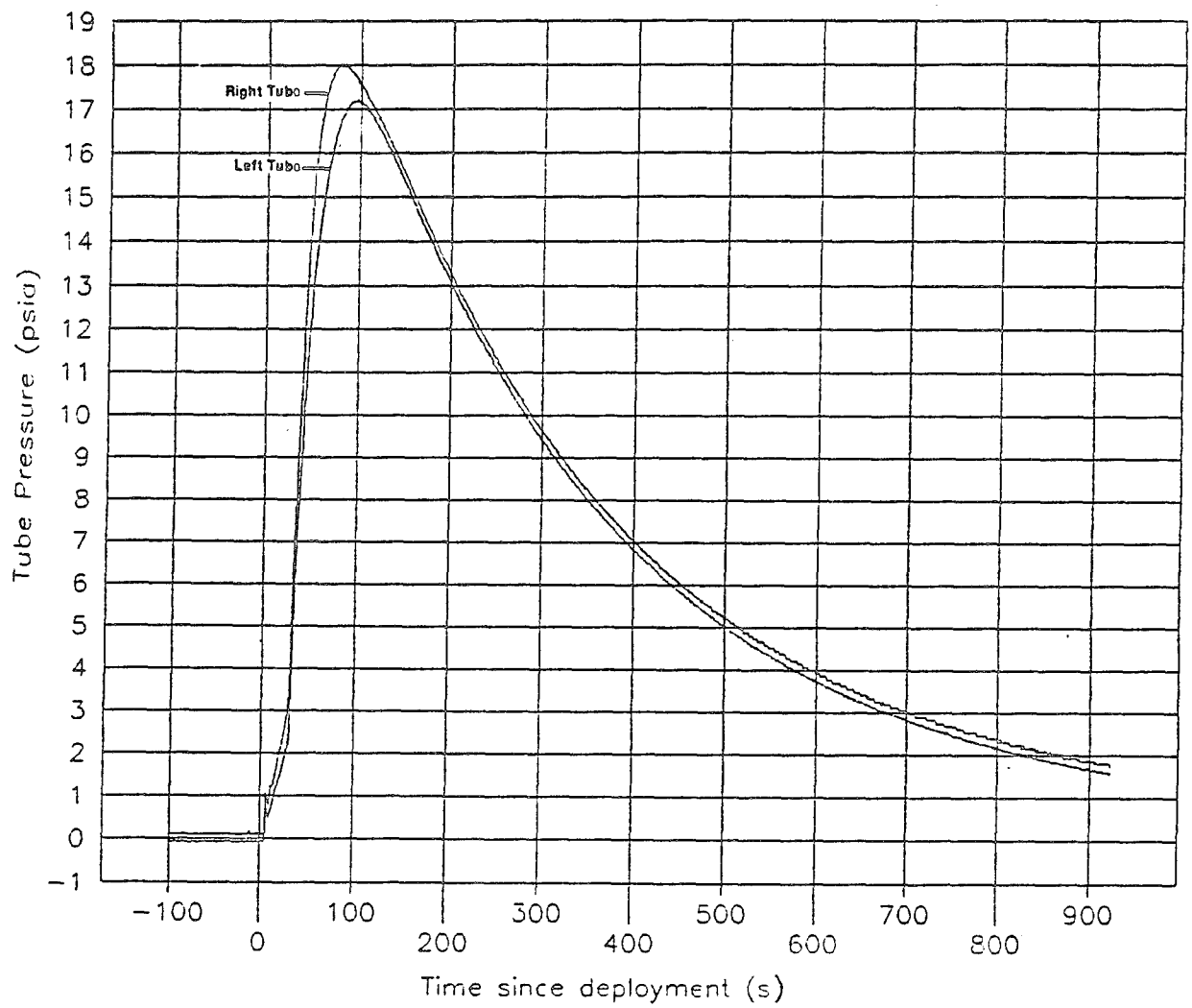

Figure 115. Tube pressure versus time.

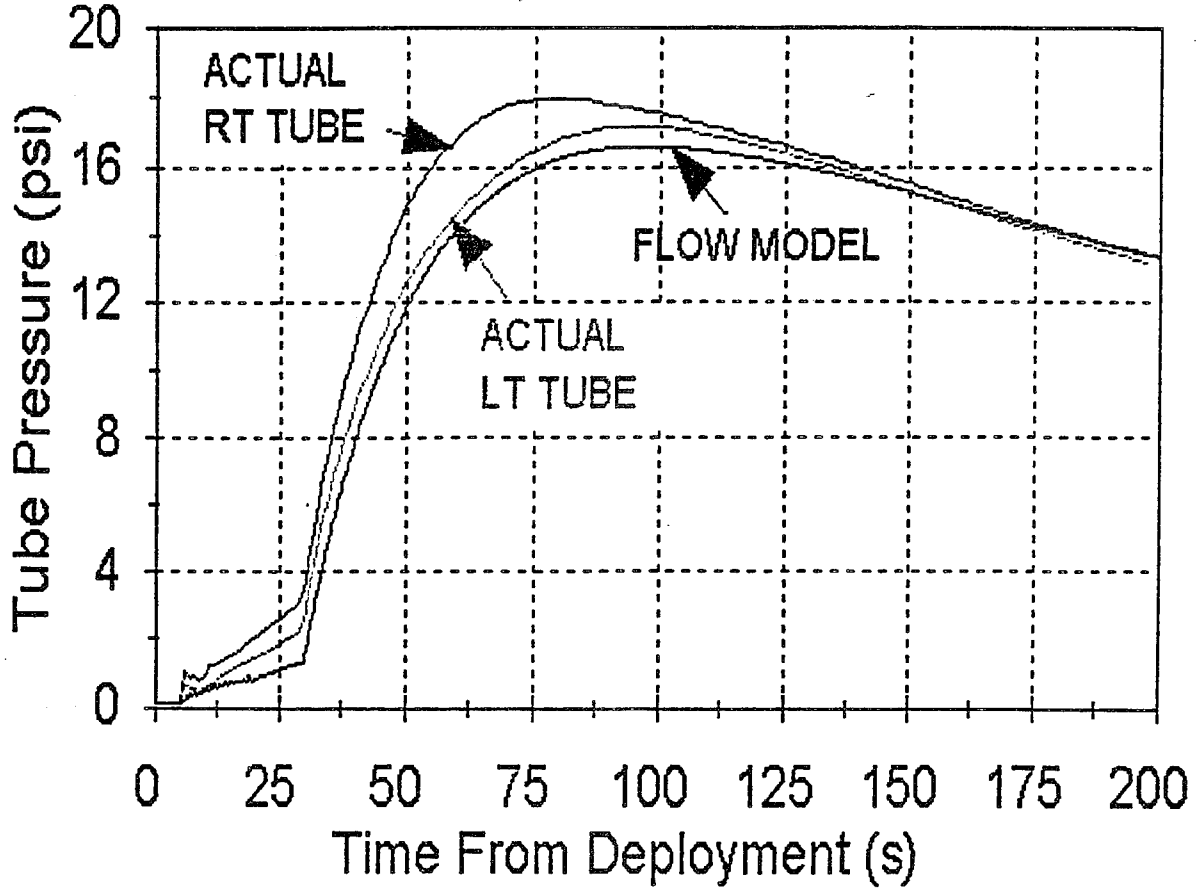

Figure 116. Tube pressure versus time-first 200 s.

The strength of the tubes at this rigidization pressure is still adequate; Reference 11 finds that the safety factor in bending is still 10.26 at a rigidizing pressure of 17 psi.

The average tank temperature versus time is shown in Figure 117. The tank temperature drops by a small amount due to the expansion of the gas, but nowhere near the freezing point of the nitrogen.

The temperatures of the blanket and the tubes are given in Figure 118. Note that the temperature of the blanket drops faster than the tubes due to its lower thermal mass.

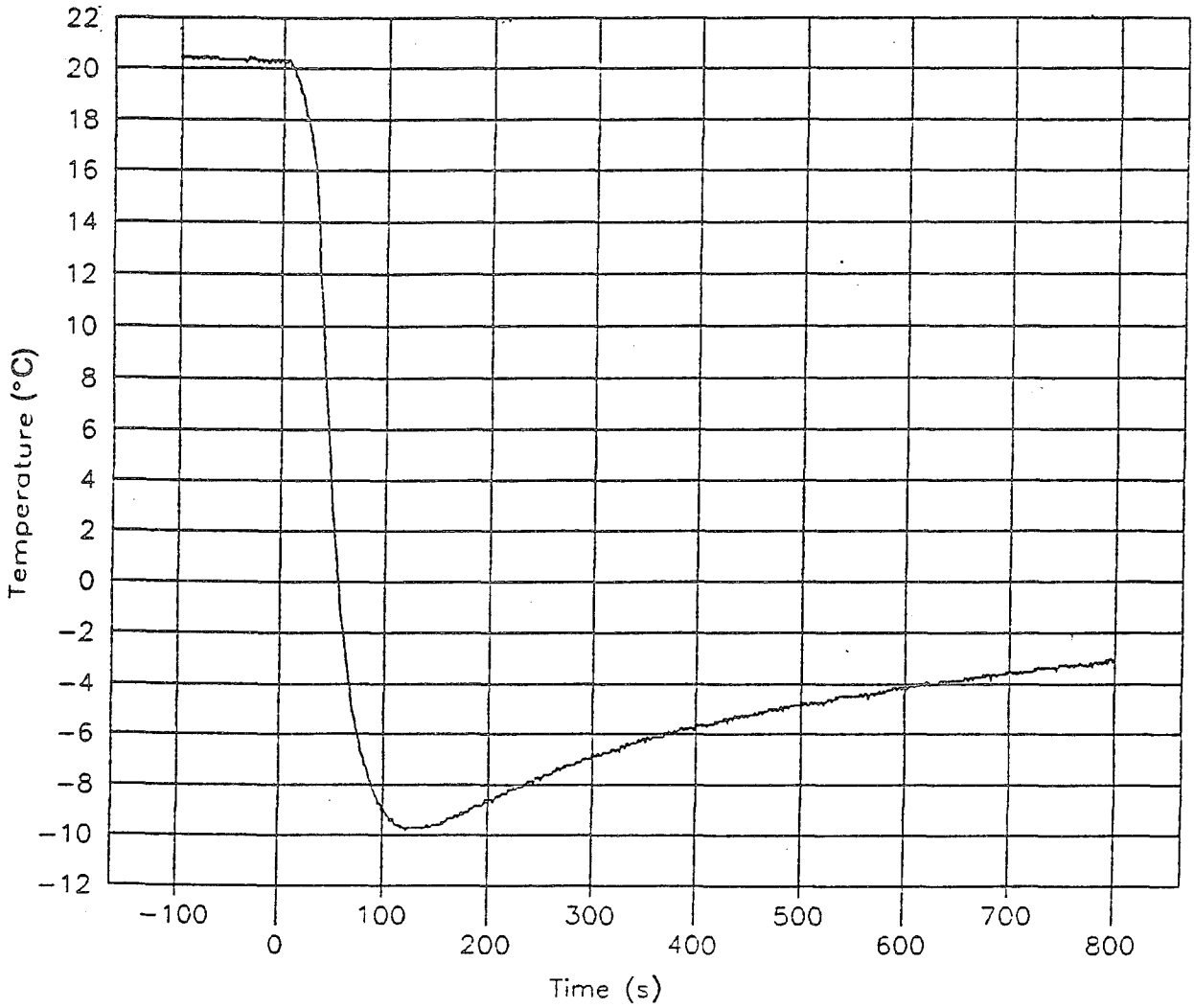

Figure 117. Tank temperature versus time.

Figure 119 shows the tube temperature compared to the pretest predictions from Reference 33. The two curves for the predicted case show the temperature of the top of the tube (colder curve) and the bottom of the tube (warmer curve). These predictions were somewhat conservative; a steeper drop in the temperature was predicted.

There was no damage to the solar array due to deployment. All of the 217 working solar cells were intact. Electrical I-V tests conducted before and after the NRL test show no change in the power output of the array (Subsection 4.7.3).

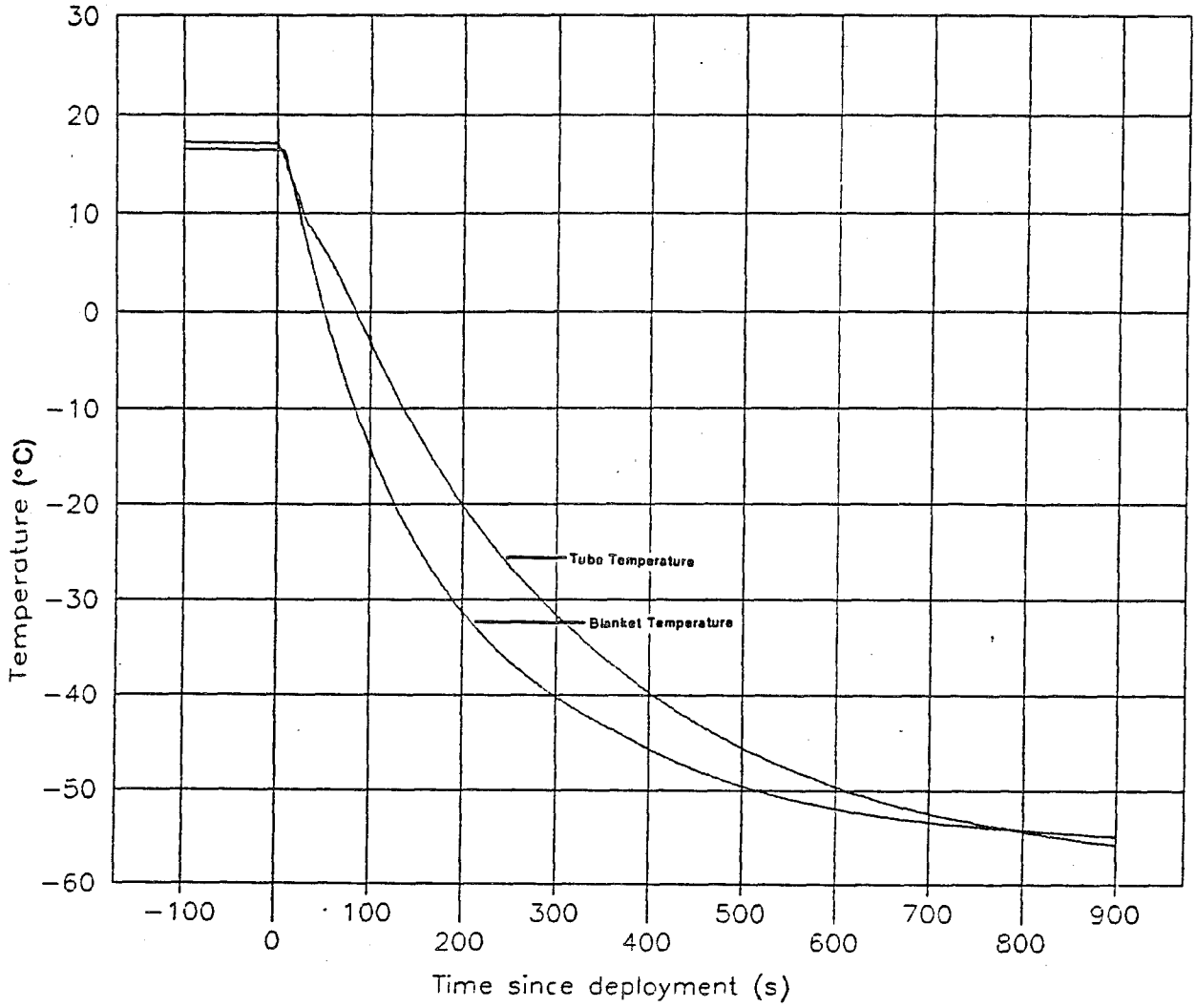

Figure 118. Tube blanket temperature versus time (average temperatures).

Of the 465 glass simulator cells, 5 cracks were noted after the test. There is no clear way to tell if these cracks occurred during array packaging, vibration testing, shipment, or deployment. The fact that cracks occurred only in the simulated cells and not in the actual solar cells may be due to their higher fragility.

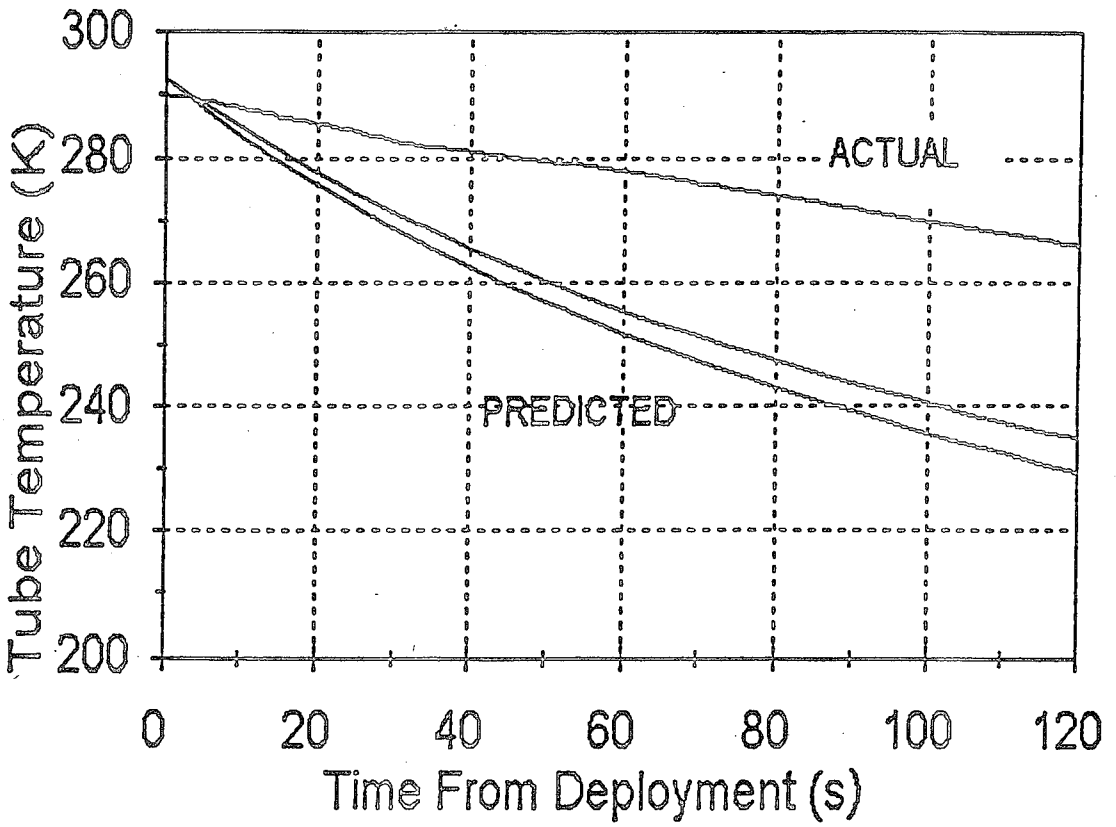

Figure 119. Tube temperature versus time.

4.7.2.2 Dynamics Test. On Wednesday, October 27th, the array was hung vertically (Fig. 120), and the exciter motor was set in position to oscillate the array about the z-axis. The temperature of the test article was allowed to reach the equilibrium temperature of the chamber, 52° C. The Charged Coupled Device (CCD) camera was set inside the chamber to view the oscillating lid for the determination of natural frequency. By advancing the videotape frame by frame, we obtained the position of the lid versus time.

There were a total of four oscillation tests planned for redundancy, each time allowing the array to damp out to zero amplitude. However, about 18 s into the first run the camera overheated due to the high chamber temperature. In addition, the camera signal started failing and gave poor data in the period between 9 and 13 s.

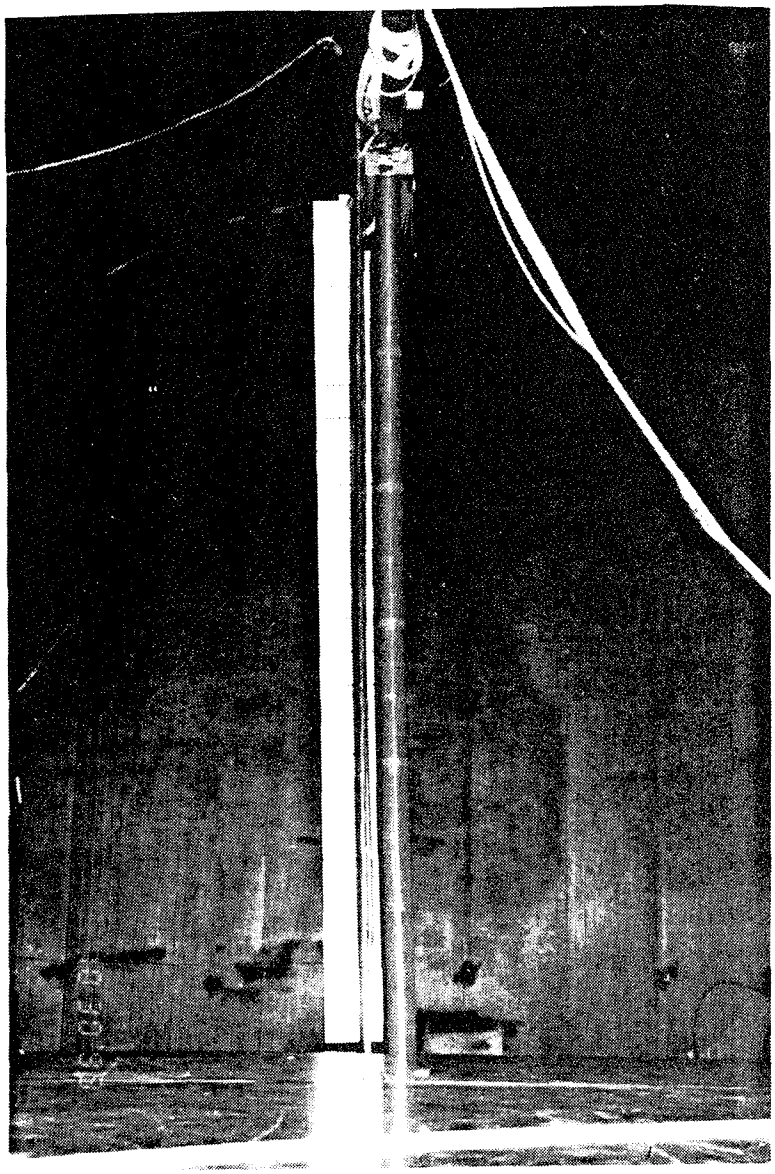

Figure 120. Dynamics test setup.

The data that were collected are given in Figure 121 and were sufficient to determine the natural frequency (1.04 Hz) and the damping characteristics of the array. The natural frequency differed from the ambient deployment test results which indicated a natural frequency of 0.904 Hz (corrected for vacuum). There are three possible explanations for this:

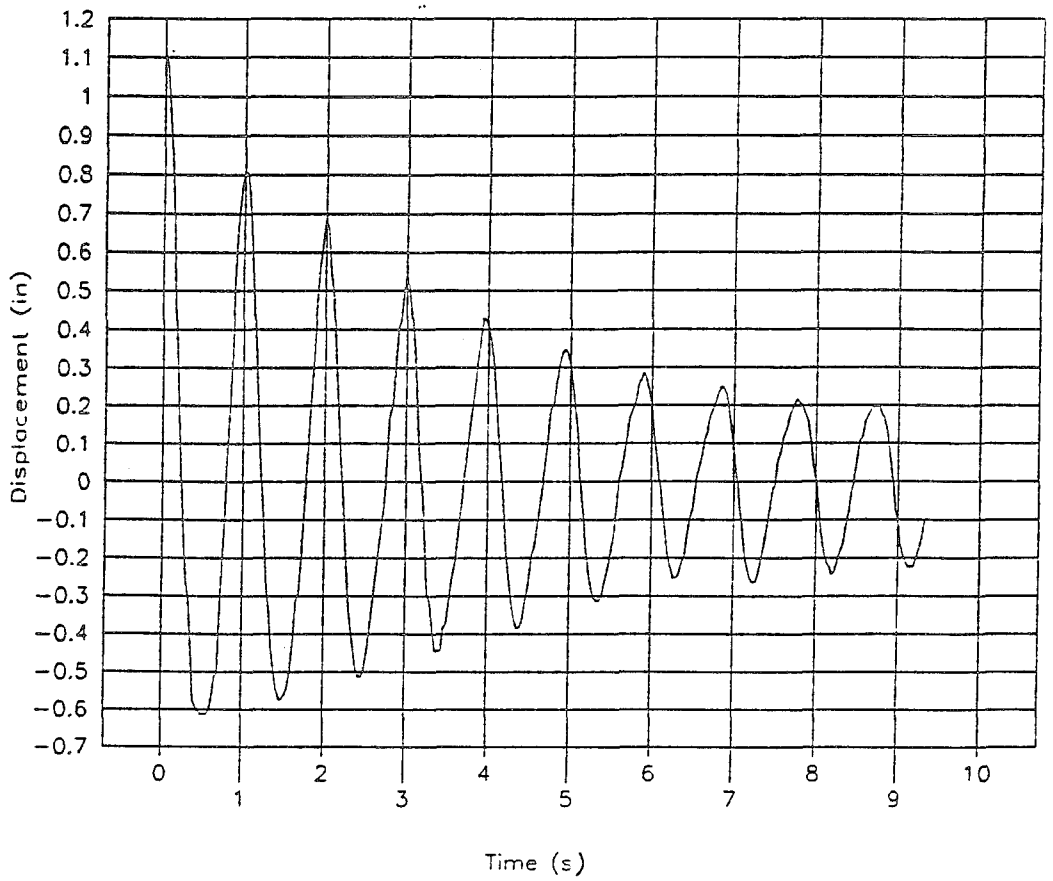

Figure 121. Oscillation of ITSAT (dynamics test).

- The ambient unit used the replica solar blanket (1027 g) while the qualification unit used the flight solar blanket (1098 g). While the heavier flight blanket should have given the lower natural frequency, this was not the case. The other possibility is the difference in damping characteristics between the two blankets. The replica used bonded Delrin strips to simulate the solar cells which may have given a lower stiffness and a resulting lower natural frequency.

- When attaching the solar blanket to the tubes, attempts were made to deflect the springs by the same amount on both test units. There is a possible source of error here.

- The ambient array was attached to a welded aluminum frame. The qualification array was attached to a steel I-beam at the top of the chamber. The difference in stiffness at the attachment point may be the cause.

The amplitude of oscillation versus the cycle number is plotted in Figure 122. A curve fit was made to the data, consisting of two exponential terms:

$$A = 0.573e^{-0.429x} + 0.519e^{-0.118x} \quad (104)$$

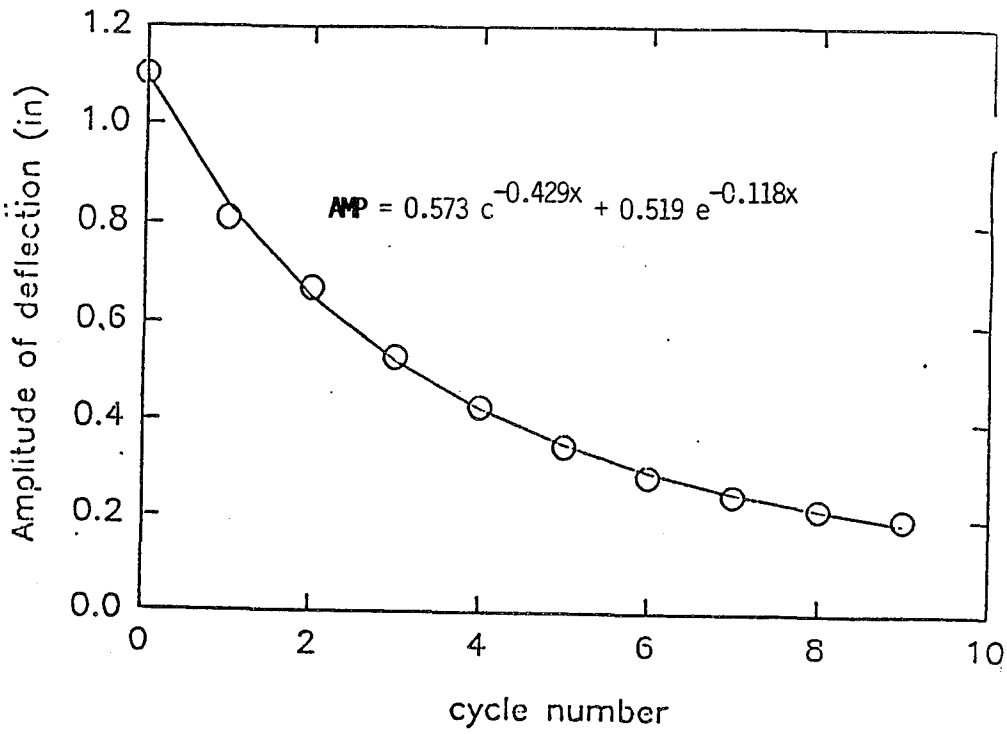

Figure 122. Vibration damping data - two-term curve fit.

Where x is the cycle number and A is the amplitude. A description of the two terms is given next:

TWO TERMS:

$0.573e^{-0.429x}$

- 35 percent of amplitude reduced each cycle.
- 57 percent of energy reduced each cycle.
- Probably due to the tubes.

$0.519e^{-0.118x}$

- 11 percent of amplitude reduced each cycle.
- 21 percent of energy reduced each cycle.
- Probably due to the housing.

4.7.2.3 Thermal Cycling. From 2:00 a.m. on Thursday, October 28th until 10:45 a.m. on Saturday, October 30th, the deployed ITSAT was thermal cycled nominally from -85 to +70°C. Figure 123 shows the average tube temperature (average, front and back of both tubes). Notice it follows the shroud temperature quite closely.

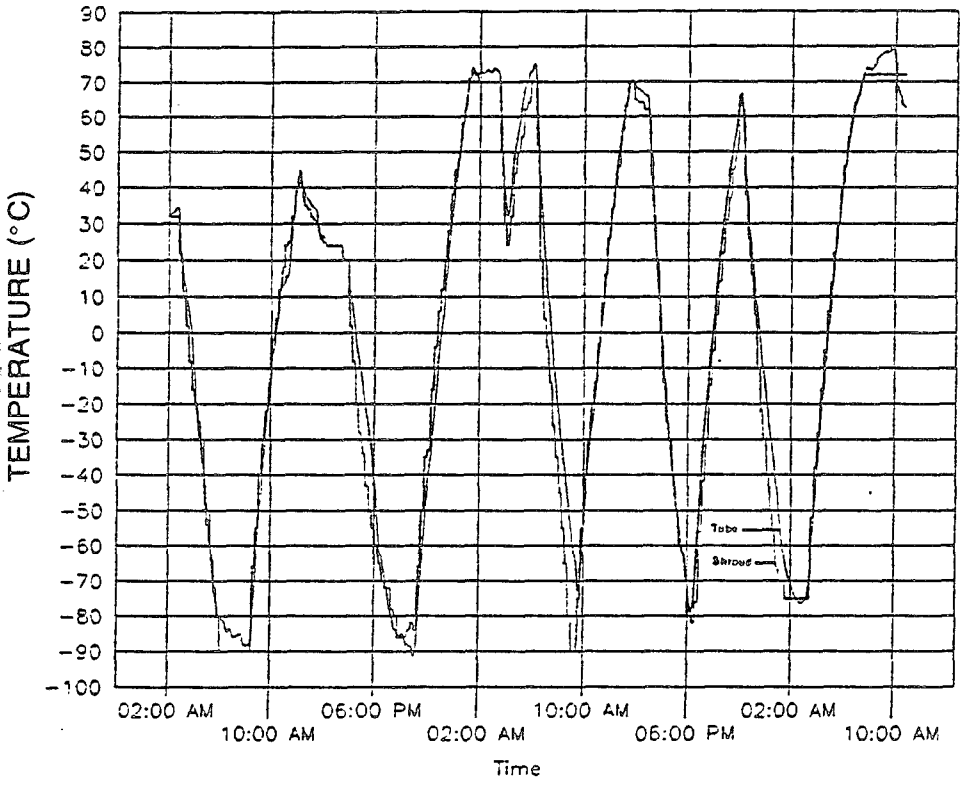

Figure 123. Thermal cycle data, 10/28 to 10/30, average tube temperature.

Figure 124 shows a close-up portion of the tube temperature graph during a cold soak. Notice that the difference between the front and rear of the tube varies by only 9°C even though it is exposed to a temperature difference of about 100°C. The radiative heat transfer between the front and back sides of the tube is large enough to overcome the large difference in exposure temperatures.

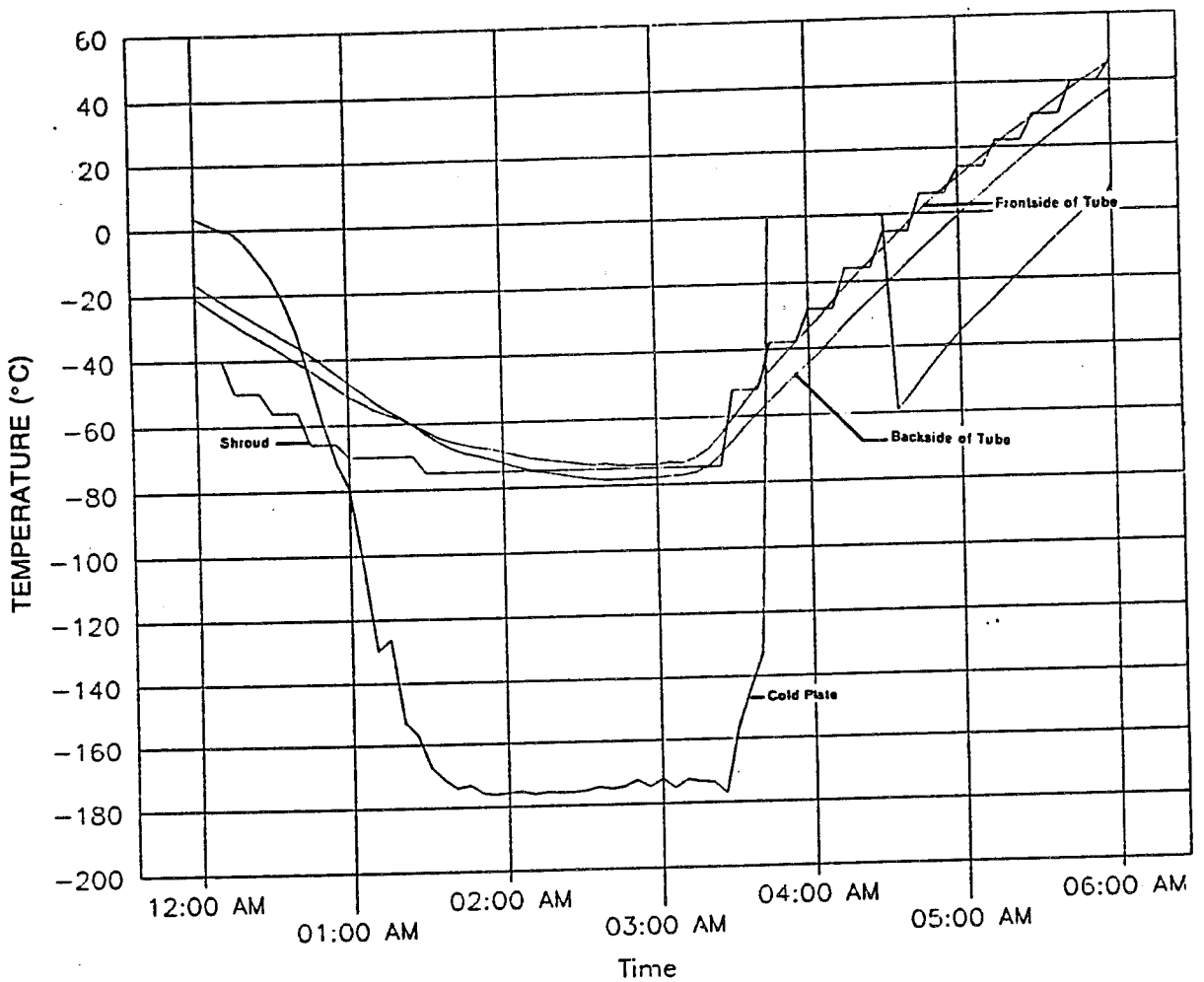

Figure 124. Thermal cycle data, 10/30/93, left tube temperature.

During the thermal cycling a secondary objective was to assess the bowing in the tubes due to the front to back side temperature gradient. During the test setup the cold plates behind the tubes were mistakenly placed too close to the lid, constraining the tubes from bowing. Hence, no conclusive data on the tube bow was obtained from this test.

Figure 125 shows the average blanket temperature (average of the 13 working RTDs). It also follows the shroud temperature closely due to its low thermal mass.

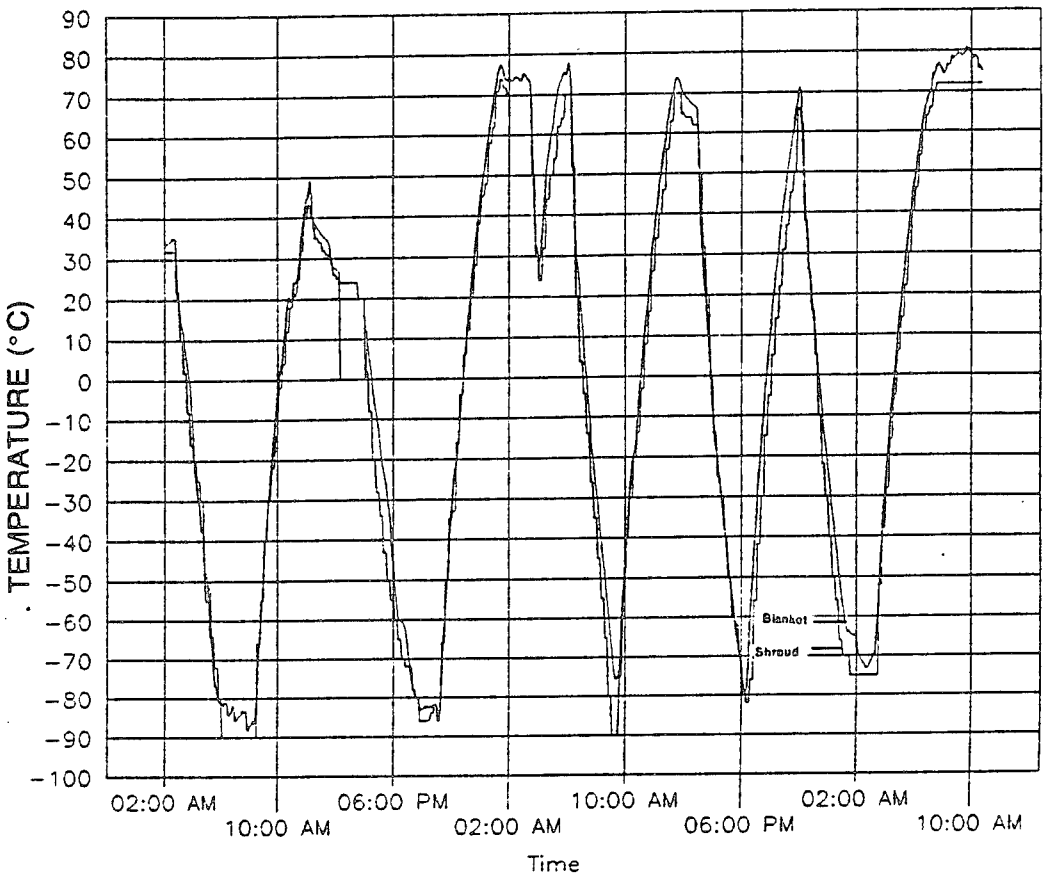

Figure 125. Thermal cycle data, 10/28 to 10/30, average blanket temperature.

4.7.2.4 NRL Test Summary. The testing at NRL was a success.

- The ITSAT can deploy successfully in a vacuum and in a simulated eclipse situation.

- The ITSAT has a natural frequency of 1.04 Hz about its z-axis which is higher than the contract requirement of 1.00 Hz. While the natural frequency about the x- or y-axes was not tested at NRL, it was determined that the z-axis has a lower natural frequency

than the y-axis during the ambient deployment test. Also the array was found to be difficult to excite about the x-axis.

- The ITSAT was thermal cycled through five complete thermal cycles with extremes of -85 to 70°C, with no physical damage noted.

The following anomalies were encountered during the testing:

- Several of the shroud sections on the bottom of the chamber were not working and remained near room temperature during the test.

- After rigidization the weight of the solar blanket caused it to sag slightly, pulling inward on the tubes. The left tube buckled at its midpoint. This will not occur in flight due to the absence of gravity.

- During backfill of the chamber after the deployment test, the tubes were not pressurized until one tube started to crush slightly. At this point and for all subsequent backfills, the tubes were pressurized with an external gas source to keep the tube pressure 1-3 psi above the chamber pressure.

- The CCD camera failed during the dynamics test as discussed previously.

- The tube bow test was inconclusive due to the incorrect mounting method.

4.7.3 I-V Tests Before and After Deployment

This subsection contains test data and results from I-V tests of the solar cell strings on the ITSAT blanket. These tests were conducted before and after deployment of the blanket at NRL. The complete details of the tests are given in References 34 and 35. The I-V tests of

the full-sized ITSAT blanket were conducted in accordance with L'Garde Procedure No. 21775*.

Each string was tested three times before deployment and three times after deployment. The temperature of the strings were 28 $\pm$ 2°C for all tests. As shown in Reference 36, temperature effects for this small variation are negligible.

4.7.3.1 Comparison of Before and After Tests. Table 42 compares the open circuit voltage, short circuit and maximum power for the before and after deployment cases. As shown in the table, there is no significant change in the string's behavior between the tests. The maximum percent variation between tests is about 4.0 percent, which is likely due to slightly different test and environment conditions between the July 1993 test ("before" the deployment test) and the December 1993 test ("after" the deployment test).

Table 42. Solar cell string I-V test results before and after deployment.

STRING	AVERAGE Voc (V)			AVERAGE Isc (Amp)			AVERAGE Pmax (W)		
	Before	After	% Change	Before	After	% Change	Before	After	% Change
01	16.3871	16.4216	+0.2	0.2729	0.2747	+0.7	3.3259	3.2663	-1.8
02	16.1312	16.4615	+2.0	0.2707	0.2757	+1.8	3.2624	3.2624	+0.0
03	16.7660	16.4172	-2.1	0.2725	0.2742	+0.6	3.30948	3.2697	-1.2
04	16.8294	16.5730	-1.5	0.2692	0.2614	-0.3	3.0861	3.1358	+1.6
05	18.3059	18.4268	+0.7	0.2866	0.2775	-3.3	3.3846	3.5256	+4.0
06	16.5161	16.5686	+0.3	0.2734	0.2692	-1.6	3.1502	3.1917	+1.3
07	16.6107	16.4866	-0.8	0.2773	0.2672	-3.8	3.1491	3.1335	-0.5

Figure 126 shows the percent variation in open circuit voltage, short circuit current, and maximum power between the before and after tests. These data show that the strings did not degrade in performance due to packaging, environmental testing, and deployment.

*L'Garde Procedure No. 21775 for I-V Testing a Solar Cell String

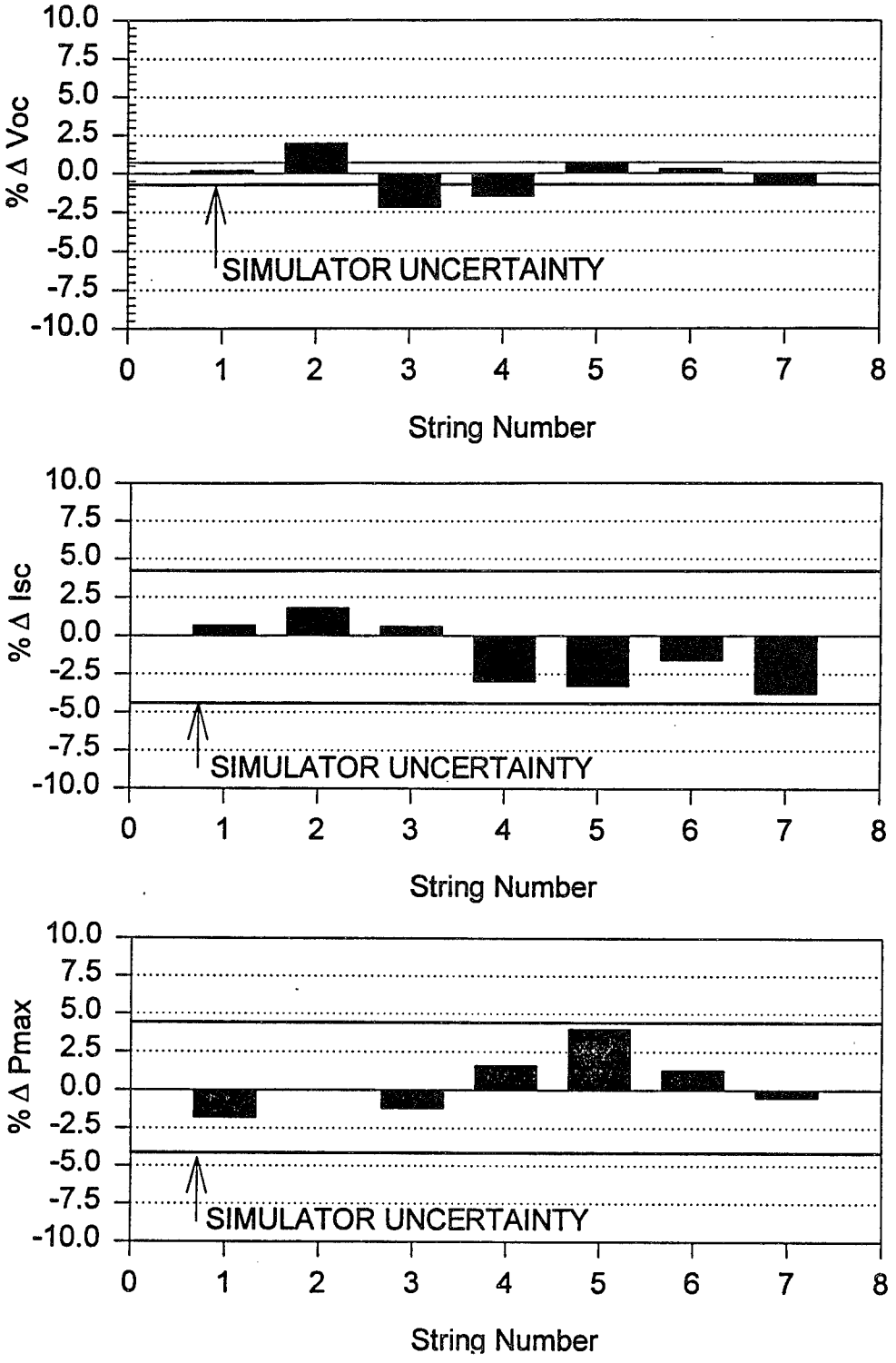

Figure 126. Cell performance comparisons.

Figure 127 presents the results first shown in Reference 36 which suggest that a partial covering on the order of 20 percent of one cell area, of one cell in a 31-cell string would be apparent in the I-V curve. For this figure the cell partially covered was in the 7-cell group of the 31-cell string (each string contains three 8-cell groups and one 7-cell group). Figures 128 to 134 show the comparison of the before and after I-V curves.

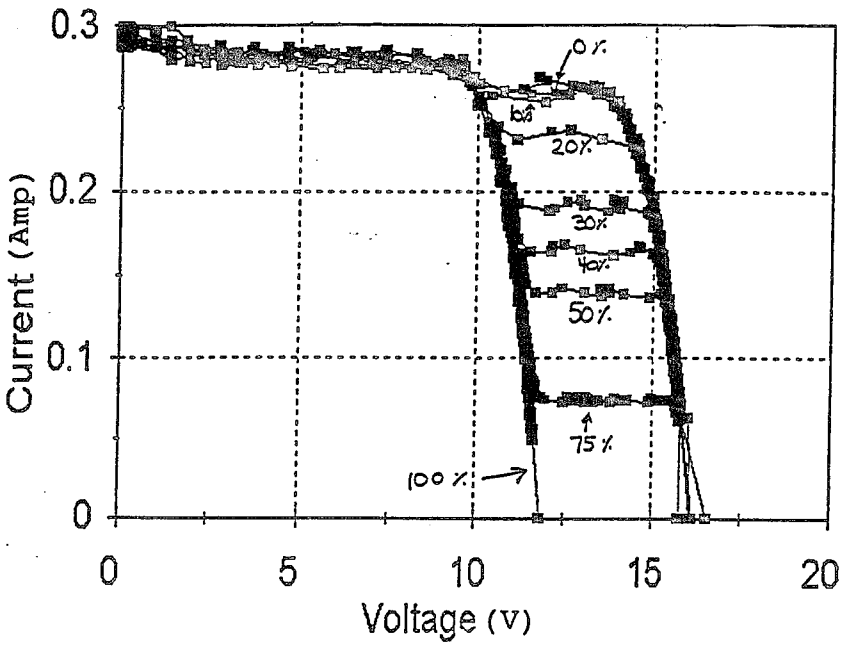

Figure 127. Effect of partial covering one cell on I-V curve.

No difference can be found in the before and after I-V curves. Any change in the curves is less than that shown in Figure 127. It can be stated that the strings did not degrade significantly in performance due to vacuum deployment. Any change in the string behavior was limited to less than 10 percent of one cell in the string, which has been shown to be at the threshold of the measurements.

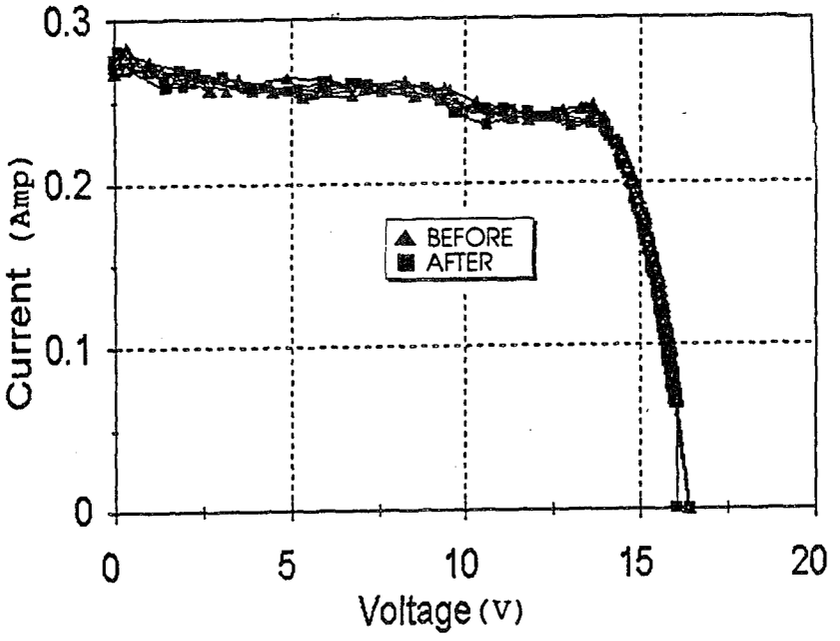

Figure 128. String 01 comparison.

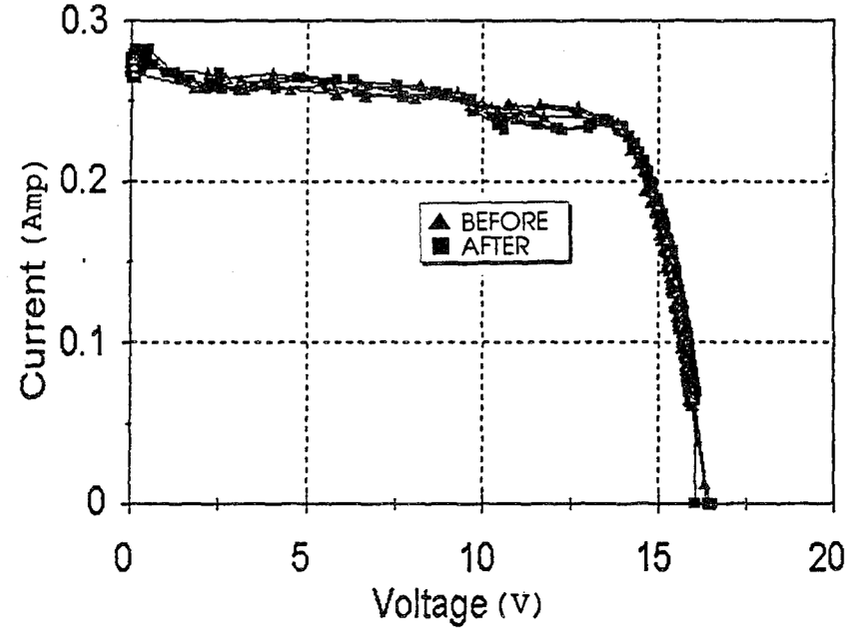

Figure 129. String 02 comparison.

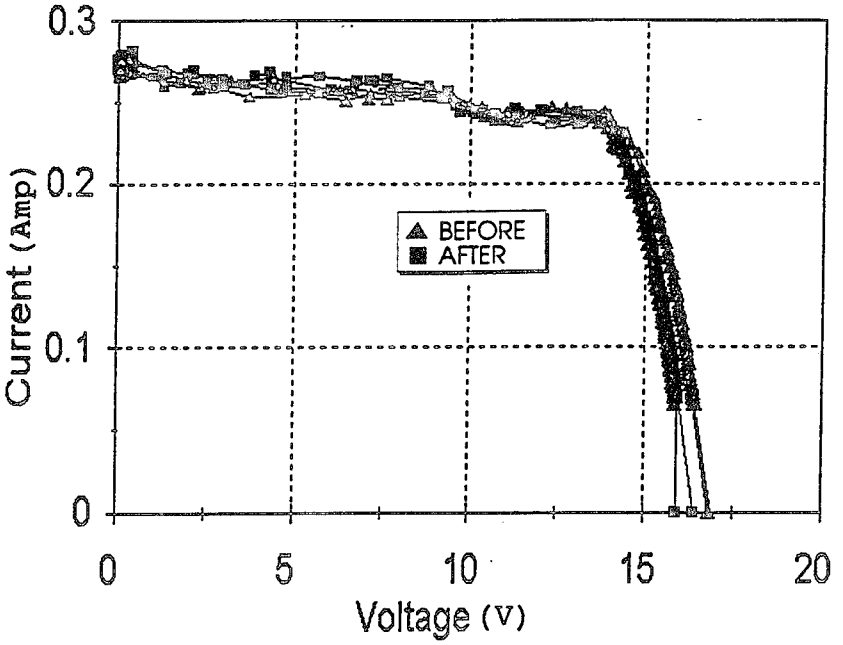

Figure 130. String 03 comparison.

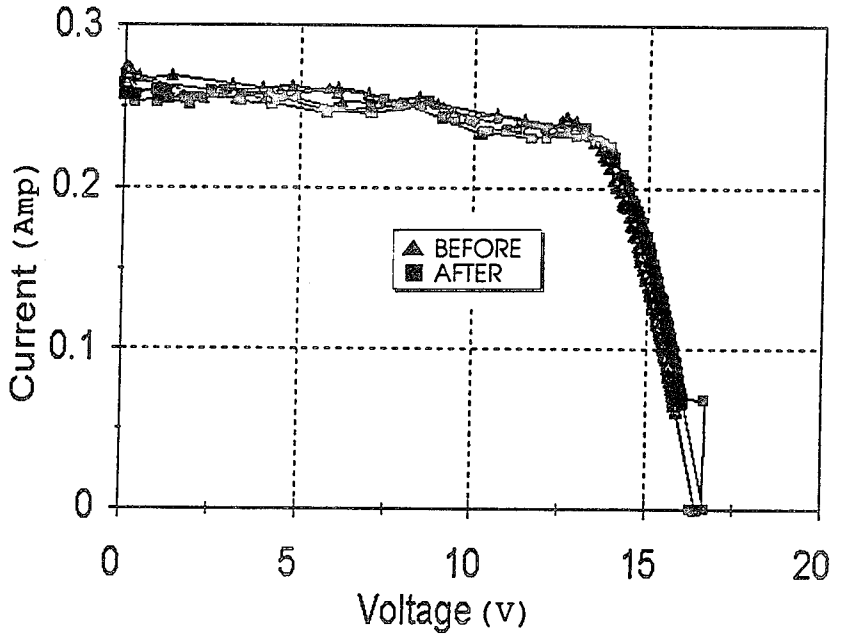

Figure 131. String 04 comparison.

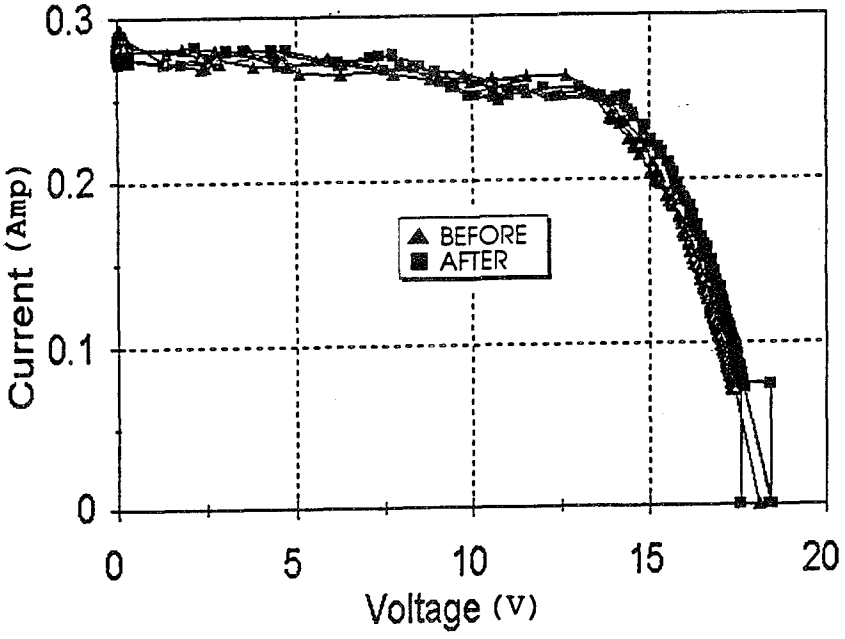

Figure 132. String 05 comparison.

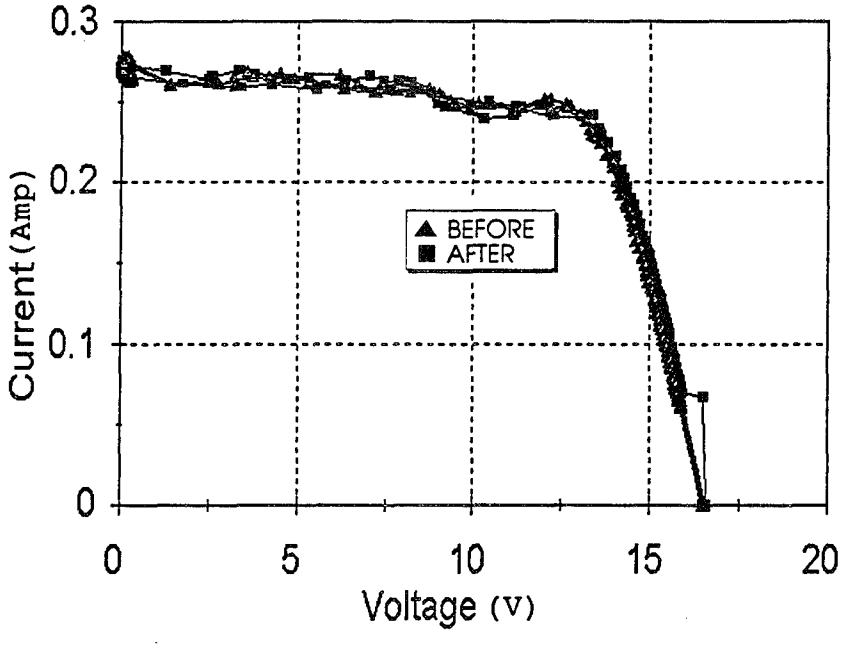

Figure 133. String 06 comparison.

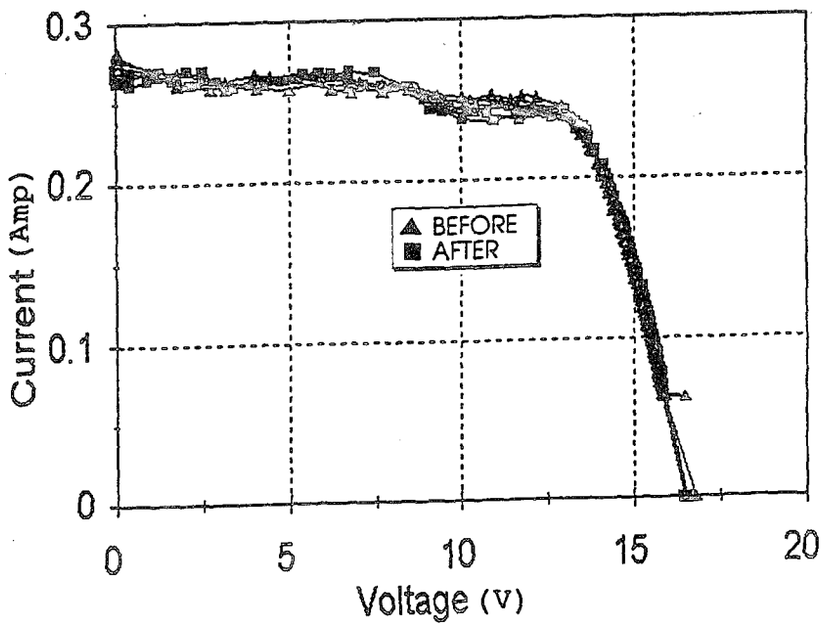

Figure 134. String 07 comparison.

4.7.3.2 Conclusions. From the I-V tests of the solar cell strings before and after vacuum deployment, the following conclusions can be reached:

- All strings functioned normally after vacuum deployment.
- No significant damage to the strings occurred from vacuum deployment.
- The electrical performance of the strings did not change due to vacuum deployment.
- L'Garde's solar simulator provided a repeatable test-bed for measuring the solar cell performance, with resolution to 20 percent covering of one cell in a 31-cell string.

5.0 SUMMARY/CONCLUSIONS

5.1 PERFORMANCE

The ITSAT Phase II demonstration program has made a significant gain in power density over state-of-practice solar array systems. The power density of the protoflight unit is 59.1 W/kg with an areal density of 113 W/m^2. The unit is designed for a 3-year life in a 600-800 km orbit at any inclination. The test results have demonstrated that the ITSAT will deploy orderly and efficiently. There was no cell breakage due to deployment signifying that an operable system will be in place while on orbit. The production unit has a power density capability of up to 93 W/kg using crystalline silicon solar cells.

5.2 CURRENT DESIGN

The current design uses 4-in diameter structural tubes, a graphite-epoxy enclosure, state-of-practice silicon crystalline solar cells, state-of-the-art solar blanket, and novel inflation deployment system. This design was fabricated using space-qualified materials and subsystems. The result is a power density well over double the state of practice.

5.3 PERFORMANCE ENHANCEMENTS/RECOMMENDATIONS

Several design enhancements can be incorporated to the current design to boost the power density to as high as 93 W/kg at no or low risk to invalidating the previous testing.

Initially the enclosure can be optimized by adding lightening holes and/or modifying the configuration slightly. The deployable laminate tubes can be made smaller. During Phase II, the 4-in diameter was chosen based on customer direction and previous data developed during the Phase I and II efforts. The calculations showed that the tubes could be made substantially smaller due to the low loading environment. While tubes as small as 1-in diameter could theoretically be used, a minimum was set at 2.5 in due to the difficulty in manufacturing them any smaller. It was demonstrated during Phase II that a 2.88-in diameter would support the current design loads. Using these test data, a 2.5-in tube diameter design margin can be extrapolated.

The deployment tubes utilize a 1.5-mil thick bladder. This material was an off-the-shelf purchase. Further weight optimization can be accomplished using a custom bladder made from 0.5-mil thick material.

Another area where mass can be reduced is the inflation system. The current design uses a simple blowdown system (i.e., a tank of pressurized gas is opened and allowed to fill a larger volume at a lower pressure). Several approaches could be developed: (1) use lighter weight components such as filament wound tanks versus steel and a magnesium versus aluminum manifold assembly; (2) use a different inflatant (a solid or liquid that would have an appropriate vapor pressure to accomplish the task); and (3) use a pyrotechnic gas generator similar to that used on automobile air bags (Sodium-Azide). Any combination of these approaches will enhance the ITSAT performance.

The last enhancement area is the solar array itself. Soon to be available are several advanced cell technologies. The most promising is the thin-film technology. Within each of these technologies there are various architectures that can be used. Gains of 5 to 15 percent can be realized depending upon the cost, risk, and reliability requirements.

Recommendations for the production units in the near term would include using the optimized enclosure, using smaller support tubes, and optimizing the inflation system using the cold gas inflatant approach. In the future as more advanced cell technology becomes available, these technologies would be desirable. In summary, a variety of performance enhancements can be incorporated into the ITSAT design, Table 43 presents a list of areas where mass can be saved.

5.4 PROJECTED COSTS

The projected costs are shown in Table 44. The recurring and nonrecurring costs are separated. The ITSAT system is very attractive with $2,300-$3,100 per watt when compared to the state-of-practice costs of about $4,000-$6,000 per watt. When the additional advantages, including storage conformity and reliability are considered, the ITSAT is an exceptional value.

Table 43. Component mass comparison.

	PROTOFLIGHT UNIT	PRODUCTION DESIGN
Component	Mass (kg)	Mass (kg)
TUBES AND CAPS		
Tubes	0.936	0.516
Bladders	0.062	0.044
Tube Clamp Rings	0.047	0.015
Tube End Caps	0.132	0.041
Subtotal	1.177	0.616
ENCLOSURE		
Housing	0.554	0.265
Lid	0.285	0.158
Cable Cutters	0.057	0.032
Holddown Cables	0.005	0.005
Subtotal	0.901	0.460
INFLATION SYSTEM		
Puncture Cutter (for tank)	0.070	0.012
Pyro Valve Manifold	0.119	0.079
Diaphragm	0.010	0.007
Inflatant Tank	0.524	0.126
Vent Piston	0.001	0.001
Fill Valve	0.009	0.009
Tubing	0.016	0.016
Inflatant	0.100	0.009
Subtotal	0.849	0.259

	PROTOFLIGHT UNIT	PRODUCTION DESIGN
Component	Mass (kg)	Mass (kg)
MISCELLANEOUS		
Interleaving foam pads	0.154	0.077
End Pads	0.034	0.017
Miscellaneous	0.411	0.411
Subtotal	0.599	0.505
SOLAR BLANKET		
Blanket Mass	1.098	1.098 (* see below)
Total Non-Blanket Mass	3.526	1.840
TOTAL MASS	4.624	2.938
Structure % of Mass	76%	63%

[a] Note the mass of the ITSAT blanket (crystalline silicon) is given here. This could be substantially reduced by incorporating thin film solar cells.

Table 44. Projected costs[a].

Cost estimates with recurring and nonrecurring separated.

ARRAY SYSTEM	DELIVERY TIME FOLLOWING FAB AND ACCEPTANCE TESTING	ROM PRICE $ (Millions)	RECURRING PRICE EST.	NONRECURRING PRICE EST.
200	14 Months ARO	$0.61	$0.59	$0.02
600	16 Months ARO	$1.41	$1.33	$0.08
1000	18 Months ARO	$2.33	$2.22	$0.11

[a] Price does not include integration effort that may be required.

5.5 PROGRAMMATICS

5.5.1 Phase II Accomplishments

Table 45 presents the major subheadings of the Statement of Work. The supporting columns show the status of each item.

Table 45. Statement of work summary, Phase II.

SOW PARA	DESCRIPTION	REQUIREMENT MET ?	HOW
4.2	Optional Phase II		
4.2.1	Definition	Yes	TI/TD Meeting to discuss definition.
4.2.2	Task-1 Requirements	Yes	Generated/approved Requirements Document.
4.2.3	Task-2 Design	Yes	Documented on drawings, ICD 21201.
4.2.4	Task-3 Fabrication	Yes	Fabricated subsystems documented on shop orders.
4.2.5	Test-4 Testing	Yes	Testing accomplished, documented in test reports.
4.2.8	Task-5 Analysis	Yes	Analysis generated to support design and test, documented in reports.
4.2.7	Task-6 Management and Documentation	Yes	Management documentation presented in monthly status and financial reports, others submitted in accordance with CDRLs.

5.5.2 Lessons Learned From the ITSAT Program

1. The corner joint developed during Phase I of the program was difficult to fabricate. Excessive leakage and problems with the bond strength added to the decision to abandon it in favor of the simpler Phase II "straight tube" design.

2. At the beginning of the program it was thought the tubes had to be pressurized high enough to completely remove all the wrinkles for adequate strength. This was not the case; The tube strength is only slightly degraded at lower pressures. Hence, the visual appearance of the tube surface is not a good indicator of strength as previously thought.

3. During folding of the tubes during development tests, pinholes were produced causing excessive leakage. An internal bladder was added to correct this problem at a small expense to the system mass. The result was a significantly lower leak rate design.

4. More deployment/burst tests should be performed on full length tubes with bladders to increase the statistical confidence.

5. During testing of the qualification unit at NRL, the venting of the tubes was insufficient to keep them from crushing while backfilling the chamber. This required externally pressurizing them during backfill. This method will be used for all similar tests in the future, although it has no bearing on a flight situation.

6. The ITSAT can be optimized further in subsequent designs. Some of the preliminary design calculations were overly conservative, leading us to fabricate a unit that was heavier than necessary. Examples of recommended improvements include:

   - Reduce the tube diameter

   - Redesign the housing and lid; the weight of these can be substantially reduced by the addition of lightening holes.

- Reduce the safety margin on the inflatant tank. Also, use a material with a higher strength-to-weight ratio than the 4130 steel, such as titanium.

- Use lighter weight pyro devices. Several options have been identified.

- Use lighter weight materials (i.e., magnesium for the machined parts).

- Use thinner foam padding (1/8 in instead of 1/4 in) between the folds of the solar blanket.

- Use a different mounting scheme for the tube end caps. Mount them outside the lid and housing to reduce the thickness of the enclosure.

5.5.3 Phase III Program Plan

A Phase III flight test effort is planned. Figure 135 presents a proposed program plan to meet the flight test and evaluation objectives. The nominal program length is 12 months though, depending on the mission, launch vehicle, budgetary requirements, etc., the schedule could be as short as 10 months or as long as 18 months. Mission support is difficult to determine at this date. A nominal period of performance for this effort would be about 1 year with a significant portion at the beginning of the period (i.e., during the experiment deployment and initial monitoring effort).

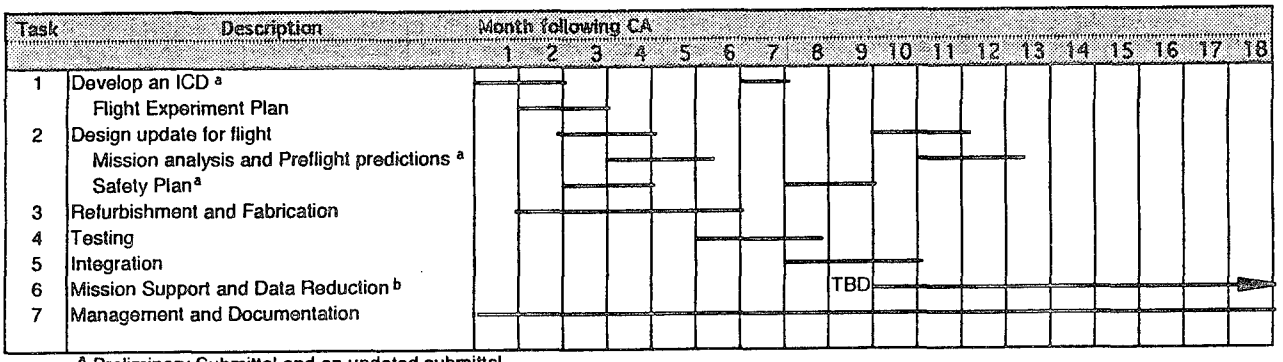

[a] Preliminary Submittal and an updated submittal

[b] Mission support is TBD. Will be defined when mission manifest is announced.

Figure 135. Phase III program plan.

REFERENCES

1. Williams, G., "ITSAT Requirements Document", L'Garde Specification #21211, April 1992.

2. Williams, Geoff, "ITSAT Design Calculations", L'Garde Technical Report, LTR-92-GW-042

3. Davey, K., "Thermal Analysis of ITSAT Tubes and Canister", L'Garde Technical Report LTR-93-KD-055A, September 1993.

4. "NISA User's Manual", Engineering Mechanics Research Corporation, 1992.

5. Tada, H.Y., et al, "Solar Cell Radiation Handbook", 2nd Edition, Prentice Hall, 1981.

6. Encyclopedia of Polymer Science and Technology, 1985, J Kroschwitz, Williamson, NY.

7. A. Paillons, Certs/Derts. 2, Avenue E. Belin, b.p. 4025, 31055 Toulouse Cedex, France.

8. General Dynamics Test Data contained in:
   Bruhn, E.F., "Analysis and Design of Flight Vehicle Structures", S. R. Jacobs and Associates, Inc., June 1973. Pages C8.5 - C8.10.

9. MDAC Test Data contained in:
   Veal, G., "Design of Solar Rocket Torus", L'Garde Information Release #280, March 3, 1986.

10. NASA Test Data from:
    Weingarten, V., Seide, P., and Peterson, J., "Buckling of Thin Walled Circular Cylinders", NASA Special Publication SP-8007, NASA Langley Research Center, August 1986, Pages 7,35.

11. Williams, G., "ITSAT II Tube Bending Test at Various Rigidization Pressures", L'Garde Technical Report #LTR-93-GW-057, September, 1993.

12. Veal, G., "The Inflatable Antenna Experiment, Interim Report - Phase B", L'Garde Technical Report LTR-93-GV-001, January 1992.

13. Test Certification, OCM Test Laboratory, Sample Test 921214A, December 7, 1992

14. Davey, K., "ITSAT II Leak Rate Theoretical Model" L'Garde Technical Report, LTR-93-KJD-025, April 1993.

15. Roark and Young, "Formulas for Stress and Strain", Fifth Edition 1975.

16. Oberg, E., et al "Machinery's Handbook", 22nd Edition, Industrial Press, Inc., New York, NY, 1984.

17. Thompson, W., "Theory of Vibrations with Applications", 2nd edition, Prentice Hall, 1981.

18. Williams, G., "Bypass Diode Sample Blankets", L'Garde Technical Report LTR-92-GW-059, December 1992.

19. Westen, H.P., Editor "Reference Data for Radio Engineers", International Telephone & Telegraph Corporation, 1962.

20. Kurland, R., "Advanced Photovoltaic Solar Array Prototype Development & Testing", TRW Report #51760-6005-UT-00, JPL Contract #957990 (Mod 10), August 12, 1991.

21. Williams, G., "ASEC CIC Acceptance & Electrical Results" L'Garde Technical Report LTR-93-GW-008, February 1993.

22. Williams, G., "ITSAT II Thermal Cycle of Tube Materials", L'Garde Technical Report LTR-93-GW-063, October 1993.

23. Brandt, D., "ITSAT II Fixed Volume Blowdown Test Results", L'Garde Technical Report LTR-93-DFB-034, May 1993.

24. Brandt, D., "ITSAT II Ascent Vent Test Results", L'Garde Technical Report LTR-93-DFB-024, April 1993.

25. Brandt, D., "ITSAT II Inflatable Tank Proof/Burst Tests" L'Garde Technical Report LTR-93-DFB-016, March 1993.

26. Brandt, D., "ITSAT II Vacuum Inflation Test of Five-Foot Tube", L'Garde Technical Report LTR-93-DRB-038, June 1993.

27. Williams, G., "Thermal Cycling of NASA Coupon", L'Garde Technical Report LTR-93-GW-036, June 1993.

28. Williams, G., "Single Tube Tests for ITSAT II", L'Garde Technical Report LTR-93-GTW-022, April 1993.

29. Williams, G., "Bladder for ITSAT II Tubes", L'Garde Technical Report, LTR-93-GW-027, April 1993.

30. Davey, K., "Preliminary Calculations on Natural Frequency in Vacuum", September 2, 1993.

31. Williams, G., "ITSAT II Random Vibration Test Results", L'Garde Technical Report LTR-93-GW-062, October 1993.

32. Williams, G., "ITSAT II Thermal Vacuum Test Report - Revision A", L'Garde Technical Report LTR-93-GW-069A, December 1993.

33. Davey, K., "Predicted Temperature and Pressure of ITSAT at NRL", L'Garde Technical Report LTR-93-KD-064, October 1.

34. Davey, K., "ITSAT I-V Tests Before Vacuum Deployment Test", L'Garde Technical Report LTR-93-KD-048, July 1993.

35. Davey, K., "ITSAT I-V Tests Before and After Vacuum Deployment Test", L'Garde Technical Report LTR-93-KD-071, November 1993.

36. Davey, K., "Solar Simulator Test Results", L'Garde Technical Report LTR-93-KD-028, May 1993.

APPENDIX A

GROUPING OF CELLS

Table A-1. Electrical data for cell strings #6 (highest efficiency).

Lot	Cell	Voc	Isc	IL	Cff	Eff
104	62	542.8	313.8	297.9	78.7	12.4
104	56	540.9	313.9	296.5	78.6	12.3
104	15	541.9	311.6	296.2	78.9	12.3
104	96	544.3	311.3	295.7	78.5	12.3
104	100	540.8	311.5	295.6	78.9	12.3
104	12	543.5	310.5	295.1	78.7	12.3
104	32	550.1	311.1	295.1	77.6	12.3
104	103	544.1	309.3	295.0	78.9	12.3
104	6	542.1	314.2	294.2	77.7	12.2
104	69	542.5	311.5	294.1	78.3	12.2
104	52	540.8	309.2	294.0	79.1	12.2
104	35	544.2	310.4	293.9	78.3	12.2
101	65	547.3	307.1	293.7	78.6	12.2
104	14	538.1	310.9	293.7	79.0	12.2
104	93	542.5	312.1	293.6	78.0	12.2
104	7	536.8	311.9	293.4	78.8	12.2
104	11	540.9	312.5	293.4	78.1	12.2
101	5	547.6	304.4	293.2	79.1	12.2
102	49	545.4	306.8	293.1	78.8	12.2
104	5	538.1	310.7	293.1	78.9	12.2
104	8	540.5	310.3	293.1	78.6	12.2
104	90	538.8	312.0	293.1	78.5	12.2
101	48	549.3	305.5	292.9	78.5	12.2
104	64	538.7	311.8	292.9	78.5	12.2
103	41	543.6	309.1	292.8	78.4	12.2
104	21	534.8	312.6	292.8	78.8	12.2
104	10	541.8	307.4	292.5	79.0	12.2
104	53	540.1	313.2	292.5	77.8	12.2
101	61	548.6	305.9	292.0	78.3	12.1
104	84	544.5	309.4	291.9	78.0	12.1
101	20	550.3	302.4	291.6	78.9	12.1
	AVERAGE:	542.0	310.1	293.8	78.5	12.2

Table A-2. Electrical data for cell string #7 (2nd highest efficiency).

Lot	Cell	Voc	Isc	IL	Cff	Eff
104	60	538.9	311.3	291.6	78.2	12.1
102	22	539.5	309.8	291.4	78.5	12.1
103	10	540.1	310.9	291.2	78.1	12.1
104	99	537.3	311.0	291.2	78.4	12.1
101	57	545.7	306.1	291.1	78.4	12.1
104	4	540.0	310.9	291.0	78.0	12.1
101	47	546.9	303.0	290.8	79.0	12.1
104	19	538.8	310.5	290.8	78.2	12.1
104	48	540.3	309.2	290.8	78.3	12.1
101	24	546.9	303.0	290.7	78.9	12.1
104	76	534.1	310.4	290.7	78.9	12.1
104	87	540.5	309.7	290.7	78.1	12.1
104	54	538.3	310.5	290.6	78.2	12.1
101	15	546.6	302.5	290.5	79.0	12.1
102	21	537.4	307.7	290.5	79.1	12.1
104	63	541.0	311.0	290.5	77.7	12.1
103	22	541.1	310.5	290.3	77.8	12.1
102	19	541.6	310.7	290.3	77.6	12.1
104	16	541.9	310.7	290.2	77.5	12.1
101	40	540.9	306.2	290.1	78.8	12.1
102	38	538.6	307.8	290.0	78.7	12.1
101	66	548.6	301.6	289.9	78.9	12.1
101	19	549.1	305.2	289.8	77.8	12.0
104	59	540.1	309.3	289.8	78.1	12.0
104	102	533.0	312.1	289.8	78.4	12.0
101	43	541.6	304.0	289.7	79.2	12.0
101	58	549.1	304.2	289.7	78.0	12.0
104	71	539.5	308.7	289.7	78.3	12.0
101	6	548.6	302.5	289.6	78.5	12.0
101	41	551.0	299.9	289.6	78.9	12.0
104	46	536.8	310.6	289.6	78.2	12.0
	AVERAGE:	541.0	307.8	290.4	78.4	12.1

Table A-3. Electrical data for cell string #4 (3rd highest efficiency).

Lot	Cell	Voc	Isc	IL	Cff	Eff
103	26	536.8	309.7	289.3	78.3	12.0
104	38	531.9	311.8	289.2	78.5	12.0
101	51	549.8	301.3	289.1	78.5	12.0
104	39	539.0	306.9	289.1	78.6	12.0
101	7	541.6	305.1	289.0	78.7	12.0
101	71	548.1	303.9	289.0	78.1	12.0
104	1	536.4	307.4	289.0	78.9	12.0
104	26	536.6	307.7	289.0	78.8	12.0
104	68	538.3	308.3	289.0	78.4	12.0
102	76	538.6	307.5	289.0	78.5	12.0
101	11	549.3	300.2	288.9	78.8	12.0
104	3	537.9	308.7	288.9	78.3	12.0
101	28	547.9	302.8	288.8	78.3	12.0
104	34	530.4	313.6	288.8	78.1	12.0
101	21	549.5	300.9	288.7	78.6	12.0
101	25	548.1	304.7	288.7	77.8	12.0
104	65	539.8	309.9	288.7	77.7	12.0
101	62	548.0	305.9	288.6	77.5	12.0
104	104	537.4	308.5	288.6	78.3	12.0
102	50	538.6	306.6	288.5	78.6	12.0
101	3	547.6	305.3	288.5	77.6	12.0
101	56	550.5	300.7	288.5	78.5	12.0
101	23	546.7	300.9	288.3	78.9	12.0
104	2	538.6	308.5	288.3	78.1	12.0
101	13	541.1	303.4	288.2	79.0	12.0
101	14	539.8	305.8	288.2	78.6	12.0
101	60	546.3	306.3	288.2	77.5	12.0
102	28	538.8	305.8	288.2	78.7	12.0
102	79	536.2	306.2	288.1	79.0	12.0
103	13	536.9	310.4	288.1	77.8	12.0
104	18	539.1	309.0	288.1	77.8	12.0
	AVERAGE:	541.0	306.2	288.7	78.3	12.0

Table A-4. Electrical data for cell string #3 (4th highest efficiency).

Lot	Cell	Voc	Isc	IL	Cff	Eff
101	1	548.5	300.4	287.9	78.6	12.0
101	31	546.6	300.4	287.9	78.9	12.0
102	55	539.4	305.6	287.9	78.6	12.0
101	53	539.8	304.4	287.8	78.8	12.0
102	36	536.6	307.9	287.8	78.4	12.0
102	62	538.7	304.6	287.8	78.9	12.0
102	68	538.2	305.7	287.8	78.7	12.0
101	42	546.3	300.1	287.7	78.9	12.0
102	41	544.1	305.1	287.7	78.0	12.0
103	47	537.0	310.2	287.7	77.7	12.0
101	69	540.3	306.6	287.6	78.1	12.0
104	43	534.6	310.0	287.6	78.1	12.0
104	36	530.2	311.8	287.5	78.2	12.0
104	78	536.3	308.8	287.5	78.1	12.0
101	49	548.4	297.6	287.4	79.2	11.9
101	54	539.7	302.7	287.4	79.2	12.0
102	77	537.4	306.3	287.4	78.6	12.0
104	81	538.1	311.0	287.3	77.3	11.9
101	18	538.8	304.8	287.2	78.7	11.9
102	18	537.4	305.9	287.2	78.6	11.9
102	20	537.7	307.4	287.2	78.2	11.9
102	40	538.8	305.9	287.2	78.4	11.9
102	82	537.8	307.3	287.1	78.2	11.9
103	3	543.3	307.9	287.1	77.2	11.9
103	24	538.1	309.6	286.9	77.5	11.9
101	55	547.2	305.2	286.8	77.3	11.9
102	4	537.4	304.9	286.8	78.8	11.9
102	70	542.9	303.2	286.8	78.4	11.9
104	51	537.7	310.6	286.8	77.3	11.9
102	83	539.3	306.2	286.8	78.2	11.9
102	59	536.7	305.3	286.7	78.7	11.9
	AVERAGE:	539.0	305.9	287.4	78.3	12.0

Table A-5. Electrical data for cell string #2 (5th highest efficiency).

Lot	Cell	Voc	Isc	IL	Cff	Eff
102	6	536.5	305.6	286.6	78.6	11.9
102	51	539.4	304.3	286.6	78.6	11.9
103	2	532.2	309.1	286.6	78.4	11.9
104	97	525.6	313.1	286.6	78.4	11.9
101	17	549.2	302.2	286.4	77.7	11.9
102	54	537.0	305.4	286.4	78.6	11.9
102	90	539.1	306.0	286.4	78.1	11.9
101	32	541.3	301.7	286.3	78.9	11.9
101	35	548.4	298.7	286.3	78.5	11.9
102	52	542.8	302.8	286.3	78.4	11.9
101	9	539.0	302.5	286.2	79.0	11.9
102	24	536.7	307.2	286.2	78.1	11.9
102	53	536.6	304.0	286.1	78.9	11.9
102	84	535.0	305.5	286.1	78.8	11.9
102	31	535.8	310.7	286.0	77.3	11.9
102	78	537.6	303.8	286.0	78.8	11.9
102	30	536.4	308.6	285.9	77.7	11.9
104	40	536.0	308.8	285.9	77.7	11.9
101	52	545.6	302.8	285.8	77.8	11.9
102	71	540.0	307.4	285.8	77.7	11.9
102	74	537.4	302.8	285.8	79.0	11.9
104	42	533.3	310.7	285.8	77.6	11.9
102	75	538.1	302.9	285.7	78.9	11.9
101	16	538.8	301.8	285.6	79.0	11.9
101	33	539.3	301.7	285.6	79.0	11.9
102	10	536.6	305.6	285.5	78.3	11.9
102	58	534.6	307.0	285.5	78.3	11.9
104	25	537.1	308.6	285.5	77.5	11.9
102	64	538.3	304.8	285.4	78.3	11.9
101	2	550.3	300.0	285.2	77.7	11.9
101	63	542.6	300.8	285.2	78.6	11.9
	AVERAGE:	538.0	305.1	286.0	78.3	11.9

Table A-6. Electrical data for cell string #1 (6th highest efficiency).

Lot	Cell	Voc	Isc	IL	Cff	Eff
102	65	537.8	304.6	285.1	78.3	11.9
104	49	535.0	308.7	285.1	77.7	11.9
101	22	535.7	305.6	285.0	78.3	11.9
102	46	536.3	305.3	285.0	78.3	11.9
103	5	537.5	311.2	285.0	76.7	11.9
103	8	539.3	309.5	285.0	76.8	11.9
104	29	534.5	307.1	285.0	78.1	11.9
102	44	536.1	310.4	284.8	77.0	11.8
102	35	542.5	305.8	284.8	77.3	11.8
104	41	538.2	312.2	284.8	76.3	11.8
101	26	537.4	303.1	284.7	78.7	11.8
104	13	540.1	309.6	284.7	76.6	11.8
104	24	533.3	309.9	284.7	77.5	11.8
104	31	538.5	313.9	284.7	75.8	11.8
102	57	535.9	307.1	284.6	77.8	11.8
102	85	534.7	304.7	284.6	78.6	11.8
102	88	534.3	304.3	284.6	78.8	11.8
101	10	547.7	296.4	284.5	78.9	11.8
104	88	532.5	311.2	284.5	77.3	11.8
102	32	539.0	303.8	284.4	78.1	11.8
102	66	538.4	304.1	284.4	78.2	11.8
101	27	542.5	300.8	284.2	78.4	11.8
102	89	539.8	306.0	284.2	77.4	11.8
103	16	532.3	311.2	284.2	77.2	11.8
101	70	546.0	303.5	284.1	77.1	11.8
102	5	535.7	304.2	284.1	78.4	11.8
102	29	535.9	304.9	284.1	78.2	11.8
101	12	537.9	300.7	283.9	79.0	11.8
102	25	544.5	301.8	283.9	77.7	11.8
102	60	537.8	302.0	283.9	78.7	11.8
104	30	535.4	311.1	283.9	76.7	11.8
	AVERAGE:	537.0	306.3	284.5	77.7	11.8
AVERAGE FOR 8 MIL CELLS:		540.0	306.9	288.5	78.3	12.0

APPENDIX B

TEMPERATURE PROFILE FOR THERMAL CYCLING OF TUBE MATERIALS

(See Subsection 4.2.5)

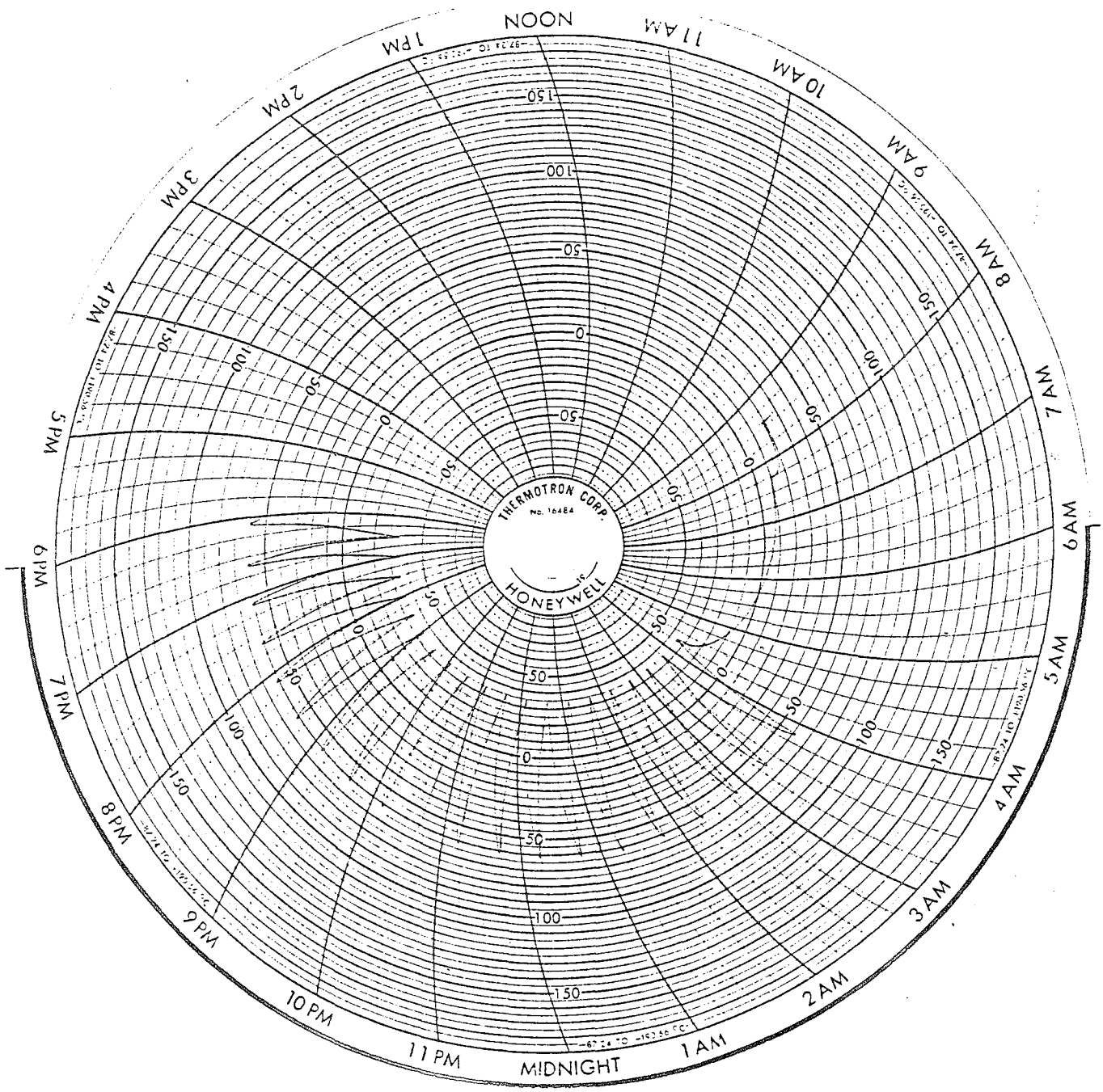

Figure B-1. Thermotron printout.

DISTRIBUTION LIST

AUL/LSE
Bldg 1405 - 600 Chennault Circle
Maxwell AFB, AL 36112-6424 1 cy

DTIC/OCC
Cameron Station
Alexandria, VA 22304-6145 2 cys

AFSAA/SAI
1580 Air Force Pentagon
Washington, DC 20330-1580 1 cy

PL/SUL
Kirtland AFB, NM 87117-5776 2 cys

PL/HO
Kirtland AFB, NM 87117-5776 1 cy

Official Record Copy
PL/VTPC/Lt R Boswell 1 cy

PL/VT
Dr. R.V. Wick
Kirtland AFB, NM 87117-5776 1 cy